

Phenomenological applications in CP-violating systems in the SM and beyond



VNIVERSITAT
DE VALÈNCIA

Tesis doctoral
Programa de Doctorado en Física
Julio 2019

Héctor Gisbert Mullor
IFIC, Universitat de València - CSIC
Departament de Física Teòrica

Director de tesis:
Antonio Pich Zardoya

Als meus pares

Antonio Pich Zardoya, catedrático de la Universidad de Valencia,

Certifica:

Que la presente memoria “Phenomenological applications in CP-violating systems in the SM and beyond” ha sido realizada bajo su dirección en el Instituto de Física Corpuscular, centro mixto de la Universidad de Valencia y del CSIC, por Héctor Gisbert Mullor y constituye su Tesis para optar al grado de Doctor en Física.

Y para que así conste, en cumplimiento de la legislación vigente, presenta en el Departamento de Física Teórica de la Universidad de Valencia la referida Tesis Doctoral, y firma el presente certificado.

Valencia, a 8 de Julio de 2019.

Antonio Pich Zardoya

Contents

Preface	1
1 Deepening into Flavour Physics	3
1.1 The Gauge Interactions of the Standard Model	3
1.1.1 Strong interaction	3
1.1.2 Electroweak interactions	6
1.2 Spontaneous Symmetry Breaking	13
1.2.1 Global symmetry: Goldstone theorem	14
1.2.2 Local gauge symmetry: Higgs mechanism	16
1.2.3 The Higgs boson and its interactions	18
1.2.4 The Yukawa Lagrangian	18
1.3 The CKM matrix	21
1.3.1 Unitarity of the CKM matrix	23
1.4 CP violation in Neutral Meson Systems	26
1.4.1 Neutral Meson Mixing	27
1.4.2 Neutral Meson Decay	37
1.4.3 Types of CP violation in neutral meson systems	39
2 The Toolbox: EFTs, OPEs and RGEs	41
2.1 What are EFTs and why we use them?	41
2.2 General aspects of EFT	42

2.2.1	Operator product expansion	42
2.2.2	Behaviour of local operators	47
2.3	Effective weak interactions	48
2.3.1	General description	49
2.3.2	Phenomenological application	51
2.3.3	Some final comments or remarks	65
3	Direct CP violation in kaon decays	67
3.1	Historical prelude	67
3.2	Anatomy of ε'/ε	72
3.3	Short-distance contributions	76
3.4	Hadronic matrix elements	78
3.5	Effective field theory description	83
3.5.1	Chiral perturbation theory	83
3.5.2	Chiral realization of the $\Delta S = 1$ effective Lagrangian	87
3.6	Matching	88
3.7	The χ PT $K \rightarrow \pi\pi$ amplitudes	94
3.7.1	Chiral loop corrections	96
3.7.2	Local $\mathcal{O}(p^4)$ contributions	99
3.8	The SM prediction for ε'/ε	100
3.9	Discussion and outlook	104
4	Isospin violation in kaon decays	109
4.1	Introduction	109
4.2	$K \rightarrow \pi\pi$ amplitudes at NLO	111
4.2.1	Isospin breaking structure of the amplitudes	113
4.3	Determination of chiral LECs	115
4.3.1	Weak couplings at $\mathcal{O}(G_F p^2)$ and $\mathcal{O}(e^2 G_8 p^0)$	115
4.3.2	Weak couplings at $\mathcal{O}(G_F p^4)$ and $\mathcal{O}(e^2 G_8 p^2)$	116

4.3.3	Strong couplings of $\mathcal{O}(p^4)$ and $\mathcal{O}(p^6)$	117
4.3.4	Electromagnetic couplings of $\mathcal{O}(e^2p^2)$	119
4.4	Anatomy of isospin-breaking parameters	120
4.5	Numerical results	121
4.5.1	Amplitudes at NLO	121
4.5.2	χ PT fit to $K \rightarrow \pi\pi$ data	123
4.5.3	Isospin-breaking parameters in the CP-odd sector	124
4.6	Impact on the ε'/ε prediction	128
5	Neutral meson mixing in Multi-Higgs-Doublet Models	131
5.1	Introduction	131
5.2	Theoretical framework	133
5.2.1	Multi-Higgs-Doublet Model	133
5.2.2	Yukawa interactions and alignment	134
5.2.3	$M^0 - \bar{M}^0$ mixing within the SM and beyond	136
5.2.4	GIM mechanism	143
5.2.5	Comparison with the literature	144
5.3	Numerical results	145
5.3.1	Standard Model predictions	146
5.3.2	Aligned Two-Higgs-Doublet Model	147
5.3.3	Aligned Three-Higgs-Doublet Model	155
5.4	Conclusions	159
6	Improved bounds on heavy quark electric dipole moments	161
6.1	Introduction	161
6.2	Renormalization group equations	162
6.3	Extracting the new bounds	165
	Appendix	171

A	OPE in the charged-current SM Lagrangian	171
B	Feynman rules for $q_1 \bar{q}_3 \rightarrow q_2 \bar{q}_4$	175
C	Inputs values of Chapter 3	177
D	NLO $\Delta S = 1$ Wilson coefficients	179
	D.1 Effective $\Delta S = 1$ short-distance Hamiltonian	179
	D.2 Renormalization group equations	179
	D.3 General evolution matrix	180
	D.4 QCD evolution matrix	181
	D.5 QED evolution matrix	183
	D.6 Wilson coefficients at $\mu < m_c$	185
	D.7 Wilson coefficient in the HV scheme	189
	D.8 Errors on the Wilson coefficients	190
E	Parameters of large-N_C matching at NLO	193
	E.1 $(g_8 N_i)$ couplings	193
	E.2 $(g_8 Z_i)$ couplings	194
F	Updated estimate of λ_3^{SS}	195
G	Feynman rules for meson mixing	197
H	Loop functions for meson mixing	199
I	Colour factors	203
J	Fierz transformations	205
K	GIM mechanism in $C_{\text{SM } 2\text{SRR}}^{ij}$	207
	K.1 B mixing	211
	K.2 K mixing	212

Contents	xi
<hr/>	
K.3 Matching procedure	212
K.4 Renormalization procedure	215
L Hadronic matrix elements for meson mixing	217
M Renormalization group short-distance QCD effects	219
M.1 η -Factors for $B_{s,d}^0 - \bar{B}_{s,d}^0$ mixing	220
M.2 η -Factors for $K^0 - \bar{K}^0$ mixing	221
N Inputs for meson mixing	225
O Computation of $(\gamma_e)_{12}^{(0)}$	227
O.1 Feynman diagrams	227
O.2 Feynman Rules	228
O.3 Computation	228
O.4 Extracting the anomalous dimension matrix	230
P Resum de la tesi	233
P.1 Objectius assolits	234
P.2 Metodologia	235
P.2.1 El model estàndard de la física de partícules	235
P.2.2 Teoria de camps efectius	241
P.3 Resultats i conclusions	246
P.3.1 Violació directa de CP en la desintegració de $K \rightarrow \pi\pi$	247
P.3.2 Violació d'isospín en la desintegració de $K \rightarrow \pi\pi$	247
P.3.3 Mescla de mesons neutres en extensions del Model Estàndard	248
P.3.4 Millora als moments dipolars electrics dels quarks pesats	248
Bibliography	253

Preface

The current knowledge on the structure of matter is the result of a huge experimental and theoretical effort. Our Universe is composed of elementary particles governed by the four fundamental forces: gravitational, weak, electromagnetic and strong forces.

The Standard Model (SM) of particle physics is the simplest theoretical description of how these particles and forces, except for the gravitational force, are related to each other. Along the years, the SM has been able to explain all the experimental data with high accuracy, culminating in 2012 with the discovery of the Higgs boson. Its elegance, simplicity and high predictivity have converted the SM in the best theoretical reference framework to date.

Despite being a successful description of the reality, there are some phenomena that the SM does not explain such as the large matter-antimatter asymmetry. In the early Universe, the Big Bang should have resulted in the same proportions of matter and antimatter, but nowadays we observe that almost everything around us is made of matter except for a small amount of antimatter. One of the grand challenges facing physics is understanding why we observe this asymmetry.

CP violation is one of the necessary ingredients to generate this large asymmetry. In spite of including all needed ingredients, the SM is unable to completely generate the observed asymmetry. Therefore, extensions of the SM with new sources of CP violation could explain the size of this asymmetry. The main objective of this work is precisely the study of phenomenological systems where the CP symmetry is violated.

This thesis is divided in seven chapters. In Chapter 1, we present a comprehensive overview of the SM, showing how its interactions emerge from symmetry principles. The last part is dedicated to the flavour sector of the SM where the CP violation phenomena is introduced through the Cabibbo-Kobawashi-Maskawa (CKM) matrix. Finally, we present the different ways in which this phenomena can appear in nature.

The concept of Effective Field Theory (EFT) is introduced in Chapter 2, providing a powerful theoretical approach for the physical systems studied along this thesis.

The theoretical determination of the direct CP-violating ratio ε'/ε in the SM is the first phenomenological application presented in this thesis which can be found in Chapter 3. Using the theoretical framework of Chiral Perturbation Theory (χ PT), we obtain a SM prediction in complete agreement with its experimental measurement. Finally, in Chapter 4 we update the previous prediction including the known isospin-breaking corrections.

In Chapter 5, we perform a one-loop computation of the short-distance contributions for the neutral meson mixing in a quite general extension of the SM, the Aligned-Multi-Higgs-Doublet Model (AMHDM). This extension accommodates new sources of CP violation that could reproduce the size of the observed matter-antimatter asymmetry of the Universe. Finally, these sources are strongly constrained from the current flavour data.

In Chapter 6, we obtain new limits for the charm and bottom quark electric dipole moments (EDMs) using the renormalization group equations (RGEs) and the strong bounds on their chromo-EDMs.

Chapter 1

Deepening into Flavour Physics

The Standard Model (SM) of particle physics is the simplest theory based on symmetry principles that is able to describe the experimental data with high accuracy. The SM is composed by two gauge theories, $SU(3)_C$ and $SU(2)_L \otimes U(1)_Y$, which lead into two types of interactions, strong and electroweak interactions, respectively. In this chapter, we give a general overview of the SM, paying special attention to the flavour sector. For further reading, you can consult Refs. [1–5].

1.1 The Gauge Interactions of the Standard Model

In this section, we study how the fundamental interactions of the SM emerge from gauge symmetry principles.

1.1.1 Strong interaction

Quantum chromodynamics (QCD) is the gauge theory of the strong interactions with $SU(3)_C$ as the underlying gauge group [6–9]. The matter fields of QCD are the so-called *quarks* which are spin-1/2 fermions with six different flavours (3 light flavours up u , down d , strange s and 3 heavy flavours charm c , bottom b , top t) and three possible colour charges (red, blue or green). Applying the gauge principle to the $SU(3)_C$ group, we can

obtain the QCD Lagrangian from the free quark Lagrangian. For that purpose, let us consider

$$\mathcal{L}_0 = \sum_f \sum_\alpha \bar{q}_f^\alpha (i \not{\partial} - m_f) q_f^\alpha = \sum_f \bar{q}_f (i \not{\partial} - m_f) q_f , \quad (1.1.1)$$

where $\not{\partial} \equiv \gamma^\mu \partial_\mu$ and $q_f \equiv (q_f^1, q_f^2, q_f^3)^T$ is the colour triplet field with components q_f^α , being α and f the colour and the flavour indices, respectively. Notice that \mathcal{L}_0 is invariant under the global $SU(3)_C$ transformations,

$$q_f \xrightarrow{SU(3)_C} q'_f = U q_f , \quad \bar{q}_f \xrightarrow{SU(3)_C} \bar{q}'_f = \bar{q}_f U^\dagger , \quad (1.1.2)$$

where U is a unitary matrix with $\det U = 1$ that is conveniently written as

$$U = \exp \left\{ i \sum_{a=1}^8 \frac{\lambda^a}{2} \theta_a \right\} . \quad (1.1.3)$$

θ_a are arbitrary real parameters without physical meaning and the eight linearly independent matrices λ^a are the Gell-Mann matrices which play the role of the generators of $SU(3)_C$. They are traceless and satisfy the following commutation relations

$$\left[\frac{\lambda^a}{2}, \frac{\lambda^b}{2} \right] = i \sum_{c=1}^8 f^{abc} \frac{\lambda^c}{2} , \quad (1.1.4)$$

where f^{abc} are the totally antisymmetric real structure constants which give a measure of the non-commutativity of $SU(3)_C$,

$$f_{abc} = \frac{1}{4i} \text{Tr}([\lambda_a, \lambda_b] \lambda_c) . \quad (1.1.5)$$

Let the θ_a parameters depend on the space-time coordinates, $\theta_a = \theta_a(x)$. Then, due to the derivative acting on the quark field, the Lagrangian given by Eq. (1.1.1) is no longer invariant,

$$\mathcal{L}'_0 = \mathcal{L}_0 - \sum_{a=1}^8 (\partial_\mu \theta_a) J_a^\mu , \quad (1.1.6)$$

where

$$J_a^\mu \equiv \sum_f \sum_{\alpha, \beta} \bar{q}_f^\alpha \gamma^\mu \left(\frac{\lambda^a}{2} \right)_{\alpha\beta} q_f^\beta \quad (1.1.7)$$

is the conserved current given by the Noether theorem associated with the global symmetry (1.1.2).

To keep the invariance under local transformations, one has to apply the gauge principle to the $SU(3)_C$ group which consists in adding extra pieces to the Lagrangian, transforming it in such a way that they cancel the additional term in (1.1.6). Then, we must introduce $3^2 - 1$ gauge fields G_μ^a , transforming as

$$G_\mu \equiv \frac{\lambda^a}{2} G_\mu^a \xrightarrow{SU(3)_C} G'_\mu = U G_\mu U^\dagger + \frac{i}{g_s} (\partial_\mu U) U^\dagger, \quad (1.1.8)$$

where g_s corresponds to the strong coupling constant, and define the *covariant derivative* D_μ as

$$D_\mu q_f \equiv (\partial_\mu + i g_s G_\mu) q_f, \quad (1.1.9)$$

which transforms, by construction, as the quark field.

Then, replacing ∂_μ by D_μ in Eq. (1.1.1), we obtain the following Lagrangian

$$\mathcal{L} = \sum_f \bar{q}_f (i \not{D} - m_f) q_f = \sum_f \bar{q}_f (i \not{\partial} - m_f) q_f - g_s J_a^\mu G_\mu^a, \quad (1.1.10)$$

which is invariant under the local transformation given by Eq. (1.1.2). The gauge principle provides a flavour-independent interaction between quark and gauge fields called *gluons*. In order to propagate these new fields, it is necessary to add a kinetic term. The only quantity with dimension four that does not violate the fundamental symmetries and is invariant under a local $SU(3)_C$ transformation, is

$$\mathcal{L}_{\text{kin}} = -\frac{1}{2} \text{Tr} (G^{\mu\nu} G_{\mu\nu}) = -\frac{1}{4} G_a^{\mu\nu} G_{\mu\nu}^a, \quad (1.1.11)$$

where

$$G^{\mu\nu} = -\frac{i}{g_s} [D^\mu, D^\nu] = \partial^\mu G^\nu - \partial^\nu G^\mu + i g_s [G^\mu, G^\nu] \equiv \frac{\lambda^a}{2} G_a^{\mu\nu}, \quad (1.1.12)$$

and transforms under $SU(3)_C$ as

$$G_{\mu\nu} \xrightarrow{SU(3)_C} G'_{\mu\nu} = U G_{\mu\nu} U^\dagger. \quad (1.1.13)$$

Finally, the QCD Lagrangian reads

$$\begin{aligned} \mathcal{L}_{\text{QCD}} = & -\frac{1}{4} (\partial^\mu G_a^\nu - \partial^\nu G_a^\mu) (\partial_\mu G_\nu^a - \partial_\nu G_\mu^a) + \sum_f \bar{q}_f (i \not{\partial} - m_f) q_f - g_s J_a^\mu G_\mu^a \\ & + \frac{g_s}{2} f^{abc} (\partial^\mu G_a^\nu - \partial^\nu G_a^\mu) G_\mu^b G_\nu^c - \frac{g_s^2}{4} f^{abc} f_{ade} G_b^\mu G_c^\nu G_\mu^d G_\nu^e. \end{aligned} \quad (1.1.14)$$

In the first line of Eq. (1.1.14), one finds from left to right the gluon and quark kinetic terms and the quark-gluon interaction, while in the last line, the gluon self-interactions involving vertices with three and four gauge fields as shown in Figure 1.1.

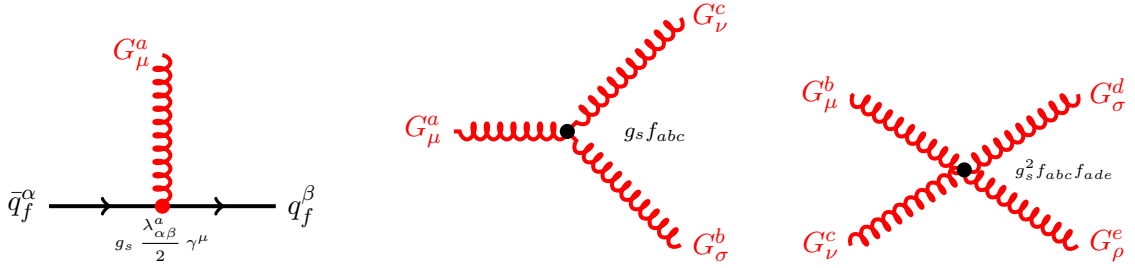


Figure 1.1: Feynman vertices for the strong interaction.

The $SU(3)_C$ symmetry does not allow a mass term for gluons, since $m_G^2 G_a^\mu G_\mu^a$ breaks the gauge invariance. The last two terms in the first line of Eq. (1.1.14) would be formally identical to the Quantum Electrodynamics (QED) Lagrangian with an appropriate redefinition of the gauge field. Unlike QED, QCD has triple and quartic self-interactions between gluon fields. The existence of these terms explain the fundamental features of the strong interaction such as *asymptotic freedom* (strong interactions become weaker at short-distances) and *confinement* (the strong interaction increases at long-distances). Further details can be found in Refs. [10–12].

1.1.2 Electroweak interactions

The Electroweak Standard Model (EWSM) is a $SU(2)_L \otimes U(1)_Y$ gauge theory that describes weak and electromagnetic interactions through the exchange of spin-1 gauge fields, similar to gluons in QCD. In the EWSM, one has a massless *photon* for the electromagnetic interaction and 3 massive *weak bosons*, W^\pm and Z^0 , for the weak interaction [13–15].

The fermionic sector is organized in 3 generations with identical properties. The only differences are their masses and their flavour quantum numbers. The particle content in each generation is

- **First generation:** $\begin{bmatrix} \nu_e \\ e^- \end{bmatrix}_L$, $\begin{bmatrix} u \\ d' \end{bmatrix}_L$, e_R^- , u_R , d'_R
- **Second generation:** $\begin{bmatrix} \nu_\mu \\ \mu^- \end{bmatrix}_L$, $\begin{bmatrix} c \\ s' \end{bmatrix}_L$, μ_R^- , c_R , s'_R
- **Third generation:** $\begin{bmatrix} \nu_\tau \\ \tau^- \end{bmatrix}_L$, $\begin{bmatrix} t \\ b' \end{bmatrix}_L$, τ_R^- , t_R , b'_R

with their corresponding antiparticles. $\mathcal{X}_{R,L} \equiv P_{R,L}\mathcal{X}$ with $P_{R,L} = (1 \pm \gamma_5)/2$ for $\mathcal{X} = q_u, q_d, \nu_l, l^-$. Each generation has 1 (1 lepton field) plus 3 (1 quark field with 3 colours) left-handed fields that transform as $SU(2)_L$ doublets, in addition to 1 (1 lepton field) plus 6 (2 quark field with 3 colours) right-handed fields that transform as $SU(2)_L$ singlets.

For simplicity, let us consider just one generation,

$$Q_1(x) = \begin{bmatrix} q_u \\ q_d \end{bmatrix}_L, \quad Q_2(x) = q_{uR}, \quad Q_3(x) = q_{dR}, \quad (1.1.15)$$

$$L_1(x) = \begin{bmatrix} \nu_l \\ l^- \end{bmatrix}_L, \quad L_2(x) = l_R^-, \quad (1.1.16)$$

with the following representations under the gauge $SU(3)_C \otimes SU(2)_L \otimes U(1)_Y$,

$$Q_1(x) = (3, 2, 1/6), \quad Q_2(x) = (3, 1, 2/3), \quad Q_3(x) = (3, 1, -1/3),$$

$$L_1(x) = (1, 2, -1/2), \quad L_2(x) = (1, 1, -1).$$

The free Lagrangian is given by

$$\mathcal{L}_{\text{free}} \equiv i \sum_{j=1}^3 \bar{Q}_j(x) \not{\partial} Q_j(x) + i \sum_{k=1}^2 \bar{L}_k(x) \not{\partial} L_k(x), \quad (1.1.17)$$

which is invariant under global $SU(2)_L \otimes U(1)_Y$ transformations,

$$\begin{aligned}
Q_1(x) &\xrightarrow{SU(2)_L \otimes U(1)_Y} Q'_1(x) \equiv \exp\{i y_1^q \beta\} U_L Q_1(x) , \\
Q_{2,3}(x) &\xrightarrow{SU(2)_L \otimes U(1)_Y} Q'_{2,3}(x) \equiv \exp\{i y_{2,3}^q \beta\} Q_{2,3}(x) , \\
L_1(x) &\xrightarrow{SU(2)_L \otimes U(1)_Y} L'_1(x) \equiv \exp\{i y_1^l \beta\} U_L L_1(x) , \\
L_2(x) &\xrightarrow{SU(2)_L \otimes U(1)_Y} L'_2(x) \equiv \exp\{i y_2^l \beta\} L_2(x) ,
\end{aligned} \tag{1.1.18}$$

where U_L is the non-Abelian matrix associated to the global $SU(2)_L$ transformation,

$$U_L = \exp\left\{i \sum_{j=1}^3 \frac{\sigma_j}{2} \alpha_j\right\} , \tag{1.1.19}$$

and σ_j are the Pauli matrices and the parameters $y_i^{q,l}$ are the quark and lepton hypercharges which play a similar role as the electric charge Q for $U(1)_Q$ in QED.

In order to have a Lagrangian invariant under local $SU(2)_L \otimes U(1)_Y$ transformation, as in QCD, we have to replace the Dirac derivatives by covariant ones. In $SU(2)_L \otimes U(1)_Y$, we have 4 gauge parameters, $\alpha^i(x)$ and $\beta(x)$, which imply 3 vectorial bosons, $W_\mu^i(x)$, one for each $SU(2)_L$ generator, and another one, $B_\mu(x)$, for $U(1)_Y$. Then, the covariant derivatives are given by

$$\begin{aligned}
D_\mu Q_1(x) &\equiv \left[\partial_\mu + i g \widetilde{W}_\mu(x) + i g' y_1^q B_\mu(x) \right] Q_1(x) , \\
D_\mu Q_{2,3}(x) &\equiv \left[\partial_\mu + i g' y_{2,3}^q B_\mu(x) \right] Q_{2,3}(x) , \\
D_\mu L_1(x) &\equiv \left[\partial_\mu + i g \widetilde{W}_\mu(x) + i g' y_1^l B_\mu(x) \right] L_1(x) , \\
D_\mu L_2(x) &\equiv \left[\partial_\mu + i g' y_2^l B_\mu(x) \right] L_2(x) ,
\end{aligned} \tag{1.1.20}$$

where $\widetilde{W}_\mu(x) \equiv \frac{\sigma_i}{2} W_\mu^i(x)$, while g and g' are the $SU(2)_L$ and $U(1)_Y$ coupling constants which characterize the strength of the electroweak interaction. The gauge fields $B_\mu(x)$

and $\widetilde{W}_\mu(x)$ transform under $SU(2)_L \otimes U(1)_Y$ as

$$\begin{aligned} B_\mu(x) &\xrightarrow{SU(2)_L \otimes U(1)_Y} B'_\mu(x) \equiv B_\mu(x) - \frac{1}{g'} \partial_\mu \beta(x), \\ \widetilde{W}_\mu(x) &\xrightarrow{SU(2)_L \otimes U(1)_Y} \widetilde{W}'_\mu(x) \equiv U_L(x) \widetilde{W}_\mu(x) U_L^\dagger(x) + \frac{i}{g} [\partial_\mu U_L(x)] U_L^\dagger(x), \end{aligned} \quad (1.1.21)$$

which are obtained imposing that $D_\mu Q_i(x)$ and $D_\mu L_i(x)$ transform exactly in the same way as the $Q_i(x)$ and $L_i(x)$ fields, respectively.

Replacing all the fermionic derivatives by their corresponding covariant derivatives, we obtain a Lagrangian invariant under local $SU(2)_L \otimes U(1)_Y$ transformations,

$$\mathcal{L} = i \sum_{j=1}^3 \overline{Q}_j(x) \gamma^\mu D_\mu Q_j(x) + i \sum_{k=1}^2 \overline{L}_k(x) \gamma^\mu D_\mu L_k(x), \quad (1.1.22)$$

with the following kinetic terms

$$\mathcal{L}_{\text{kin}} = -\frac{1}{4} B_{\mu\nu} B^{\mu\nu} - \frac{1}{4} W_{\mu\nu}^i W_i^{\mu\nu}, \quad (1.1.23)$$

where

$$B_{\mu\nu} \equiv \partial_\mu B_\nu - \partial_\nu B_\mu, \quad W_{\mu\nu}^i \equiv \partial_\mu W_\nu^i - \partial_\nu W_\mu^i - g \epsilon^{ijk} W_\mu^j W_\nu^k, \quad (1.1.24)$$

which transform as

$$B_{\mu\nu} \xrightarrow{SU(2)_L \otimes U(1)_Y} B_{\mu\nu}, \quad W_{\mu\nu}^i \xrightarrow{SU(2)_L \otimes U(1)_Y} U_L W_{\mu\nu}^i U_L^\dagger. \quad (1.1.25)$$

Finally, we obtain the EWSM Lagrangian

$$\mathcal{L}_{\text{EWSM}} = -\frac{1}{4} B_{\mu\nu} B^{\mu\nu} - \frac{1}{4} W_{\mu\nu}^i W_i^{\mu\nu} + i \sum_j \left(\overline{Q}_j \not{D} Q_j + \overline{L}_j \not{D} L_j \right), \quad (1.1.26)$$

which can be expanded as

$$\begin{aligned} \mathcal{L}_{\text{EWSM}} &= -\frac{1}{4} (\partial^\mu B_\nu^a - \partial^\nu B_\mu^a) (\partial_\mu B_\nu^a - \partial_\nu B_\mu^a) - \frac{1}{4} (\partial^\mu W_\nu^a - \partial^\nu W_\mu^a) (\partial_\mu W_\nu^a - \partial_\nu W_\mu^a) \\ &\quad + i \sum_{j=1}^3 \overline{Q}_j \not{D} Q_j + i \sum_{k=1}^2 \overline{L}_k \not{D} L_k - g' J_Y^\mu B_\mu - g \sum_{a=1}^3 \widetilde{J}_a^\mu W_\mu^a \\ &\quad + \frac{g}{2} \epsilon^{abc} (\partial^\mu W_\nu^a - \partial^\nu W_\mu^a) W_\mu^b W_\nu^c - \frac{g^2}{4} \epsilon^{abc} \epsilon_{ade} W_b^\mu W_c^\nu W_\mu^d W_\nu^e, \end{aligned} \quad (1.1.27)$$

where

$$\begin{aligned} J_Y^\mu &\equiv \sum_{i=1}^3 y_i^q \bar{Q}_i \gamma^\mu Q_i + \sum_{i=1}^2 y_i^l \bar{L}_i \gamma^\mu L_i , \\ \tilde{J}_a^\mu &\equiv \bar{Q}_1 \gamma^\mu \frac{\sigma^a}{2} Q_1 + \bar{L}_1 \gamma^\mu \frac{\sigma^a}{2} L_1 , \end{aligned} \quad (1.1.28)$$

are the conserved currents. The first line of Eq. (1.1.27) contains the kinetic terms of the bosonic fields B_μ and W_μ^a . The second line contains the free Dirac Lagrangians for quarks and leptons, and the interaction Lagrangians between fermions and gauge bosons. The last line contains the typical interactions of non-Abelian groups, the three and four gauge self-interactions for W_μ^a bosons. As in QCD, the mass terms of gauge bosons break gauge symmetry. Furthermore, it is not allowed to include fermionic mass terms, since they mix left and right field components which follow different transformations properties, so that, these terms explicitly break gauge symmetry. Therefore, the EWSM Lagrangian, given by Eq. (1.1.27), only contains massless fields. In the following subsections, we describe in more detail all different pieces that compose the EWSM Lagrangian.

1.1.2.1 The charged-current sector



Figure 1.2: Feynman vertices for charged-currents interactions.

The EWSM Lagrangian contains interactions between fermion and gauge bosons,

$$\begin{aligned} \mathcal{L}_{\text{EWSM}} &\supset -g' J_Y^\mu B_\mu - g \sum_{a=1}^3 \tilde{J}_a^\mu W_\mu^a \\ &= -g' B_\mu \sum_{i=1}^3 y_i^q \bar{Q}_i \gamma^\mu Q_i - g \bar{Q}_1 \gamma^\mu \tilde{W}_\mu Q_1 - g' B_\mu \sum_{i=1}^2 y_i^l \bar{L}_i \gamma^\mu L_i - g \bar{L}_1 \gamma^\mu \tilde{W}_\mu L_1 . \end{aligned} \quad (1.1.29)$$

The terms with \widetilde{W}_μ fields correspond to the charged-current interactions with a boson field $W_\mu \equiv \frac{1}{\sqrt{2}}(W_\mu^1 + iW_\mu^2)$ and its complex conjugate $W_\mu^\dagger \equiv \frac{1}{\sqrt{2}}(W_\mu^1 - iW_\mu^2)$. The charged-current interactions for quarks and leptons are

$$\mathcal{L}_{\text{CC}} = -\frac{g}{\sqrt{2}} W_\mu^\dagger \left(\bar{q}_u(x) \gamma^\mu P_L q_d(x) + \bar{\nu}_l(x) \gamma^\mu P_L l^-(x) \right) + \text{h.c.} \quad (1.1.30)$$

1.1.2.2 The neutral-current sector



Figure 1.3: Feynman vertices for neutral-current interaction.

The Eq. (1.1.29) also contains interactions between neutral gauge fields W_μ^3 and B_μ which we would like to identify with the Z boson and the photon γ . However, since the photon field A_μ has the same right and left chiral fermionic interactions, the B_μ field can not be the photon field. It would only happen if $y_1^q = y_2^q = y_3^q$, $y_1^l = y_2^l = y_3^l$, $g' y_j^q = e Q_j^q$ and $g' y_j^l = e Q_j^l$ which can not be satisfied simultaneously. We can try with an arbitrary combination between them,

$$\begin{bmatrix} W_\mu^3 \\ B_\mu \end{bmatrix} \equiv \begin{bmatrix} c_\theta & s_\theta \\ -s_\theta & c_\theta \end{bmatrix} \begin{bmatrix} Z_\mu \\ A_\mu \end{bmatrix}, \quad (1.1.31)$$

where $s_\theta \equiv \sin \theta_W$ and $c_\theta \equiv \cos \theta_W$. In terms of Z_μ and A_μ , the neutral-current Lagrangian can be written as

$$\begin{aligned} \mathcal{L}_{\text{NC}} = & -\sum_{j=1}^3 \bar{Q}_j \left\{ \not{A} \left[g \frac{\sigma_3}{2} s_\theta + g' y_j^q c_\theta \right] + \not{Z} \left[g \frac{\sigma_3}{2} c_\theta - g' y_j^q s_\theta \right] \right\} Q_j \\ & -\sum_{j=1}^2 \bar{L}_j \left\{ \not{A} \left[g \frac{\sigma_3}{2} s_\theta + g' y_j^l c_\theta \right] + \not{Z} \left[g \frac{\sigma_3}{2} c_\theta - g' y_j^l s_\theta \right] \right\} L_j, \end{aligned} \quad (1.1.32)$$

where $\not{A} \equiv \gamma_\mu A^\mu$ and $\not{Z} \equiv \gamma_\mu Z^\mu$. Then, in order to obtain the QED Lagrangian, one has to impose

$$\begin{aligned} g \sin \theta_W &= g' \cos \theta_W = e , \\ Y &= Q - T_3 , \end{aligned} \quad (1.1.33)$$

where $T_3 = \sigma_3/2$ is the third component of the weak isospin, while Q is the electric charge. The first equality relates the g and g' couplings with the electromagnetic coupling e , providing the unification of the electroweak interactions. The second equality fixes the fermionic hypercharges in terms of the electric charges and the weak isospin,

$$y_1^q = Q_{qu} - \frac{1}{2} = Q_{qd} + \frac{1}{2} , \quad y_2^q = Q_{qu} , \quad y_3^q = Q_{qd} , \quad (1.1.34)$$

$$y_1^l = Q_{\nu l} - \frac{1}{2} = Q_{l^-} + \frac{1}{2} , \quad y_2^l = Q_{l^-} . \quad (1.1.35)$$

Therefore, the neutral-current Lagrangian can be expressed as

$$\mathcal{L}_{\text{NC}} = \mathcal{L}_{\text{QED}} + \mathcal{L}_{\text{NC}}^Z , \quad (1.1.36)$$

where \mathcal{L}_{QED} and $\mathcal{L}_{\text{NC}}^Z$ are the QED and Z neutral-current Lagrangians respectively,

$$\mathcal{L}_{\text{QED}} = -e \sum_j \left(\bar{Q}_j \not{A} Q_j^q + \bar{L}_j \not{A} Q_j^l \right) , \quad (1.1.37)$$

$$\mathcal{L}_{\text{NC}}^Z = -\frac{e}{2 \sin \theta_W \cos \theta_W} \sum_f \bar{f} \not{Z} (v_f - a_f \gamma_5) f , \quad (1.1.38)$$

with $a_f \equiv T_3^f$, $v_f \equiv T_3^f (1 - 4 |\mathcal{Q}_f| \sin^2 \theta_W)$ and f is the fermion field.

1.1.2.3 Self-interactions of the weak gauge bosons

The kinetic Lagrangian, given by Eq. (1.1.23), contains triple and quartic self-interactions, see Figure 1.4,

$$\begin{aligned} \mathcal{L}_3 = & + i e \cot \theta_W \left\{ w^{\mu\nu} W_\mu^\dagger Z_\nu - w^{\mu\nu\dagger} W_\mu Z_\nu + W_\mu W_\nu^\dagger Z^{\mu\nu} \right\} \\ & + i e \left\{ w^{\mu\nu} W_\mu^\dagger A_\nu - w^{\mu\nu\dagger} W_\mu A_\nu + W_\mu W_\nu^\dagger F^{\mu\nu} \right\} , \end{aligned} \quad (1.1.39)$$

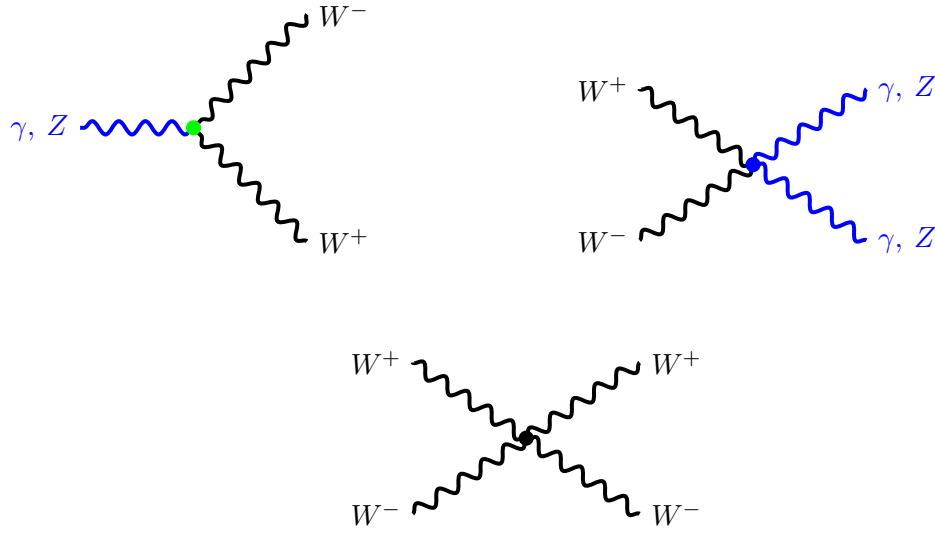


Figure 1.4: Self interactions vertices of the weak gauge bosons.

$$\begin{aligned}
\mathcal{L}_4 = & - \frac{e^2}{2 \sin^2 \theta_W} \left\{ (W_\mu^\dagger W^\mu)^2 - W_\mu^\dagger W^{\mu\dagger} W_\nu W^\nu \right\} \\
& - e^2 \cot^2 \theta_W \left\{ W_\mu^\dagger W^\mu Z_\nu Z^\nu - W_\mu^\dagger Z^\mu W_\nu Z^\nu \right\} \\
& - e^2 \cot \theta_W \left\{ 2 W_\mu^\dagger W^\mu Z_\nu A^\nu - W_\mu^\dagger Z^\mu W_\nu A^\nu - W_\mu^\dagger A^\mu W_\nu Z^\nu \right\} \\
& - e^2 \left\{ W_\mu^\dagger W^\mu A_\nu A^\nu - W_\mu^\dagger A^\mu W_\nu A^\nu \right\}, \tag{1.1.40}
\end{aligned}$$

where $w_{\mu\nu} = \partial_\mu W_\nu - \partial_\nu W_\mu$, $w_{\mu\nu}^\dagger = \partial_\mu W_\nu^\dagger - \partial_\nu W_\mu^\dagger$ and $Z_{\mu\nu} = \partial_\mu Z_\nu - \partial_\nu Z_\mu$.

1.2 Spontaneous Symmetry Breaking

Promoting the $SU(2)_L \otimes U(1)_Y$ group as a local gauge symmetry, we have determined all the electroweak fermion and boson interactions. However, in contrast to the gauge bosons of QED and QCD, the electroweak gauge bosons are massive. Since, the gauge symmetry does not allow mass terms for the gauge bosons, this requires a new ingredient in order to solve this problem, *spontaneous symmetry breaking*. The Spontaneous Symmetry

Breaking (SSB) appears when a system defined by a Lagrangian symmetric under a certain transformation has a vacuum state that is not symmetric. In this section, we show how the SSB leads to the appearance of scalar fields with zero mass called *Goldstone particles* and then we give mass to the W^\pm and Z^0 bosons of the SM through the *Higgs mechanism*.

1.2.1 Global symmetry: Goldstone theorem

Let us consider a complex scalar field $\phi(x)$ with the following Lagrangian

$$\mathcal{L} = (\partial_\mu \phi)^\dagger (\partial^\mu \phi) - V(\phi), \quad V(\phi) \equiv \mu^2 (\phi^\dagger \phi) + h (\phi^\dagger \phi)^2, \quad (1.2.41)$$

which is invariant under global phase transformations,

$$\phi \longrightarrow \phi' \equiv \exp\{i\theta\} \phi, \quad \phi^\dagger \longrightarrow \phi'^\dagger \equiv \phi^\dagger \exp\{-i\theta\}, \quad (1.2.42)$$

where θ is an arbitrary constant.

The potential is bounded from below, then $\lambda > 0$. For μ^2 , we have two possibilities depending on its sign, see Figure 1.5:

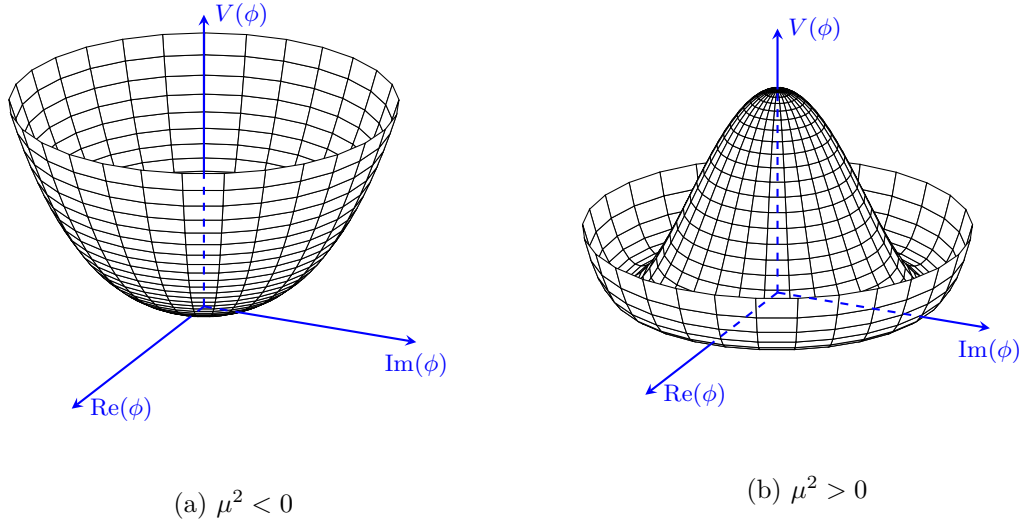
1. $\mu^2 > 0$: The potential $V(\phi)$ has a unique minimum, $\phi_0(x) \equiv |\langle 0|\phi(x)|0\rangle| = 0$. The term involving μ^2 is a mass term, therefore $\phi(x)$ has mass μ .
2. $\mu^2 < 0$: The minimum corresponds to the configurations of $\phi(x)$ that satisfy

$$\phi_0(x) \equiv \frac{v}{\sqrt{2}} \exp\{i\theta\}, \quad v = \sqrt{-\frac{\mu^2}{h}}. \quad (1.2.43)$$

Due to the global U(1) invariance, there are an infinite number of minimum energy states that are connected through Eq. (1.2.43).

For $\mu^2 < 0$, we can build a perturbation theory through the expansion of the scalar field around one of these minima given by Eq. (1.2.43). For that purpose, we introduce the following parametrization

$$\phi(x) = \frac{1}{\sqrt{2}} \left(v + \varphi_1(x) \right) \exp \left\{ i \left(\theta + \frac{\varphi_2(x)}{v} \right) \right\}, \quad (1.2.44)$$

Figure 1.5: Scalar potential $V(\phi)$.

where $\varphi_1(x)$ and $\varphi_2(x)$ are real fields that describe small perturbations of the modulus and the phase of $\phi(x)$ from the chosen minimum. The choice of one of these minima, via the parameter θ , leads to SSB. Inserting the parametrization given by Eq. (1.2.44) into Eq.(1.2.41),

$$\begin{aligned} \mathcal{L} = & \frac{1}{2} (\partial_\mu \varphi_1)(\partial^\mu \varphi_1) + \frac{1}{2} \left(1 + \frac{\varphi_1}{v}\right)^2 (\partial_\mu \varphi_2)(\partial^\mu \varphi_2) \\ & - \frac{\mu^2 v^2}{2} \left(1 + \frac{\varphi_1}{v}\right)^2 - \frac{h v^2}{2} \left(1 + \frac{\varphi_1}{v}\right)^4, \end{aligned} \quad (1.2.45)$$

where we find the following aspects:

- $\varphi_1(x)$ is a scalar field with mass μ which describes the radial oscillations of ϕ around $v/\sqrt{2}$. The mass results from non-vanishing radial curvature of $V(\phi)$.
- $\varphi_2(x)$ is a massless scalar field called *Goldstone boson*. It is massless due to the vanishing curvature along the potential minima, $\partial^2 V / \partial \varphi_2^2 = 0$.
- $\varphi_1(x)$ interacts with $\varphi_2(x)$ only through derivatives of $\varphi_2(x)$. In the limit of zero momenta, the Goldstone bosons do not interact with $\varphi_1(x)$.

Although this conclusions correspond to a particular model, it is an example of a more general result, known as *Goldstone theorem* [16, 17]:

If a Lagrangian is invariant under a continuous symmetry group G , but the vacuum is only invariant under a subgroup $H \subset G$, then there are as many massless particles with zero spin (Goldstone bosons) as generators of G that are not of H , in other words, the number of symmetries that have been broken.

In this quite general example, there is only one Goldstone boson because when we have chosen the minimum, we have broken the only symmetry of the vacuum.

1.2.2 Local gauge symmetry: Higgs mechanism

We have studied how a SSB of a global symmetry produces a massless particle. This seems to be unuseful for giving mass to the gauge bosons. However, when we consider a SSB of a local gauge symmetry, the problem is completely solved. First, we have to build the scalar Lagrangian which requires the choice of the scalar field representation. This choice demands that the field with a nonzero vacuum value is electrically neutral, then the photon remains massless, while it have to carry nonzero values of T_3 and Y . The simplest choice is an $SU(2)_L$ doublet of complex scalar fields [18–20]

$$\Phi(x) = \begin{bmatrix} \phi^{(+)}(x) \\ \phi^{(0)}(x) \end{bmatrix}. \quad (1.2.46)$$

We can write the scalar Lagrangian invariant under $SU(2)_L \otimes U(1)_Y$ as

$$\begin{aligned} \mathcal{L}_{\text{scalar}} &= (D_\mu \Phi)^\dagger (D^\mu \Phi) - \mu^2 \Phi^\dagger \Phi - h (\Phi^\dagger \Phi)^2, \\ D_\mu \Phi &= \left[\partial_\mu + i g \widetilde{W}_\mu + i g' Y_\Phi B_\mu(x) \right] \Phi, \end{aligned} \quad (1.2.47)$$

where $Y_\Phi = Q_\Phi - T_3 = \frac{1}{2}$. The value of the scalar hypercharge Y_Φ is set to have the correct coupling between $\Phi(x)$ and $A^\mu(x)$. The photon is not coupled to $\phi^{(0)}$, this is crucial to have a massless photon.

For $h > 0$ and $\mu^2 < 0$, the situation is very similar to the Goldstone model, see Figure 1.5. There are an infinite number of minima, satisfying

$$|\langle 0|\phi^{(0)}|0\rangle| = \frac{v}{\sqrt{2}}, \quad v = \sqrt{-\frac{\mu^2}{h}}. \quad (1.2.48)$$

All of them connected by an $SU(2)_L \otimes U(1)_Y$ transformation (4 generators). When we choose one of these minima, the symmetry is spontaneously broken leading a remaining $U(1)_Q$ symmetry (1 generator), which gives rise to the appearance of $4 - 1 = 3$ massless scalar fields (Goldstone theorem).

As in the global symmetry case, we parametrize the scalar doublet in terms of the radial $H(x)$ and the phase $\theta^i(x)$ excitations around the physical vacuum,

$$\Phi(x) = \exp\left\{i \frac{\sigma_i}{2} \theta^i(x)\right\} \frac{1}{\sqrt{2}} \begin{bmatrix} 0 \\ v + H(x) \end{bmatrix}. \quad (1.2.49)$$

Using the gauge invariance of the Lagrangian, we can transform $\Phi(x)$ into another field in which the three $\theta^i(x)$ fields (Goldstone bosons) do not appear and so preserving the Higgs boson as the only physical scalar field $H(x)$,

$$\Phi(x) = \frac{1}{\sqrt{2}} \begin{bmatrix} 0 \\ v + H(x) \end{bmatrix}. \quad (1.2.50)$$

These three degrees of freedom, that are apparently lost, become the longitudinal polarizations of the gauge bosons W^\pm and Z^0 . After the SSB, they become massive fields as can be seen inserting Eq. (1.2.50) into Eq. (1.2.47),

$$(D_\mu \Phi)^\dagger (D^\mu \Phi) = (v + H)^2 \left\{ \frac{g^2}{4} W_\mu^\dagger W^\mu + \frac{g^2}{8 \cos^2 \theta_W} Z_\mu Z^\mu \right\} + \dots,$$

which contains the mass terms for the weak bosons W^\pm and Z^0 ,

$$M_Z \cos \theta_W = M_W = \frac{1}{2} v g, \quad (1.2.51)$$

and the photon stays massless. Then, the W^\pm and Z^0 bosons acquire masses through a SSB of a local gauge symmetry with the following pattern:

$$SU(2)_L \otimes U(1)_Y \xrightarrow{\text{SSB}} U(1)_Q. \quad (1.2.52)$$

1.2.3 The Higgs boson and its interactions

The scalar Lagrangian, given by Eq. (1.2.47), has introduced a new scalar particle: the Higgs boson. In terms of physical fields (unitary gauge), it becomes

$$\mathcal{L}_{\text{scalar}} = \frac{1}{4} h v^4 + \mathcal{L}_H + \mathcal{L}_{HG^2} , \quad (1.2.53)$$

where

$$\mathcal{L}_H = \frac{1}{2} \partial_\mu H \partial^\mu H - \frac{1}{2} M_H^2 H^2 - \frac{M_H^2}{2v} H^3 - \frac{M_H^2}{8v^2} H^4 , \quad (1.2.54)$$

$$\mathcal{L}_{HG^2} = \left(M_W^2 W_\mu^\dagger W^\mu + \frac{1}{2} M_Z^2 Z_\mu Z^\mu \right) \left\{ 1 + \frac{2}{v} H + \frac{H^2}{v^2} \right\} , \quad (1.2.55)$$

and the Higgs mass is given by $M_H = \sqrt{-2\mu^2} = \sqrt{2} \bar{h} v$. In Figure 1.6, we show the Higgs interactions with gauge bosons and fermions.

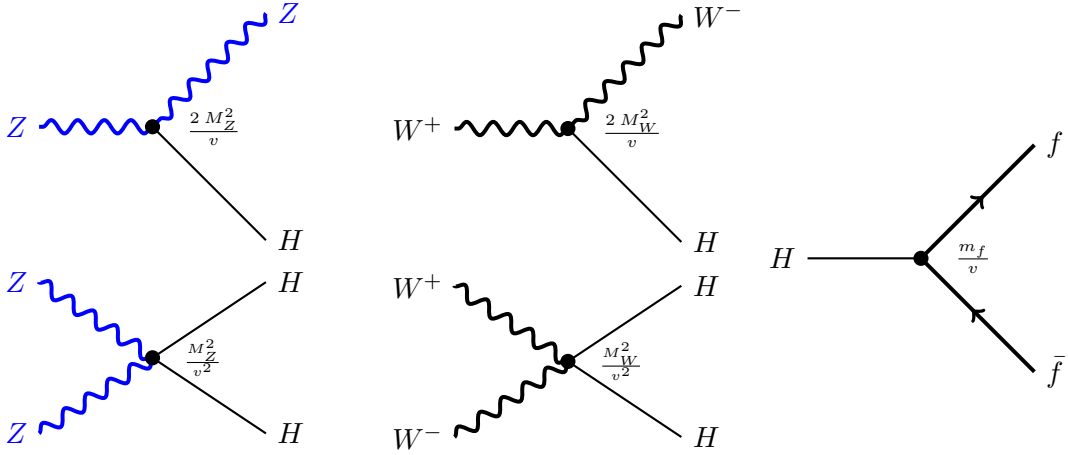


Figure 1.6: Higgs interactions with gauge bosons and fermions.

1.2.4 The Yukawa Lagrangian

In the previous section, we have been able to produce all weak boson masses via the Higgs mechanism. In this section, we show that the $SU(2)_L$ scalar doublet allows us to

add new terms to the Lagrangian which are invariant under the gauge symmetry. These interactions will be responsible of generating the mass for all fermions in the SM.

Let us consider n generations of fermions, denoted by ν'_j, l'_j, u'_j, d'_j , where the members of each generation j ($j = 1, \dots, n$) have the usual $SU(2)_L \otimes U(1)_Y$ transformations. Due to the insertion of the scalar doublet, a large variety of fermion-scalar doublet couplings are allowed by the gauge symmetry. The most general interaction is the *Yukawa Lagrangian*,

$$\mathcal{L}_Y = - \sum_{j,k} \left\{ \bar{Q}'_{1j} Y_{jk}^{(d)} \Phi Q'_{3k} + \bar{Q}'_{1j} Y_{jk}^{(u)} \tilde{\Phi} Q'_{2k} + \bar{L}'_{1j} Y_{jk}^{(l)} \Phi L'_{2k} \right\} + \text{h.c.}, \quad (1.2.56)$$

where $Y_{jk}^{(d)}$, $Y_{jk}^{(u)}$ and $Y_{jk}^{(l)}$ are the three Yukawa couplings, arbitrary $n \times n$ complex matrices, and $\tilde{\Phi} \equiv i\sigma_2 \Phi^*$ is the conjugate representation of the scalar doublet Φ . In the unitary gauge, the Yukawa Lagrangian can be written as

$$\mathcal{L}_Y = - \left(1 + \frac{H}{v} \right) \left\{ \bar{d}'_L \mathcal{M}'_d d'_R + \bar{u}'_L \mathcal{M}'_u u'_R + \bar{l}'_L \mathcal{M}'_l l'_R \right\} + \text{h.c.}, \quad (1.2.57)$$

where d' , u' and l' are n -dimensional vectors in flavour space and

$$(\mathcal{M}'_d)_{ij} \equiv Y_{ij}^{(d)} \frac{v}{\sqrt{2}}, \quad (\mathcal{M}'_u)_{ij} \equiv Y_{ij}^{(u)} \frac{v}{\sqrt{2}}, \quad (\mathcal{M}'_l)_{ij} \equiv Y_{ij}^{(l)} \frac{v}{\sqrt{2}}, \quad (1.2.58)$$

are the mass matrices. In general, the \mathcal{M}'_d matrix can be decomposed as

$$\mathcal{M}'_d = H_d U_d = S_d^\dagger \mathcal{M}_d S_d U_d, \quad (1.2.59)$$

where $H_d \equiv \sqrt{\mathcal{M}'_d \mathcal{M}'_d{}^\dagger}$ is a hermitian positive definite matrix while U_d is a unitary matrix. Furthermore, H_d can be diagonalized through another unitary matrix S_d . Therefore, the final result is a diagonal, hermitian and positive definite matrix \mathcal{M}_d . For \mathcal{M}'_u and \mathcal{M}'_l , we can do the same:

$$\begin{aligned} \mathcal{M}_d &= \text{diag}(m_d, m_s, m_b, \dots), \\ \mathcal{M}_u &= \text{diag}(m_u, m_c, m_t, \dots), \\ \mathcal{M}_l &= \text{diag}(m_e, m_\mu, m_\tau, \dots), \end{aligned} \quad (1.2.60)$$

and finally, the Yukawa Lagrangian becomes

$$\mathcal{L}_Y = - \left(1 + \frac{H}{v} \right) \left\{ \bar{d} \mathcal{M}_d d + \bar{u} \mathcal{M}_u u + \bar{l} \mathcal{M}_l l \right\}, \quad (1.2.61)$$

where we have defined the mass eigenstates as

$$\begin{aligned} d_L &\equiv S_d d'_L, & u_L &\equiv S_u u'_L, & l_L &\equiv S_l l'_L, \\ d_R &\equiv S_d U_d d'_R, & u_R &\equiv S_u U_u u'_R, & l_R &\equiv S_l U_l l'_R. \end{aligned} \quad (1.2.62)$$

The diagonalization of the Yukawa Lagrangian has strong physical implications on the previous Lagrangians, since we have to put them in terms of the mass eigenstates. These implications are the foundations of flavour physics in the SM,

- *Neutral-currents do not mix flavour in the SM*, this is known as the Glashow-Iliopoulos-Maiani mechanism [21]. The neutral-current Lagrangian, given by Eq. (1.1.36), does not change when it is expressed in terms of the mass eigenstates,

$$\bar{f}'_{L,R} f'_{L,R} = \bar{f}_{L,R} f_{L,R}. \quad (1.2.63)$$

- *Charged-currents are the only interactions that mix flavour in the SM*. The charged-current Lagrangian, given by Eq. (1.1.30), mixes both \bar{u} fermion states with d and \bar{v}_l fermion states with l . After diagonalizing the mass matrices,

$$\bar{u}'_L d'_L = \bar{u}_L S_u S_d^\dagger d_L \equiv \bar{u}_L V d_L. \quad (1.2.64)$$

In general, $S_u \neq S_d$, then when we express the weak eigenstates in terms of the mass eigenstates, it appears the product $S_u S_d^\dagger$ which is an $n \times n$ unitary matrix denoted by V . Therefore, the charged-current Lagrangian becomes

$$\mathcal{L}_{CC} = -\frac{g}{\sqrt{2}} W_\mu^\dagger \left[\sum_{ij} \bar{u}_i \gamma^\mu P_L V_{ij} d_j + \sum_l \bar{v}_l \gamma^\mu P_L l \right] + \text{h.c.} \quad (1.2.65)$$

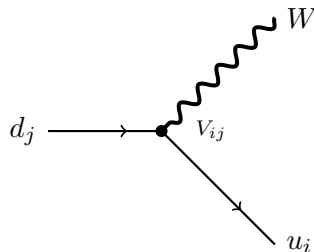


Figure 1.7: Feynman vertex for flavour-changing interactions.

- If a right-handed neutrino ν_R is included in the SM, we would have additional terms in the Yukawa Lagrangian that would lead to a mass piece,

$$(\mathcal{M}'_{\nu})_{ij} \equiv Y_{ij}^{(\nu)} \frac{v}{\sqrt{2}} . \quad (1.2.66)$$

This would accommodate massive neutrinos in addition of Lepton Flavour Violation (LFV). This violation would be parametrized by a mixing matrix that would be analogous to the CKM matrix of the quark sector. Another way to implement the neutrino masses in the SM is through the addition of a right-handed Majorana neutrino mass term [22]. In the last case, the neutrino would be its own antiparticle.

1.3 The CKM matrix

The quark mixing matrix V is an $n \times n$ unitary matrix, characterized by n^2 real parameters: $n(n-1)/2$ modulus and $n(n+1)/2$ phases. Since the SM Lagrangian (except the charged-current Lagrangian) is invariant under phase transformations of the quark fields, $u_i \rightarrow e^{i\phi_i} u_i$ and $d_j \rightarrow e^{i\theta_j} d_j$, some of these parameters are redundant. The $V_{ij} \rightarrow V_{ij} e^{i(\theta_j - \phi_i)}$ transformation allows us to eliminate $2n-1$ phases which reduces the parameters to $n(n-1)/2$ modulus (mixing angles) and $(n-1)(n-2)/2$ complex phases (CP violating phases).

For $n=2$ generations, the CP violation phenomena can not be explained because there are no complex phases. For $n=3$, the quark mixing matrix is called Cabibbo-Kobayashi-Maskawa (CKM) matrix [23, 24] which has 3 mixing angles and 1 complex phase. In

the literature, the CKM matrix can be found in different equivalent parameterizations. One of the most popular is the standard CKM parameterization, introduced by Chau and Keung [25],

$$\begin{aligned}
V &= \begin{pmatrix} 1 & 0 & 0 \\ 0 & c_{23} & s_{23} \\ 0 & -s_{23} & c_{23} \end{pmatrix} \begin{pmatrix} c_{13} & 0 & s_{13} e^{-i\delta_{13}} \\ 0 & 1 & 0 \\ -s_{13} e^{i\delta_{13}} & 0 & c_{13} \end{pmatrix} \begin{pmatrix} c_{12} & s_{12} & 0 \\ -s_{12} & c_{12} & 0 \\ 0 & 0 & 1 \end{pmatrix} \\
&= \begin{pmatrix} c_{12} c_{13} & c_{13} s_{12} & s_{13} e^{-i\delta_{13}} \\ -c_{23} s_{12} - c_{12} s_{13} s_{23} e^{i\delta_{13}} & c_{12} c_{23} - s_{12} s_{13} s_{23} e^{i\delta_{13}} & c_{13} s_{23} \\ s_{12} s_{23} - c_{12} c_{23} s_{13} e^{i\delta_{13}} & -c_{12} s_{23} - c_{23} s_{12} s_{13} e^{i\delta_{13}} & c_{13} c_{23} \end{pmatrix}, \quad (1.3.67)
\end{aligned}$$

where $c_{ij} \equiv \cos \theta_{ij}$ and $s_{ij} \equiv \sin \theta_{ij}$, i and j are the generation labels ($i, j = 1, 2, 3$). The θ_{ij} angles are defined in the $[0, \frac{\pi}{2}]$ range through a proper redefinition of the quark phases, so $c_{ij} \geq 0$, $s_{ij} \geq 0$ and $0 \leq \delta_{13} \leq 2\pi$ and then δ_{13} is the only source that generates CP violation in the SM. In fact, this was the reason for advocating [24] the existence of a third family before the discovery of the bottom quark and the tau lepton, since with only two families, the SM could not explain the CP violation observed in the kaon system.

Experimentally it is known that $s_{13} \ll s_{23} \ll s_{12} \ll 1$. A convenient parameterization is the Wolfenstein expansion with three mixing parameters (λ, A, ρ) and one source of CP violation η . In this parametrization, λ plays the role of the expansion parameter. Defining $s_{12} \equiv \lambda = |V_{us}|/\sqrt{|V_{ud}|^2 + |V_{us}|^2}$, $s_{23} \equiv A \lambda^2 = \lambda |V_{cb}|/|V_{us}|$ and $s_{13} e^{i\delta_{13}} \equiv A \lambda^3 (\rho + i\eta) = V_{ub}^*$ [26–28], we can explicitly show the hierarchy in the size of mixing angles through orders of λ ,

$$V = \begin{pmatrix} 1 - \frac{1}{2} \lambda^2 & \lambda & A \lambda^3 (\rho - i \eta) \\ -\lambda & 1 - \frac{1}{2} \lambda^2 & A \lambda^2 \\ A \lambda^3 (1 - \rho - i \eta) & -A \lambda^2 & 1 \end{pmatrix} + \mathcal{O}(\lambda^4). \quad (1.3.68)$$

where

$$A \approx \frac{|V_{cb}|}{\lambda^2}, \tag{1.3.69}$$

$$\sqrt{\rho^2 + \eta^2} \approx \left| \frac{V_{ub}}{\lambda V_{cb}} \right|. \tag{1.3.70}$$

Then, diagonal transitions (V_{ud}, V_{cs}, V_{tb}) are $\mathcal{O}(1)$, transitions between the first and the second generation (V_{us}, V_{cd}) are $\mathcal{O}(\lambda)$, transitions between the second and the third generation (V_{cb}, V_{ts}) are $\mathcal{O}(\lambda^2)$ and transitions between the first and the third generation (V_{ub}, V_{td}) are $\mathcal{O}(\lambda^3)$.

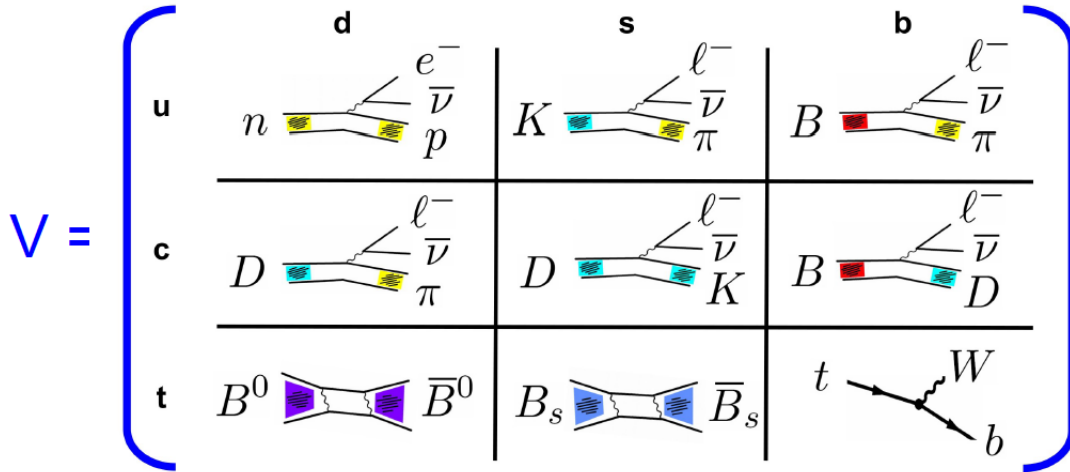


Figure 1.8: Principal processes used to determine the CKM matrix elements [29].

1.3.1 Unitarity of the CKM matrix

The unitarity of the CKM matrix allows us to test the consistency of the SM, then it is important to determine the matrix elements with high accuracy. The accurate determination of these matrix elements supposes a challenge because it involves the study of hadronic decays that introduce large theoretical uncertainties. The Figure 1.8 shows which processes are used to determine the CKM matrix elements. An apparent violation of the

unitarity of the CKM matrix could indicate signs of new physics beyond the SM. For instance, this could lead to a fourth generation or exotic heavy quarks, so the submatrix 3×3 would cease to be unitary by itself. Alternatively, this could involve new interactions such as supersymmetry (SUSY), leptoquarks, or a heavy W' boson (coupled to right-handed currents) or a gauge Z' boson that have not been included in the analysis and therefore would lead to an incorrect determination of some elements of the CKM matrix.

The unitarity of the CKM matrix imposes that

$$V^\dagger V = V V^\dagger = I, \quad (1.3.71)$$

in matrix form

$$\sum_i V_{ij} V_{il}^* = \delta_{jl}, \quad \sum_j V_{ij} V_{kj}^* = \delta_{ik}. \quad (1.3.72)$$

This fixes the rows and columns normalization,

$$\begin{aligned} |V_{ud}|^2 + |V_{us}|^2 + |V_{ub}|^2 &= 1, & |V_{ud}|^2 + |V_{cd}|^2 + |V_{td}|^2 &= 1, \\ |V_{cd}|^2 + |V_{cs}|^2 + |V_{cb}|^2 &= 1, & |V_{us}|^2 + |V_{cs}|^2 + |V_{ts}|^2 &= 1, \\ |V_{td}|^2 + |V_{ts}|^2 + |V_{tb}|^2 &= 1, & |V_{ub}|^2 + |V_{cb}|^2 + |V_{tb}|^2 &= 1, \end{aligned} \quad (1.3.73)$$

and six unitarity relations,

$$\begin{aligned} V_{ud} V_{us}^* + V_{cd} V_{cs}^* + V_{td} V_{ts}^* &= 0, & V_{ud} V_{cd}^* + V_{us} V_{cs}^* + V_{ub} V_{cb}^* &= 0, \\ V_{ud} V_{ub}^* + V_{cd} V_{cb}^* + V_{td} V_{tb}^* &= 0, & V_{ud} V_{td}^* + V_{us} V_{ts}^* + V_{ub} V_{tb}^* &= 0, \\ V_{us} V_{ub}^* + V_{cs} V_{cb}^* + V_{ts} V_{tb}^* &= 0, & V_{cd} V_{td}^* + V_{cs} V_{ts}^* + V_{cb} V_{tb}^* &= 0. \end{aligned} \quad (1.3.74)$$

Plotting the unitarity relations as a sum of three complex numbers whose sum is zero, they form a triangle, see Figure 1.9. The area of these triangles is $\mathcal{J}/2$, where \mathcal{J} is the Jarlskog invariant. In the SM any CP violation is proportional to this invariant quantity. The Jarlskog invariant is given by [30]

$$\text{Im} \left[V_{ij} V_{kl} V_{il}^* V_{kj}^* \right] = \mathcal{J} \sum_{m,n=1}^3 \epsilon_{ikm} \epsilon_{jln}, \quad (1.3.75)$$

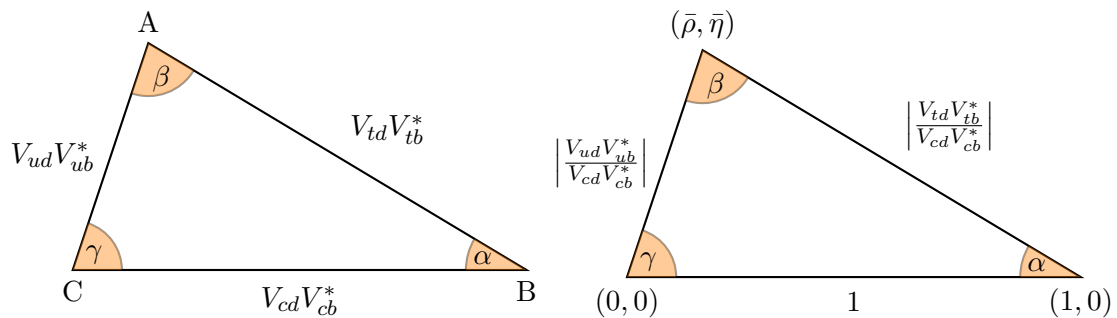


Figure 1.9: Unitarity triangle of the CKM matrix.

being

$$\mathcal{J} = c_{12} c_{23} c_{13}^2 s_{12} s_{23} s_{13} \sin \delta_{13} = A^2 \lambda^6 \eta \left(1 - \frac{\lambda^2}{2}\right) + \mathcal{O}(\lambda^{10}). \quad (1.3.76)$$

Taking into account the Wolfenstein parameterization, we observe how the identities (1.3.74) satisfy the following relations between the triangle sides: $\lambda : \lambda : \lambda^5$ for the first equation and $\lambda^4 : \lambda^2 : \lambda^2$ for the third equation, showing that there is always one side that is suppressed. In the second equation, we observe that all triangle sides are $\mathcal{O}(\lambda^3)$. Dividing each side in the left-hand-side equation by $V_{cb}^* V_{cd}$, we obtain a triangle, see Figure 1.9, with vertices in $(0, 0)$, $(1, 0)$ and $(\bar{\rho}, \bar{\eta}) \approx (1 - \lambda^2/2)(\rho, \eta)$. Many experimental measurements in flavour physics can be shown in the plane $(\bar{\rho}, \bar{\eta})$ giving important determinations and constraints for the CKM matrix elements. Some of these measurements come from decay amplitudes that depend on the CP violation angles α , β and γ ,

$$\alpha \equiv \arg \left[-\frac{V_{td}V_{tb}^*}{V_{ud}V_{ub}^*} \right], \quad \beta \equiv \arg \left[-\frac{V_{cd}V_{cb}^*}{V_{td}V_{tb}^*} \right], \quad \gamma \equiv \arg \left[-\frac{V_{ud}V_{ub}^*}{V_{cd}V_{cb}^*} \right]. \quad (1.3.77)$$

The current experimental constraints are shown in Figure 1.10. One of the triangle sides has been calculated using Eq. (1.3.70) through $|V_{ub}/V_{cb}|$ (dark green region). The other side can be obtained using the $B_d^0 - \bar{B}_d^0$ mixing (yellow region), $\Delta M_d = 0.5064 \pm 0.0019 \text{ ps}^{-1}$ [31, 32]. Additional information has been obtained from the $B_s^0 - \bar{B}_s^0$ mixing, $\Delta M_s = 17.757 \pm 0.021 \text{ ps}^{-1}$ [31, 32] and from the experimental fraction $\Delta M_d/\Delta M_s$ (orange region). In addition, constraints on the η parameter are determined through $K^0 \rightarrow \pi\pi$ decay with the measured value of $|\varepsilon_K| = (2.228 \pm 0.011) \cdot 10^{-3}$ [31] which determines the

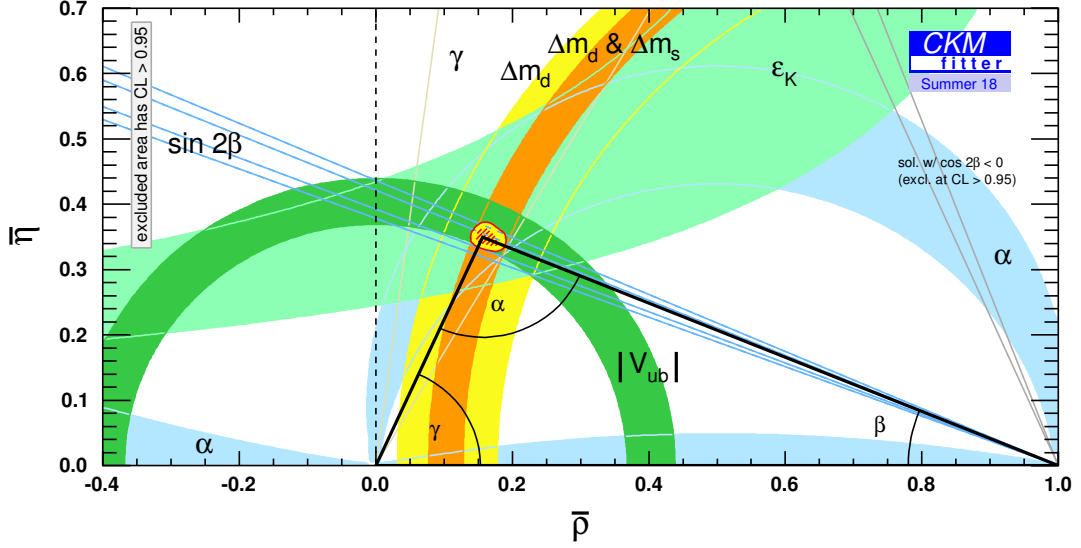


Figure 1.10: Experimental constraints on the SM unitarity triangle [28].

light green parabolic region. The B^0 decays into CP self-conjugate final states provide independent ways to determine the angles of the unitarity triangle. One of the most important decays is $B_d^0 \rightarrow J/\psi K_S$, which gives us a very good measure of the angle β , $\sin(2\beta) = 0.691 \pm 0.017$ [32]. The determinations of the other two angles α and γ , have already been obtained, and included in the global fit. The different sets of data fit very well and provide a very accurate determination of the vertices of the unitarity triangle.

1.4 CP violation in Neutral Meson Systems

In this section, we introduce a general formalism to study CP violation phenomena in the mixing and the decay of a generic neutral meson M^0 being $M^0 \equiv K^0, D^0, B^0, B_s^0$.

1.4.1 Neutral Meson Mixing

1.4.1.1 Formalism

Let us consider a superposition of two meson states, $|M^0\rangle$ and $|\bar{M}^0\rangle$, which are eigenstates of the strong and electromagnetic interactions with common mass m_0 but different flavour content,

$$|\psi(t)\rangle = a(t) |M^0\rangle + b(t) |\bar{M}^0\rangle \equiv \begin{bmatrix} a(t) \\ b(t) \end{bmatrix}, \quad (1.4.78)$$

where $a(t)$ and $b(t)$ are the time-dependent coefficients for the M^0 and \bar{M}^0 states, respectively. In general, M^0 and \bar{M}^0 mix together through weak interactions and they can also decay into other states $|n\rangle$. We simplify the problem by considering only two states M^0 and \bar{M}^0 . Therefore, the time evolution of these coefficients is valid for times which are much larger than the typical strong interaction scale.

The time evolution of $|\psi(t)\rangle$ is governed by an effective Hamiltonian which is a sum of the strong, electromagnetic and weak Hamiltonians,

$$\mathcal{H} = \mathcal{H}_s + \mathcal{H}_{\text{em}} + \mathcal{H}_w, \quad (1.4.79)$$

which obeys the non-relativistic Schrödinger equation,

$$i \frac{\partial}{\partial t} |\psi(t)\rangle = \mathcal{H} |\psi(t)\rangle. \quad (1.4.80)$$

Splitting into a Hermitian and anti-Hermitian parts, the 2×2 complex matrix \mathcal{H} can be written in the meson rest frame as

$$\mathcal{H} = \mathcal{M} - \frac{i}{2} \Gamma, \quad (1.4.81)$$

where both \mathcal{M} and Γ are Hermitian,

$$\mathcal{M} = \frac{1}{2} (\mathcal{H} + \mathcal{H}^\dagger) = \mathcal{M}^\dagger, \quad \Gamma = i (\mathcal{H} - \mathcal{H}^\dagger) = \Gamma^\dagger. \quad (1.4.82)$$

Since \mathcal{M} and Γ are Hermitian, their diagonal elements are real, $M_{21} = M_{12}^*$ and $\Gamma_{21} = \Gamma_{12}^*$. The CPT invariance requires $M_{11} = M_{22}$ and $\Gamma_{11} = \Gamma_{22}$. Notice that \mathcal{H} is not Hermitian,

otherwise the meson states would just mix and not decay into other states. Furthermore, these non-Hermiticity is also reflected in the probability to observe either M^0 or \bar{M}^0 , since it is not conserved, it goes down with time

$$\frac{\partial}{\partial t} \langle \psi(t) | \psi(t) \rangle = -\langle \psi(t) | \Gamma | \psi(t) \rangle \leq 0. \quad (1.4.83)$$

In general, \mathcal{H} can be described through three physical quantities: two modulus ($|M_{12}|$ and $|\Gamma_{12}|$) and one CP phase ϕ

$$\phi = \arg\left(-\frac{M_{12}}{\Gamma_{12}}\right), \quad (1.4.84)$$

which is the relative phase difference between the off-shell (dispersive) and on-shell (absorptive) contributions. So, the mass and width differences are

$$\Delta M \equiv M_+ - M_- = 2|M_{12}|, \quad \Delta \Gamma \equiv \Gamma_+ - \Gamma_- = 2|\Gamma_{12}| \cos \phi, \quad (1.4.85)$$

up to numerically irrelevant corrections of order $\mathcal{O}(|\Gamma_{12}|/M_{12}|^2)$. M_{\pm} and Γ_{\pm} are the masses and decay rates of the physical eigenstates $|M_{\pm}\rangle$, respectively. Diagonalizing the Hamiltonian, we find the eigenvalues (masses and decay rates) and eigenvectors (physical eigenstates),

$$\lambda_{\pm} = M_{11} - \frac{i}{2} \Gamma_{11} \pm \Delta, \quad \Delta \equiv \sqrt{\left(M_{12} - \frac{i}{2} \Gamma_{12}\right) \left(M_{12}^* - \frac{i}{2} \Gamma_{12}^*\right)} \quad (1.4.86)$$

and¹

$$|M_{\pm}\rangle = \frac{p|M^0\rangle \pm q|\bar{M}^0\rangle}{\sqrt{|p|^2 + |q|^2}}, \quad \frac{q}{p} \equiv \frac{1 - \bar{\varepsilon}}{1 + \bar{\varepsilon}} = \sqrt{\frac{M_{12}^* - \frac{i}{2} \Gamma_{12}^*}{M_{12} - \frac{i}{2} \Gamma_{12}}}, \quad (1.4.87)$$

which can be rewritten as

$$\begin{aligned} |M^0\rangle &= \frac{\sqrt{|p|^2 + |q|^2}}{2p} [|M_+\rangle + |M_-\rangle], \\ |\bar{M}^0\rangle &= \frac{\sqrt{|p|^2 + |q|^2}}{2q} [|M_+\rangle - |M_-\rangle]. \end{aligned} \quad (1.4.88)$$

¹We use the CP convention $\mathcal{CP}|M^0\rangle = -|\bar{M}^0\rangle$.

From Eq. (1.4.86), we immediately obtain

$$M_{\pm} = M_{11} \pm \text{Re}(\Delta) , \quad \Gamma_{\pm} = -[\Gamma_{11} \pm 2 \text{Im}(\Delta)] . \quad (1.4.89)$$

Another interesting phenomenological observable is the CP asymmetry for flavour-specific final states a_{fs} , which relates q/p to the mixing phase ϕ ,

$$a_{\text{fs}} \equiv 2 \left(1 - \left| \frac{q}{p} \right| \right) = \text{Im} \left(\frac{\Gamma_{12}}{M_{12}} \right) = \frac{|\Gamma_{12}|}{|M_{12}|} \sin \phi = \frac{\Delta \Gamma}{\Delta M} \tan \phi . \quad (1.4.90)$$

1.4.1.2 Time evolution

The $|M_{\pm}\rangle$ are the mass eigenstates that diagonalize the Hamiltonian. Then, from Eq. (1.4.80), the usual time dependence is

$$|M_{\pm}(t)\rangle = e^{-i(M_{\pm} - \frac{i}{2}\Gamma_{\pm})t} |M_{\pm}(0)\rangle . \quad (1.4.91)$$

Combining Eqs. (1.4.87), (1.4.88) and (1.4.91), we obtain the following time evolution of $|M^0\rangle$ and $|\bar{M}^0\rangle$

$$\begin{bmatrix} |M^0(t)\rangle \\ |\bar{M}^0(t)\rangle \end{bmatrix} = \begin{bmatrix} g_+(t) & \frac{q}{p} g_-(t) \\ \frac{p}{q} g_-(t) & g_+(t) \end{bmatrix} \begin{bmatrix} |M^0(0)\rangle \\ |\bar{M}^0(0)\rangle \end{bmatrix} , \quad (1.4.92)$$

where

$$\begin{bmatrix} g_+(t) \\ g_-(t) \end{bmatrix} = e^{-i M t} e^{-\frac{1}{2} \Gamma t} \begin{bmatrix} \cos \left[\frac{(x - i y) \Gamma t}{2} \right] \\ -i \sin \left[\frac{(x - i y) \Gamma t}{2} \right] \end{bmatrix} , \quad (1.4.93)$$

with the following definitions

$$M \equiv \frac{1}{2} (M_+ + M_-) , \quad \Gamma \equiv \frac{1}{2} (\Gamma_+ + \Gamma_-) , \quad (1.4.94)$$

and

$$x \equiv \frac{\Delta M}{\Gamma} , \quad y \equiv \frac{\Delta \Gamma}{2\Gamma} . \quad (1.4.95)$$

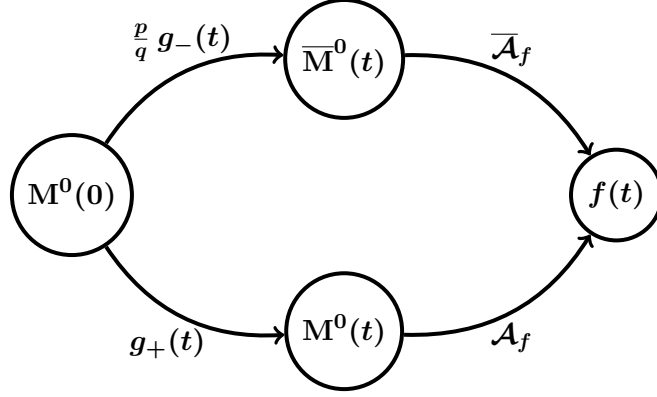


Figure 1.11: Diagrammatic casuistry of neutral meson mixing transitions.

1.4.1.3 Mixing in the Standard Model

At second order in perturbation theory, M_{ij} and Γ_{ij} are given by

$$M_{ij} = m_0 \delta_{ij} + \langle i | \mathcal{H}_w | j \rangle + \sum_n \mathcal{P} \left(\frac{\langle i | \mathcal{H}_w | n \rangle \langle n | \mathcal{H}_w | j \rangle}{m_0 - E_n} \right), \quad (1.4.96)$$

$$\Gamma_{ij} = 2\pi \sum_n \langle i | \mathcal{H}_w | n \rangle \langle n | \mathcal{H}_w | j \rangle \delta(m_0 - E_n), \quad (1.4.97)$$

where $m_0 = \langle M^0 | (\mathcal{H}_s + \mathcal{H}_{\text{em}}) | M^0 \rangle = \langle \bar{M}^0 | (\mathcal{H}_s + \mathcal{H}_{\text{em}}) | \bar{M}^0 \rangle$ is the unperturbed mass of M^0 and \bar{M}^0 , E_n is the energy of the intermediate states n and \mathcal{P} indicates the principal part. The diagonal elements M_{11} and Γ_{11} are real parameters that would correspond to the mass and width of the neutral mesons in the ideal world in which the weak interaction is switch-off. The off-diagonal elements, M_{12} and Γ_{12} , encode the physics behind the neutral meson transitions. While the dispersive part M_{12} quantifies the short-distance $\Delta F = 2$ contributions coming from box diagrams and non-local contributions involving two $\Delta F = 1$ transitions, the absorptive contribution Γ_{12} encodes all on-shell intermediate states in which M^0 and \bar{M}^0 can both decay. In Figure 1.11, we show diagrammatically the interplay between mixing and decay.

In the following, we explain how to perform the calculation of the mixing parameters in the SM. The mass width ΔM is dominated by short-distance $\Delta F = 2$ contributions. These contributions appear at one-loop level in the SM due to the GIM mechanism.

They are represented by the Feynman diagrams popularly known as box diagrams, see Figure 1.12 ($M^0 \equiv q_1 \bar{q}_2$ and $\bar{M}^0 \equiv \bar{q}_1 q_2$). In general, the computation of these diagrams

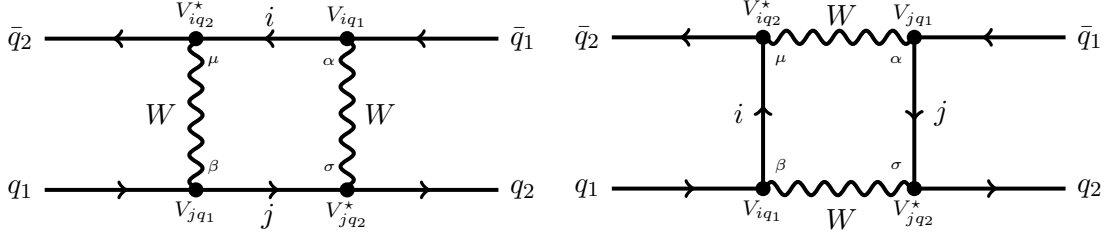


Figure 1.12: Box diagrams contributing to neutral meson mixing.

is quite complicated because they contain 4 external four-momenta, 4 propagators and a sum of three quarks flowing into the loop. In the limit of zero external four-momenta and zero external quark masses, the computation is simplified considerably and the physical amplitude (in the unitary gauge) is given by (left diagram in Fig. 1.12)

$$\mathcal{A}_{M^0} = \frac{g^4}{4} \sum_{ij} \lambda_i \lambda_j \cdot \int \frac{d^4 k}{(2\pi)^4} \left(\frac{g^{\mu\beta} - \frac{k^\mu k^\beta}{M_W^2}}{k^2 - M_W^2} \right) \cdot \left(\frac{g^{\alpha\sigma} - \frac{k^\alpha k^\sigma}{M_W^2}}{k^2 - M_W^2} \right) \cdot \left[\bar{u}_{q_2}(0) \gamma_\sigma P_L \frac{(\not{k} + m_j)}{k^2 - m_j^2} \gamma_\beta P_L u_{q_1}(0) \right] \cdot \left[\bar{v}_{q_2}(0) \gamma_\mu P_L \frac{(\not{k} + m_i)}{k^2 - m_i^2} \gamma_\alpha P_L v_{q_1}(0) \right], \quad (1.4.98)$$

where we can see the weak coupling $g^2 \equiv 4\sqrt{2}G_F M_W^2$ to the fourth power, the four CKM matrix elements $\lambda_i \equiv V_{iq_2}^* V_{iq_1}$, the two W propagators, the two internal quark propagators and the external quark and anti-quark spinors. Using the following Fierz identity,

$$(\bar{u}_1 A P_L u_2)(\bar{u}_3 P_R B u_4) = \frac{1}{2} (\bar{u}_3 \gamma^\mu P_L u_2)(\bar{u}_1 A \gamma_\mu P_R B u_4), \quad (1.4.99)$$

being A and B two arbitrary matrices and Lorentz invariance,

$$\int \frac{d^4 k}{(2\pi)^4} f(k^2) k_\mu k_\nu = \int \frac{d^4 k}{(2\pi)^4} f(k^2) \frac{k^2}{D} g_{\mu\nu}, \quad (1.4.100)$$

where D is the space-time dimension², the amplitude given by Eq. (1.4.98) plus a similar expression from the second Feynman diagram can be reduced to the following effective Hamiltonian

$$\mathcal{H}_{\text{eff}}^{\Delta F=2} = \frac{G_F^2 M_W^2}{4 \pi^2} \sum_{ij} \lambda_i \lambda_j \tilde{S}(m_i^2, m_j^2) \mathcal{O}_{\text{VLL}} , \quad (1.4.101)$$

where $\mathcal{O}_{\text{VLL}} \equiv [\bar{q}_2(x) \gamma_\mu P_L q_1(x)] [\bar{q}_2(x) \gamma^\mu P_L q_1(x)]$ is a local dimension-six operator and

$$\tilde{S}(m_i^2, m_j^2) \equiv \left(1 + \frac{1}{4} \beta_i \beta_j \right) M_W^2 D_2(m_i^2, m_j^2, M_W^2) - 2 \beta_i \beta_j M_W^4 D_0(m_i^2, m_j^2, M_W^2) ,$$

where $\beta_i \equiv m_i^2/M_W^2$ and $D_{0,2}$ are loop functions

$$\begin{aligned} D_0(a, b, c, d) &\equiv \frac{b \ln\left(\frac{b}{a}\right)}{(b-a)(b-c)(b-d)} + \frac{c \ln\left(\frac{c}{a}\right)}{(c-a)(c-b)(c-d)} \\ &+ \frac{d \ln\left(\frac{d}{a}\right)}{(d-a)(d-b)(d-c)} , \end{aligned} \quad (1.4.102)$$

$$\begin{aligned} D_2(a, b, c, d) &\equiv \frac{b^2 \ln\left(\frac{b}{a}\right)}{(b-a)(b-c)(b-d)} + \frac{c^2 \ln\left(\frac{c}{a}\right)}{(c-a)(c-b)(c-d)} \\ &+ \frac{d^2 \ln\left(\frac{d}{a}\right)}{(d-a)(d-b)(d-c)} . \end{aligned} \quad (1.4.103)$$

Assuming the sum over all different flavours that are flowing into the loop, imposing the unitarity of the CKM matrix through $\lambda_u + \lambda_c + \lambda_t = 0$ and taking $m_{u,d} \rightarrow 0$, the $\Delta F = 2$ effective Hamiltonian can be expressed as

$$\mathcal{H}_{\text{eff}}^{\Delta F=2} = \frac{G_F^2 M_W^2}{16 \pi^2} \left\{ \lambda_t^2 \mathcal{C}_{\text{VLL}}^{tt} + \lambda_c^2 \mathcal{C}_{\text{VLL}}^{cc} + 2 \lambda_t \lambda_c \mathcal{C}_{\text{VLL}}^{ct} \right\} \mathcal{O}_{\text{VLL}} , \quad (1.4.104)$$

with

$$\begin{aligned} \mathcal{C}_{\text{VLL}}^{ij} &= \tilde{S}(0, 0) - \frac{1}{2} \tilde{S}(m_i^2, 0) - \frac{1}{2} \tilde{S}(m_j^2, 0) - \frac{1}{2} \tilde{S}(0, m_i^2) - \frac{1}{2} \tilde{S}(0, m_j^2) \\ &+ \frac{1}{2} \tilde{S}(m_i^2, m_j^2) + \frac{1}{2} \tilde{S}(m_j^2, m_i^2) . \end{aligned} \quad (1.4.105)$$

²In unitarity gauge, there are UV divergences. However, since they are independent of internal quark masses, the divergences disappear when the unitarity of the CKM matrix is assumed.

Then, we obtain an analytical expression which involves three pieces, the first piece depends on m_t^2/M_W^2 , the second piece depends on m_c^2/M_W^2 and the last piece with a more complicated dependence on both m_t^2/M_W^2 and m_c^2/M_W^2 . These corrections $\mathcal{C}_{\text{VLL}}^{ij}$ are popularly known as Inami-Lim factors [33]. In the Table 1.1, we give the size of these three corrections together with the corresponding CKM matrix elements.

		CKM factors ($\lambda_i \lambda_j$)		
(i, j)	$\mathcal{C}_{\text{VLL}}^{ij}/4$	K^0	B^0	B_s^0
(t, t)	2.37	$A^4 \lambda^{10} 1 - \rho - i\eta ^2$	$A^2 \lambda^6 1 - \rho - i\eta ^2$	$A^2 \lambda^4$
(c, c)	$2.6 \cdot 10^{-4}$	λ^2	$A^2 \lambda^6$	$A^2 \lambda^4$
(c, t)	$2.3 \cdot 10^{-3}$	$A^2 \lambda^6 1 - \rho - i\eta $	$A^2 \lambda^6 1 - \rho - i\eta $	$-A^2 \lambda^4$

Table 1.1: Inami-Lim factors and CKM matrix elements for different mixings.

From Table 1.1, we immediately extract the following conclusions,

1. Since $\lambda_t \ll \lambda_c$, K^0 mixing is largely dominated by the (c, c) diagram, while the (t, t) and (c, t) diagrams represent small corrections.
2. In the B^0 and B_s^0 mixings, $\lambda_t \approx \lambda_c$ and $m_t \gg m_c$, then they are completely dominated by the (t, t) diagram.

Taking into account these conclusions and

$$\Delta M_{M^0} = \frac{|\langle M^0 | \mathcal{H}_{\text{eff}}^{\Delta F=2} | \bar{M}^0 \rangle|}{m_0}, \quad (1.4.106)$$

we obtain the following mass differences for the B and K systems,

$$\Delta M_{B_q^0} = \frac{G_F^2 M_W^2}{6\pi^2} f_{B_q^0}^2 M_{B_q^0} \hat{\mathcal{B}}_{B_q^0} \left[\eta_{B_q^0} \frac{\mathcal{C}_{\text{VLL}}^{tt}}{4} \lambda_t^2 \right], \quad (1.4.107)$$

$$\Delta M_{K^0} = \frac{G_F^2 M_W^2}{6\pi^2} f_{K^0}^2 M_{K^0} \hat{\mathcal{B}}_{K^0} \left[\eta_{tt} \frac{\mathcal{C}_{\text{VLL}}^{tt}}{4} \lambda_t^2 + \eta_{ct} \frac{\mathcal{C}_{\text{VLL}}^{ct}}{4} 2 \lambda_c \lambda_t + \eta_{cc} \frac{\mathcal{C}_{\text{VLL}}^{cc}}{4} \lambda_c^2 \right],$$

where f_{K^0} and $f_{B_q^0}$ are the K^0 and B_q^0 decay constants, M_{K^0} and $M_{B_q^0}$ are the K^0 and B_q^0 masses. Furthermore, $\hat{\mathcal{B}}_{K^0}$ and $\hat{\mathcal{B}}_{B_q^0}$ are the renormalization group invariant parameters defined by

$$\hat{\mathcal{B}}_{K^0} = \mathcal{B}_{K^0}(\mu) \left[\alpha_s^{(3)}(\mu) \right]^{-2/9} \left[1 + \frac{\alpha_s^{(3)}(\mu)}{4\pi} J_3 \right], \quad (1.4.108)$$

$$\hat{\mathcal{B}}_{B_q^0} = \mathcal{B}_{B_q^0}(\mu) \left[\alpha_s^{(5)}(\mu) \right]^{-6/23} \left[1 + \frac{\alpha_s^{(5)}(\mu)}{4\pi} J_5 \right], \quad (1.4.109)$$

with

$$\langle M^0 | \mathcal{O}_{VLL}(\mu) | \bar{M}^0 \rangle = \frac{2}{3} m_0^2 f_{M^0}^2 \mathcal{B}_{M^0}(\mu), \quad (1.4.110)$$

where $\alpha_s^{(f)}$ is the strong coupling constant in an effective three flavour theory, $J_3 = 1.895$ and $J_5 = 1.627$ in the Naive Dimensional Regularization (NDR) scheme [34–36]. In addition, the short-distance QCD effects are described through the correction factors $\hat{\eta}_{B_q^0}$, $\hat{\eta}_{tt}$, $\hat{\eta}_{ct}$ and $\hat{\eta}_{cc}$ [37–41].

On the other hand, Γ_{12} involves the computation of box diagrams with on-shell internal quarks. For B^0 and B_s^0 mixings, the dominant contribution comes from the $b \rightarrow c\bar{c}s$ transition. Since $b \rightarrow c\bar{c}s$ is a tree-level transition, Γ_{12} is expected to be less sensitive to new physics than M_{12} . It can be written as [42]

$$\Gamma_{12} = -\frac{G_F^2 m_b^2}{8\pi^2} \left[\lambda_t^2 + \lambda_t \lambda_c \mathcal{O} \left(\frac{m_c^2}{m_b^2} \right) + \lambda_c^2 \mathcal{O} \left(\frac{m_c^2}{m_b^2} \right) \right] \eta'_{B_q^0} f_{B_q^0}^2 M_{B_q^0} \hat{\mathcal{B}}_{B_q^0}, \quad (1.4.111)$$

where the QCD corrections are encoded in the factor $\eta'_{B_q^0}$. Notice that M_{12} and Γ_{12} have the same dependence on the non-perturbative parameter $f_{B_q^0}^2 \hat{\mathcal{B}}_{B_q^0}$, then one should expect that the short-distance prediction for Γ_{12}/M_{12} has a smaller theoretical uncertainty than Γ_{12} and M_{12} separately. Then, from Eqs. (1.4.107), (1.4.111) and (1.4.85),

$$\frac{\Delta\Gamma_{B_q^0}}{\Delta M_{B_q^0}} \approx 3\pi \frac{m_b^2}{M_W^2} \frac{1}{C_{VLL}^{tt}} \approx \frac{1}{250}, \quad (1.4.112)$$

which is approximately independent of the CKM matrix elements and therefore the same for both B -systems. Furthermore, since $\frac{\Delta\Gamma_{B_q^0}}{\Delta M_{B_q^0}}$ is proportional to $\frac{m_b^2}{M_W^2}$, we have $\Delta\Gamma_{B_q^0} \ll$

$\Delta M_{B_q^0}$ in the SM. Since ΔM and $\Delta\Gamma$ are proportional to λ_t^2 for B-systems, the phase difference between M_{12} and Γ_{12} is 180° and ϕ is very small in the SM. Moreover, Eq. (1.4.85) implies that $\Delta\Gamma > 0$.

1.4.1.4 Behaviour of flavour oscillations

The mixing phenomena $D^0 - \bar{D}^0$, $K^0 - \bar{K}^0$, $B^0 - \bar{B}^0$ and $B_s^0 - \bar{B}_s^0$ show different oscillation behaviours, since they have all different values of Γ , $\Delta\Gamma$ and ΔM . Let us compute the probability to observe a M^0 meson at time t if one starts with a M^0 meson

$$P(M^0(0) \rightarrow M^0(t)) \equiv |\langle M^0(0) | M^0(t) \rangle|^2 = |g_+(t)|^2, \quad (1.4.113)$$

and the probability to observe a \bar{M}^0 meson at time t if one starts with a M^0 meson

$$P(M^0(0) \rightarrow \bar{M}^0(t)) \equiv |\langle M^0(0) | \bar{M}^0(t) \rangle|^2 = |g_-(t)|^2 \left| \frac{q}{p} \right|^2, \quad (1.4.114)$$

and

$$|g_\pm(t)|^2 = \frac{e^{-\Gamma t}}{2} \left(\cosh(y \Gamma t) \pm \cos(x \Gamma t) \right), \quad (1.4.115)$$

where x and y are the dimensionless parameters controlling the oscillation time scales defined in Eq. (1.4.95). Our experimental knowledge about these oscillation parameters is summarized in Table 1.2. Assuming the SM as the ultimate theory, we can try to explain the size of the ΔM values in Table 1.2. For instance, in the $D^0 - \bar{D}^0$ mixing, if we consider the contribution from the heaviest quark that is flowing into the loop m_b^2 , this is not enough to compensate the strong suppression of the CKM matrix elements $|V_{ub}V_{cb}^*|^2$. Then, the light quarks dominate ΔM_{D^0} and since it is proportional to $|V_{us}V_{cs}^*|^2 m_s^2 \sim \lambda^2 m_s^2$, we expect a small value of ΔM_{D^0} . The $B^0 - \bar{B}^0$ mixing is clearly dominated by the top quark loop, so $|V_{tb}V_{td}^*|^2 m_t^2 \sim \lambda^6 m_t^2$ and therefore the D^0 oscillation is clearly suppressed compared to B^0 oscillation. For $B_s^0 - \bar{B}_s^0$ mixing, we expect a value for the mass width larger than the $B^0 - \bar{B}^0$ value, since $|V_{tb}V_{ts}^*|^2 m_t^2 \sim \lambda^4 m_t^2$. Finally, K^0 mixing is dominated by the charm quark, $|V_{cd}V_{cs}^*|^2 m_c^2 \sim \lambda^2 m_c^2$.

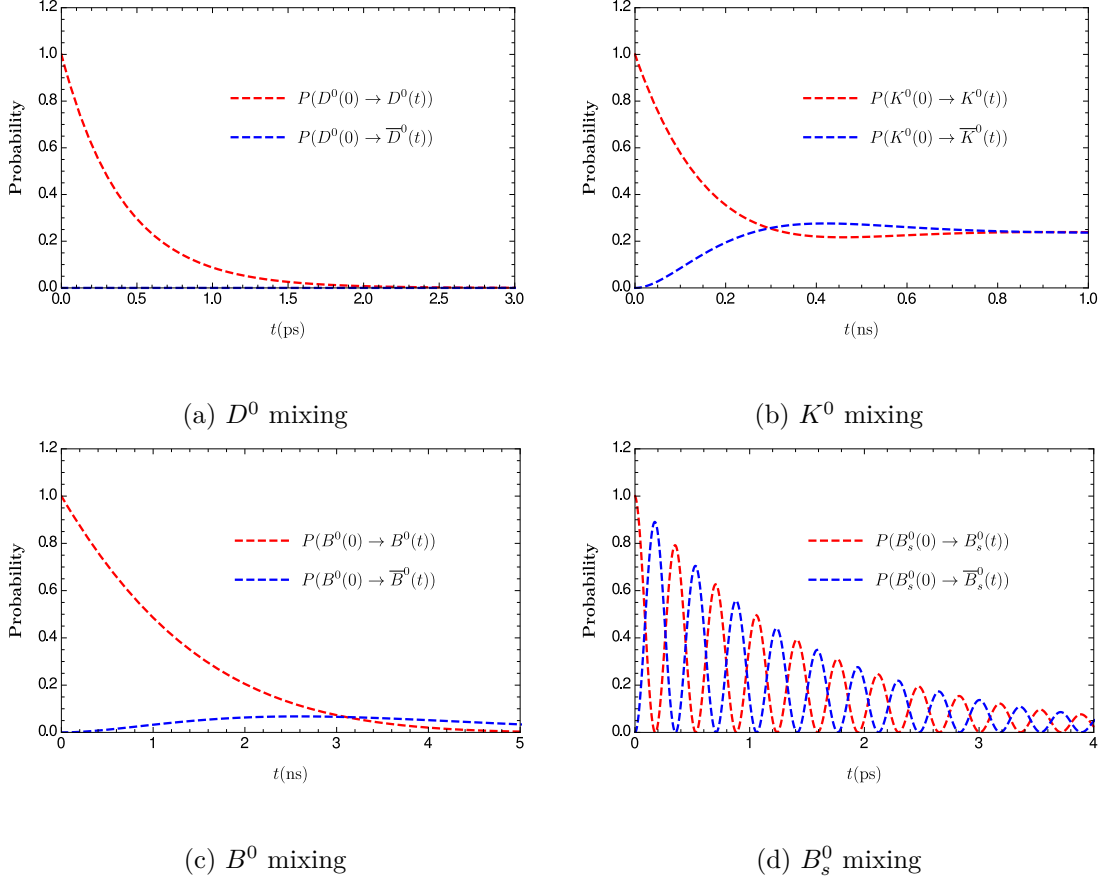


Figure 1.13: Probability to observe a M^0 or a \bar{M}^0 meson at time t .

In Table 1.2, we observe that there is a large casuistry depending on the value of x and y . From Eq. (1.4.115), we observe that x is the frequency of the flavour oscillations. Depending on the x value:

- $x \ll 1$: Since $\cos(x \Gamma t) \approx 1$, the meson has no time to oscillate and then the flavour is mostly conserved. We call this case *slow oscillation*. It corresponds to the $D^0 - \bar{D}^0$ mixing, see Figure 1.13a where we plot the probability for the inputs of Table 1.2.
- $x \gg 1$: The meson oscillates many times before decaying, thus flavour is not conserved. We call this case *fast oscillation*. It corresponds to the $B_s^0 - \bar{B}_s^0$ mixing, see Figure 1.13d.

System	Γ (10^{11} s^{-1})	ΔM (10^{12} s^{-1})	x	y
$D^0 - \bar{D}^0$	24.384	0.010	$3.2 \cdot 10^{-3}$	$6.9 \cdot 10^{-3}$
$K^0 - \bar{K}^0$	0.056	0.005	0.945	-0.991
$B^0 - \bar{B}^0$	6.579	0.506	0.770	0.000
$B_s^0 - \bar{B}_s^0$	6.627	17.757	26.795	0.066

Table 1.2: Mixing parameters of neutral mesons systems [31].

- $x \sim 1$: In this case, there is a nice interplay between the oscillation and the decay of the meson. It corresponds to the $K^0 - \bar{K}^0$ and $B^0 - \bar{B}^0$ mixings, see Figure 1.13b and 1.13c.

We can also study and combine the y parameter with the previous x casuistry:

- $|y| \ll 1$ and $y \ll x$: In this case the width difference is irrelevant. It corresponds to the B mixings.
- $|y| \sim x$: In this case the width difference and the mass width are relevant. It corresponds to the $D^0 - \bar{D}^0$ and $K^0 - \bar{K}^0$ mixings.

There are other limits that we do not analyze since they have not been observed.

1.4.2 Neutral Meson Decay

We have studied a quite general formalism to describe neutral meson systems. However, since we have been more focused in the understanding of the mixing phenomena, we did not include the decay of the meson into a final state f , instead we have considered a non-Hermitian Hamiltonian. In this section, we include the meson decay, constructing a more general formalism. Let us consider M^0 and \bar{M}^0 meson decays into two possible final

states f and \bar{f} . Phenomenologically, there are only four independent quantities,

$$\begin{aligned}\mathcal{A}_f &= \langle f | \mathcal{T} | M^0 \rangle, & \bar{\mathcal{A}}_f &= \langle f | \mathcal{T} | \bar{M}^0 \rangle, \\ \mathcal{A}_{\bar{f}} &= \langle \bar{f} | \mathcal{T} | M^0 \rangle, & \bar{\mathcal{A}}_{\bar{f}} &= \langle \bar{f} | \mathcal{T} | \bar{M}^0 \rangle,\end{aligned}\quad (1.4.116)$$

where \mathcal{T} is the transition matrix. Then, using Eq. (1.4.92), the different expressions for the time-dependent decay rates are

$$\Gamma_{M^0 \rightarrow f} = |\mathcal{A}_f|^2 \left\{ |g_+(t)|^2 + |\lambda_f|^2 |g_-(t)|^2 + 2 \operatorname{Re} (\lambda_f g_+^*(t) g_-(t)) \right\}, \quad (1.4.117)$$

$$\Gamma_{M^0 \rightarrow \bar{f}} = |\bar{\mathcal{A}}_f|^2 \left| \frac{q}{p} \right|^2 \left\{ |g_-(t)|^2 + |\bar{\lambda}_f|^2 |g_+(t)|^2 + 2 \operatorname{Re} (\bar{\lambda}_f g_+(t) g_-^*(t)) \right\}, \quad (1.4.118)$$

$$\Gamma_{\bar{M}^0 \rightarrow f} = |\mathcal{A}_f|^2 \left| \frac{p}{q} \right|^2 \left\{ |g_-(t)|^2 + |\lambda_f|^2 |g_+(t)|^2 + 2 \operatorname{Re} (\lambda_f g_+(t) g_-^*(t)) \right\}, \quad (1.4.119)$$

$$\Gamma_{\bar{M}^0 \rightarrow \bar{f}} = |\bar{\mathcal{A}}_f|^2 \left\{ |g_+(t)|^2 + |\bar{\lambda}_f|^2 |g_-(t)|^2 + 2 \operatorname{Re} (\bar{\lambda}_f g_+^*(t) g_-(t)) \right\}, \quad (1.4.120)$$

where $\Gamma_{I \rightarrow F}(t) \equiv |\langle F | \mathcal{T} | I \rangle|^2$ give us the probability that a state I at $t = 0$ decays into the final state F at time t . Furthermore, we have defined the following complex parameters

$$\lambda_f \equiv \frac{q}{p} \frac{\bar{\mathcal{A}}_f}{\mathcal{A}_f}, \quad \bar{\lambda}_f \equiv \frac{1}{\lambda_f}, \quad \lambda_{\bar{f}} \equiv \frac{q}{p} \frac{\bar{\mathcal{A}}_{\bar{f}}}{\mathcal{A}_{\bar{f}}}, \quad \bar{\lambda}_{\bar{f}} \equiv \frac{1}{\lambda_{\bar{f}}}. \quad (1.4.121)$$

Notice that in Eqs. (1.4.117) - (1.4.120), the terms proportional to $|\mathcal{A}_f|^2$ or $|\bar{\mathcal{A}}_f|^2$ are associated with decays that occur without any net oscillation, while terms proportional to $|\mathcal{A}_f|^2 \left| \frac{p}{q} \right|^2$ or $|\bar{\mathcal{A}}_f|^2 \left| \frac{q}{p} \right|^2$ are associated with decays following a net oscillation. The terms with $g_+^*(t) g_-(t)$ or $g_+(t) g_-^*(t)$ correspond to the interference between these two cases.

Finally, taking into account Eq. (1.4.93), we obtain the time-dependent decay rates for neutral mesons in terms of x and y ,

$$\begin{aligned}\frac{\Gamma_{M^0 \rightarrow f}(t)}{\tilde{\Gamma}_f(t)} &= \cosh(y\tau) + D_f \sinh(y\tau) + C_f \cos(x\tau) - S_f \sin(x\tau), \\ \frac{\Gamma_{M^0 \rightarrow \bar{f}}(t)}{\tilde{\Gamma}_{\bar{f}}(t)} &= \left| \frac{q}{p} \right|^2 \left(\cosh(y\tau) + \bar{D}_{\bar{f}} \sinh(y\tau) - \bar{C}_{\bar{f}} \cos(x\tau) + \bar{S}_{\bar{f}} \sin(x\tau) \right), \\ \frac{\Gamma_{\bar{M}^0 \rightarrow f}(t)}{\tilde{\Gamma}_f(t)} &= \left| \frac{p}{q} \right|^2 \left(\cosh(y\tau) + D_f \sinh(y\tau) - C_f \cos(x\tau) + S_f \sin(x\tau) \right), \\ \frac{\Gamma_{\bar{M}^0 \rightarrow \bar{f}}(t)}{\tilde{\Gamma}_{\bar{f}}(t)} &= \cosh(y\tau) + \bar{D}_{\bar{f}} \sinh(y\tau) + \bar{C}_{\bar{f}} \cos(x\tau) - \bar{S}_{\bar{f}} \sin(x\tau). \quad (1.4.122)\end{aligned}$$

where $\tau \equiv \Gamma t$,

$$\tilde{\Gamma}_f(t) \equiv |\mathcal{A}_f|^2 \frac{e^{-\Gamma t}}{2} (1 + |\lambda_f|^2), \quad \tilde{\Gamma}_{\bar{f}}(t) \equiv |\bar{\mathcal{A}}_{\bar{f}}|^2 \frac{e^{-\Gamma t}}{2} (1 + |\bar{\lambda}_{\bar{f}}|^2), \quad (1.4.123)$$

and

$$D_f \equiv \frac{2 \operatorname{Re}(\lambda_f)}{1 + |\lambda_f|^2}, \quad C_f \equiv \frac{1 - |\lambda_f|^2}{1 + |\lambda_f|^2}, \quad S_f \equiv \frac{2 \operatorname{Im}(\lambda_f)}{1 + |\lambda_f|^2}, \quad (1.4.124)$$

$$\bar{D}_{\bar{f}} \equiv \frac{2 \operatorname{Re}(\bar{\lambda}_{\bar{f}})}{1 + |\bar{\lambda}_{\bar{f}}|^2}, \quad \bar{C}_{\bar{f}} \equiv \frac{1 - |\bar{\lambda}_{\bar{f}}|^2}{1 + |\bar{\lambda}_{\bar{f}}|^2}, \quad \bar{S}_{\bar{f}} \equiv \frac{2 \operatorname{Im}(\bar{\lambda}_{\bar{f}})}{1 + |\bar{\lambda}_{\bar{f}}|^2}, \quad (1.4.125)$$

which satisfy

$$|D_f|^2 + |C_f|^2 + |S_f|^2 = 1, \quad |\bar{D}_{\bar{f}}|^2 + |\bar{C}_{\bar{f}}|^2 + |\bar{S}_{\bar{f}}|^2 = 1. \quad (1.4.126)$$

From Eqs. (1.4.122), one realizes that the fundamental quantities necessary to completely describe a meson neutral system are four, x , y , λ_f and $\bar{\lambda}_{\bar{f}}$. Notice in Eqs. (1.4.122) how $\left| \frac{q}{p} \right|^2$ is a pure global factor.

1.4.3 Types of CP violation in neutral meson systems

The CP violation appears in neutral meson systems through two types of phenomena, mixing and decay. For completeness, we give a classification of the three types of CP violation effects [43].

1. **CP violation in decay** (also called **direct CP violation**) is defined by

$$\left| \frac{\bar{\mathcal{A}}_f}{\mathcal{A}_f} \right| \neq 1, \quad (1.4.127)$$

This is the case of the interference between two decay amplitudes with necessary different weak and strong phases. These last phases due to rescattering.

In charged mesons where there is no mixing, the only type of CP violation is

$$a_{f^\pm} \equiv \frac{\Gamma(M^- \rightarrow f^-) - \Gamma(M^+ \rightarrow f^+)}{\Gamma(M^- \rightarrow f^-) + \Gamma(M^+ \rightarrow f^+)} = \frac{\left| \frac{\bar{\mathcal{A}}_{f^-}}{\mathcal{A}_{f^+}} \right|^2 - 1}{\left| \frac{\bar{\mathcal{A}}_{f^-}}{\mathcal{A}_{f^+}} \right|^2 + 1}. \quad (1.4.128)$$

2. **CP violation in mixing** (also called **indirect CP violation**) is defined by

$$\left| \frac{q}{p} \right| \neq 1. \quad (1.4.129)$$

This type of CP violation is originated through the interference between the absorptive and dispersive mixing amplitudes, see Eq. (1.4.87).

One example of CP violation in mixing is the asymmetry of *wrong-sign* decays in charged-current semi-leptonic neutral meson decays $M^0, \bar{M}^0 \rightarrow l^\pm X$ which only occurs if there is meson oscillation,

$$a_{\text{SL}} = \frac{\Gamma(M^0 \rightarrow l^+ X) - \Gamma(\bar{M}^0 \rightarrow l^- X)}{\Gamma(M^0 \rightarrow l^+ X) + \Gamma(\bar{M}^0 \rightarrow l^- X)} = \frac{1 - \left| \frac{q}{p} \right|^4}{1 + \left| \frac{q}{p} \right|^4}. \quad (1.4.130)$$

where the initial neutral meson can be \bar{B}^0, \bar{K}^0 or D^0 .

3. **CP violation in interference between a decay without mixing, $M^0 \rightarrow f$, and a decay with mixing $M^0 \rightarrow \bar{M}^0 \rightarrow f$** is defined by

$$\arg(\lambda_f) + \arg(\lambda_{\bar{f}}) \neq 0, \quad (1.4.131)$$

with the following asymmetry for neutral meson decays into CP eigenstates

$$a_{f_{\text{CP}}} \equiv \frac{\Gamma(M^0 \rightarrow f_{\text{CP}}) - \Gamma(\bar{M}^0 \rightarrow f_{\text{CP}})}{\Gamma(M^0 \rightarrow f_{\text{CP}}) + \Gamma(\bar{M}^0 \rightarrow f_{\text{CP}})} \approx \text{Im}(\lambda_{f_{\text{CP}}}) \sin(x \Gamma t). \quad (1.4.132)$$

Chapter 2

The Toolbox: EFTs, OPEs and RGEs

In the previous chapter, we have introduced the foundations of flavour physics. In addition, we have studied the CP violation phenomena in the SM which is unable to reproduce the large matter-antimatter asymmetry that we observe in our Universe. We have presented different phenomenological applications in which the CP violation can appear, *i.e.* mixing, decay or both. In this chapter, we introduce the concept of Effective Field Theory (EFT) which represents a formidable approach to describe a physical system with the appropriate degrees of freedom. Using the Fermi's theory [44] as a toy model, we introduce the general aspects of EFT, paying special attention to those that are close to the field of flavour physics. Further information can be found in Refs. [45–50].

2.1 What are EFTs and why we use them?

An EFT is a simplified description of an underlying physical theory. EFT provides an excellent formalism to describe physical problems involving several energy scales. Its principle is to use the appropriate degrees of freedom to describe a physical system at some energy scale in which one is interested. For instance, a heavy particle (1 degree of

freedom) can not be created at energy scales smaller than its mass, then it can not be a dynamical degree of freedom of the low-energy effective theory. The EFT approach works better when there is a large energy gap between the scale of interest and the scale of the underlying dynamics. The dynamics at low energies do not depend on the details of the dynamics at high energies, this is guaranteed by the *decoupling theorem* [51] which states that the degrees of freedom of heavy particles decouple at energy scales much lower than their mass. By decoupling, we mean that the contributions to physical amplitudes of these degrees of freedom are suppressed by inverse powers of the heavy masses (up to logarithmic corrections). Then, high-energy physics or physics beyond the SM is suppressed at low energies. This seems to forbid extracting information on the fundamental theory from the low-energy measurements, but this is not true. Indications of new physics can be found through small deviations on the low-energy parameters of the effective Lagrangian, because they encode information in terms of masses of heavy degrees of freedom. Therefore, the high-precision in low-energy experiments can be used to probe high-energy dynamics and provide an alternative to high energy experiments.

2.2 General aspects of EFT

2.2.1 Operator product expansion

Let us consider a QFT composed by a heavy scalar field Φ with mass M and a light scalar field ϕ with mass $m \ll M$,

$$\mathcal{L} = \underbrace{-\frac{1}{2}\phi(\square + m^2)\phi}_{\mathcal{L}_{\text{kin}}^\phi} - \underbrace{\frac{1}{2}\Phi(\square + M^2)\Phi}_{\mathcal{L}_{\text{kin}}^\Phi} + J\Phi, \quad (2.2.1)$$

where $\square \equiv \partial_\mu \partial^\mu$ and J is the source of Φ . Suppose that we want to study some phenomenological application at energies $E \ll M$ and obtain its scattering amplitude up to some power of E/M . In the following, we show the steps that one has to follow in order to build the effective Lagrangian.

The normalized generating functional for this scalar field theory is given by

$$Z[J] \equiv \frac{\int [\mathcal{D}\phi] [\mathcal{D}\Phi] e^{i S[\phi, \Phi, J]}}{\int [\mathcal{D}\phi] [\mathcal{D}\Phi] e^{i S[\phi, \Phi, 0]}} , \quad (2.2.2)$$

where $S[\phi, \Phi, J] \equiv \int d^D x \mathcal{L}$ is the action and D is the dimension of the space-time.

At low energy scales ($E < M$), we can perform an integration over the Φ in Eq. (2.2.2). However, notice that the field Φ is an integration variable and it does not satisfy the equation of motion. Let us introduce an auxiliary field Φ_0 :

$$\Phi = \Phi_0 + \tilde{\Phi} , \quad (2.2.3)$$

where Φ_0 satisfies the equation of motion

$$\left(\square + M^2 \right) \Phi_0 = J(x) , \quad (2.2.4)$$

with the following solution

$$\Phi_0 = - \int d^D y \Delta_F^\Phi(x-y) J(y) , \quad (2.2.5)$$

being Δ_F^Φ the Feynman propagator of the field Φ ,

$$\Delta_F^\Phi(x-y) \equiv \int \frac{d^D k}{(2\pi)^D} \frac{e^{-ik(x-y)}}{k^2 - M^2 - i\epsilon} . \quad (2.2.6)$$

Expanding the Lagrangian around Φ_0 , it can be written as

$$\begin{aligned} \mathcal{L}[\phi, \Phi_0 + \tilde{\Phi}] &= -\frac{1}{2} \phi \left(\square + m^2 \right) \phi - \frac{1}{2} (\Phi_0 + \tilde{\Phi}) \left(\square + M^2 \right) (\Phi_0 + \tilde{\Phi}) + J(\Phi_0 + \tilde{\Phi}) \\ &= \mathcal{L}_{\text{kin}}^\phi - \frac{1}{2} \Phi_0 \left(\square + M^2 \right) \Phi_0 - \frac{1}{2} \Phi_0 \left(\square + M^2 \right) \tilde{\Phi} - \frac{1}{2} \tilde{\Phi} \left(\square + M^2 \right) \Phi_0 \\ &\quad - \frac{1}{2} \tilde{\Phi} \left(\square + M^2 \right) \tilde{\Phi} + J \Phi_0 + J \tilde{\Phi} , \end{aligned} \quad (2.2.7)$$

which can be reduced to

$$\mathcal{L}[\phi, \Phi_0 + \tilde{\Phi}] = \mathcal{L}_{\text{kin}}^\phi + \frac{1}{2} J \Phi_0 - \frac{1}{2} \tilde{\Phi} \left(\square + M^2 \right) \tilde{\Phi} - \frac{1}{2} \partial_\mu \left(\Phi_0 \partial^\mu \tilde{\Phi} - \tilde{\Phi} \partial^\mu \Phi_0 \right) , \quad (2.2.8)$$

using Eq.(2.2.4) and the identity

$$\Phi_0 \square \tilde{\Phi} - \tilde{\Phi} \square \Phi_0 = \partial_\mu \left(\Phi_0 \partial^\mu \tilde{\Phi} - \tilde{\Phi} \partial^\mu \Phi_0 \right) . \quad (2.2.9)$$

Therefore, the action can be expressed as

$$S[\phi, \tilde{\Phi}, J] = \int d^D x \left(\mathcal{L}_{\text{kin}}^\phi + \frac{1}{2} J \Phi_0 - \frac{1}{2} \tilde{\Phi} (\square + M^2) \tilde{\Phi} \right), \quad (2.2.10)$$

where the last term in Eq. (2.2.8) has been eliminated using the Gauss's law. Inserting Eq. (2.2.5) into the action given by Eq. (2.2.10), we obtain

$$S[\phi, \tilde{\Phi}, J] = \int d^D x \left(\mathcal{L}_{\text{kin}}^\phi - \frac{1}{2} \tilde{\Phi} (\square + M^2) \tilde{\Phi} \right) - \frac{1}{2} \int d^D x d^D y J(x) \Delta_F^\Phi(x-y) J(y), \quad (2.2.11)$$

and the normalized generating functional becomes

$$Z[J] = e^{-\frac{i}{2} \int d^D x d^D y J(x) \Delta_F^\Phi(x-y) J(y)}, \quad (2.2.12)$$

which has the following Lagrangian,

$$\mathcal{L} = -\frac{1}{2} \int d^D y J(x) \Delta_F^\Phi(x-y) J(y). \quad (2.2.13)$$

It is interesting to point out that all the dependence of $Z[0]$ on the heavy field Φ has canceled out with the normalization $Z[0]$. In the literature, one says that the heavy field has been *integrated out*.

Let us consider $x \approx y$ and perform a Taylor expansion of $J(y)$,

$$J(y) = \lim_{N \rightarrow \infty} \sum_{n=0}^N \frac{(-1)^n}{n!} \hat{J}_{\mu_1 \dots \mu_n}(x) (x-y)^{\mu_1} \dots (x-y)^{\mu_n}, \quad (2.2.14)$$

where $\hat{J}_{\mu_1 \dots \mu_n}(x) \equiv \left(\partial_{\mu_1}^z \dots \partial_{\mu_n}^z J(z) \right) \Big|_{z=x}$. Then, introducing Eqs. (2.2.6) and (2.2.14) into Eq. (2.2.13), we obtain

$$\begin{aligned} \mathcal{L} = & -\frac{1}{2} \lim_{N \rightarrow \infty} \sum_{n=0}^N \frac{(-1)^n}{n!} J(x) \hat{J}_{\mu_1 \dots \mu_n}(x) \cdot \\ & \cdot \int \frac{d^D k}{(2\pi)^D} \frac{1}{k^2 - M^2} \int d^D y (x-y)^{\mu_1} \dots (x-y)^{\mu_n} e^{-ik(x-y)}, \end{aligned} \quad (2.2.15)$$

which using the following identity

$$\partial_k^{\mu_1} \dots \partial_k^{\mu_n} e^{-ik(x-y)} = (-i)^n (x-y)^{\mu_1} \dots (x-y)^{\mu_n} e^{-ik(x-y)}, \quad (2.2.16)$$

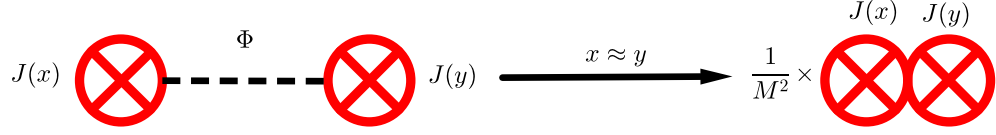


Figure 2.1: Diagrammatic representation of the OPE.

can be reduced to

$$\begin{aligned}
\mathcal{L} &= -\frac{1}{2} \lim_{N \rightarrow \infty} \sum_{n=0}^N \frac{(-i)^n}{n!} J(x) \hat{J}_{\mu_1 \dots \mu_n}(x) \int \frac{d^D k}{(2\pi)^D} \frac{1}{k^2 - M^2} \partial_k^{\mu_1} \dots \partial_k^{\mu_n} \int d^D y e^{-ik(x-y)} \\
&= -\frac{1}{2} \lim_{N \rightarrow \infty} \sum_{n=0}^N \frac{(-i)^n}{n!} J(x) \hat{J}_{\mu_1 \dots \mu_n}(x) \int \frac{d^D k}{(2\pi)^D} \frac{1}{k^2 - M^2} \partial_k^{\mu_1} \dots \partial_k^{\mu_n} \int d^D z e^{ikz} \\
&= -\frac{1}{2} \lim_{N \rightarrow \infty} \sum_{n=0}^N \frac{(-i)^n}{n!} J(x) \hat{J}_{\mu_1 \dots \mu_n}(x) \int d^D k \frac{1}{k^2 - M^2} \partial_k^{\mu_1} \dots \partial_k^{\mu_n} \delta^{(D)}(k) \\
&= -\frac{1}{2} \lim_{N \rightarrow \infty} \sum_{n=0}^N \frac{(-i)^n}{n!} J(x) \hat{J}_{\mu_1 \dots \mu_n}(x) \int d^D k (-1)^n \partial_k^{\mu_1} \dots \partial_k^{\mu_n} \left(\frac{1}{k^2 - M^2} \right) \delta^{(D)}(k) \\
&= -\frac{1}{2} \lim_{N \rightarrow \infty} \sum_{n=0}^N \frac{(i)^n}{n!} J(x) \hat{J}_{\mu_1 \dots \mu_n}(x) \partial_k^{\mu_1} \dots \partial_k^{\mu_n} \left(\frac{1}{k^2 - M^2} \right) \Big|_{k=0} \\
&= -\frac{1}{2} \lim_{N \rightarrow \infty} \sum_{n=0}^N \frac{(i)^n}{n!} J(x) \hat{J}_{\mu_1 \dots \mu_n}(x) P^{\mu_1 \dots \mu_n}(0) \\
&= -\frac{1}{2} \lim_{N \rightarrow \infty} \sum_{n=0}^{\frac{N}{2}} \frac{(-1)^n}{(2n)!} J(x) \hat{J}_{\mu_1 \dots \mu_{2n}}(x) P^{\mu_1 \dots \mu_{2n}}(0) \\
&= \frac{1}{2} \frac{1}{M^2} \lim_{N \rightarrow \infty} \sum_{n=0}^{\frac{N}{2}} \left(-\frac{1}{M^2} \right)^n J(x) \hat{J}_{\mu_1 \dots \mu_{2n}}(x) g_{\mu_1 \mu_2} \dots g_{\mu_{2n-1} \mu_{2n}} \\
&= \frac{1}{2} \frac{1}{M^2} \lim_{N \rightarrow \infty} \sum_{n=0}^{\frac{N}{2}} J(x) \left(-\frac{\square}{M^2} \right)^n J(x), \tag{2.2.17}
\end{aligned}$$

where

$$P^{\mu_1 \cdots \mu_n}(a) \equiv \partial_k^{\mu_1} \cdots \partial_k^{\mu_n} \left(\frac{1}{k^2 - M^2} \right) \Big|_{k=a}. \quad (2.2.18)$$

In the following, we give some comments on the proof of Eq. (2.2.17):

- From the first line to the second line, we perform a change of variable: $z \equiv y - x$.
- From the second line to the third line, we use the definition of the Dirac delta function:

$$\int d^D z e^{ikz} = (2\pi)^D \delta^{(D)}(k).$$

- From the third line to the fourth line, we apply recursively the following property of the Dirac delta function:

$$\int d^D k f(k) \delta^{(D)'}(k) = - \int d^D k f'(k) \delta^{(D)}(k),$$

where f is a generic function and the prime means a derivative.

- From fourth line to fifth line, we use

$$\int d^D k f(k) \delta^{(D)}(k - a) = f(a).$$

- From the fifth line to the last line, we use

$$P^{\mu_1 \cdots \mu_{2n+1}}(0) = 0, \\ P^{\mu_1 \cdots \mu_{2n}}(0) = -\frac{(2n)!}{(M^2)^{n+1}} g_{\mu_1 \mu_2} \cdots g_{\mu_{2n-1} \mu_{2n}}, \quad \forall n.$$

Finally, we show that \mathcal{L} can be written as

$$\mathcal{L} = \frac{1}{2} \frac{1}{M^2} \lim_{N \rightarrow \infty} \sum_{n=0}^{\frac{N}{2}} J(x) \left(-\frac{\square}{M^2} \right)^n J(x), \quad (2.2.19)$$

when $x \approx y$. This expression can be truncated for some value of N ,

$$\mathcal{L}_{\text{eff}}^N \approx \frac{1}{2} \frac{1}{M^2} \sum_{n=0}^{\frac{N}{2}} J(x) \left(-\frac{\square}{M^2} \right)^n J(x), \quad (2.2.20)$$

and since $E < M$, the $N + 1$ missing corrections are smaller than the N corrections which guarantees the convergence of our predictions.

In summary, we have performed a Taylor expansion of a non-local Lagrangian given by Eq. (2.2.13), obtaining as a result an infinite sum of local operators that depend on the source $J(x)$. Finally, truncating this Lagrangian up to some value of N (depending in how accurate we want to be in our predictions), we have obtained an effective Lagrangian given by Eq. (2.2.20) which is a finite sum of local operators. This process is called Operator Product Expansion (OPE) and it is closely related with the suppression in the decoupling theorem. In Figure 2.1, we show a schematic representation of the OPE approach.

2.2.2 Behaviour of local operators

We have proved that an effective Lagrangian can be expressed as a finite sum of local operators \mathcal{O}_i multiplied by certain coefficients C_i :

$$\mathcal{L}_{\text{eff}} = \sum_i C_i \mathcal{O}_i, \quad (2.2.21)$$

where the coefficients C_i encode all high-energy information in terms of heavy masses, while the operators \mathcal{O}_i describe the dynamics at low energies. The different operators \mathcal{O}_i can be classified using *naive dimensional analysis* ($\hbar = c = 1$). If we define the dimension of the operator \mathcal{O}_i as E^{d_i} , the dimension of the coefficients C_i must be Λ^{D-d_i} being Λ some heavy integrated-out scale (M in our previous example). Therefore, the effective action has the following behaviour

$$S_{\text{eff}} \equiv \int d^D x \mathcal{L}_{\text{eff}} = \sum_i c_i \left(\frac{E}{\Lambda} \right)^{d_i - D}, \quad (2.2.22)$$

where c_i are dimensionless constants of $\mathcal{O}(1)$. The energy dependence given by Eq. (2.2.22) leads to the following cases:

- $d_i > D$: these operators are called *irrelevant*, since they are suppressed at low energies. However, this does not mean that their contribution is not important, in fact they are crucial in some cases where they are the only type of operators that

contribute, this only means that they are weak at low energies. These operators correspond to *non-renormalizable* operators.

- $d_i = D$: these operators are called *marginal*. Their contributions do not depend on the ratio E/Λ , with the exception of logarithmic corrections. These operators correspond to *renormalizable* operators.
- $d_i < D$: these operators are called *relevant* and they are important at low energies. These operators are usually forbidden by symmetries, otherwise they cause problems due to their effects at high energy scales. These operators correspond to *super-renormalizable* operators.

Notice that we can take into account the predictability of the EFT. Let us imagine that we are interested in computing some phenomenological process to some level of accuracy ϵ , therefore we have to truncate the Lagrangian for those operators with dimension d_i that satisfy

$$d_i \lesssim D + \frac{\ln \epsilon}{\ln \left(\frac{E}{\Lambda} \right)}. \quad (2.2.23)$$

In the OPE example, we have started with the fundamental Lagrangian given by Eq. (2.2.1), composed by two irrelevant mass operators $[\phi \phi] = [\Phi \Phi] = D - 2$, and three marginal operators: two kinetic operators $[\phi \square \phi] = [\Phi \square \Phi] = D$ and one interacting operator $[J \Phi] = D$, and we have finished with an effective Lagrangian in which all the interacting operators are irrelevant $[J(x) J(x)] = D + 2$. It is interesting to point out the marginal operators do not have a strong energy-scale dependence on their couplings.

2.3 Effective weak interactions

Let us consider the charged-current Lagrangian given by Eq. (1.2.65) which is the only flavour-changing interaction in the SM. As in the Lagrangian given by Eq. (2.2.1), we can also obtain the charged-current EFT realization for $E \ll M_W$. Similarly, we can integrate out the W^\pm bosons, leading into a sum of local four-fermion operators which can

be truncated to some order. After all this process, we obtain the effective weak Lagrangian, popularly called Fermi's theory [44] of weak interactions:

$$\mathcal{L}_{\text{eff}}^{\text{weak}} = -4 \frac{G_F}{\sqrt{2}} \mathcal{J}_\mu^\dagger \mathcal{J}^\mu + \mathcal{O}\left(\frac{p^2}{M_W^2}\right), \quad (2.3.24)$$

where $\frac{G_F}{\sqrt{2}} \equiv \frac{g^2}{8M_W^2}$ is the Fermi constant and

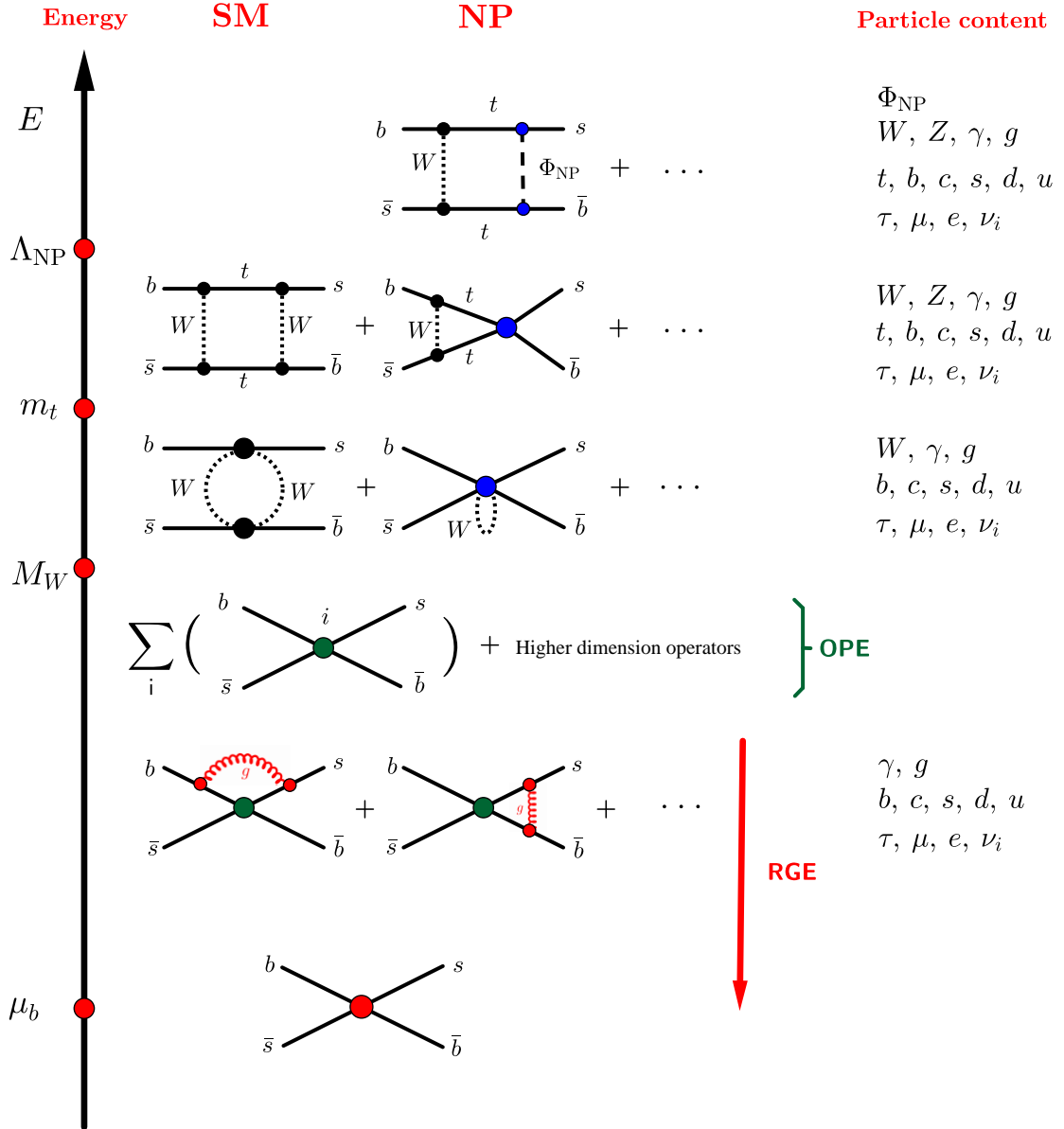
$$\mathcal{J}_\mu^\dagger = \sum_{ij} V_{ij} \bar{u}_i \gamma_\mu P_L d_j + \sum_l \bar{\nu}_l \gamma_\mu P_L l. \quad (2.3.25)$$

In Appendix A, we give a detailed proof of Eq. (2.3.24). Notice that the first contribution is composed by an irrelevant operator of dimension six. The next higher-order contribution is also an irrelevant operator of dimension eight and so on. The coupling constant associated with the operator of dimension six is suppressed by two powers of M_W which is the typical behaviour that one finds when integrating out the heavy fields from the fundamental theory (usually constructed with marginal operators) in the way down to low energies, as in the example of Section 2.2.1. The Fermi's theory was proposed to describe the weak interactions before the formulation of the SM with its weak gauge bosons. During that time, there was a strong belief that the scale of the weak force should be around $\left(\frac{\sqrt{2}}{G_F}\right)^{\frac{1}{2}} \approx 10^2$ GeV. Therefore, the discovery of the weak gauge bosons around this scale was a very important success for the particle physics community, both because of the unification of weak and electromagnetic forces and because of the powerful prediction via the EFT reasoning.

2.3.1 General description

The Lagrangian given by Eq. (2.3.24) is quite far from a realistic description, since it does not take into account the strong interactions which are relevant at low energies. Our EFT needs to take into account these effects, the perturbative QCD contributions are encoded by the well-known *Wilson coefficients* \mathcal{C}_i while the non-perturbative QCD effects appear in the local operators \mathcal{O}_i ,

$$\mathcal{L}_{\text{eff}}^{\text{weak}} = -4 \frac{G_F}{\sqrt{2}} \sum_i \lambda_i \mathcal{C}_i(\mu) \mathcal{O}_i, \quad (2.3.26)$$

Figure 2.2: EFT picture of B_s^0 mixing.

where λ_i contains CKM factors. The \mathcal{O}_i operators have been constructed with the light degrees of freedom (quarks and lepton fields) using low-energy symmetry principles. We do not consider dimension eight or higher-dimension operators because they are suppressed

by inverse powers of M_W^2 . The Wilson coefficients \mathcal{C}_i are the strengths with which a given operator \mathcal{O}_i contributes to some phenomenological process. They are independent of the particle process and only depend on masses of the heavy particles that have been integrated out. The values of the Wilson coefficients can be determined using four ingredients:

1. The Wilson coefficients \mathcal{C}_i have to be determined perturbatively at high energy scales in some fundamental theory. This can be done because QCD has asymptotic freedom.
2. By construction, the low-energy EFT has the same infrared behaviour that the fundamental theory, the differences only appear at high energies where the fundamental theory has additional degrees of freedom, for instance it could have new fields Φ_{NP} .
3. Determining the amplitude for some phenomenological process in both the effective and the fundamental theories allows one to determine $\mathcal{C}_i(\mu_H)$ for $\mu_H > M_W$ through the matching condition:

$$\mathcal{A}_{\text{eff}} = \mathcal{A}_{\text{fun}} \longrightarrow \sum_i \lambda_i \mathcal{C}_i(\mu_H) \langle f | \mathcal{O}_i(\mu_H) | i \rangle = \sum_i \mathcal{X}_i(\mu_H) \langle f | \mathcal{O}_i(\mu_H) | i \rangle ,$$

where $|i\rangle$ and $|f\rangle$ are the initial and final particle states, while \mathcal{X}_i are functions that depend on parameters from the fundamental theory.

4. Finally, we can use the *Renormalization Group Equations* (RGEs) to transform the Wilson coefficients $\mathcal{C}_i(\mu_H)$ at some high energy scale $\mu_H > M_W$ into the Wilson coefficients $\mathcal{C}_i(\mu_L)$ at a low energy scale $\mu_L \ll M_W$.

In Figure 2.2, we illustrate these points through the EFT description of B_s^0 mixing in some extension of the SM with new particles Φ_{NP} .

2.3.2 Phenomenological application

Since the previous ideas are very technical, let us consider the following phenomenological application, $q_1 \bar{q}_3 \rightarrow q_2 \bar{q}_4$ in the SM. Notice that we do not specify the flavour of the

quarks involved. The effective weak Hamiltonian is given by

$$\mathcal{H}_{\text{eff}} = \frac{G_F}{\sqrt{2}} V_{q_1 q_2} V_{q_3 q_4}^* \left[C_1(\mu) Q_1 + C_2(\mu) Q_2 \right], \quad (2.3.27)$$

where $Q_1 \equiv 4 [\bar{q}_2^\alpha \gamma^\mu P_L q_1^\beta] [\bar{q}_3^\beta \gamma^\mu P_L q_4^\alpha]$ and $Q_2 \equiv 4 [\bar{q}_2^\alpha \gamma^\mu P_L q_1^\alpha] [\bar{q}_3^\beta \gamma^\mu P_L q_4^\beta]$.

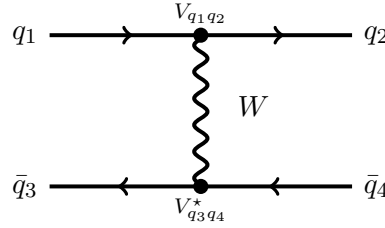


Figure 2.3: Tree-level contribution for $q_1 \bar{q}_3 \rightarrow q_2 \bar{q}_4$ in the SM.

In an ideal world where QCD does not exist, the Wilson coefficients of this effective Hamiltonian would take the following values:

$$C_1(\mu) = 0, \quad C_2(\mu) = 1, \quad (2.3.28)$$

which can also be seen in Figure 2.3, where there is not exchange of colour between both currents. However, in the real world, where QCD effects are not negligible, this transition has additional QCD contributions. In Figure 2.4, we show all one-loop QCD corrections. In the diagrams (c), (d), (e) and (f), there is an exchange of colours between currents which clearly produces a C_1 contribution through the following Fierz rearrangement of the Gell-Mann matrices,

$$T_{\alpha\beta}^a T_{\gamma\rho}^a = -\frac{1}{2 N_C} \delta_{\alpha\beta} \delta_{\gamma\rho} + \frac{1}{2} \delta_{\alpha\rho} \delta_{\gamma\beta}. \quad (2.3.29)$$

2.3.2.1 Computation of the fundamental amplitude

In the following, we give a detailed overview of the computation for each Feynman diagram in Figure 2.4. Before we start with it, we must specify the prescriptions adopted:

- The Feynman rules are defined in Appendix B.

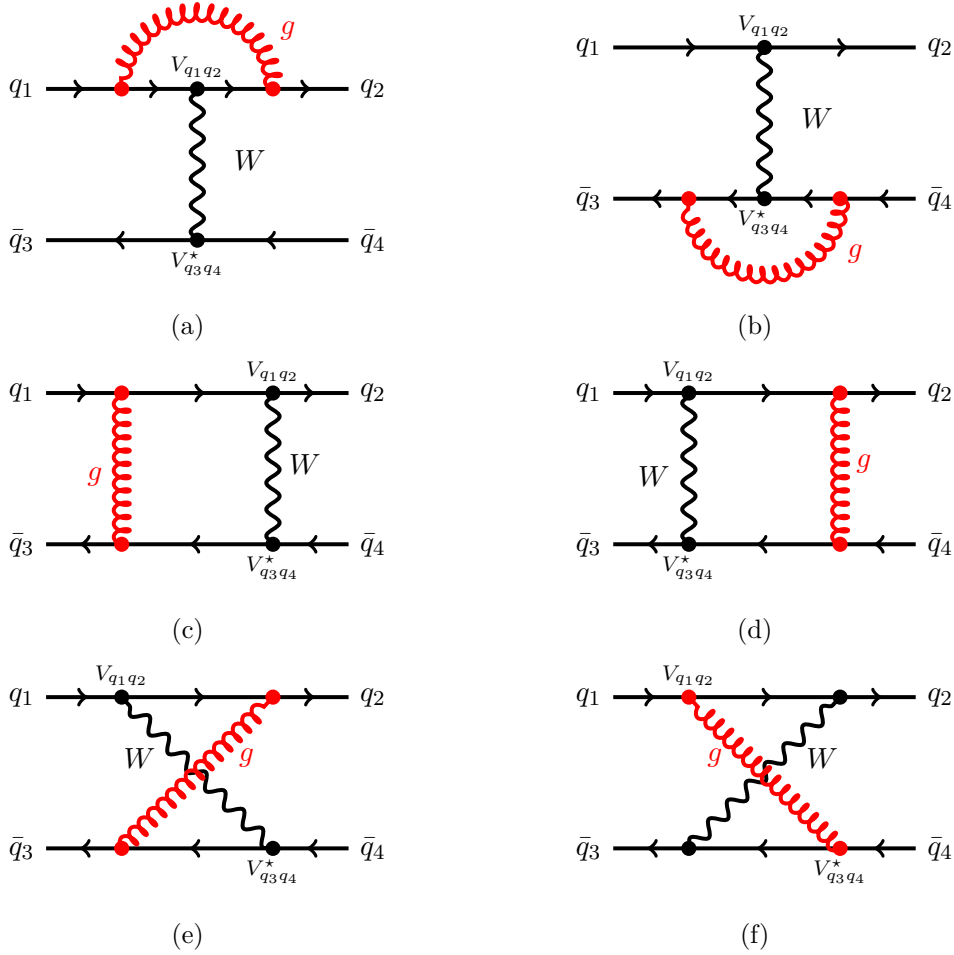


Figure 2.4: One-loop QCD corrections for $q_1 \bar{q}_3 \rightarrow q_2 \bar{q}_4$ in the SM.

- The computation is performed in 't-Hooft-Feynman gauge, $\xi_W = \xi_g = 1$.
- All external momenta are equal $p_1 = p_2 = p_3 = p_4 = p$.
- All non-logarithmic momentum dependence is fixed on-shell ($p^2 = m_{q_i}^2$).
- All external quark masses are fixed to zero.
- We neglect constant contributions of $\mathcal{O}(\alpha_s)$.
- We do not add the quark field renormalization. Later, we explain why we can do it.

Feynman diagram (0)

The amplitude for the Feynman diagram **(0)** is

$$\begin{aligned} \mathcal{M}_{(0)} &= \left(\frac{ig}{\sqrt{2}} \right)^2 \frac{i}{M_W^2} V_{q_1 q_2} V_{q_3 q_4}^* \left[\bar{v}_{q_3}^\alpha(p_3) \gamma_\mu P_L v_{q_4}^\alpha(p_4) \right] \left[\bar{u}_{q_2}^\beta(p_2) \gamma^\mu P_L u_{q_1}^\beta(p_1) \right] \\ &= -i \frac{G_F}{\sqrt{2}} V_{q_1 q_2} V_{q_3 q_4}^* S_2, \end{aligned} \quad (2.3.30)$$

where

$$S_1 \equiv \left[\bar{v}_{q_3}^\alpha(p_3) \gamma_\mu (1 - \gamma_5) v_{q_4}^\beta(p_4) \right] \left[\bar{u}_{q_2}^\beta(p_2) \gamma^\mu (1 - \gamma_5) u_{q_1}^\alpha(p_1) \right], \quad (2.3.31)$$

$$S_2 \equiv \left[\bar{v}_{q_3}^\alpha(p_3) \gamma_\mu (1 - \gamma_5) v_{q_4}^\alpha(p_4) \right] \left[\bar{u}_{q_2}^\beta(p_2) \gamma^\mu (1 - \gamma_5) u_{q_1}^\beta(p_1) \right]. \quad (2.3.32)$$

Feynman diagram (a)

The amplitude for the Feynman diagram **(a)** is

$$\begin{aligned} \mathcal{M}_{(a)} &= \left(\frac{ig}{\sqrt{2}} \right)^2 \frac{i}{M_W^2} V_{q_1 q_2} V_{q_3 q_4}^* \int \frac{d^D k}{(2\pi)^D} \left[\bar{v}_{q_3}^\gamma(p_3) \gamma_\mu P_L v_{q_4}^\gamma(p_4) \right] \left(-\frac{i}{k_1^2} \delta_{ab} \right) g^{\alpha_1 \alpha_2} \cdot \\ &\cdot \left[\bar{u}_{q_2}^\beta(p_2) (-i g_s \gamma_{\alpha_1} T_{\beta\gamma}^a) \frac{i(k_3^2 + m_{q_2}^2)}{k_3^2 - m_{q_2}^2} \gamma^\mu P_L \frac{i(k_2^2 + m_{q_1}^2)}{k_2^2 - m_{q_1}^2} (-i \gamma_{\alpha_2} T_{\gamma\alpha}^b) u_{q_1}^\beta(p_1) \right] \\ &= 16 \sqrt{2} \pi G_F \alpha_s C_F V_{q_1 q_2} V_{q_3 q_4}^* \int \frac{d^D k}{(2\pi)^D} \frac{k_3^{\alpha_1} k_2^{\alpha_2}}{k_1^2 k_2^2 k_3^2} \cdot \\ &\cdot \left[\bar{v}_{q_3}^\alpha(p_3) \gamma_\mu P_L v_{q_4}^\alpha(p_4) \right] \left[\bar{u}_{q_2}^\beta(p_2) \gamma_{\alpha_2} \gamma^\mu \gamma_{\alpha_1} P_L u_{q_1}^\beta(p_1) \right], \end{aligned} \quad (2.3.33)$$

where $\alpha_s \equiv \frac{g_s^2}{4\pi}$, $k_1 \equiv k$, $k_2 \equiv k + p$ and $k_3 \equiv k + p$. In addition, we have made use of the following Dirac algebra identity

$$\gamma_{\mathfrak{X}} \gamma^{\alpha_1} \gamma^\mu \gamma^{\alpha_2} \gamma^{\mathfrak{X}} = -2 \gamma^{\alpha_2} \gamma^\mu \gamma^{\alpha_1}, \quad (2.3.34)$$

and the Gell-Mann identity

$$(T^a T^a)_{\alpha\beta} = C_F \delta_{\alpha\beta}, \quad C_F \equiv \frac{N_C^2 - 1}{2N_C}, \quad (2.3.35)$$

which can be directly extracted from Eq. (2.3.29). The integral in Eq. (2.3.33) can be computed using dimensional regularization with the following result:

$$\int \frac{d^D k}{(2\pi)^D} \frac{k^{\alpha_1} k^{\alpha_2}}{k^4 (k-p)^2} = -\frac{i}{(4\pi)^2} \frac{\mu^{2\epsilon}}{4} g^{\alpha_1 \alpha_2} \left[\frac{1}{\hat{\epsilon}} + \ln \left(\frac{p^2}{\mu^2} \right) \right]. \quad (2.3.36)$$

where $D \equiv 4 + 2\epsilon$ and

$$\frac{1}{\hat{\epsilon}} \equiv \frac{1}{\epsilon} + \gamma_E - \ln(4\pi), \quad (2.3.37)$$

where $\gamma_E = 0.57721 \dots$ is the Euler-Mascheroni constant. Finally, the amplitude becomes

$$\mathcal{M}_{(a)} = +i \frac{G_F}{\sqrt{2}} V_{q_1 q_2} V_{q_3 q_4}^* \left(\frac{\alpha_s(\mu)}{4\pi} \right) C_F \left[\frac{1}{\hat{\epsilon}} + \ln \left(\frac{p^2}{\mu^2} \right) \right] S_2, \quad (2.3.38)$$

where $\alpha_s(\mu) \equiv \frac{g_s^2 \mu^{2\epsilon}}{4\pi}$.

Feynman diagrams (b), (c), (d), (e) and (f)

Similarly to the Feynman diagram (a), we obtain the following amplitudes for the other Feynman diagrams

$$\mathcal{M}_{(b)} = \mathcal{M}_{(a)}, \quad (2.3.39)$$

$$\mathcal{M}_{(c)} = \mathcal{M}_{(d)} = -i \frac{G_F}{\sqrt{2}} V_{q_1 q_2} V_{q_3 q_4}^* \left(\frac{\alpha_s(\mu)}{4\pi} \right) \ln \left(\frac{p^2}{M_W^2} \right) \left[\frac{1}{2N_C} S_2 - \frac{1}{2} S_1 \right], \quad (2.3.40)$$

$$\mathcal{M}_{(e)} = \mathcal{M}_{(f)} = -i \frac{G_F}{\sqrt{2}} V_{q_1 q_2} V_{q_3 q_4}^* \left(\frac{\alpha_s(\mu)}{4\pi} \right) \ln \left(\frac{p^2}{M_W^2} \right) \left[2 S_1 - \frac{2}{N_C} S_2 \right]. \quad (2.3.41)$$

Total sum

Finally, the fundamental amplitude is given by

$$\begin{aligned} \mathcal{A}_{\text{fun}} &= i \left(\mathcal{M}_{(0)} + 2 \mathcal{M}_{(a)} + 2 \mathcal{M}_{(c)} + 2 \mathcal{M}_{(e)} \right) \\ &= \frac{G_F}{\sqrt{2}} V_{q_1 q_2} V_{q_3 q_4}^* \left\{ \left(1 + 2 C_F \left(\frac{\alpha_s(\mu)}{4\pi} \right) \left[-\frac{1}{\hat{\epsilon}} + \ln \left(\frac{\mu^2}{M_W^2} \right) \right] \right) S_2 \right. \\ &\quad \left. + \frac{3}{N_C} \left(\frac{\alpha_s(\mu)}{4\pi} \right) \ln \left(\frac{M_W^2}{p^2} \right) S_2 - 3 \left(\frac{\alpha_s(\mu)}{4\pi} \right) \ln \left(\frac{M_W^2}{p^2} \right) S_1 \right\}. \quad (2.3.42) \end{aligned}$$

2.3.2.2 Computation of the effective amplitude

In the computation of the effective amplitude, we use the same prescriptions as for the fundamental amplitude. In Figures 2.5 and 2.6, we show the diagrams from the effective theory with and without QCD corrections respectively. Since the calculation is quite similar to the fundamental case, we just give the final amplitudes for each Feynman diagram.

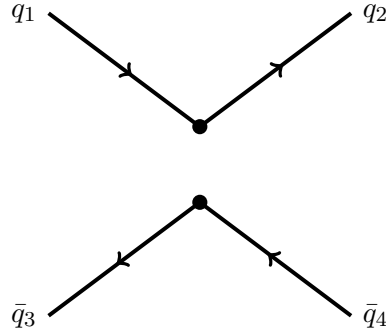


Figure 2.5: Tree-level contribution for $q_1 \bar{q}_3 \rightarrow q_2 \bar{q}_4$ in the EFT.

Feynman diagram (0)

The amplitude for the Feynman diagram (0) is

$$\mathcal{M}_{(0)}^i = -i \frac{G_F}{\sqrt{2}} V_{q_1 q_2} V_{q_3 q_4}^* C_i(\mu) S_i ,$$

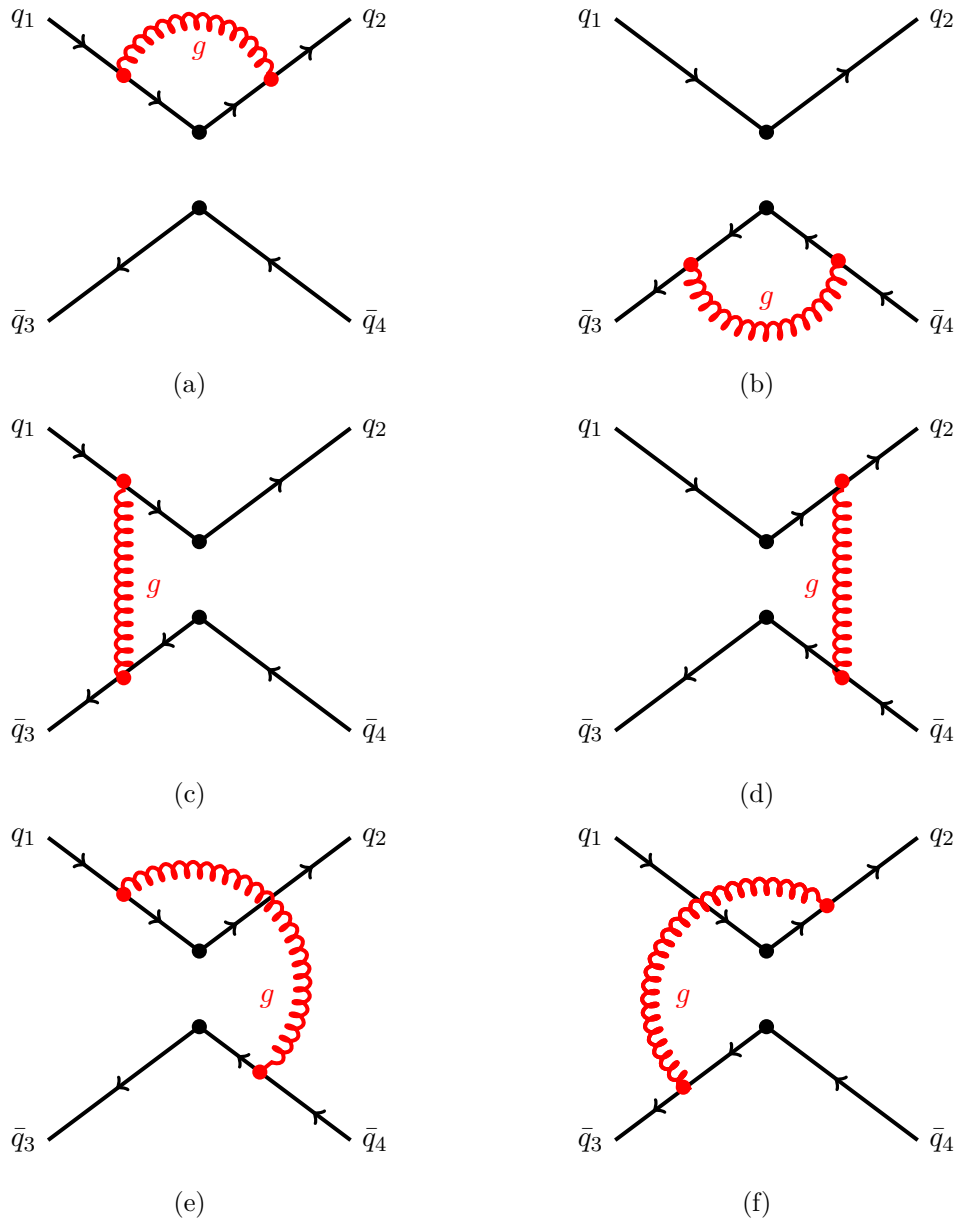
where $i = 1, 2$ depending on the local operator.

Feynman diagram (a)

The amplitude for the Feynman diagram (a) is

$$\mathcal{M}_{(a)}^1 = +i \frac{G_F}{\sqrt{2}} V_{q_1 q_2} V_{q_3 q_4}^* C_1(\mu) \left(\frac{\alpha_s(\mu)}{4\pi} \right) \left[\frac{1}{\hat{\epsilon}} + \ln \left(\frac{p^2}{\mu^2} \right) \right] \left(-\frac{1}{2N_C} S_1 + \frac{1}{2} S_2 \right) ,$$

$$\mathcal{M}_{(a)}^2 = +i \frac{G_F}{\sqrt{2}} V_{q_1 q_2} V_{q_3 q_4}^* C_2(\mu) \left(\frac{\alpha_s(\mu)}{4\pi} \right) \left[\frac{1}{\hat{\epsilon}} + \ln \left(\frac{p^2}{\mu^2} \right) \right] C_F S_2 .$$

Figure 2.6: One-loop QCD corrections for $q_1 \bar{q}_3 \rightarrow q_2 \bar{q}_4$ in the EFT.

Feynman diagram (b)

The amplitude for the Feynman diagram **(b)** is

$$\begin{aligned}\mathcal{M}_{(b)}^1 &= \mathcal{M}_{(a)}^1, \\ \mathcal{M}_{(b)}^2 &= \mathcal{M}_{(a)}^2.\end{aligned}$$

Feynman diagram (c)

The amplitude for the Feynman diagram **(c)** is

$$\begin{aligned}\mathcal{M}_{(c)}^1 &= +i \frac{G_F}{\sqrt{2}} V_{q_1 q_2} V_{q_3 q_4}^* C_1(\mu) \left(\frac{\alpha_s(\mu)}{4\pi} \right) \left[\frac{1}{\hat{\epsilon}} + \ln \left(\frac{p^2}{\mu^2} \right) \right] C_F S_1, \\ \mathcal{M}_{(c)}^2 &= +i \frac{G_F}{\sqrt{2}} V_{q_1 q_2} V_{q_3 q_4}^* C_2(\mu) \left(\frac{\alpha_s(\mu)}{4\pi} \right) \left[\frac{1}{\hat{\epsilon}} + \ln \left(\frac{p^2}{\mu^2} \right) \right] \left(-\frac{1}{2N_C} S_2 + \frac{1}{2} S_1 \right).\end{aligned}$$

Feynman diagram (d)

The amplitude for the Feynman diagram **(d)** is

$$\begin{aligned}\mathcal{M}_{(d)}^1 &= \mathcal{M}_{(c)}^1, \\ \mathcal{M}_{(d)}^2 &= \mathcal{M}_{(c)}^2.\end{aligned}$$

Feynman diagram (e)

The amplitude for the Feynman diagram **(e)** is

$$\begin{aligned}\mathcal{M}_{(e)}^1 &= -i \frac{G_F}{\sqrt{2}} V_{q_1 q_2} V_{q_3 q_4}^* C_1(\mu) \left(\frac{\alpha_s(\mu)}{4\pi} \right) \left[\frac{1}{\hat{\epsilon}} + \ln \left(\frac{p^2}{\mu^2} \right) \right] \left(2 S_2 - \frac{2}{N_C} S_1 \right), \\ \mathcal{M}_{(e)}^2 &= -i \frac{G_F}{\sqrt{2}} V_{q_1 q_2} V_{q_3 q_4}^* C_2(\mu) \left(\frac{\alpha_s(\mu)}{4\pi} \right) \left[\frac{1}{\hat{\epsilon}} + \ln \left(\frac{p^2}{\mu^2} \right) \right] \left(2 S_1 - \frac{2}{N_C} S_2 \right).\end{aligned}$$

Feynman diagram (f)

The amplitude for the Feynman diagram (f) is

$$\begin{aligned}\mathcal{M}_{(f)}^1 &= \mathcal{M}_{(e)}^1, \\ \mathcal{M}_{(f)}^2 &= \mathcal{M}_{(e)}^2.\end{aligned}$$

Total sum

Finally, the effective amplitudes are

$$\begin{aligned}\mathcal{A}_{\text{eff}}^1 &= i \left(\mathcal{M}_{(0)}^1 + 2 \mathcal{M}_{(a)}^1 + 2 \mathcal{M}_{(c)}^1 + 2 \mathcal{M}_{(e)}^1 \right) \\ &= \frac{G_F}{\sqrt{2}} V_{q_1 q_2} V_{q_3 q_4}^* C_1(\mu) \left\{ \left(1 + 2 C_F \left(\frac{\alpha_s(\mu)}{4 \pi} \right) \left[-\frac{1}{\hat{\epsilon}} + \ln \left(\frac{\mu^2}{p^2} \right) \right] \right) S_1 \right. \\ &\quad \left. + \frac{3}{N_C} \left(\frac{\alpha_s(\mu)}{4 \pi} \right) \left[-\frac{1}{\hat{\epsilon}} + \ln \left(\frac{\mu^2}{p^2} \right) \right] S_1 - 3 \left(\frac{\alpha_s(\mu)}{4 \pi} \right) \left[-\frac{1}{\hat{\epsilon}} + \ln \left(\frac{\mu^2}{p^2} \right) \right] S_2 \right\} \\ &\equiv \frac{G_F}{\sqrt{2}} V_{q_1 q_2} V_{q_3 q_4}^* C_1(\mu) \langle Q_1 \rangle^{(0)},\end{aligned}\tag{2.3.43}$$

$$\begin{aligned}\mathcal{A}_{\text{eff}}^2 &= i \left(\mathcal{M}_{(0)}^2 + 2 \mathcal{M}_{(a)}^2 + 2 \mathcal{M}_{(c)}^2 + 2 \mathcal{M}_{(e)}^2 \right) \\ &= \frac{G_F}{\sqrt{2}} V_{q_1 q_2} V_{q_3 q_4}^* C_2(\mu) \left\{ \left(1 + 2 C_F \left(\frac{\alpha_s(\mu)}{4 \pi} \right) \left[-\frac{1}{\hat{\epsilon}} + \ln \left(\frac{\mu^2}{p^2} \right) \right] \right) S_2 \right. \\ &\quad \left. + \frac{3}{N_C} \left(\frac{\alpha_s(\mu)}{4 \pi} \right) \left[-\frac{1}{\hat{\epsilon}} + \ln \left(\frac{\mu^2}{p^2} \right) \right] S_2 - 3 \left(\frac{\alpha_s(\mu)}{4 \pi} \right) \left[-\frac{1}{\hat{\epsilon}} + \ln \left(\frac{\mu^2}{p^2} \right) \right] S_1 \right\} \\ &\equiv \frac{G_F}{\sqrt{2}} V_{q_1 q_2} V_{q_3 q_4}^* C_2(\mu) \langle Q_2 \rangle^{(0)}.\end{aligned}\tag{2.3.44}$$

where $\langle Q_{1,2} \rangle^{(0)}$ are the unrenormalized current-current matrix elements.

In the first terms of Eqs (2.3.43) and (2.3.44), there are diagonal divergences proportional to C_F . These divergences can be eliminated through the quark field renormalization,

$$Z_q = 1 + \frac{1}{\hat{\epsilon}} \frac{\alpha_s(\mu)}{4 \pi} C_F \quad (\overline{\text{MS}} \text{ scheme}).\tag{2.3.45}$$

However, after the renormalization of the external legs, the current-current matrix elements are still divergent. To eliminate the remaining divergences, it is necessary to perform an *operator renormalization*,

$$\langle Q_i \rangle^{(0)} = Z_q^{-2} \mathcal{Z}_{ij} \langle Q_i \rangle . \quad (2.3.46)$$

where $\langle Q_i \rangle$ are the renormalized current-current matrix elements and \mathcal{Z} is the 2×2 renormalization matrix. Introducing Eqs. (2.3.43), (2.3.44) and (2.3.45) into Eq. (2.3.46), we obtain

$$\mathcal{Z} = 1 - \frac{\alpha_s(\mu)}{4\pi} \frac{1}{\hat{\epsilon}} \begin{bmatrix} 3/N_C & -3 \\ -3 & 3/N_C \end{bmatrix} \quad (\overline{\text{MS}} \text{ scheme}) , \quad (2.3.47)$$

and then the renormalized matrix elements are given by

$$\begin{aligned} \langle Q_1 \rangle &= \left[1 + 2 C_F \frac{\alpha_s(\mu)}{4\pi} \ln \left(\frac{\mu^2}{p^2} \right) \right] S_1 + \frac{3}{N_C} \frac{\alpha_s(\mu)}{4\pi} \ln \left(\frac{\mu^2}{p^2} \right) S_1 \\ &\quad - 3 \frac{\alpha_s(\mu)}{4\pi} \ln \left(\frac{\mu^2}{p^2} \right) S_2 , \end{aligned} \quad (2.3.48)$$

$$\begin{aligned} \langle Q_2 \rangle &= \left[1 + 2 C_F \frac{\alpha_s(\mu)}{4\pi} \ln \left(\frac{\mu^2}{p^2} \right) \right] S_2 + \frac{3}{N_C} \frac{\alpha_s(\mu)}{4\pi} \ln \left(\frac{\mu^2}{p^2} \right) S_2 \\ &\quad - 3 \frac{\alpha_s(\mu)}{4\pi} \ln \left(\frac{\mu^2}{p^2} \right) S_1 . \end{aligned} \quad (2.3.49)$$

2.3.2.3 Matching condition

At this point, we are in the disposition to compute the Wilson coefficients through the following *matching condition*,

$$\mathcal{A}_{\text{fun}} = \mathcal{A}_{\text{eff}}^i , \quad i = 1, 2 . \quad (2.3.50)$$

Since in the fundamental theory, we have not renormalized the quark fields, when using Eq. (2.3.50), we must also not renormalize them in the effective theory. To obtain a correct estimation of the Wilson coefficients, it is crucial to treat the fundamental theory in the

same way as the effective theory. Since both theories have the same ultraviolet and infrared behaviour for the dynamical light degrees of freedom, the prescriptions followed during the computation of the amplitudes exactly cancel when the matching condition is applied. Finally, one obtains the Wilson coefficients which do not depend on prescriptions followed during the computation, otherwise physics would depend too. Therefore, inserting both amplitudes with the same prescriptions in Eqs. (2.3.50), we obtain the Wilson coefficients $C_{1,2}(\mu)$ performing a Taylor expansion around $\alpha_s(\mu) \approx 0$:

$$C_1(\mu) = -3 \frac{\alpha_s(\mu)}{4\pi} \ln \left(\frac{M_W^2}{\mu^2} \right), \quad (2.3.51)$$

$$C_2(\mu) = 1 + \frac{3}{N_C} \frac{\alpha_s(\mu)}{4\pi} \ln \left(\frac{M_W^2}{\mu^2} \right). \quad (2.3.52)$$

2.3.2.4 Operator mixing and diagonalization

We have seen how gluonic corrections generate contributions to the original matrix element $\langle Q_1 \rangle$ ($\langle Q_2 \rangle$) and also to the other operator $\langle Q_2 \rangle$ ($\langle Q_1 \rangle$), when this occurs we say that *the operator mix under renormalization*. In the following sections, it is useful to diagonalize these current-current matrix elements through the following change of basis

$$Q_{\pm} = \frac{Q_2 \pm Q_1}{2}, \quad C_{\pm} = C_2 \pm C_1. \quad (2.3.53)$$

The advantage of this basis is that the operators can be renormalized independently,

$$\langle Q_{\pm} \rangle^{(0)} = Z_q^{-2} \mathcal{Z}_{\pm} \langle Q_{\pm} \rangle, \quad (2.3.54)$$

being

$$\mathcal{Z}_{\pm} = 1 - \frac{\alpha_s(\mu)}{4\pi} \frac{1}{\hat{\epsilon}} \frac{3(1 \mp N_C)}{N_C} \quad (\overline{\text{MS}} \text{ scheme}). \quad (2.3.55)$$

2.3.2.5 Large logarithmic corrections

In principle, we can obtain the values of the Wilson coefficients $C_{1,2}(\mu)$ at any energy scale μ using Eqs. (2.3.51) and (2.3.52). However, there is an important technical limitation in

these equations. In our application, there are two energy scales with a very large splitting, $\mu \ll M_W$. Analyzing the size of the perturbative corrections of $C_{1,2}$, we observe that $\frac{\alpha_s(\mu)}{4\pi} \ln\left(\frac{M_W^2}{\mu^2}\right) \sim 0.4$ for $\mu \sim 1$ GeV. Then, the perturbative expansion is broken due to these large logarithmic corrections. This is not a particular case, in fact, when we study a more generic problem with different energy scales, the presence of logarithmic corrections is a general feature that emerges when the frequency modes of the fields are integrated out in the way down to low energies.

2.3.2.6 Renormalization-group improved perturbation theory

In the literature, the solution of this problem is called *Renormalization-Group Improved* (RGI) perturbation theory. It consists in re-summing all these logarithmic corrections $\left[\frac{\alpha_s(\mu)}{4\pi} \ln\left(\frac{M_W^2}{\mu^2}\right)\right]^n$ to all orders of n . This involves to solve the RGEs taking in mind the following counting rules:

$$\frac{\alpha_s(\mu)}{4\pi} \ln\left(\frac{M_W^2}{\mu^2}\right) \sim \mathcal{O}(1), \quad \frac{\alpha_s(\mu)}{4\pi} \ll 1. \quad (2.3.56)$$

For that purpose, let us consider the following physical amplitude,¹

$$\mathcal{A} = \sum_{i=\pm} C_i(\mu) \langle Q_i(\mu) \rangle. \quad (2.3.57)$$

Since \mathcal{A} is a physical observable, it can not depend on the scale μ , then we obtain

$$C_i(\mu) \frac{d\langle Q_i(\mu) \rangle}{d\mu} + \frac{dC_j(\mu)}{d\mu} \langle Q_j(\mu) \rangle = 0, \quad (2.3.58)$$

where sum over repeated indices is understood. Rewriting Eq. (2.3.58), we obtain the RGEs for the Wilson coefficients $C_{\pm}(\mu)$

$$\frac{dC_{\pm}(\mu)}{d\ln\mu} = \gamma_{\pm}(\mu) C_{\pm}(\mu), \quad (2.3.59)$$

where γ_{\pm} is the *anomalous dimension* in the diagonal basis,

$$\gamma_{\pm}(\mu) \equiv -\frac{1}{\langle Q_{\pm}(\mu) \rangle} \frac{d\langle Q_{\pm}(\mu) \rangle}{d\ln\mu} = \frac{1}{\mathcal{Z}_{\pm}(\mu)} \frac{d\mathcal{Z}_{\pm}(\mu)}{d\ln\mu} = \left(\frac{\alpha_s(\mu)}{4\pi}\right) \gamma_{\pm}^{(0)}, \quad (2.3.60)$$

¹In Eq. (2.3.57), we have omitted some global factors because they do not have any physical repercussion.

where

$$\gamma_{\pm}^{(0)} \equiv -6 \frac{(1 \mp N_C)}{N_C} . \quad (2.3.61)$$

Since the anomalous dimension matrix depend only on μ through $\alpha_s(\mu)$, we can consider the running of the strong coupling

$$\frac{d\alpha_s(\mu)}{d\ln\mu} = \beta , \quad (2.3.62)$$

where β is the QCD β -function given by

$$\beta = -2\alpha_s(\mu) \left[\beta_0 \frac{\alpha_s(\mu)}{4\pi} + \beta_1 \left(\frac{\alpha_s(\mu)}{4\pi} \right)^2 \right] + \mathcal{O}(\alpha_s^4) , \quad (2.3.63)$$

with

$$\beta_0 \equiv \frac{11 N_C - 2 f}{3} , \quad \beta_1 \equiv \frac{34}{3} N_C^2 - \frac{10}{3} N_C f - 2 C_F f , \quad (2.3.64)$$

and f the number of active flavours. Then, taking into account Eq. (2.3.62), the RGEs become

$$\frac{d C_{\pm}(\mu)}{d\alpha_s(\mu)} = \frac{\gamma_{\pm}(\alpha_s(\mu))}{\beta(\alpha_s(\mu))} C_{\pm}(\mu) , \quad (2.3.65)$$

which has the following solution

$$C_{\pm}(\mu_L) = \exp \left[\int_{\alpha_s(\mu_L)}^{\alpha_s(\mu_H)} d\alpha \frac{\gamma_{\pm}(\alpha)}{\beta(\alpha)} \right] C_{\pm}(\mu_H) , \quad \mu_L < \mu_H , \quad (2.3.66)$$

where μ_L and μ_H correspond to some low and high energy scales. This problem can also be solved in the non-diagonal basis,

$$\frac{d \vec{\mathcal{C}}(\mu)}{d\ln\mu} = \hat{\gamma}^T(\mu) \vec{\mathcal{C}}(\mu) , \quad (2.3.67)$$

where the solution is

$$\vec{\mathcal{C}}(\mu_L) = T_{\alpha} \exp \left[\int_{\alpha_s(\mu_L)}^{\alpha_s(\mu_H)} d\alpha \frac{\hat{\gamma}^T(\alpha)}{\beta(\alpha)} \right] \vec{\mathcal{C}}(\mu_H) , \quad \mu_L < \mu_H , \quad (2.3.68)$$

being $\vec{\mathcal{C}}(\mu) = (C_1(\mu), C_2(\mu))$ and T_{α} the α -ordering operator which arranges the Taylor expansion of the exponential function in such a way that coupling constants increase from

right to left. This is necessary because $\hat{\gamma}(\alpha)$ is a non-diagonal matrix that in general does not commute, $[\hat{\gamma}(\alpha_s(\mu_1)), \hat{\gamma}(\alpha_s(\mu_2))] \neq 0$.

Finally, we have re-summed all these large logarithmic corrections and the problem is reduced to the analytical computation of three quantities: $C_{\pm}(\mu_H)$, $\gamma_{\pm}(\alpha_s(\mu))$ and $\beta(\alpha_s(\mu))$. Integrating Eq. (2.3.66), we obtain the following solution

$$C_{\pm}(\mu_L) = \left[\frac{\alpha_s(\mu_L)}{\alpha_s(\mu_H)} \right]^{-\frac{\gamma_{\pm}^{(0)}}{2\beta_0}} C_{\pm}(\mu_H), \quad (2.3.69)$$

which clearly re-sum all these large logarithms,

$$\left[\frac{\alpha_s(\mu_L)}{\alpha_s(\mu_H)} \right]^{-\frac{\gamma_{\pm}^{(0)}}{2\beta_0}} = 1 + \gamma_{\pm}^{(0)} \frac{\alpha_s(\mu_H)}{4\pi} \ln\left(\frac{\mu_L}{\mu_H}\right) + \mathcal{O}\left(\alpha_s^2(\mu_H) \ln^2\left(\frac{\mu_L}{\mu_H}\right)\right).$$

In Figures 2.7, we plot the dependence of the Wilson coefficients as function of low energy scale μ_L . We have taken $C_1(M_W) = 0$ and $C_2(M_W) = 1$ from Eqs. (2.3.51) and (2.3.52). The plot shows that the mixing between the operators has a significant impact to low energies at few GeVs.

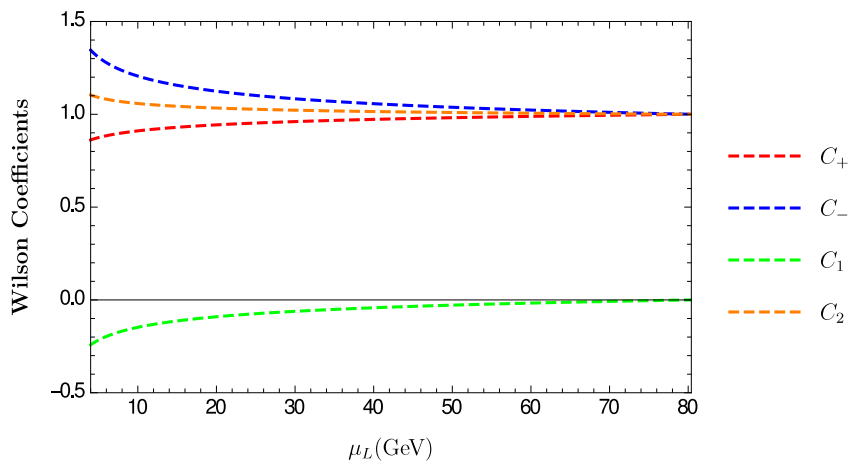


Figure 2.7: Wilson coefficients as function of μ_L

2.3.3 Some final comments or remarks

In the previous example, we have used the RGEs to go down from the electroweak scale to the charm quark scale. For $m_c < \mu_L < m_b$, the bottom quark field ceases to be a dynamical degree of freedom and leads into an EFT with 4 flavours instead of 5. In this EFT transition, there are QCD corrections that are known as *threshold effects*, further details can be found in Refs. [49, 50].

In addition, we would like to point out how the numbers $-2/9$ and $-6/23$ in Eqs. (1.4.108) and (1.4.109) respectively correspond to simple gluonic QCD corrections to the typical current-current operators that govern the neutral meson mixing. These numbers come from the power $-\frac{\gamma_+^{(0)}}{2\beta_0}$ for $f = 3$ and $f = 5$ respectively.

In this chapter, we have not introduced the EFT for non-perturbative regimes below 1 GeV, Chiral Perturbation Theory (χ PT). We prefer to introduce it in the next chapter where we study the direct CP violating ratio ε'/ε from $K^0 \rightarrow \pi\pi$ in the SM. For this prediction, it is necessary to use some non-perturbative tools like χ PT, large- N_C , etc. Then, some of the powerful non-perturbative techniques used in particle physics are introduced there.

Chapter 3

Direct CP violation in kaon decays

In 1988 the NA31 experiment presented the first evidence of direct CP violation in the $K^0 \rightarrow \pi\pi$ decay amplitudes. A clear signal with a 7.2σ statistical significance was later established with the full data samples from the NA31, E731, NA48 and KTeV experiments, confirming that CP violation is associated with a $\Delta S = 1$ quark transition, as predicted by the SM. However, the theoretical prediction for the measured ratio ε'/ε has been a subject of strong controversy along the years. Although the underlying physics was already clarified in 2001, the recent release of improved lattice data has revived again the theoretical debate. In this chapter, we review the current status, discussing in detail the different ingredients that enter into the calculation of this observable and the reasons why seemingly contradictory predictions were obtained in the past by several groups. Finally, an update of the SM prediction is presented and the prospects for future improvements are analysed. The content of this chapter is based on Ref. [52].

3.1 Historical prelude

The investigation of kaon decays [53] has a fruitful record of very important scientific achievements, being at the origin of many of the fundamental ingredients that have given rise to the current structure of the EWSM [13–15]: the flavour concept of strangeness

[54, 55], parity violation [56, 57], meson-antimeson oscillations [58], quark mixing [23], GIM mechanism [21] and CP violation [24, 59]. Since their discovery in 1947 [60], kaons have played a very significant role in our understanding of fundamental physics, providing accurate tests of quantum mechanics and uncovering the existence of higher-mass scales such as the charm [21, 61] and the top quarks [24, 62]. Nowadays, the kaon decay data continue having a major impact on flavour phenomenology and impose very stringent constraints on plausible scenarios of New Physics (NP).

The measured ratios of $K_L \rightarrow \pi\pi$ and $K_S \rightarrow \pi\pi$ decay amplitudes,

$$\eta_{00} \equiv \frac{A(K_L \rightarrow \pi^0\pi^0)}{A(K_S \rightarrow \pi^0\pi^0)} \equiv \varepsilon - 2\varepsilon', \quad \eta_{+-} \equiv \frac{A(K_L \rightarrow \pi^+\pi^-)}{A(K_S \rightarrow \pi^+\pi^-)} \equiv \varepsilon + \varepsilon', \quad (3.1.1)$$

exhibit a clear violation of the CP symmetry at the per-mill level [63]

$$|\varepsilon| = \frac{1}{3} |\eta_{00} + 2\eta_{+-}| = (2.228 \pm 0.011) \cdot 10^{-3}, \quad (3.1.2)$$

which originates in a $\Delta S = 2$ transition between the K^0 and the \bar{K}^0 states [53, 59]. A more subtle effect is the existence of a tiny difference between η_{00} and η_{+-} that has been experimentally established through the ratio [64–72]

$$\text{Re}(\varepsilon'/\varepsilon) = \frac{1}{3} \left(1 - \left| \frac{\eta_{00}}{\eta_{+-}} \right| \right) = (16.6 \pm 2.3) \cdot 10^{-4}, \quad (3.1.3)$$

demonstrating the existence of direct CP violation in the $K^0 \rightarrow \pi\pi$ decay amplitudes. This measurement plays a crucial role in our understanding of the dynamical origin of the CP violation, since it confirms that it is associated with a $\Delta S = 1$ transition, as predicted by the SM with the CKM mechanism [23, 24].

The theoretical prediction of ε'/ε has a quite controversial history [73–92] because the first next-to-leading order (NLO) calculations [75–80] claimed SM values one order of magnitude smaller than (3.1.3), contradicting the clear signal observed in 1988 by the CERN NA31 collaboration [64, 65] and giving support to the null result obtained by the E731 experiment at Fermilab [69]. The final confirmation that $\text{Re}(\varepsilon'/\varepsilon) \sim 10^{-3}$, with the NA48 [66–68] and KTeV [70–72] data, triggered then a large number of new-physics

explanations for that exciting “flavour anomaly”.¹ However, it was soon realized that the former SM predictions had missed completely the important role of the final pion dynamics [86,87]. Once long-distance contributions were properly taken into account, the theoretical prediction was found to be in good agreement with the experimental value, albeit with unfortunately large uncertainties of non-perturbative origin [88].

Numerical QCD simulations on a discretised space-time volume are an appropriate tool to address non-perturbative problems. However, lattice calculations of the $K \rightarrow \pi\pi$ amplitudes face many technical challenges, associated with their Minkowskian nature (the physical amplitudes cannot be extracted from standard Euclidean lattice simulations [93]), the presence of several competing operators with a very involved dynamical interplay, and the vacuum quantum numbers of the isoscalar $\pi\pi$ final state (a large vacuum-state contribution must be subtracted, which deteriorates the signal to noise ratio). For many years, a quantitative lattice corroboration of the known enhancement of the $\Delta I = 1/2$ amplitude remained unsuccessful, while attempts to estimate ε'/ε were unreliable, often obtaining negative values due to an insufficient signal in the isoscalar decay amplitude [94–97]. The situation has changed in recent years, thanks to the development of more sophisticated techniques and the increasing power of modern computers. A quite successful calculation of the $\Delta I = 3/2$ $K^+ \rightarrow \pi^+\pi^0$ amplitude has been achieved by the RBC-UKQCD collaboration [98–100], and the first statistically-significant signal of the $\Delta I = 1/2$ enhancement has recently been reported [101], confirming the qualitative dynamical understanding achieved long time ago with analytical methods [102–111].²

From its most recent lattice data, the RBC-UKQCD collaboration has also extracted a first estimate for the direct CP-violation ratio: $\text{Re}(\varepsilon'/\varepsilon) = (1.38 \pm 5.15 \pm 4.59) \cdot 10^{-4}$ [100,113]. Although the quoted errors are still large, the low central value would imply a

¹Many papers addressing the claimed discrepancy can be found at the Inspire data basis. We refrain from quoting them here.

²A large enhancement of the isoscalar $K \rightarrow \pi\pi$ amplitude has also been found at unphysical quark masses ($M_K \sim 2M_\pi$), using PACS-CS gauge configurations generated with the Iwasaki action and the $\mathcal{O}(a)$ -improved Wilson fermion action [112].

2.1 σ deviation from the experimental value in Eq. (3.1.3). This discrepancy has revived some of the old SM calculations predicting low values of ε'/ε [114–116] (missing again the crucial pion dynamics), and has triggered new studies of possible contributions from physics beyond the SM [117–143].

Before claiming any evidence for new physics, one should realize the technical limitations of the current lattice result. In order to access the Minkowskian kinematics with physical interacting pions, evading the Maini-Testa no-go theorem [93], the RBC-UKQCD simulation follows the elegant method developed by Lellouch and Lüscher [144] to relate the infinite-volume and finite-volume results. At finite volumes there is a discrete spectrum and the box size can be tuned to get pions with the desired momentum; moreover, the Lüscher quantization condition [145, 146] allows one to compute the needed S-wave phase shift of the final $\pi\pi$ state. The $(\pi\pi)_I$ phase shifts, δ_I ($I = 0, 2$), play a crucial role in the calculation and provide a quantitative test of the lattice result. While the extracted $I = 2$ phase shift is only 1σ away from its physical value, the lattice analysis of Ref. [113] finds a result for δ_0 which disagrees with the experimental value by 2.9σ , a much larger discrepancy than the one quoted for ε'/ε . Obviously, nobody is looking for any NP contribution to the $\pi\pi$ elastic scattering phase shifts. Nevertheless, although it is still premature to derive strong physics implications from these lattice results, they look already quite impressive and show that substantial improvements could be achieved in the near future [147, 148].

Meanwhile, it seems worth to revise and update the analytical SM calculation of ε'/ε [88], which is already 18 years old. A very detailed study of electromagnetic and isospin-violating corrections, which play a very important role in ε'/ε , was accomplished later [149–151]. Although the main numerical implications for the ε'/ε prediction were reported in some unpublished conference proceedings [92] and have been quoted in more recent reviews [53], a complete phenomenological analysis including properly these corrections has never been presented. The penguin matrix elements that dominate the CP-violating $K \rightarrow \pi\pi$ amplitudes are also quite sensitive to the numerical inputs adopted for the light quark masses. Thanks to the impressive lattice progress achieved in recent years [152],

the quark masses are nowadays determined with a much better precision and their impact on ε'/ε must be investigated. Moreover, we have now a better understanding of several non-perturbative ingredients entering the calculation such as chiral low-energy constants and large- N_C relations [153–169].

A convenient decomposition of the $K \rightarrow \pi\pi$ amplitudes [150] that allows us to incorporate electromagnetic and isospin-violating corrections, closely following the familiar isospin notation, is presented in Section 3.2. We also review there the phenomenological expressions needed to compute ε'/ε and the isospin-breaking corrections computed in Refs. [149–151] and updated in the next chapter. The short-distance contributions to ε'/ε are detailed in Section 3.3, where large logarithmic corrections $\sim \alpha_s^k(\mu) \log^n(M_W/\mu)$ are summed up with the renormalization group, at the NLO ($k = n, n + 1$). The hadronic matrix elements of the relevant four-quark operators are discussed in Section 3.4. Their chiral $SU(3)_L \otimes SU(3)_R$ symmetry properties are analysed, emphasizing the reasons why the strong and electroweak penguin operators Q_6 and Q_8 dominate the CP-odd kaon decay amplitudes into final pions with $I = 0$ and 2, respectively. Using the large- N_C limit we also provide there a first simplified estimate of ε'/ε that exhibits the presence of a subtle numerical cancellation. This estimate allows us to easily understand the numerical values quoted in Ref. [116]. Sections 3.5, 3.6 and 3.7 present a much more powerful EFT approach to the problem. The low-energy realization of the short-distance $\Delta S = 1$ effective Lagrangian is analysed in Section 3.5, using the well-known techniques of χ PT [170–176] that make possible to pin down the long-distance contributions to the $K \rightarrow \pi\pi$ amplitudes and unambiguously determine the logarithmic chiral corrections. Section 3.6 discusses the matching between the short-distance Lagrangian and χ PT and shows how the chiral couplings can be determined at $N_C \rightarrow \infty$. The kaon decay amplitudes are worked out in Section 3.7, at the NLO in the chiral expansion. The one-loop chiral corrections are rather large and have a very important impact on ε'/ε because they destroy the numerical cancellation present in simplified analyses. This is explained in Section 3.8, which contains the updated determination of the CP-violating ratio. A detailed discussion of the current result and the prospects for future improvements are finally given in Section 3.9. The

input values adopted for the different parameters entering in the analysis are collected in the Appendix C.

3.2 Anatomy of ε'/ε

The $K \rightarrow \pi\pi$ decay amplitudes can be parametrized in the general form³ [150]

$$\begin{aligned} A(K^0 \rightarrow \pi^+\pi^-) &= \mathcal{A}_{1/2} + \frac{1}{\sqrt{2}} (\mathcal{A}_{3/2} + \mathcal{A}_{5/2}) = A_0 e^{i\chi_0} + \frac{1}{\sqrt{2}} A_2 e^{i\chi_2}, \\ A(K^0 \rightarrow \pi^0\pi^0) &= \mathcal{A}_{1/2} - \sqrt{2} (\mathcal{A}_{3/2} + \mathcal{A}_{5/2}) = A_0 e^{i\chi_0} - \sqrt{2} A_2 e^{i\chi_2}, \\ A(K^+ \rightarrow \pi^+\pi^0) &= \frac{3}{2} \left(\mathcal{A}_{3/2} - \frac{2}{3} \mathcal{A}_{5/2} \right) = \frac{3}{2} A_2^+ e^{i\chi_2^+}, \end{aligned} \quad (3.2.4)$$

which expresses the three physical amplitudes in terms of three complex quantities $\mathcal{A}_{\Delta I}$ that are generated by the $\Delta I = \frac{1}{2}, \frac{3}{2}, \frac{5}{2}$ components of the electroweak effective Hamiltonian, in the limit of isospin conservation. Writing $\mathcal{A}_{1/2} \equiv A_0 e^{i\chi_0}$, $\mathcal{A}_{3/2} + \mathcal{A}_{5/2} \equiv A_2 e^{i\chi_2}$ and $\mathcal{A}_{3/2} - \frac{2}{3}\mathcal{A}_{5/2} \equiv A_2^+ e^{i\chi_2^+}$, our notation closely follows the usual isospin decomposition. In the CP-conserving limit the amplitudes, A_0 , A_2 and A_2^+ are real and positive by definition.

In the SM, $\mathcal{A}_{5/2} = 0$ in the absence of electromagnetic interactions. If isospin symmetry is assumed, A_0 and $A_2 = A_2^+$ correspond to the decay amplitudes into the $(\pi\pi)_{I=0,2}$ final states. The phases χ_0 and $\chi_2 = \chi_2^+$ can then be identified with the S-wave $\pi\pi$ scattering phase shifts δ_I at $\sqrt{s} = M_K$, up to isospin-breaking effects [150, 151].

In the isospin limit (keeping the physical meson masses in the phase space), A_0 , A_2 and the phase difference $\chi_0 - \chi_2$ can be directly extracted from the measured $K \rightarrow \pi\pi$

³Including electromagnetic corrections, this parametrization holds for the infrared-finite amplitudes after the Coulomb and infrared parts are removed and treated in combination with real photon emission [150].

branching ratios [177]:

$$\begin{aligned} A_0 &= (2.704 \pm 0.001) \cdot 10^{-7} \text{ GeV} , \\ A_2 &= (1.210 \pm 0.002) \cdot 10^{-8} \text{ GeV} , \\ \chi_0 - \chi_2 &= (47.5 \pm 0.9)^\circ . \end{aligned} \quad (3.2.5)$$

They exhibit a strong enhancement of the isoscalar amplitude with respect to the isotensor one (the so-called “ $\Delta I = \frac{1}{2}$ rule”),

$$\omega \equiv \frac{\text{Re}A_2}{\text{Re}A_0} \approx \frac{1}{22} , \quad (3.2.6)$$

and a large phase-shift difference between the two isospin amplitudes, which mostly originates in the strong S-wave rescattering of the two final pions with $I = 0$. This implies that 50% of the $\mathcal{A}_{1/2}/\mathcal{A}_{3/2}$ ratio originates from the absorptive contribution:

$$\frac{\text{Abs}(\mathcal{A}_{1/2}/\mathcal{A}_{3/2})}{\text{Dis}(\mathcal{A}_{1/2}/\mathcal{A}_{3/2})} = 1.09 . \quad (3.2.7)$$

We would see later their strong implications on ε'/ε .

When CP violation is turned on, the amplitudes A_0 , A_2 and A_2^+ acquire imaginary parts. The direct CP-violating signal is generated by the interference of the two possible $K^0 \rightarrow \pi\pi$ decay amplitudes, with different weak and strong phases. To first order in CP violation,

$$\varepsilon' = \frac{1}{3} (\eta_{+-} - \eta_{00}) = -\frac{i}{\sqrt{2}} e^{i(\chi_2 - \chi_0)} \hat{\omega} \left[\frac{\text{Im}A_0}{\text{Re}A_0} - \frac{\text{Im}A_2}{\text{Re}A_2} \right] , \quad (3.2.8)$$

with

$$\hat{\omega} = \frac{\omega}{1 - \frac{\omega}{\sqrt{2}} e^{i(\chi_2 - \chi_0)} - \omega^2 e^{2i(\chi_2 - \chi_0)}} \approx \omega . \quad (3.2.9)$$

Thus, ε' is suppressed by the small dynamical ratio ω . The global phase $\phi_{\varepsilon'} = \chi_2 - \chi_0 + \pi/2 = (42.5 \pm 0.9)^\circ$ is very close to $\phi_\varepsilon \approx \tan^{-1} [2(m_{K_L} - m_{K_S})/(\Gamma_{K_S} - \Gamma_{K_L})] = (43.52 \pm 0.05)^\circ$ [63], the so-called superweak phase. This implies that $\cos(\phi_{\varepsilon'} - \phi_\varepsilon) \approx 1$ and ε'/ε is approximately real.

Eq. (3.2.8) involves a very delicate numerical balance between the two isospin contributions. In order to minimize hadronic uncertainties, the CP-conserving amplitudes $\text{Re}A_I$

are usually set to their experimentally determined values. A first-principle calculation is only needed for the CP-odd amplitudes $\text{Im}A_0$ and $\text{Im}A_2$, which are dominated by the strong and electromagnetic penguin contributions, respectively, to be discussed in the next section. However, naive estimates of $\text{Im}A_I$ result in a large numerical cancellation between the two terms, leading to unrealistically low values of ε'/ε [75–80]. The true SM prediction is then very sensitive to the precise values of the two isospin contributions [83, 85]. Small corrections to any of the two amplitudes get strongly amplified in Eq. (3.2.8) because they destroy the accidental numerical cancellation.

Isospin violation plays a very important role in ε'/ε due to the large ratio $1/\omega$. Small isospin-violating corrections to the dominant decay amplitude A_0 generate very sizeable contributions to A_2 , which have obviously a direct impact on ε'/ε . Isospin-breaking effects in $K \rightarrow \pi\pi$ decays have been systematically analysed in Refs. [149–151], including corrections from electromagnetic interactions, at NLO in χ PT. To first order in isospin violation, ε' can be expressed in the following form, which makes explicit all sources of isospin breaking:

$$\varepsilon' = -\frac{i}{\sqrt{2}} e^{i(\chi_2 - \chi_0)} \omega_+ \left[\frac{\text{Im}A_0^{(0)}}{\text{Re}A_0^{(0)}} \left(1 + \Delta_0 + f_{5/2}\right) - \frac{\text{Im}A_2}{\text{Re}A_2^{(0)}} \right]. \quad (3.2.10)$$

From the (isospin conserving) phenomenological fit in Eq. (3.2.5), one actually extracts $\omega_+ = \text{Re}A_2^+/\text{Re}A_0$, which differs from ω by a pure $\Delta I = \frac{5}{2}$ correction induced by the electromagnetic interaction at NLO, *i.e.*, at $\mathcal{O}(e^2 p^2)$ [53, 149–151],

$$f_{5/2} = \frac{\text{Re}A_2}{\text{Re}A_2^+} - 1 = \frac{\omega_+}{\omega} - 1 = (8.44 \pm 0.02_{\text{exp}} \pm 2.5_{\text{th}}) \cdot 10^{-2}. \quad (3.2.11)$$

The superscript (0) on the amplitudes denotes the isospin limit and [149, 150]

$$\Delta_0 = \frac{\text{Im}A_0}{\text{Im}A_0^{(0)}} \frac{\text{Re}A_0^{(0)}}{\text{Re}A_0} - 1 = (8.4 \pm 3.6) \cdot 10^{-2}, \quad (3.2.12)$$

includes corrections of $\mathcal{O}[(m_u - m_d)p^2, e^2 p^2]$. The final numerical result for Δ_0 is governed to a large extent by the electromagnetic penguin contribution to $\text{Im}A_0$.

The expression (3.2.10) takes already into account that $\text{Im}A_2$ is itself of first order in isospin violation. It is convenient to separate the leading contribution of the electromag-

netic penguin operator from the isospin-breaking effects generated by other four-quark operators:

$$\text{Im}A_2 = \text{Im}A_2^{\text{emp}} + \text{Im}A_2^{\text{non-emp}} . \quad (3.2.13)$$

This separation is renormalization-scheme dependent,⁴ but allows one to identify those isospin-violating contributions which are enhanced by the ratio $1/\omega$ and write them explicitly as corrections to the $I = 0$ side through the parameter [149, 150]

$$\Omega_{\text{IB}} = \frac{\text{Re}A_0^{(0)}}{\text{Re}A_2^{(0)}} \frac{\text{Im}A_2^{\text{non-emp}}}{\text{Im}A_0^{(0)}} = (22.7 \pm 7.6) \cdot 10^{-2} . \quad (3.2.14)$$

This quantity includes a sizeable contribution from π^0 - η mixing [178] which dominates the full NLO correction from strong isospin violation: $\Omega_{\text{IB}}^{\alpha=0} = (15.9 \pm 4.5) \cdot 10^{-2}$. Electromagnetic contributions are responsible for the numerical difference with the value in Eq. (3.2.14).

The phenomenological analysis of ε'/ε can then be more easily performed with the expression

$$\text{Re}(\varepsilon'/\varepsilon) = -\frac{\omega_+}{\sqrt{2}|\varepsilon|} \left[\frac{\text{Im}A_0^{(0)}}{\text{Re}A_0^{(0)}} (1 - \Omega_{\text{eff}}) - \frac{\text{Im}A_2^{\text{emp}}}{\text{Re}A_2^{(0)}} \right] , \quad (3.2.15)$$

with [149, 150]

$$\Omega_{\text{eff}} = \Omega_{\text{IB}} - \Delta_0 - f_{5/2} = (6.0 \pm 7.7) \cdot 10^{-2} . \quad (3.2.16)$$

Notice that there is a large numerical cancellation among the different isospin-breaking corrections. Although the separate strong and electromagnetic contributions are sizeable, they interfere destructively leading to a final isospin-violation correction of moderate size. In the next chapter, an update of these isospin violating effects is presented, in this chapter we use the values adopted in Ref. [52].

⁴ The renormalization-scheme ambiguity is only present in the electromagnetic contribution. The splitting between $\text{Im}A_2^{\text{emp}}$ and $\text{Im}A_2^{\text{non-emp}}$ has been performed (in the $\overline{\text{MS}}$ scheme with naive dimensional regularization) matching the short-distance Hamiltonian and χ PT effective descriptions (see the next sections) at leading order in $1/N_C$.

3.3 Short-distance contributions

In the SM, the flavour-changing $\Delta S = 1$ transition proceeds through the exchange of a W boson between two weak charged currents. Since $M_K \ll M_W$, the heavy W boson can be integrated out and the effective interaction reduces to a local four-fermion operator, $[\bar{s}\gamma^\mu(1 - \gamma_5)u][\bar{u}\gamma_\mu(1 - \gamma_5)d]$, multiplied by the Fermi coupling $G_F/\sqrt{2} = g^2/(8M_W^2)$ and the relevant CKM factors $V_{ud}V_{us}^*$. The inclusion of gluonic corrections generates additional four-fermion operators, which mix under renormalization [179–183] as we have seen in Chapter 2:

$$\begin{aligned} Q_1 &= (\bar{s}_\alpha u_\beta)_{V-A} (\bar{u}_\beta d_\alpha)_{V-A} , & Q_2 &= (\bar{s} u)_{V-A} (\bar{u} d)_{V-A} , \\ Q_3 &= (\bar{s} d)_{V-A} \sum_{q=u,d,s} (\bar{q} q)_{V-A} , & Q_4 &= (\bar{s}_\alpha d_\beta)_{V-A} \sum_{q=u,d,s} (\bar{q}_\beta q_\alpha)_{V-A} , \\ Q_5 &= (\bar{s} d)_{V-A} \sum_{q=u,d,s} (\bar{q} q)_{V+A} , & Q_6 &= (\bar{s}_\alpha d_\beta)_{V-A} \sum_{q=u,d,s} (\bar{q}_\beta q_\alpha)_{V+A} , \end{aligned} \quad (3.3.17)$$

where $V \pm A$ indicates the Lorentz structure $\gamma_\mu (1 \pm \gamma_5)$ and α, β denote color indices. When colour labels are not explicit, colour-singlet currents are understood ($\bar{q}\Gamma q \equiv \bar{q}_\alpha \Gamma q_\alpha$). The first two operators originate in the W -exchange topology of Figure 3.1a, while the QCD penguin diagram in Figure 3.1b gives rise to $Q_{3,4,5,6}$.

Four additional four-quark operators appear when one-loop electroweak corrections are incorporated. The electroweak penguin diagrams in Figure 3.1c generate the structures [184–188]

$$\begin{aligned} Q_7 &= \frac{3}{2} (\bar{s}d)_{V-A} \sum_{q=u,d,s} e_q (\bar{q}q)_{V+A} , & Q_8 &= \frac{3}{2} (\bar{s}_\alpha d_\beta)_{V-A} \sum_{q=u,d,s} e_q (\bar{q}_\beta q_\alpha)_{V+A} , \\ Q_9 &= \frac{3}{2} (\bar{s}d)_{V-A} \sum_{q=u,d,s} e_q (\bar{q}q)_{V-A} , & Q_{10} &= \frac{3}{2} (\bar{s}_\alpha d_\beta)_{V-A} \sum_{q=u,d,s} e_q (\bar{q}_\beta q_\alpha)_{V-A} , \end{aligned} \quad (3.3.18)$$

where e_q denotes the corresponding quark charge in units of $e = \sqrt{4\pi\alpha}$.

The presence of very different mass scales ($M_\pi < M_K \ll M_W$) amplifies the gluonic corrections to the $K \rightarrow \pi\pi$ amplitudes with large logarithms that can be summed up all the way down from M_W to scales $\mu < m_c$, using the OPE and the RGEs as we have seen

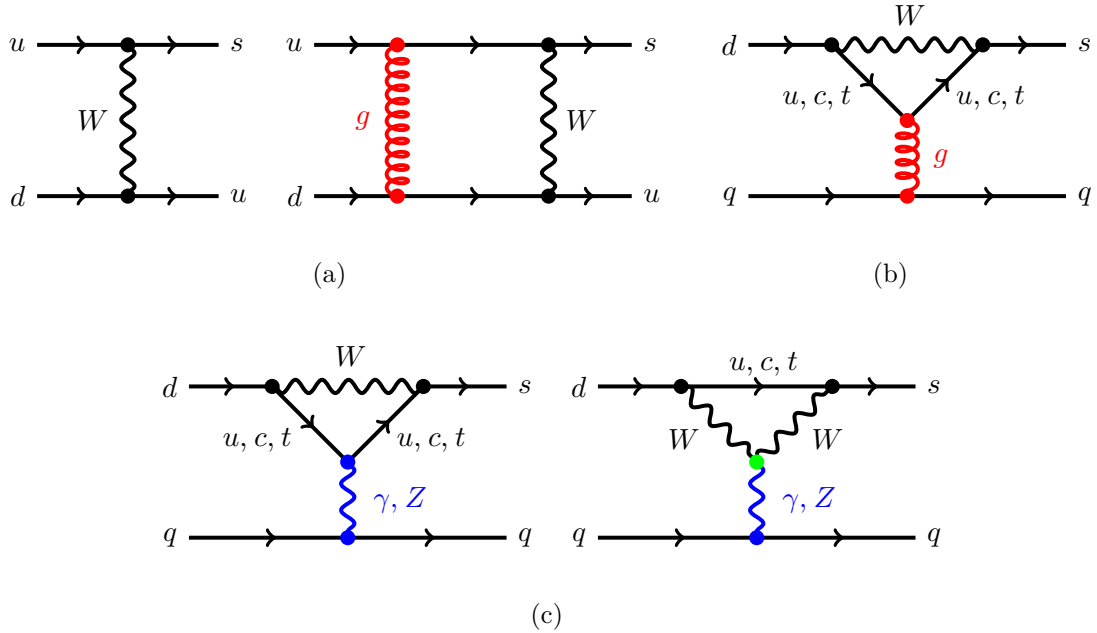


Figure 3.1: SM Feynman diagrams contributing to $\Delta S = 1$ transitions: current–current (a), QCD penguin (b) and electroweak penguin (c) topologies.

in Chapter 2. One finally gets a short-distance effective Lagrangian [49],

$$\mathcal{L}_{\text{eff}}^{\Delta S=1} = -\frac{G_F}{\sqrt{2}} V_{ud} V_{us}^* \sum_{i=1}^{10} C_i(\mu) Q_i(\mu) , \quad (3.3.19)$$

defined in the three-flavour theory, with the different local operators modulated by Wilson coefficients $C_i(\mu)$ that are functions of the heavy masses ($M_{Z,W}, m_{t,b,c} > \mu$) and CKM parameters:

$$C_i(\mu) = z_i(\mu) + \tau y_i(\mu) , \quad \tau \equiv -\frac{V_{td} V_{ts}^*}{V_{ud} V_{us}^*} . \quad (3.3.20)$$

For convenience, the global normalization in Eq. (3.3.19) incorporates the tree-level dependence on CKM factors, so that $C_i = \delta_{i2}$ at lowest order (LO), and the unitarity of the CKM matrix has been used to remove the dependences on $V_{cd} V_{cs}^*$.

The Wilson coefficients $C_i(\mu)$ are known at the next-to-leading logarithmic order [189–192]. This includes all corrections of $\mathcal{O}(\alpha_s^n t^n)$ and $\mathcal{O}(\alpha_s^{n+1} t^n)$, where $t \equiv \log(M_1/M_2)$ refers to the logarithm of any ratio of heavy mass scales $M_1, M_2 \geq \mu$. Moreover, the full

m_t/M_W dependence (at LO in α_s) is taken into account. Some next-to-next-to-leading-order (NNLO) corrections are already known [193, 194] and efforts towards a complete short-distance calculation at the NNLO are currently under way [195].

In Table 3.1 we provide the numerical values of the Wilson coefficients, computed at NLO with a renormalization scale $\mu = 1$ GeV. The results are displayed in the $\overline{\text{MS}}$ renormalization scheme for two different definitions of γ_5 within dimensional regularization: the NDR and 't Hooft-Veltman (HV) schemes [34–36, 196]. The inputs adopted for the relevant SM parameters are detailed in the Appendix C, in Table C.1. The dependence of the Wilson coefficients on the renormalization scheme and scale should cancel with a corresponding dependence on the hadronic matrix elements of the four-quark operators. However, given their non-perturbative character, a rigorous evaluation of these matrix elements, keeping full control of the QCD renormalization conventions, is a very challenging task. As shown in Table 3.1, the Wilson coefficients have a sizeable sensitivity to the chosen scheme for γ_5 , which limits the currently achievable precision. The table illustrates also their variation with the input value of the strong coupling, which has been taken in the range $\alpha_s^{(n_f=3)}(m_\tau) = 0.325 \pm 0.015$ [63, 197]. Further technical details can be found in the Appendix D.

To generate CP-violating effects, the SM requires at least three fermion families so that the CKM matrix incorporates a measurable complex phase. For the $K \rightarrow \pi\pi$ transitions, this implies that direct violations of CP can only originate from penguin diagrams where the three generations play an active role. Thus, the CP-violating parts of the decay amplitudes, $\text{Im}A_I$, are proportional to the $y_i(\mu)$ components of the Wilson coefficients, which are only non-zero for $i > 2$. In the Wolfenstein parametrization [26], $\text{Im}\tau \approx -\lambda^4 A^2 \eta \sim -6 \cdot 10^{-4}$, exhibiting the strong suppression of these effects in the SM.

3.4 Hadronic matrix elements

Symmetry considerations allow us to better understand the dynamical role of the different four-quark operators. The difference $Q_- \equiv Q_2 - Q_1$ and the QCD penguin operators

	NDR scheme	HV scheme	$\alpha_s(M_\tau)$ error
z_1	-0.4967	-0.6238	± 0.04
z_2	1.2697	1.3587	± 0.03
z_3	0.0115	0.0064	± 0.002
z_4	-0.0321	-0.0143	± 0.006
z_5	0.0073	0.0034	± 0.0007
z_6	-0.0318	-0.0124	± 0.006
z_7/α	0.0107	-0.0017	± 0.003
z_8/α	0.0121	0.0082	± 0.003
z_9/α	0.0169	0.0037	± 0.004
z_{10}/α	-0.0072	-0.0082	± 0.001
y_3	0.0318	0.0367	± 0.003
y_4	-0.0575	-0.0607	± 0.004
y_5	0.0000	0.0161	± 0.003
y_6	-0.1081	-0.0948	± 0.02
y_7/α	-0.0364	-0.0349	± 0.0004
y_8/α	0.1605	0.1748	± 0.02
y_9/α	-1.5087	-1.5103	± 0.04
y_{10}/α	0.6464	0.6557	± 0.06

Table 3.1: $\Delta S = 1$ Wilson coefficients at $\mu = 1$ GeV ($y_1 = y_2 = 0$).

$Q_{3,4,5,6}$ transform as $(8_L, 1_R)$ under chiral $SU(3)_L \otimes SU(3)_R$ transformations in the flavour space, and induce pure $\Delta I = \frac{1}{2}$ transitions. Thus, they do not contribute to the A_2 amplitude if isospin is conserved. $\Delta I = \frac{3}{2}$ transitions can only be generated through the complementary combination $Q^{(27)} \equiv 2Q_2 + 3Q_1 - Q_3$, which transforms as a $(27_L, 1_R)$

operator and can also give rise to processes with $\Delta I = \frac{1}{2}$. Owing to their explicit dependence on the quark charges e_q , the electroweak penguin operators do not have definite chiral and isospin quantum numbers. The operators Q_7 and Q_8 contain $(8_L, 1_R)$ and $(8_L, 8_R)$ components, while Q_9 and Q_{10} are combinations of $(8_L, 1_R)$ and $(27_L, 1_R)$ pieces.

The chiralities of the different Q_i operators play also a very important dynamical role. Making a Fierz rearrangement, one can rewrite all operators in terms of colour-singlet quark currents. While the $(V - A) \otimes (V - A)$ operators remain then with a similar Lorentz structure,

$$Q_4 = \sum_{q=u,d,s} (\bar{s}q)_{V-A} (\bar{q}d)_{V-A} , \quad Q_{10} = \frac{3}{2} \sum_{q=u,d,s} e_q (\bar{s}q)_{V-A} (\bar{q}d)_{V-A} , \quad (3.4.21)$$

the two $(V - A) \otimes (V + A)$ operators transform into a product of scalar/pseudoscalar currents,

$$Q_6 = -8 \sum_{q=u,d,s} (\bar{s}_L q_R) (\bar{q}_R d_L) , \quad Q_8 = -12 \sum_{q=u,d,s} e_q (\bar{s}_L q_R) (\bar{q}_R d_L) . \quad (3.4.22)$$

For light quarks, the hadronic matrix elements of this type of operators turn out to be much larger than the $(V - A) \otimes (V - A)$ ones.

This chiral enhancement can be easily estimated in the limit of a large number of QCD colours [198, 199], because the product of two colour-singlet quark currents factorizes at the hadron level into two current matrix elements:

$$\langle J \cdot J \rangle = \langle J \rangle \langle J \rangle \{1 + \mathcal{O}(1/N_C)\} . \quad (3.4.23)$$

Thus, when $N_C \rightarrow \infty$,⁵

$$\begin{aligned} \langle \pi^+ \pi^- | (\bar{s}_L \gamma^\mu u_L) (\bar{u}_L \gamma_\mu d_L) | K^0 \rangle &= \langle \pi^+ | \bar{u}_L \gamma_\mu d_L | 0 \rangle \langle \pi^- | \bar{s}_L \gamma^\mu u_L | K^0 \rangle \\ &= \frac{i\sqrt{2}}{4} F_\pi (M_K^2 - M_\pi^2) \left\{ 1 + \mathcal{O}\left(\frac{M_\pi^2}{F_\pi^2}\right) \right\} , \end{aligned} \quad (3.4.24)$$

⁵The convention for $F_{\pi,K}$ in Chapters 3 and 4 is different from the one introduced in Chapters 1 and 5, both are related through $f_{M^0} = \sqrt{2} F_{M^0}$.

while

$$\begin{aligned} \langle \pi^+ \pi^- | (\bar{s}_L u_R)(\bar{u}_R d_L) | K^0 \rangle &= \langle \pi^+ | \bar{u}_R d_L | 0 \rangle \langle \pi^- | \bar{s}_L u_R | K^0 \rangle \\ &= \frac{i\sqrt{2}}{4} F_\pi \left[\frac{M_K^2}{m_d(\mu) + m_s(\mu)} \right]^2 \left\{ 1 + \mathcal{O}\left(\frac{M_K^2}{F_\pi^2}\right) \right\}, \end{aligned} \quad (3.4.25)$$

where $F_\pi = 92.1$ MeV is the pion decay constant. Notice the μ dependence of this last matrix element, which arises because the scalar and pseudoscalar currents get renormalized, but keeping the products $m_q \bar{q}(1, \gamma_5) q$ invariant under renormalization. On the other side, the vector and axial currents are renormalization invariant, since they are protected by chiral symmetry. This different short-distance behaviour has important consequences in the analysis of ε'/ε . At $\mu = 1$ GeV, the relative ratio between the matrix elements in Eqs. (3.4.25) and (3.4.24) is a large factor $M_K^2/[m_s(\mu) + m_d(\mu)]^2 \sim 14$.

Owing to their chiral enhancement, the operators Q_6 and Q_8 dominate the CP-odd amplitudes $\text{Im}A_0^{(0)}$ and $\text{Im}A_2^{\text{emp}}$, respectively, in Eq. (3.2.15). As shown in Table 3.1, Q_6 has in addition the largest Wilson coefficient $y_i(\mu)$. Ignoring all other contributions to the CP-violating decay amplitudes, one can then make a rough estimate of ε'/ε with their matrix elements [185, 200]:

$$\text{Im}A_0|_{Q_6} = G_F A^2 \lambda^5 \eta y_6(\mu) 4 (F_K - F_\pi) \left[\frac{M_K^2}{m_d(\mu) + m_s(\mu)} \right]^2 B_6^{(1/2)}, \quad (3.4.26)$$

$$\text{Im}A_2|_{Q_8} = -\frac{G_F}{\sqrt{2}} A^2 \lambda^5 \eta y_8(\mu) 2 F_\pi \left[\frac{M_K^2}{m_d(\mu) + m_s(\mu)} \right]^2 B_8^{(3/2)}, \quad (3.4.27)$$

where $F_K = (1.193 \pm 0.003) F_\pi$ [152] is the kaon decay constant and the factors $B_6^{(1/2)}$ and $B_8^{(3/2)}$ parametrize the deviations of the true hadronic matrix elements from their large- N_C approximations; *i.e.*, $B_6^{(1/2)} = B_8^{(3/2)} = 1$ at $N_C \rightarrow \infty$.⁶ The renormalization-scale dependence of $y_6(\mu)$ and $y_8(\mu)$ is cancelled to a large extent by the running quark masses, leaving a very soft residual dependence on μ for the unknown parameters $B_6^{(1/2)}$

⁶Actually, the expressions (3.4.26) and (3.4.27) receive small chiral corrections even at $N_C \rightarrow \infty$. We will take them later into account, using an appropriate effective field theory framework.

and $B_8^{(3/2)}$. This very fortunate fact originates in the large- N_C structure of the anomalous dimension matrix γ_{ij} of the four-quark operators Q_i . At $N_C \rightarrow \infty$, all entries of this matrix are zero, except γ_{66} and γ_{88} [201]. This just reflects the factorization property in Eq. (3.4.23) and the fact that the product $m_q \bar{q} q$ is renormalization invariant.

Inserting these two matrix elements in Eq. (3.2.15) and taking the experimental values for all the other inputs, one finds

$$\text{Re}(\varepsilon'/\varepsilon) \approx 2.2 \cdot 10^{-3} \left\{ B_6^{(1/2)} (1 - \Omega_{\text{eff}}) - 0.48 B_8^{(3/2)} \right\}. \quad (3.4.28)$$

With $B_6^{(1/2)} = B_8^{(3/2)} = 1$ and $\Omega_{\text{eff}} = 0.06$, this gives $\text{Re}(\varepsilon'/\varepsilon) \approx 1.0 \cdot 10^{-3}$ as the expected order of magnitude for the SM prediction. However, there is a subtle cancellation among the three terms in Eq. (3.4.28), making the final number very sensitive to the exact values of these three inputs. For instance, with the inputs adopted in Ref. [116], $B_6^{(1/2)} = 0.57$, $B_8^{(3/2)} = 0.76$ and $\Omega_{\text{eff}} = 0.15$, one finds instead $\text{Re}(\varepsilon'/\varepsilon) \approx 2.6 \cdot 10^{-4}$, which is nearly one order of magnitude smaller and in clear conflict with the experimental value in Eq. (3.1.3). Which such a choice of inputs, the cancellation is so strong that contributions from other four-quark operators become then sizeable. On the other side, a moderate increase of $B_6^{(1/2)}$ over its large- N_C prediction, *i.e.*, $B_6^{(1/2)} > 1$, gets amplified in Eq. (3.4.28), which results in much larger values of ε'/ε .

The crucial observation made in Refs. [86–88] is that the chiral dynamics of the final-state pions generates large logarithmic corrections to the two relevant decay amplitudes, $A_0|_{Q_6}$ and $A_2|_{Q_8}$, which are of NLO in $1/N_C$. These logarithmic corrections can be rigorously computed with standard χ PT methods and are tightly related to the large phase-shift difference in Eq. (3.2.5). They turn out to be positive for $A_0|_{Q_6}$ and negative for $A_2|_{Q_8}$, destroying the numerical cancellation in Eq. (3.4.28) and bringing, therefore, a sizeable enhancement of the SM prediction for ε'/ε , in good agreement with its experimental value.

3.5 Effective field theory description

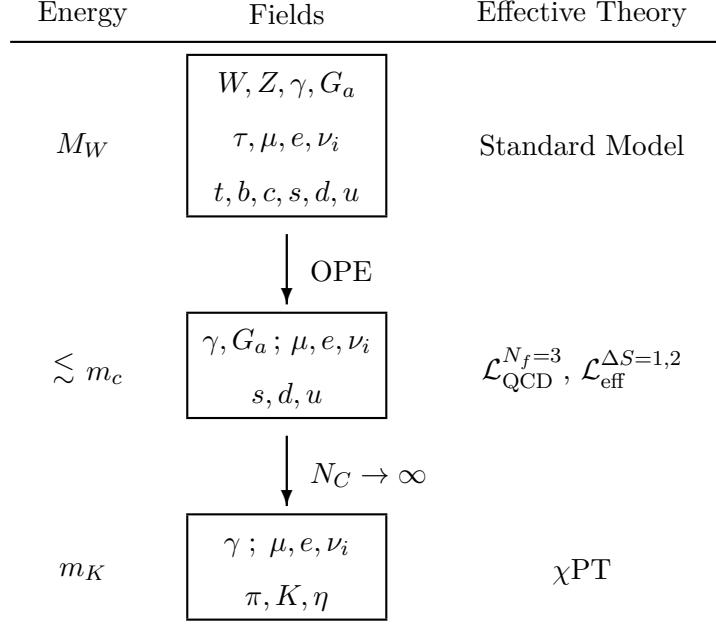
EFT provides the appropriate framework to address the multi-scale dynamics involved in kaon decays. While the short-distance electroweak transitions occur at the W mass scale, kaons and pions are the lightest particles in the QCD spectrum and their dynamics is governed by the non-perturbative regime of the strong interaction. A proper description of non-leptonic kaon decays requires then a good theoretical control of short-distance and long-distance contributions, through a combined application of perturbative and non-perturbative techniques.

We have already displayed in Eq. (3.3.19) the relevant short-distance effective Lagrangian at scales μ just below the charm mass, where perturbation theory remains still valid. This Lagrangian corresponds to an effective field theory description with all heavy ($M > \mu$) fields integrated out. Only the three light quarks (and $e, \mu, \nu_i, \gamma, G_a$) are kept as explicit dynamical fields. All informations on the heavy fields that are no longer in the effective theory are captured by the Wilson coefficients $C_i(\mu)$, which can be conveniently calculated with the OPE and renormalization-group methods as we have explained in Chapter 2.

Chiral symmetry considerations allow us to formulate another EFT that is valid at the kaon mass scale where perturbation theory can no longer be applied. Since kaons and pions are the Goldstone modes of the QCD chiral symmetry breaking, their dynamics is highly constrained by chiral symmetry, which provides a very powerful tool to describe kaon decays in a rigorous way [53]. Figure 3.2 shows schematically the chain of effective theories entering the analysis of the kaon decay dynamics.

3.5.1 Chiral perturbation theory

At very low energies, below the ρ mass scale, the hadronic spectrum only contains the pseudoscalar meson octet; *i.e.*, the Goldstone modes ϕ_a associated with the dynamical breaking of chiral symmetry by the QCD vacuum, which are conveniently parametrized

Figure 3.2: Evolution from M_W to the kaon mass scale.

through the 3×3 unitary matrix [174]

$$U(\phi) \equiv \exp \{i\sqrt{2} \Phi(x)/F\}, \quad (3.5.29)$$

where

$$\Phi(x) \equiv \sum_{a=1}^8 \frac{\lambda^a}{\sqrt{2}} \phi_a(x) = \begin{pmatrix} \frac{1}{\sqrt{2}}\pi^0 + \frac{1}{\sqrt{6}}\eta_8 & \pi^+ & K^+ \\ \pi^- & -\frac{1}{\sqrt{2}}\pi^0 + \frac{1}{\sqrt{6}}\eta_8 & K^0 \\ K^- & \bar{K}^0 & -\frac{2}{\sqrt{6}}\eta_8 \end{pmatrix}. \quad (3.5.30)$$

Under a chiral transformation $(g_L, g_R) \in SU(3)_L \otimes SU(3)_R$ in the flavour space $q \equiv (u, d, s)^T$, $q_L \rightarrow g_L q_L$, $q_R \rightarrow g_R q_R$, $U(\phi)$ transforms as $g_R U(\phi) g_L^\dagger$, inducing a non-linear transformation on the Goldstone fields $\phi_a(x)$.

The low-energy effective realization of QCD is obtained by writing the most general Lagrangian involving the matrix $U(\phi)$ that is consistent with chiral symmetry [170]. The Lagrangian can be organised through an expansion in powers of momenta (derivatives) and explicit breakings of chiral symmetry (light quark masses, electromagnetic coupling,

etc.):

$$\mathcal{L}_{\text{eff}} = \mathcal{L}_2 + \mathcal{L}_4 + \mathcal{L}_6 + \dots . \quad (3.5.31)$$

Parity conservation requires the number of derivatives to be even, and a minimum of two derivatives is needed to generate non-trivial interactions because $UU^\dagger = 1$. The terms with a minimum number of derivatives will dominate at low energies. To lowest order, $\mathcal{O}(p^2)$, the effective Lagrangian is given by [172]:

$$\mathcal{L}_2 = \frac{F^2}{4} \langle D_\mu U^\dagger D^\mu U + U^\dagger \chi + \chi^\dagger U \rangle , \quad (3.5.32)$$

where $\langle \dots \rangle$ denotes the three-dimensional flavour trace, $D_\mu U = \partial_\mu U - ir_\mu U + iU\ell_\mu$ is the covariant chiral derivative, in the presence of arbitrary right-handed and left-handed (matrix-valued) external sources r_μ and ℓ_μ , and $\chi \equiv 2B_0(s + ip)$ with s and p external scalar and pseudoscalar sources, respectively. Taking $s = \mathcal{M}$, $p = 0$, and $r_\mu = \ell_\mu = e\mathcal{Q}A_\mu$ allows one to incorporate the explicit chiral symmetry breakings generated by the non-zero quark masses and electric charges:

$$\mathcal{M} = \text{diag}(m_u, m_d, m_s) , \quad \mathcal{Q} = \frac{1}{3} \text{diag}(2, -1, -1) . \quad (3.5.33)$$

Moreover, taking derivatives with respect to the external sources one can easily obtain the effective realization of the QCD quark currents in terms of the Goldstone bosons [174]. One then finds that F is the pion decay constant in the chiral limit ($m_q = 0$), while the constant B_0 is related to the quark condensate.

While only two low-energy constants (LECs) appear at $\mathcal{O}(p^2)$, F and B_0 , ten additional couplings L_i characterize the $\mathcal{O}(p^4)$ χ PT Lagrangian [172],

$$\begin{aligned} \mathcal{L}_4 = & L_1 \langle D_\mu U^\dagger D^\mu U \rangle^2 + L_2 \langle D_\mu U^\dagger D_\nu U \rangle \langle D^\mu U^\dagger D^\nu U \rangle + L_3 \langle D_\mu U^\dagger D^\mu U D_\nu U^\dagger D^\nu U \rangle \\ & + L_4 \langle D_\mu U^\dagger D^\mu U \rangle \langle U^\dagger \chi + \chi^\dagger U \rangle + L_5 \langle D_\mu U^\dagger D^\mu U (U^\dagger \chi + \chi^\dagger U) \rangle \\ & + L_6 \langle U^\dagger \chi + \chi^\dagger U \rangle^2 + L_7 \langle U^\dagger \chi - \chi^\dagger U \rangle^2 + L_8 \langle \chi^\dagger U \chi^\dagger U + U^\dagger \chi U^\dagger \chi \rangle \\ & - iL_9 \langle F_R^{\mu\nu} D_\mu U D_\nu U^\dagger + F_L^{\mu\nu} D_\mu U^\dagger D_\nu U \rangle + L_{10} \langle U^\dagger F_R^{\mu\nu} U F_{L\mu\nu} \rangle , \end{aligned} \quad (3.5.34)$$

with $F_R^{\mu\nu} = \partial^\mu r^\nu - \partial^\nu r^\mu - i [r^\mu, r^\nu]$ and $F_L^{\mu\nu} = \partial^\mu \ell^\nu - \partial^\nu \ell^\mu - i [\ell^\mu, \ell^\nu]$, and 90 LECs more would be needed to compute corrections of $\mathcal{O}(p^6)$:⁷

$$\mathcal{L}_6 = F^{-2} \sum_{i=1}^{90} X_i O_i^{p^6}. \quad (3.5.35)$$

The explicit form of the $\mathcal{O}(p^6)$ operators can be found in Ref. [175]. The current knowledge on all these LECs has been summarized in Ref. [167].

Quantum loops with Goldstone boson propagators in the internal lines generate non-polynomial contributions, with logarithms and threshold factors as required by unitarity. Each loop increases the chiral dimension by two powers of momenta [170]. Thus, to achieve an $\mathcal{O}(p^4)$ accuracy one needs to compute tree-level contributions with a single insertion of \mathcal{L}_4 plus one-loop graphs with only \mathcal{L}_2 vertices. These chiral one-loop corrections are then fully predicted in terms of F_π and the meson masses. Two-loop corrections with only \mathcal{L}_2 vertices contribute at $\mathcal{O}(p^6)$, together with one-loop graphs with a single insertion of \mathcal{L}_4 and tree-level diagrams with one insertion of \mathcal{L}_6 .

The ultraviolet divergences generated by quantum loops get reabsorbed by the corresponding LECs contributing to the same order in momenta. This induces a dependence of the renormalized LECs on the chiral renormalization scale ν_χ :

$$L_i = L_i^r(\nu_\chi) + \Gamma_i \Lambda(\nu_\chi), \quad (3.5.36)$$

with

$$\Lambda(\nu_\chi) = \frac{\nu_\chi^{d-4}}{16\pi^2} \left\{ \frac{1}{d-4} - \frac{1}{2} [\log(4\pi) + \Gamma'(1) + 1] \right\}, \quad (3.5.37)$$

the divergent subtraction constant in the usual χ PT renormalization scheme. Similar expressions apply for the other $\mathcal{O}(p^4)$ and $\mathcal{O}(e^2 p^2)$ LECs (K_i, N_i, D_i, Z_i) that will be dis-

⁷ There are, in addition, 2 contact terms without Goldstone bosons at $\mathcal{O}(p^4)$, and 4 more at $\mathcal{O}(p^6)$, which are only needed for renormalization. The $\mathcal{O}(p^6)$ LECs are usually denoted $C_i \equiv F^{-2} X_i$. We have changed the notation to avoid possible confusions with the short-distance Wilson coefficients. The χ PT Lagrangian contains also the $\mathcal{O}(p^4)$ Wess-Zumino-Witten term that has no free parameters and accounts for the QCD chiral anomaly [202, 203].

cussed next, while the $\mathcal{O}(p^6)$ LECs X_i require a two-loop subtraction [176]. The divergent parts of all these χ PT couplings are fully known [172, 176, 204–207].

In order to include loop corrections with virtual photon propagators, one needs to consider also the electromagnetic Lagrangian [153, 204, 208]

$$\mathcal{L}_{\text{em}} = e^2 Z F^4 \langle Q U^\dagger Q U \rangle + e^2 F^2 \sum_{i=1}^{14} K_i O_i^{e^2 p^2} + \mathcal{O}(e^2 p^4). \quad (3.5.38)$$

The presence of the quark charge matrix allows for a chiral structure without derivatives. The corresponding LEC of this $\mathcal{O}(e^2 p^0)$ term is determined by the electromagnetic pion mass difference [153]

$$Z = \frac{1}{8\pi\alpha F^2} (M_{\pi^\pm}^2 - M_{\pi^0}^2) \approx 0.8. \quad (3.5.39)$$

3.5.2 Chiral realization of the $\Delta S = 1$ effective Lagrangian

Strangeness-changing weak interactions with $\Delta S = 1$ are incorporated in the low-energy theory as a perturbation to the strong Lagrangian. At LO, the most general effective Lagrangian with the same transformation properties as the short-distance Lagrangian given by Eq. (3.3.19) contains three terms [184, 209, 210]:

$$\begin{aligned} \mathcal{L}_2^{\Delta S=1} &= G_8 F^4 \langle \lambda D^\mu U^\dagger D_\mu U \rangle + G_{27} F^4 \left(L_{\mu 23} L_{11}^\mu + \frac{2}{3} L_{\mu 21} L_{13}^\mu \right) \\ &+ e^2 G_8 g_{\text{ewk}} F^6 \langle \lambda U^\dagger Q U \rangle, \end{aligned} \quad (3.5.40)$$

where $\lambda = (\lambda_6 - i\lambda_7)/2$ projects into the $\bar{s} \rightarrow \bar{d}$ transition and $L_\mu = iU^\dagger D_\mu U$ represents the octet of $V - A$ currents to lowest order in derivatives. Under chiral transformations, these three terms transform as $(8_L, 1_R)$, $(27_L, 1_R)$ and $(8_L, 8_R)$, respectively. To simplify notation, we have reabsorbed the Fermi coupling and the CKM factors into effective LECs:

$$G_{8,27} \equiv -\frac{G_F}{\sqrt{2}} V_{ud} V_{us}^* g_{8,27}, \quad (3.5.41)$$

where g_8 , g_{27} and g_{ewk} are dimensionless couplings.

The G_8 and G_{27} chiral operators contain two derivatives and, therefore, lead to amplitudes that vanish at zero momenta. However, the electromagnetic penguin operator has a

chiral realization at $\mathcal{O}(e^2 p^0)$, given by the term proportional to $G_8 g_{\text{ewk}}$. The absence of derivatives implies a chiral enhancement that we have already seen before in Eq. (3.4.25).

The NLO effective Lagrangians have been worked out in Refs. [205–207] and include χ PT operators of $\mathcal{O}(p^4)$ and $\mathcal{O}(e^2 p^2)$:

$$\mathcal{L}_4^{\Delta S=1} = G_8 F^2 \sum_{i=1}^{22} N_i O_i^8 + G_{27} F^2 \sum_{i=1}^{28} D_i O_i^{27} + e^2 G_8 F^4 \sum_{i=1}^{14} Z_i O_i^{\text{EW}}. \quad (3.5.42)$$

3.6 Matching

In principle, the chiral LECs could be computed through a matching calculation between the three-flavour quark effective theory and χ PT. This is however a formidable non-perturbative task. Therefore, one needs to resort to phenomenological determinations, using the available hadronic data [167]. Nevertheless, a very good understanding of the strong LECs has been achieved in the large- N_C limit, where the meson scattering amplitudes reduce to tree-level diagrams with physical hadrons exchanged [155]. The contributions from tree-level meson resonance exchanges have been shown to saturate the phenomenologically known LECs at $\nu_\chi \sim M_\rho$ [153–156]. Nowadays, lattice simulations are also able to provide quantitative values of some of the $\mathcal{O}(p^4)$ L_i couplings [152].

In the limit $N_C \rightarrow \infty$, thanks to the factorization property in Eq. (3.4.23), the electroweak χ PT couplings can be related to strong LECs because the QCD currents have well-known chiral realizations. The quark currents are obtained as functional derivatives with respect to the appropriate external sources of the QCD generating functional $Z[v_\mu, a_\mu, s, p]$, defined via the path integral formula

$$\begin{aligned} \exp\{iZ\} &= \int \mathcal{D}q \mathcal{D}\bar{q} \mathcal{D}G_\mu \exp\left\{i \int d^4x [\mathcal{L}_{QCD} + \bar{q}\gamma^\mu(v_\mu + \gamma_5 a_\mu)q - \bar{q}(s - i\gamma_5 p)q]\right\} \\ &= \int \mathcal{D}U \exp\left\{i \int d^4x \mathcal{L}_{\text{eff}}\right\}. \end{aligned} \quad (3.6.43)$$

The corresponding derivatives of the χ PT generating functional determine the chiral expressions of the QCD currents. At $N_C \rightarrow \infty$, the generating functional reduces to the classical action because quantum loops are suppressed by powers of $1/N_C$. The left and

right vector currents are then easily computed, by taking derivatives of \mathcal{L}_{eff} with respect to $\ell_\mu^{ji} \equiv (v_\mu - a_\mu)^{ji}$ and $r_\mu^{ji} \equiv (v_\mu + a_\mu)^{ji}$, respectively [174]. One easily finds:

$$\begin{aligned} \bar{q}_L^j \gamma^\mu q_L^i &\doteq \frac{i}{2} \left\{ D^\mu U^\dagger U \left[F^2 + 8L_1 \langle D_\alpha U^\dagger D^\alpha U \rangle \right] \right. \\ &\quad + 4L_2 D_\alpha U^\dagger U \langle D^\alpha U^\dagger D^\mu U + D^\mu U^\dagger D^\alpha U \rangle \\ &\quad + 4L_3 \left\{ D^\mu U^\dagger U, D_\alpha U^\dagger D^\alpha U \right\} + 2L_5 \left\{ D^\mu U^\dagger U, (U^\dagger \chi + \chi^\dagger U) \right\} \\ &\quad + 2L_9 \partial_\alpha \left(D^\alpha U^\dagger D^\mu U - D^\mu U^\dagger D^\alpha U \right) \\ &\quad \left. + 2iL_9 \left(\ell_\alpha D^\mu U^\dagger D^\alpha U - D^\alpha U^\dagger D^\mu U \ell_\alpha \right) \right\}^{ij} + \mathcal{O}(p^5 N_C, p^3 N_C^0), \end{aligned} \quad (3.6.44)$$

$$\begin{aligned} \bar{q}_R^j \gamma^\mu q_R^i &\doteq \frac{i}{2} \left\{ D^\mu U U^\dagger \left[F^2 + 8L_1 \langle D_\alpha U^\dagger D^\alpha U \rangle \right] \right. \\ &\quad + 4L_2 D_\alpha U U^\dagger \langle D^\alpha U D^\mu U^\dagger + D^\mu U D^\alpha U^\dagger \rangle \\ &\quad + 4L_3 \left\{ D^\mu U U^\dagger, D_\alpha U D^\alpha U^\dagger \right\} + 2L_5 \left\{ D^\mu U U^\dagger, (\chi U^\dagger + U \chi^\dagger) \right\} \\ &\quad + 2L_9 \partial_\alpha \left(D^\alpha U D^\mu U^\dagger - D^\mu U D^\alpha U^\dagger \right) \\ &\quad \left. + 2iL_9 \left(r_\alpha D^\mu U D^\alpha U^\dagger - D^\alpha U D^\mu U^\dagger r_\alpha \right) \right\}^{ij} + \mathcal{O}(p^5 N_C, p^3 N_C^0). \end{aligned} \quad (3.6.45)$$

We have made explicit the $\mathcal{O}(p)$ contributions from the LO Lagrangian \mathcal{L}_2 , which are proportional to $F^2 \sim \mathcal{O}(N_C)$, and those $\mathcal{O}(p^3)$ contributions from \mathcal{L}_4 that are of $\mathcal{O}(N_C)$. Taking derivatives with respect to $-(s - ip)^{ji}$ and $-(s + ip)^{ji}$, one obtains the scalar bilinears

$$\begin{aligned} \bar{q}_L^j q_R^i &\doteq -\frac{B_0}{2} \left\{ U \left[F^2 + 4L_5 D_\alpha U^\dagger D^\alpha U \right. \right. \\ &\quad \left. \left. - 8L_7 \langle U^\dagger \chi - \chi^\dagger U \rangle + 8L_8 \chi^\dagger U \right] \right\}^{ij} + \mathcal{O}(p^4 N_C, p^2 N_C^0), \end{aligned} \quad (3.6.46)$$

$$\begin{aligned} \bar{q}_R^j q_L^i &\doteq -\frac{B_0}{2} \left\{ U^\dagger \left[F^2 + 4L_5 D_\alpha U D^\alpha U^\dagger \right. \right. \\ &\quad \left. \left. + 8L_7 \langle U^\dagger \chi - \chi^\dagger U \rangle + 8L_8 \chi U^\dagger \right] \right\}^{ij} + \mathcal{O}(p^4 N_C, p^2 N_C^0). \end{aligned} \quad (3.6.47)$$

The vacuum expectation value of the last two equations relates the coupling B_0 with the quark vacuum condensate: $\langle 0 | \bar{q}^j q^i | 0 \rangle = -F^2 B_0 \delta^{ij}$, at LO.

Inserting these expressions into the four-quark operators in Eq. (3.3.19), using the factorization property (3.4.23), one finds the χ PT realization of $\mathcal{L}_{\text{eff}}^{\Delta S=1}$ in the large- N_C

limit. At $\mathcal{O}(p^2)$, the three chiral structures in Eq. (3.5.40) are generated, with the following large- N_C values for their electroweak LECs [88, 150]:

$$\begin{aligned} g_8^\infty &= -\frac{2}{5} C_1(\mu) + \frac{3}{5} C_2(\mu) + C_4(\mu) - 16 L_5 B(\mu) C_6(\mu) , \\ g_{27}^\infty &= \frac{3}{5} [C_1(\mu) + C_2(\mu)] , \\ (e^2 g_8 g_{\text{ewk}})^\infty &= -3 B(\mu) C_8(\mu) - \frac{16}{3} B(\mu) C_6(\mu) e^2 (K_9 - 2 K_{10}) . \end{aligned} \quad (3.6.48)$$

In the last line, we have also taken into account the contribution to $g_8 g_{\text{ewk}}$ from electromagnetic corrections to Q_6 [150].

The LO terms in Eqs. (3.6.46) and (3.6.47) give rise to the $\mathcal{O}(p^0)$ electroweak chiral structure $Q_8 \doteq -3B_0^2 F^4 \langle \lambda U^\dagger Q U \rangle$. An analogous $\mathcal{O}(p^0)$ contribution is absent for Q_6 because $\langle \lambda U^\dagger U \rangle = \langle \lambda \rangle = 0$. Therefore, the χ PT realization of the penguin operator Q_6 starts at $\mathcal{O}(p^2)$, giving rise to the same octet structure as the $(V - A) \otimes (V - A)$ operators. The only difference is that $Q_{1,2,4}$ generate this structure with the LO terms in Eqs. (3.6.44) and (3.6.45), while in the Q_6 case it originates from the interference of the $\mathcal{O}(p^0)$ and $\mathcal{O}(p^2)$ terms in Eqs. (3.6.46) and (3.6.47). This is the reason why the C_6 contribution to g_8^∞ appears multiplied by the strong LEC L_5 , reducing the expected chiral enhancement in a very significant way.

There are no $\mathcal{O}(p^2)$ contributions from the operators Q_3 and Q_5 , at large- N_C , because they are proportional to the flavour trace of the left and right currents, respectively, which vanish identically at LO. The operators $Q_{7,9,10}$ start to contribute at $\mathcal{O}(e^2 p^2)$.

The dependence on the short-distance renormalization scale of the Wilson coefficients $C_i(\mu)$ is governed by the anomalous dimension matrix γ_{ij} of the four-quark operators Q_i , which vanishes at $N_C \rightarrow \infty$, except for the non-zero entries γ_{66} and γ_{88} . Thus, the μ dependence of $C_i(\mu)$ with $i \neq 6, 8$ disappears when $N_C \rightarrow \infty$, while that of $C_{6,8}(\mu)$ is exactly cancelled by the factor

$$B(\mu) \equiv \left(\frac{B_0^2}{F^2} \right)^\infty = \left\{ \frac{M_K^2}{[m_s(\mu) + m_d(\mu)] F_\pi} \right\}^2 \left[1 - \frac{16M_K^2}{F_\pi^2} (2L_8 - L_5) + \frac{8M_\pi^2}{F_\pi^2} L_5 \right] . \quad (3.6.49)$$

Thus, the computed LECs in Eq. (3.6.48) do not depend on μ , as it should. Notice, however, that the numerical values of the Wilson coefficients in Table 3.1 do include those $1/N_C$ corrections responsible for the QCD running and, when inserted in Eq. (3.6.48), will generate a residual μ dependence at NLO in $1/N_C$. At $N_C \rightarrow \infty$, the strong LECs are also independent on the χ PT renormalization scale ν_χ because chiral loops are suppressed by a factor $1/N_C$. The renormalization of the LECs L_i and their corresponding ν_χ dependences can only appear at NLO in the $1/N_C$ expansion.

The $\mathcal{O}(p^4)$ strong LEC L_5 plays a very important role in the ε'/ε prediction because it appears as a multiplicative factor in the $C_6(\mu)$ contribution to g_8^∞ . Its large- N_C value can be determined from resonance exchange, using the single-resonance approximation (SRA) [153, 155]:

$$L_5^\infty = \frac{F^2}{4M_S^2}. \quad (3.6.50)$$

The numerical result is, however, very sensitive to the chosen value for the scalar resonance mass. Taking $F = F_\pi$ and $M_S = 1.48$ GeV, as advocated in Ref. [211], one gets $L_5^\infty = 1.0 \cdot 10^{-3}$ [150], while $M_S = 1.0$ GeV would imply $L_5^\infty = 2.1 \cdot 10^{-3}$. An independent determination can be obtained from the pion and kaon decay constants, ignoring the $1/N_C$ suppressed loop contributions [88]:

$$L_5^\infty \approx \frac{F_\pi^2}{4(M_K^2 - M_\pi^2)} \left(\frac{F_K}{F_\pi} - 1 \right) = 1.8 \cdot 10^{-3}. \quad (3.6.51)$$

This procedure, which has actually been used in the rough estimate of the Q_6 matrix element in Eq. (3.4.26), is also subject to large uncertainties because the $SU(3)$ -breaking difference $F_K - F_\pi$ is very sensitive to logarithmic chiral corrections that are no longer present when $N_C \rightarrow \infty$.

Quantitative values for the χ PT coupling L_5 have been also extracted through lattice simulations. The determination has been obtained by the HPQCD collaboration [212], analysing F_K and F_π at different quark masses with $N_f = 2 + 1 + 1$ dynamical flavours, and is the result advocated in the FLAG compilation [152]:

$$L_5^r(M_\rho) = (1.19 \pm 0.25) \cdot 10^{-3}. \quad (3.6.52)$$

We will adopt this number in our analysis and will comment later on the sensitivity to this parameter of the ε'/ε prediction.

The combination $2L_8 - L_5$ can also be estimated in the large- N_C limit, through the SRA, and it gets determined by L_5 [155]:

$$(2L_8 - L_5)^\infty = -\frac{1}{4} L_5^\infty . \quad (3.6.53)$$

This relation is well satisfied by the lattice results that find $(2L_8^r - L_5^r)(M_\rho) = (-0.10 \pm 0.20) \cdot 10^{-3}$ [152, 212].

The electromagnetic LECs K_i can be expressed as convolutions of QCD correlators with a photon propagator [213], and their evaluation involves an integration over the virtual photon momenta. In contrast to the strong LECs L_i , the K_i couplings have then an explicit dependence on the χ PT renormalization scale ν_χ already at LO in $1/N_C$. Moreover, they also depend on the short-distance renormalization scale μ and the gauge parameter ξ . Those dependences cancel in the physical decay amplitudes with photon-loop contributions. In order to fix the combination $K_9 - 2K_{10}$ that enters g_{ewk} in Eq. (3.6.48), we follow Ref. [150] and adopt the value [213, 214]

$$(K_9^r - 2K_{10}^r)(M_\rho) = -(9.3 \pm 4.6) \cdot 10^{-3} , \quad (3.6.54)$$

which refers to the renormalized parameter at $\nu_\chi = M_\rho$, in the Feynman gauge $\xi = 1$ and with a short-distance scale $\mu = 1$ GeV.

Expanding the products of chiral currents to NLO, one obtains the large- N_C predictions for the $\mathcal{O}(p^4)$ and $\mathcal{O}(e^2 p^2)$ LECs N_i , D_i and Z_i . The explicit expressions can be found in Section 5.2 of Ref. [150].

Tables 3.2 and 3.3 show the numerical predictions obtained for the CP-even and CP-odd parts, respectively, of the LO electroweak LECs g_8 , g_{27} and $g_8 g_{\text{ewk}}$. The large- N_C limit has been only applied to the matching between the two EFTs. The full evolution from the electroweak scale down to $\mu < m_c$ has been taken into account without making any unnecessary expansion in powers of $1/N_C$; otherwise, one would miss the large short-distance corrections encoded in the Wilson coefficients $C_i(\mu)$ with $i \neq 6, 8$.

Scheme	$\text{Re}(g_8)$	g_{27}	$\text{Re}(g_8 g_{ewk})$
NDR	$1.22 \pm 0.13_{\mu} \pm 0.06_{L_i} \begin{smallmatrix} +0.03 \\ -0.02 m_s \end{smallmatrix}$	$0.46 \pm 0.02_{\mu}$	$-2.24 \pm 1.44_{\mu} \pm 0.38_{K_i} \begin{smallmatrix} +0.19 \\ -0.21 m_s \end{smallmatrix}$
HV	$1.16 \pm 0.20_{\mu} \pm 0.02_{L_i} \pm 0.01_{m_s}$	$0.44 \pm 0.02_{\mu}$	$-1.29 \pm 1.04_{\mu} \pm 0.15_{K_i} \begin{smallmatrix} +0.11 \\ -0.13 m_s \end{smallmatrix}$
NDR + HV	$1.19 \pm 0.17_{\mu} \pm 0.04_{L_i} \pm 0.02_{m_s}$	$0.45 \pm 0.02_{\mu}$	$-1.77 \pm 1.22_{\mu} \pm 0.26_{K_i} \begin{smallmatrix} +0.15 \\ -0.17 m_s \end{smallmatrix}$

Table 3.2: Large- N_C predictions for the CP-even parts of the LO electroweak LECs.

Scheme	$\text{Im}(g_8)/\text{Im}(\tau)$	$\text{Im}(g_8 g_{ewk})/\text{Im}(\tau)$
NDR	$0.93 \pm 0.22_{\mu} \pm 0.21_{L_i} \begin{smallmatrix} +0.10 \\ -0.08 m_s \end{smallmatrix}$	$-22.2 \pm 5.0_{\mu} \pm 1.3_{K_i} \begin{smallmatrix} +1.9 \\ -2.1 m_s \end{smallmatrix}$
HV	$0.81 \pm 0.23_{\mu} \pm 0.18_{L_i} \begin{smallmatrix} +0.08 \\ -0.07 m_s \end{smallmatrix}$	$-23.6 \pm 5.0_{\mu} \pm 1.1_{K_i} \begin{smallmatrix} +2.0 \\ -2.2 m_s \end{smallmatrix}$
NDR + HV	$0.87 \pm 0.22_{\mu} \pm 0.20_{L_i} \begin{smallmatrix} +0.09 \\ -0.08 m_s \end{smallmatrix}$	$-22.9 \pm 5.0_{\mu} \pm 1.2_{K_i} \begin{smallmatrix} +1.9 \\ -2.2 m_s \end{smallmatrix}$

Table 3.3: Large- N_C predictions for the CP-odd parts of the LO electroweak LECs.

The central values quoted in the tables have been obtained at $\mu = 1$ GeV . The first uncertainty has been estimated by varying the short-distance renormalization scale μ between M_ρ and m_c , taking into account the large- N_C running for the factor $(m_s + m_d)(\mu)$ in $B(\mu)$. The current uncertainties on the strong and electromagnetic LECs that appear in Eqs. (3.6.48) and (3.6.49) are reflected in the second error, while the third one corresponds to the uncertainty from the input quark masses given in Table C.1. To better assess the perturbative uncertainties, the Wilson coefficients have been evaluated in two different schemes for γ_5 , and an educated average of the two results is displayed in the tables.

It is important to realize the different levels of reliability of these predictions. The large- N_C matching is only able to capture the anomalous dimensions of the operators Q_6 and Q_8 . In fact, γ_{66} and γ_{88} are very well approximated by their leading estimates in $1/N_C$. Therefore, the contributions of these two operators to the electroweak LECs are

quite robust, within the estimated uncertainties. This implies that the predicted CP-odd components of g_8 and $g_8 g_{\text{ewk}}$ (g_{27} is CP even) are very reliable. However, this is no longer true for their CP-even parts because the anomalous dimensions of the relevant operators are completely missed at large- N_C . The parametric errors quoted in Table 3.2 are probably underestimating the actual uncertainties of the calculated CP-even components of the electroweak LECs. An accurate estimate of these components would require to perform the matching calculation at the NLO in $1/N_C$.

3.7 The χ PT $K \rightarrow \pi\pi$ amplitudes

The evaluation of the kaon decay amplitudes is a straightforward perturbative calculation within the χ PT framework. To lowest order in the chiral expansion, one only needs to consider tree-level Feynman diagrams with one insertion of $\mathcal{L}_2^{\Delta S=1}$. In the limit of isospin conservation, the $\mathcal{A}_{\Delta I}$ amplitudes defined in Eq. (3.2.4) are given by Refs. [88, 150]

$$\begin{aligned} \mathcal{A}_{1/2} &= -\sqrt{2} G_8 F \left[\left(M_K^2 - M_\pi^2 \right) - \frac{2}{3} F^2 e^2 g_{\text{ewk}} \right] - \frac{\sqrt{2}}{9} G_{27} F \left(M_K^2 - M_\pi^2 \right) , \\ \mathcal{A}_{3/2} &= -\frac{10}{9} G_{27} F \left(M_K^2 - M_\pi^2 \right) + \frac{2}{3} G_8 F^3 e^2 g_{\text{ewk}} , \end{aligned} \quad (3.7.55)$$

and $\mathcal{A}_{5/2} = 0$. From the measured values of the decay amplitudes in Eq. (3.2.5), one gets the tree-level determinations $g_8 = 5.0$ and $g_{27} = 0.25$ for the octet and 27-plet chiral couplings. The large numerical difference between these two LECs just reflects the small experimental value of the ratio ω in Eq. (3.2.6). Moreover, the sizeable difference between these LO phenomenological determinations and the large- N_C estimates in Table 3.2 makes evident that the neglected $1/N_C$ corrections are numerically important.

Inserting in Eq. (3.7.55) the large- N_C predictions for the electroweak LECs given in Eq. (3.6.48) and taking for L_5 the value in Eq. (3.6.51), one immediately gets the Q_6 and Q_8 CP-odd amplitudes estimated before in Eqs. (3.4.26) and (3.4.27), with $B_6^{(1/2)} = B_8^{(3/2)} = 1$, including in addition some small chiral corrections that were still missing there. Eq. (3.7.55) contains, moreover, the $\mathcal{O}(p^2)$ contributions from all other four-quark operators.

Note, however, that the $\pi\pi$ phase shifts are predicted to be zero at LO in χ PT, since phase shifts are generated by absorptive contributions in quantum loop diagrams. We know experimentally that the phase-shift difference $\chi_0 - \chi_2 = 47.5^\circ$ is large, which implies that chiral loop corrections are very sizeable. Chiral loops bring a $1/N_C$ suppression but they get enhanced by large logarithms. The large absorptive contributions originate in those logarithmic corrections that are related with unitarity. A large absorptive contribution implies, moreover, a large dispersive correction because they are related by analyticity. A proper understanding of the kaon dynamics cannot be achieved without the inclusion of these $1/N_C$ suppressed contributions.

At the NLO in χ PT the $\mathcal{A}_{\Delta I}$ amplitudes can be expressed as [150]

$$\begin{aligned} \mathcal{A}_{\Delta I} = & -G_8 F_\pi \left\{ (M_K^2 - M_\pi^2) \mathcal{A}_{\Delta I}^{(8)} - e^2 F_\pi^2 g_{\text{ewk}} \mathcal{A}_{\Delta I}^{(g)} \right\} \\ & - G_{27} F_\pi (M_K^2 - M_\pi^2) \mathcal{A}_{\Delta I}^{(27)} , \end{aligned} \quad (3.7.56)$$

where $\mathcal{A}_{\Delta I}^{(8)}$ and $\mathcal{A}_{\Delta I}^{(27)}$ represent the octet and 27-plet components, and $\mathcal{A}_{\Delta I}^{(g)}$ contains the electroweak penguin contributions. Each of these amplitudes can be decomposed in the form

$$\mathcal{A}_{\Delta I}^{(X)} = a_{\Delta I}^{(X)} \left[1 + \Delta_L \mathcal{A}_{\Delta I}^{(X)} + \Delta_C \mathcal{A}_{\Delta I}^{(X)} \right] , \quad (3.7.57)$$

with

$$\begin{aligned} a_{1/2}^{(8)} &= \sqrt{2} , & a_{1/2}^{(g)} &= \frac{2\sqrt{2}}{3} , & a_{1/2}^{(27)} &= \frac{\sqrt{2}}{9} , \\ a_{3/2}^{(8)} &= 0 , & a_{3/2}^{(g)} &= \frac{2}{3} , & a_{3/2}^{(27)} &= \frac{10}{9} , \end{aligned} \quad (3.7.58)$$

parametrizing the corresponding tree-level contributions, $\Delta_L \mathcal{A}_{\Delta I}^{(X)}$ the one-loop chiral corrections and $\Delta_C \mathcal{A}_{\Delta I}^{(X)}$ the NLO local corrections from $\mathcal{L}_4^{\Delta S=1}$. Since in this chapter we are not considering electromagnetic corrections, $\mathcal{A}_{5/2} = 0$.

A small part of the $\mathcal{O}(p^4)$ corrections has been reabsorbed into the physical pion decay constant F_π , which appears explicitly in the three terms of Eq. (3.7.56). The NLO relation

between F_π and the Lagrangian parameter F is given by [172]

$$F = F_\pi \left\{ 1 - \frac{4}{F^2} \left[\left(M_\pi^2 + 2M_K^2 \right) L_4^r(\nu_\chi) + M_\pi^2 L_5^r(\nu_\chi) \right] + \frac{1}{2(4\pi)^2 F^2} \left[2M_\pi^2 \log \left(\frac{M_\pi^2}{\nu_\chi^2} \right) + M_K^2 \log \left(\frac{M_K^2}{\nu_\chi^2} \right) \right] \right\}. \quad (3.7.59)$$

The chiral logarithmic corrections are obviously suppressed by the geometrical loop factor $(4\pi)^{-2}$ and two powers of the Goldstone scale $F \sim \sqrt{N_C}$. Thus, these contributions and the corresponding dependence of the renormalized $L_i^r(\nu_\chi)$ couplings on the χ PT renormalization scale ν_χ are of $\mathcal{O}(1/N_C)$. The ν_χ -independent parts of the LECs have a different scaling with $1/N_C$: while $L_4/F^2 \sim \mathcal{O}(1/N_C)$, L_5/F^2 is a leading correction of $\mathcal{O}(1)$. This implies the large- N_C result for L_5 given in Eq. (3.6.51) (the L_5 contribution to F_K is multiplied by M_K^2 instead of M_π^2).

The numerical values of the different $\mathcal{A}_{1/2}^{(X)}$ and $\mathcal{A}_{3/2}^{(X)}$ components are given in Tables 3.4 and 3.5, respectively. We comment next on the most important features of the different contributions.

X	$a_{1/2}^{(X)}$	$\Delta_L \mathcal{A}_{1/2}^{(X)}$	$[\Delta_C \mathcal{A}_{1/2}^{(X)}]^+$	$[\Delta_C \mathcal{A}_{1/2}^{(X)}]^-$
8	$\sqrt{2}$	$0.27 + 0.47 i$	0.01 ± 0.05	0.02 ± 0.05
g	$\frac{2\sqrt{2}}{3}$	$0.27 + 0.47 i$	-0.19 ± 0.01	-0.19 ± 0.01
27	$\frac{\sqrt{2}}{9}$	$1.03 + 0.47 i$	0.01 ± 0.63	0.01 ± 0.63

Table 3.4: Numerical predictions for the $\mathcal{A}_{1/2}^{(X)}$ components: $a_{1/2}^{(X)}$, $\Delta_L \mathcal{A}_{1/2}^{(X)}$, $\Delta_C \mathcal{A}_{1/2}^{(X)}$. The local NLO correction to the CP-even ($[\Delta_C \mathcal{A}_{1/2}^{(X)}]^+$) and CP-odd ($[\Delta_C \mathcal{A}_{1/2}^{(X)}]^-$) amplitudes is only different in the octet case.

3.7.1 Chiral loop corrections

The one-loop chiral corrections are generated through the Feynman topologies depicted in Figure 3.3 [86–88, 149–151, 205, 215–217]. They include one insertion of the LO weak

X	$a_{3/2}^{(X)}$	$\Delta_L \mathcal{A}_{3/2}^{(X)}$	$\Delta_C \mathcal{A}_{3/2}^{(X)}$
g	$\frac{2}{3}$	$-0.50 - 0.21 i$	-0.19 ± 0.19
27	$\frac{10}{9}$	$-0.04 - 0.21 i$	0.01 ± 0.05

Table 3.5: Numerical predictions for the $\mathcal{A}_{3/2}$ components: $a_{3/2}^{(X)}$, $\Delta_L \mathcal{A}_{3/2}^{(X)}$, $\Delta_C \mathcal{A}_{3/2}^{(X)}$.

Lagrangian $\mathcal{L}_2^{\Delta S=1}$ (filled red vertices), and the first two diagrams contain also interaction vertices from the $\mathcal{O}(p^2)$ strong Lagrangian \mathcal{L}_2 . The resulting $\Delta_L \mathcal{A}_{1/2}^{(X)}$ and $\Delta_L \mathcal{A}_{3/2}^{(X)}$ corrections given in Tables 3.4 and 3.5, respectively, exhibit a very clear pattern. The one-loop chiral corrections are always positive for all $\Delta I = 1/2$ amplitudes and negative for $\Delta I = 3/2$. Moreover, the absorptive contributions (the imaginary parts of $\Delta_L \mathcal{A}_{\Delta I}^{(X)}$) only depend on the isospin of the final $\pi\pi$ state. The elastic final-state interaction of the two pions induces a very large and positive absorptive correction when $I = 0$, while this contribution becomes much smaller and negative when $I = 2$.

The absorptive contribution fully originates in the first topology of Figure 3.3, since it is the only one where the two intermediate pions can be put on their mass-shell [88]:

$$\begin{aligned} \Delta_L \mathcal{A}_{1/2}^{(X)} &= \frac{M_K^2}{(4\pi F_\pi)^2} \left(1 - \frac{M_\pi^2}{2M_K^2} \right) \tilde{B}(M_\pi^2, M_\pi^2, M_K^2) + \dots, \\ \Delta_L \mathcal{A}_{3/2}^{(X)} &= -\frac{1}{2} \frac{M_K^2}{(4\pi F_\pi)^2} \left(1 - \frac{2M_\pi^2}{M_K^2} \right) \tilde{B}(M_\pi^2, M_\pi^2, M_K^2) + \dots, \end{aligned} \quad (3.7.60)$$

where

$$\tilde{B}(M_\pi^2, M_\pi^2, M_K^2) = \sigma_\pi \left[\log \left(\frac{1 - \sigma_\pi}{1 + \sigma_\pi} \right) + i\pi \right] + \log \left(\frac{\nu_\chi^2}{M_\pi^2} \right) + 1, \quad (3.7.61)$$

is the renormalized one-loop scalar integral with two pion propagators and $q^2 = M_K^2$, and $\sigma_\pi \equiv \sqrt{1 - 4M_\pi^2/M_K^2}$. These results reproduce the LO χ PT values for the strong $\pi\pi$ scattering phase shifts with $J = 0$ and $I = 0, 2$, at $s = M_K^2$:

$$\begin{aligned} \tan \delta_0(M_K^2) &= \frac{\sigma_\pi}{32\pi F_\pi^2} \left(2M_K^2 - M_\pi^2 \right), \\ \tan \delta_2(M_K^2) &= \frac{\sigma_\pi}{32\pi F_\pi^2} \left(2M_\pi^2 - M_K^2 \right). \end{aligned} \quad (3.7.62)$$

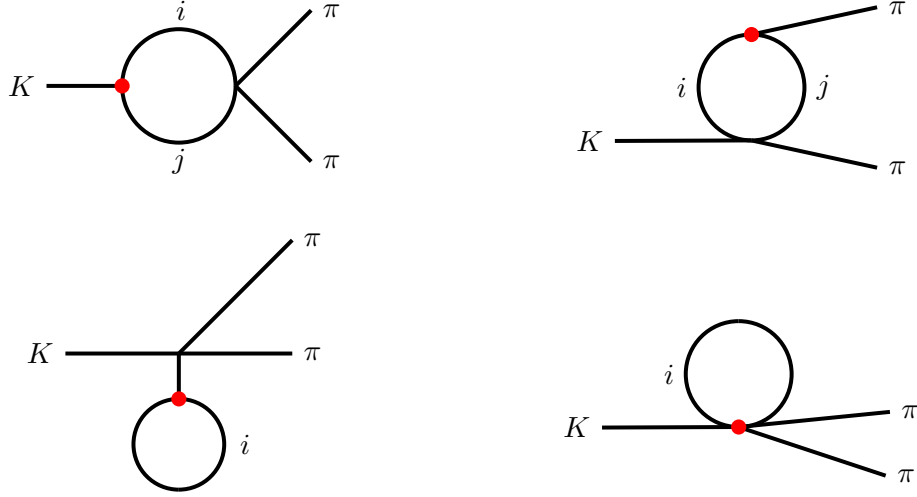


Figure 3.3: One-loop topologies contributing to $K \rightarrow \pi\pi$. The filled red circles indicate LO $\Delta S = 1$ vertices. The labels i and j represent the Goldstone bosons inside the loop. Wave-function renormalization topologies are not shown.

The predicted phase-shift difference, $\delta_0(M_K^2) - \delta_2(M_K^2) = 37^\circ$, is somewhat lower than its experimental value showing that higher-order rescattering contributions are numerically relevant. The one-loop integral in Eq. (3.7.61) contains, in addition, a large chiral logarithm of the ultraviolet scale ν_χ over the infrared scale M_π , which enhances significantly the dispersive component of the $I = 0$ amplitude and suppresses the $I = 2$ one.

The complete analytical expressions for the one-loop corrections $\Delta_L \mathcal{A}_{\Delta I}^{(X)}$ can be found in Refs. [88, 150]. The absorptive contributions are finite and, therefore, do not depend on the chiral renormalization scale. An explicit dependence on ν_χ is, however, present on the dispersive components. The numbers quoted in Tables 3.4 and 3.5 have been obtained at $\nu_\chi = M_\rho = 0.77$ GeV. The dependence on ν_χ is of course exactly cancelled by the local counterterm contributions.

One observes in Table 3.4 a huge ($\sim 100\%$) dispersive one-loop correction to the $\mathcal{A}_{1/2}^{(27)}$ amplitude. Fortunately, since the 27-plet contribution is a very small part of the total $\Delta I = \frac{1}{2}$ amplitude, this does not introduce any significant uncertainty in the final

numerical value of A_0 . Moreover, the 27-plet components do not contribute to the CP-odd amplitudes we interested in, because $\text{Im}(g_{27}) = 0$.

The corrections relevant for ε'/ε are the octet contribution to the isoscalar amplitude and the electroweak-penguin contribution to A_2 . The first one generates a very sizeable enhancement of $\text{Im}A_0$ by a factor $|1 + \Delta_L \mathcal{A}_{1/2}^{(8)}| \approx 1.35$, while the second one induces a strong suppression of $\text{Im}A_2^{\text{emp}}$ with a factor $|1 + \Delta_L \mathcal{A}_{3/2}^{(g)}| \approx 0.54$. Looking to the simplified formula in Eq. (3.4.28), one immediately realizes the obvious impact of these chiral corrections on the final value predicted for ε'/ε , since they destroy completely the accidental numerical cancellation between the Q_6 and Q_8 contributions.

3.7.2 Local $\mathcal{O}(p^4)$ contributions

Explicit expressions for the local $\Delta_C \mathcal{A}_{\Delta I}^{(X)}$ corrections in terms of the $\mathcal{O}(p^4)$ electroweak LECs can be found in Refs. [88, 150]. In the large- N_C limit, the local contribution to the $\mathcal{A}_{1/2}^{(8)}$ amplitude takes the form

$$\begin{aligned} g_8^\infty [1 + \Delta_C \mathcal{A}_{1/2}^{(8)}]^\infty &= \left[-\frac{2}{5} C_1(\mu) + \frac{3}{5} C_2(\mu) + C_4(\mu) \right] \left\{ 1 + \frac{4M_\pi^2}{F^2} L_5 \right\} \\ &\quad - 16 B(\mu) C_6(\mu) \left\{ L_5 + \frac{4M_K^2}{F^2} \delta_8^K + \frac{4M_\pi^2}{F^2} \delta_8^\pi \right\}. \end{aligned} \quad (3.7.63)$$

The NLO corrections δ_8^P depend on some $\mathcal{O}(p^6)$ LECs X_i that are not very well known. The relevant combinations can be estimated with the SRA, up to unknown contributions from couplings with two resonance fields [156]:

$$\delta_8^K = L_5 (2L_8 - L_5) + \frac{1}{4} (2X_{14} + X_{34}) \approx \frac{1}{2} L_5^2, \quad (3.7.64)$$

$$\delta_8^\pi = (8L_8^2 - 3L_5^2) + X_{12} + X_{14} + X_{17} - 3X_{19} - 4X_{20} - X_{31} \approx -\frac{15}{8} L_5^2.$$

Since the contributions from Q_6 and the other four-quark operators get different NLO corrections, the $\mathcal{O}(p^4)$ corrections to the CP-even and CP-odd octet amplitudes,

$$\text{Re}(g_8 \Delta_C \mathcal{A}_{1/2}^{(8)}) + i \text{Im}(g_8 \Delta_C \mathcal{A}_{1/2}^{(8)}) \equiv \text{Re}(g_8) [\Delta_C \mathcal{A}_{1/2}^{(8)}]^+ + i \text{Im}(g_8) [\Delta_C \mathcal{A}_{1/2}^{(8)}]^-, \quad (3.7.65)$$

are also different. The predicted numerical values for the separate corrections $[\Delta_C \mathcal{A}_{1/2}^{(8)}]^+$ and $[\Delta_C \mathcal{A}_{1/2}^{(8)}]^-$ are given in Table 3.4. The $\mathcal{O}(p^4)$ local corrections to the other $\mathcal{A}_{\Delta I}^{(X)}$ amplitudes only depend on L_5 , in the large- N_C limit:

$$\begin{aligned} \Delta_C \mathcal{A}_{1/2}^{(27)} \Big|^\infty &= \Delta_C \mathcal{A}_{3/2}^{(27)} \Big|^\infty = \frac{4M_\pi^2}{F^2} L_5, \\ \Delta_C \mathcal{A}_{1/2}^{(g)} \Big|^\infty &= \Delta_C \mathcal{A}_{3/2}^{(g)} \Big|^\infty = -\frac{4}{F^2} (M_K^2 + 5M_\pi^2) L_5. \end{aligned} \quad (3.7.66)$$

Thus, all local NLO contributions are finally determined by the input value of L_5^∞ .

The numerical predictions for the different local corrections $\Delta_C \mathcal{A}_{\Delta I}^{(X)}$ are shown in Tables 3.4 and 3.5. The main uncertainty originates in their dependence on the chiral renormalization scale ν_χ , which is totally missed by the large- N_C approximation. We take the large- N_C results as our numerical estimates at $\nu_\chi = M_\rho$. The errors have been estimated varying ν_χ between 0.6 and 1 GeV in the corresponding loop contributions $\Delta_L \mathcal{A}_{\Delta I}^{(X)}$. We have also varied the short-distance renormalization scale μ between M_ρ and m_c , but the impact on the $\Delta_C \mathcal{A}_{\Delta I}^{(X)}$ corrections is negligible compared with the ν_χ uncertainty.

The relevant corrections for our determination of ε'/ε are $[\Delta_C \mathcal{A}_{1/2}^{(8)}]^- = 0.02 \pm 0.05$ and $\Delta_C \mathcal{A}_{3/2}^{(g)} = -0.19 \pm 0.19$. They are much smaller than the corresponding loop contributions, which is also reflected in the large relative uncertainties induced by the ν_χ variation.

3.8 The SM prediction for ε'/ε

Putting all computed corrections together in Eq. (3.2.15), we obtain the updated SM prediction

$$\text{Re}(\varepsilon'/\varepsilon) = (15 \pm 2_\mu \pm 2_{m_s} \pm 2_{\Omega_{\text{eff}}} \pm 6_{1/N_C}) \times 10^{-4} = (15 \pm 7) \times 10^{-4}. \quad (3.8.67)$$

The input values adopted for the relevant SM parameters are given in Table C.1 of Appendix C. We have only calculated theoretically the CP-odd amplitudes $\text{Im}A_I$. For their CP-even counterparts (and $|\varepsilon|$) the experimental values have been taken instead. We display explicitly the four main sources of errors. The first one reflects the fluctuations under

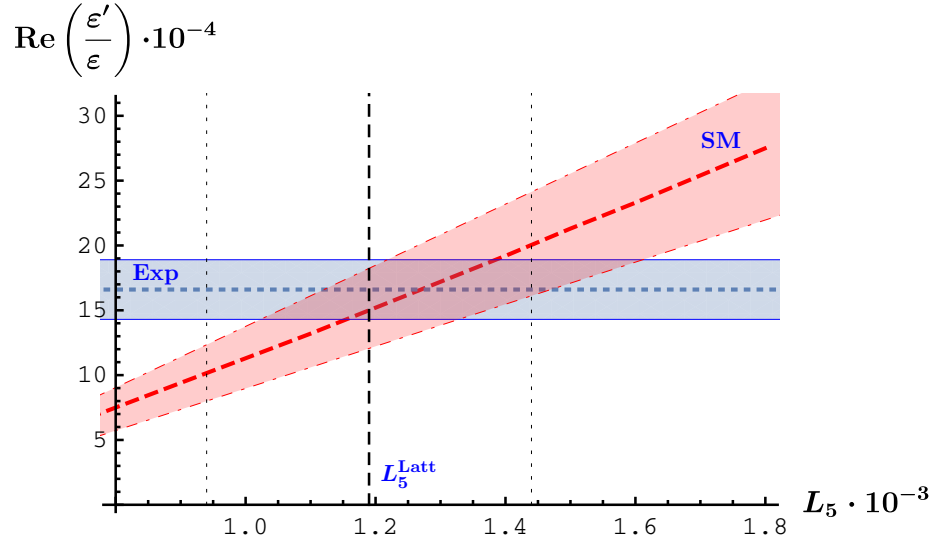


Figure 3.4: SM prediction for ε'/ε as function of L_5 (red dashed line) with 1σ errors (oblique band). The horizontal blue band displays the experimentally measured value with 1σ error bars. The dashed vertical line shows the current lattice determination of $L_5^r(M_\rho)$.

changes of the short-distance renormalization scale μ in the range between M_ρ and m_c , and the choice of scheme for γ_5 . The second uncertainty shows the sensitivity to variations of the input quark masses within their currently allowed ranges, while the third one displays the uncertainty from the isospin-breaking parameter Ω_{eff} . The fourth error accounts for the sum of squared uncertainties from the input value of L_5 ($\pm 5 \cdot 10^{-4}$) and the χ P T scale ν_χ that is varied between 0.6 and 1 GeV ($\pm 3 \cdot 10^{-4}$). This fourth error is by far the dominant one and reflects our current ignorance about $1/N_C$ -suppressed contributions in the matching process.

In Figure 3.4, we show the prediction for ε'/ε as function of the input value of L_5 . The strong dependence on this important parameter is evident from the plot. The experimental 1σ range is indicated by the horizontal band, while the dashed vertical lines display the current lattice determination of $L_5^r(M_\rho)$. The measured value of ε'/ε is nicely reproduced with the preferred lattice inputs.

In order to better appreciate the dynamical contributions that have been included in Eq. (3.8.67), it is worth to go back to the schematic description of EFTs displayed in Figure 3.2. Starting with the SM at the electroweak scale, where the underlying $\Delta S = 1$ transitions take place, we have first used the full machinery of the short-distance OPE to determine the effective Lagrangian $\mathcal{L}_{\text{eff}}^{\Delta S=1}$, defined in the three-flavour quark theory at scales just below the charm mass. We have included all NLO contributions to the Wilson coefficients $C_i(\mu)$, without making any large- N_C approximation, see Appendix D. The OPE sums up large logarithmic QCD corrections, but most of these logarithms are suppressed by factors of $1/N_C$ because the anomalous dimension matrix γ_{ij} of the Q_i operators vanishes at $N_C \rightarrow \infty$, except for γ_{66} and γ_{88} which remain non-zero. Since

$$\frac{1}{N_C} \log(M_W^2/\mu_0^2) = 2.9 \quad (3.8.68)$$

at $\mu = \mu_0 = 1 \text{ GeV}$, it would not make much sense to neglect “subleading” corrections in $1/N_C$.

At the kaon mass scale, we have made use of a different EFT that takes advantage of the chiral symmetry properties of QCD to constrain the pseudoscalar Goldstone dynamics. χ PT is the appropriate tool to describe rigorously the physics of kaons and pions, through a low-energy expansion in powers of momenta and quark masses [53]. Chiral symmetry determines the effective realization of $\mathcal{L}_{\text{eff}}^{\Delta S=1}$ at the hadronic mass scale; *i.e.*, the most general form of the low-energy χ PT structures with the same symmetry properties than the four-quark operators Q_i , at a given order in momenta. All short-distance information is encoded in LECs that are not fixed by symmetry considerations. The $K \rightarrow \pi\pi$ amplitudes can then be easily predicted in terms of those LECs. The χ PT predictions include unambiguous quantum corrections, which comply with the requirements of unitarity and analyticity.

The so-called chiral logarithmic corrections are also suppressed by factors of $1/N_C$ (quantum loops are absent from the $N_C \rightarrow \infty$ mesonic world [155]), but they cannot be ignored since they are responsible for the large $\pi\pi$ phase shifts that originate in their absorptive contributions. Moreover, the dispersive logarithmic corrections are also large

when the two pions are in a $J = 0$ state. Once again, a $1/N_C$ suppression gets compensated by a large logarithm: at $\nu_\chi = \nu_0 = 1 \text{ GeV}$,

$$\frac{1}{N_C} \log(\nu_0^2/M_\pi^2) = 1.3 . \quad (3.8.69)$$

The measured kaon decay amplitudes cannot be understood without the inclusion of these large, but $1/N_C$ suppressed, contributions. Our SM prediction in Eq. (3.8.67) includes of course the full $\mathcal{O}(p^4)$ χ PT results, without any unnecessary $1/N_C$ approximation.

The limit of a large number of QCD colours has been only used to perform the matching between the two EFTs; *i.e.*, to evaluate the numerical values of the χ PT LECs. Thanks to the factorization property in Eq. (3.4.23), the hadronic matrix elements of the four-quark operators can be reduced to matrix elements of QCD currents at $N_C \rightarrow \infty$. Since these currents have well-known χ PT realizations at low energies, the electroweak LECs can be easily determined in the large- N_C limit. The intrinsic uncertainty of this determination is of $\mathcal{O}(1/N_C)$, but it is not enhanced by any large logarithm of two widely separated mass scales.

The large- N_C structure of the anomalous dimension matrix γ_{ij} allows us to better assess the quality of our matching procedure. At $N_C \rightarrow \infty$, the only non-zero entries are γ_{66} and γ_{88} , which, moreover, are well approximated by their large- N_C estimates. Thus, the short-distance properties of Q_6 and Q_8 are very efficiently incorporated into the corresponding χ PT couplings through the large- N_C matching. In fact, the leading renormalization-scale dependence of $C_6(\mu)$ and $C_8(\mu)$ cancels exactly with the running of the light quark masses appearing through the χ PT factor $B(\mu)$ in Eq. (3.6.49). Fortunately, Q_6 and Q_8 are precisely the only two operators that really matter for the numerical prediction of ε'/ε .

This is no longer true for the other four-quark operators because their anomalous dimensions are lost at $N_C \rightarrow \infty$. The μ dependence of their Wilson coefficients cannot be compensated in the large- N_C matching process, which indicates the relevance of the missing $1/N_C$ contributions. The bulk of the $\Delta I = 1/2$ enhancement is associated with the octet operator Q_- , while $\Delta I = 3/2$ transitions originate from $Q^{(27)}$. Since the $1/N_C$ -suppressed anomalous dimensions of these two operators are a crucial ingredient of

the $K \rightarrow \pi\pi$ dynamics, an accurate prediction of the CP-even decay amplitudes will only become possible with a matching calculation at NLO in $1/N_C$ [102–104].

3.9 Discussion and outlook

The SM prediction for ε'/ε , given in Eq. (3.8.67), is in perfect agreement with the measured experimental value given by Eq. (3.1.3). The final result emerges from a delicate balance among several contributions, where the chiral dynamics of the two final pions plays a very crucial role. The $\pi\pi$ rescattering corrections destroy the naive cancellation between the Q_6 and Q_8 terms in Eq. (3.4.28), enhancing the positive Q_6 contribution and suppressing the negative contribution from Q_8 . The small corrections from other four-quark operators to $\text{Im}A_0^{(0)}$ and $\text{Im}A_2^{\text{emp}}$ are not important numerically, once the cancellation is no longer operative.

The low values of ε'/ε claimed in some recent references [114–116] originate in simplified estimates of the relevant $K \rightarrow \pi\pi$ amplitudes that neglect the long-distance contributions from pion loops. Following a $1/N_C$ -inspired approach [110], Ref. [114] has advocated the inequality $B_6^{(1/2)} \leq B_8^{(3/2)} < 1$, which has been later adopted in subsequent works. However, this very questionable result is obtained within a chiral model that only includes the $\mathcal{O}(p^4)$ L_5 structure, neglecting all other terms in Eq. (3.5.34). Moreover, the only computed $1/N_C$ corrections correspond to some non-factorizable divergent contributions of the form $\log(\Lambda^2/M^2)$, with Λ an UV cut-off that is identified with the short-distance renormalization scale μ , and M a badly-defined infrared scale of $\mathcal{O}(M_K)$. All other quantum corrections (including the important absorptive contributions) are just ignored. Notice also that in order to properly define the parameter $B_6^{(1/2)}$, one needs first to specify L_5^∞ , which in Ref. [114] is fixed at the large value shown in Eq. (3.6.51).

It has been well known for many years that the elastic scattering of two pions with zero relative angular momentum is very strong and generates a large phase-shift difference between the $I = 0$ and $I = 2$ states [218]. This important dynamical effect is well understood and has been rigorously predicted within the χ PT framework. The relevant

quantum corrections have been computed by many groups for $K \rightarrow \pi\pi$ [86–88, 149–151, 205, 215–217, 219, 220], $K_{\ell 4}$ [221–225] and $\pi\pi \rightarrow \pi\pi$ [171, 172, 226, 227], reaching a two-loop precision in the last two cases. Higher-loop effects have been also estimated with dispersive methods and many successful phenomenological analyses of the relevant data have been put forward along the years [228–235]. The inclusion of all known χ PT corrections is a compulsory requirement for a reliable prediction of the kaon decay amplitudes [53].

The recent RBC-UKQCD lattice calculation [100, 113], which also finds a low central value for ε'/ε , follows the Lellouch-Lüscher prescription [144] in order to incorporate the Minkowskian pion dynamics into the numerical simulation. Their results look quite encouraging, since it is the first time that a clear signal of the $\Delta I = 1/2$ enhancement seems to emerge from lattice data [101]. However, the value obtained for the isoscalar $\pi\pi$ phase shift disagrees with the experimental determination by 2.9σ . This discrepancy is larger than the one quoted for ε'/ε (2.1σ), indicating that these results are still in a very premature stage and improvements are clearly needed. Efforts towards a better lattice understanding of the pion dynamics are under way and improved results are expected soon [148]. In addition, the current lattice result does not take into account any isospin-breaking effects, which are a very important ingredient of the ε'/ε prediction [149–151]. The inclusion of electromagnetic corrections in lattice simulations of the $K \rightarrow \pi\pi$ amplitudes looks difficult, but proposals to face some of the technical problems involved are already being considered [236].

The quoted uncertainty of the SM prediction of ε'/ε in Eq. (3.8.67) is three times larger than the current experimental error. This leaves ample margin to speculate with hypothetical new-physics contributions, but prevents us from making a precise test of the SM mechanism of CP violation that could give significant constraints on the CKM parameters [237].

In order to achieve a better theoretical accuracy, the different ingredients entering the calculation must be substantially refined. Improvements look possible in the near future through a combination of analytical calculations, numerical simulations and data analyses:

- A NNLO computation of the Wilson coefficients is currently being performed [195]. The known NNLO corrections to the electroweak penguin operators [193] reduce the scheme dependence of $C_8(\mu)$ in a quite significant way and slightly increase the negative Q_8 contribution to ε'/ε . A complete NNLO calculation should allow for a similar reduction of the $y_6(\mu)$ uncertainty. Since the quark-mass anomalous dimension is already known with a much better $\mathcal{O}(\alpha_s^5)$ precision [238], the large- N_C matching could be trivially promoted to NNLO accuracy in α_s , once the Wilson coefficients are determined at this order.
- The isospin-breaking correction Ω_{eff} plays a quite important role in the ε'/ε prediction because the moderate value of Ω_{eff} results from a large numerical cancellation among different electromagnetic and strong contributions. A complete re-analysis with updated inputs has been performed [239]. Detailed information of this analysis will be presented in the next chapter.
- Applying soft-pion techniques, the $\mathcal{O}(e^2 p^0)$ coupling $g_8 g_{\text{ewk}}$ can be related to a dispersive integral over the hadronic vector and axial-vector spectral functions [240–243]. This makes possible to perform a phenomenological estimate of this LEC with τ decay data. The published analyses, using the τ spectral functions measured at LEP, agree reasonably well with the large- N_C determination, but their errors are rather large [244–247]. A new phenomenological analysis, using the recently updated and more precise ALEPH τ data has been presented in Ref. [248], obtaining a compatible prediction with the large- N_C determination. Several lattice calculations of the matrix element $\langle \pi\pi | Q_8 | K \rangle$ have been also published (some of them in the chiral limit) [95, 96, 100, 112, 113, 249].
- A matching calculation of the weak LECs at NLO in $1/N_C$ is a very challenging task that so far remains unsolved. Several analytical approaches have been pursued in the past to estimate the hadronic matrix elements of the Q_i operators beyond the large- N_C approximation [81–83, 89, 90, 102–111]. A fresh look to these pioneering attempts from a modern perspective could bring new enlightenment and, perhaps,

could suggest ways to implement some of these methods within a well-defined EFT framework where a proper NLO matching calculation could be accomplished.

- The dominant two-loop χ PT corrections originate from large chiral logarithms, either associated with unitarity contributions or infrared singularities of the massless Goldstone theory [86–88, 250, 251]. A reliable estimate of these two-loop contributions should be feasible.
- In the next few years, lattice simulations are expected to provide new data on $K \rightarrow \pi\pi$ transitions, with improved methods and higher statistics [147, 148]. Combined with appropriate χ PT techniques, a better control of systematic uncertainties could be achieved. Moreover, analysing the sensitivity of the lattice results to several input parameters, such as quark masses and/or the electromagnetic coupling, one could try to disentangle the different contributions to the decay amplitudes and get a better understanding of the underlying dynamics. Improved lattice determinations of the strong LECs are also needed, in particular of the crucial L_5 parameter.

At present, the SM prediction of ε'/ε agrees well with the measured value and provides a qualitative confirmation of the SM mechanism of CP violation. The theoretical error is still large, but the prospects to achieve a better accuracy in the next few years are good. A significant step forward in our theoretical understanding of the kaon dynamics would allow us to perform a precise test of the electroweak theory, giving complementary and very relevant information on the CKM matrix structure in the kaon sector.

Chapter 4

Isospin violation in kaon decays

In this chapter, we perform a reanalysis of the known isospin-breaking contributions to the $K \rightarrow \pi\pi$ amplitudes, taking into account our current understanding of the quark masses and the relevant non-perturbative inputs. In addition, we present a complete numerical reappraisal of the direct CP-violating ratio ε'/ε , where these corrections play a quite significant role. After including the updated isospin-breaking effects, we obtain that the SM prediction $\text{Re}(\varepsilon'/\varepsilon) = \left(13 \begin{smallmatrix} +6 \\ -7 \end{smallmatrix}\right) \cdot 10^{-4}$ is again in very good agreement with the measured ratio. As in Chapter 3, the uncertainty, which has been estimated very conservatively, is dominated by our current ignorance about $1/N_C$ -suppressed contributions to some relevant χ PT LECs.

4.1 Introduction

While isospin symmetry is an excellent approximation for most phenomenological applications, the isospin violations induced by the quark mass difference $m_u - m_d$ and the electromagnetic interaction can get strongly enhanced in some observables [150, 207], owing to the $\Delta I = 1/2$ rule given by Eq. (3.2.6), when a tiny isospin-violating correction to the dominant amplitude feeds into the suppressed one. This is certainly the case in the direct CP-violating ratio ε'/ε , where a subtle numerical cancellation between the two

isospin contributions takes place as discussed in Section 3.4. The current theoretical effort to predict this observable with a precision similar to the experimental one [52, 100, 113] requires an improved understanding of isospin-breaking effects [149–151, 207]. This would allow to test many possible New Physics (NP) scenarios that have been recently advocated [117–142]. Assessing the role of the different isospin-breaking corrections is one of the main motivations of this chapter.

In Chapter 3, we have seen that when CP violation is turned on, the amplitudes A_0 , A_2 and A_2^+ acquire imaginary parts and ε' is given to first order in CP violation by Eq. (3.2.8), which can be expressed as

$$\varepsilon' = -\frac{i}{\sqrt{2}} e^{i(\chi_2 - \chi_0)} \omega \frac{\text{Im}A_0}{\text{Re}A_0} \left(1 - \frac{1}{\omega} \frac{\text{Im}A_2}{\text{Im}A_0} \right). \quad (4.1.1)$$

This expression makes manifest the important potential role of isospin-breaking effects. Any small correction to the ratio $\frac{\text{Im}A_2}{\text{Im}A_0}$ gets amplified by the large value of ω^{-1} . It is well-known that the further chiral enhancement of the electromagnetic penguin contributions to $\text{Im}A_2$ makes compulsory taking them into account for any reliable estimate of ε'/ε , in spite of the fact that they are isospin-violating corrections. Furthermore, Eq. (4.1.1) contains a delicate numerical balance between the two isospin contributions, making the result very sensitive to any additional isospin-breaking corrections. Indeed, some naive estimates of $\text{Im}A_I$ result in a strong cancellation between the two terms, leading unjustifiably to low values for ε'/ε [75–80, 114–116], as have been shown in Section 3.4. A proper assessment of the isospin-violating contributions to the $K \rightarrow \pi\pi$ amplitudes is then a compulsory requirement for making reliable predictions of ε'/ε .

A detailed study of isospin-breaking effects in $K \rightarrow \pi\pi$ was performed in Ref. [149–151]. While the analytical calculations reported in these references remain valid nowadays, meanwhile there have been many relevant improvements in the needed inputs that make worth to perform an updated numerical analysis of their phenomenological implications. The much better precision achieved in the determination of quark masses allows now for improved estimates of the penguin matrix elements. Moreover, we have at present a better understanding of several non-perturbative ingredients such as the chiral LECs,

which govern the χ PT $K \rightarrow \pi\pi$ amplitudes [152–169]. Implementing those improvements by updating Ref. [150] is one of the main motivations.

In Section 4.2, we describe the structure of the amplitudes at NLO in χ PT including the most relevant isospin-breaking corrections and using the same parametrization as in Eq. (3.7.57). The main limitation of the χ PT approach originates in the not very well-known LECs that encode all short-distance dynamical information. Our current knowledge on those LECs is compiled in Section 4.3. Section 4.4 gives the chiral expansion of the different isospin amplitudes to first order in isospin-breaking and CP violation. Finally, the numerical results are presented in Section 4.5.

4.2 $K \rightarrow \pi\pi$ amplitudes at NLO

Isospin-breaking corrections are accounted only at first order, *i.e.*, only corrections of $\mathcal{O}(e^2(m_d - m_u)^0)$ and $\mathcal{O}(e^0(m_d - m_u))$ are considered. Additionally, owing to the very small value of g_{27} , as can be seen from Eq. (3.2.6) and also in the fact that $\text{Im}(g_{27}) = 0$ in the large- N_C limit, we neglect isospin-breaking corrections proportional to this coupling.¹ Therefore, we must consider the following isospin-violating contributions:

- $\mathcal{O}(\epsilon^{(2)} G_8 p^2)$ with the tree-level $\pi^0 - \eta$ mixing angle $\epsilon^{(2)}$, which to first order in isospin breaking is given by

$$\begin{pmatrix} \pi_3 \\ \eta_8 \end{pmatrix} = \begin{pmatrix} 1 & -\epsilon^{(2)} \\ \epsilon^{(2)} & 1 \end{pmatrix} \begin{pmatrix} \pi^0 \\ \eta \end{pmatrix}_{\text{LO}}, \quad (4.2.2)$$

with

$$\epsilon^{(2)} = \frac{\sqrt{3}}{4} \frac{m_d - m_u}{m_s - \hat{m}} \equiv \frac{\sqrt{3}}{4R} = (1.137 \pm 0.045) \cdot 10^{-2}. \quad (4.2.3)$$

We have extracted the numerical value from the most recent FLAG average of lattice determinations of light-quark masses, with $N_f = 2 + 1$ dynamical fermions, which quotes $R = 38.1 \pm 1.5$ [259]. The corrections from $\pi^0 - \eta$ mixing enter both in the modified vertices and in the on-shell masses.

¹Isospin-breaking corrections to g_{27} can be found in Refs. [256–258]

- $\mathcal{O}(\epsilon^{(2)} G_8 p^4)$. One has:

- $\pi^0 - \eta$ mixing at NLO. Identical to the previous correction but changing $\epsilon^{(2)} \rightarrow \epsilon_S^{(4)}$ [150, 178],

$$\begin{aligned} \epsilon_S^{(4)} = & -\frac{2\epsilon^{(2)}}{3(4\pi F)^2(M_\eta^2 - M_\pi^2)} \left\{ (4\pi)^2 64 [3L_7 + L_8^r(\nu_\chi)] (M_K^2 - M_\pi^2)^2 \right. \\ & - M_\eta^2 (M_K^2 - M_\pi^2) \log \frac{M_\eta^2}{\nu_\chi^2} + M_\pi^2 (M_K^2 - 3M_\pi^2) \log \frac{M_\pi^2}{\nu_\chi^2} \\ & \left. - 2M_K^2 (M_K^2 - 2M_\pi^2) \log \frac{M_K^2}{\nu_\chi^2} - 2M_K^2 (M_K^2 - M_\pi^2) \right\} . \end{aligned} \quad (4.2.4)$$

- Isospin-conserving amplitudes, but accounting for the isospin-breaking correction to the pseudoscalar masses, either in the propagators or the on-shell external legs.
- Diagrams analogous to the isospin-conserving ones, but with vertices obtained after applying the rotation of Eq. (4.2.2), so that one of the vertices introduces an $\epsilon^{(2)}$ factor.

- $\mathcal{O}(e^2 G_8 p^0)$, coming from either the electroweak Lagrangian ($e^2 g_8 g_{\text{ewk}}$) or the non-leptonic one (g_8) when accounting for electromagnetic corrections to the external masses.

- $\mathcal{O}(e^2 G_8 p^2)$, entering through:

- $\pi^0 - \eta$ mixing at NLO. Identical to the strong isospin-breaking correction but with $\epsilon^{(2)} \rightarrow \epsilon_{EM}^{(4)}$ [150, 260],

$$\begin{aligned} \epsilon_{EM}^{(4)} = & \frac{2\sqrt{3}\alpha}{108\pi(M_\eta^2 - M_\pi^2)} \left\{ -9M_K^2 Z \left(\log \frac{M_K^2}{\nu_\chi^2} + 1 \right) \right. \\ & + 2M_K^2 (4\pi)^2 [2U_2^r(\nu_\chi) + 3U_3^r(\nu_\chi)] \\ & \left. + M_\pi^2 (4\pi)^2 [2U_2^r(\nu_\chi) + 3U_3^r(\nu_\chi) - 6U_4^r(\nu_\chi)] \right\} , \end{aligned} \quad (4.2.5)$$

where $U_i^r(\nu_\chi)$ are linear combinations of the K_i^r LECs defined in Eq. (3.5.38),

$$\begin{aligned} U_1 &= K_1 + K_2 , & U_2 &= K_5 + K_6 , \\ U_3 &= K_4 - 2 K_3 , & U_4 &= K_9 + K_{10} . \end{aligned} \quad (4.2.6)$$

- Loop corrections with one $g_8 g_{\text{ewk}}$ vertex.
- Again, isospin-conserving amplitudes, but accounting for the isospin-breaking correction to the pseudoscalar masses either in the propagators or the external legs.
- Electromagnetic loop corrections with one g_8 vertex and virtual photon propagators. In order to cancel the infrared divergences, one must also add the corresponding calculation of the $K \rightarrow \pi\pi\gamma$ rates [150].
- Tree-level diagrams with at least one electroweak vertex and a NLO insertion.

4.2.1 Isospin breaking structure of the amplitudes

Taking into account the previous discussion and inspired by the parametrization introduced in Section 3.7, we generalize this parametrization including the isospin-breaking corrections. Then, the isospin amplitudes \mathcal{A}_n ($n = 1/2, 3/2, 5/2$) can be expressed to first order in isospin-breaking as

$$\begin{aligned} \mathcal{A}_n &= -G_{27} F_\pi \left(M_K^2 - M_\pi^2 \right) \mathcal{A}_n^{(27)} - G_8 F_\pi \left(M_K^2 - M_\pi^2 \right) \left[\mathcal{A}_n^{(8)} + \epsilon^{(2)} \mathcal{A}_n^{(\epsilon)} \right] \\ &\quad + e^2 G_8 F_\pi^3 \left[\mathcal{A}_n^{(\gamma)} + Z \mathcal{A}_n^{(Z)} + g_{\text{ewk}} \mathcal{A}_n^{(g)} \right] , \end{aligned} \quad (4.2.7)$$

where $\mathcal{A}_n^{(\epsilon)}$ refers to the strong isospin-breaking contributions, $\mathcal{A}_n^{(g)}$ and $\mathcal{A}_n^{(Z)}$ are the contributions with an insertion of g_{ewk} and Z vertices, and $\mathcal{A}_n^{(\gamma)}$ are the contributions induced by the photon loops. In Eq. (4.2.7), we have replaced the Goldstone coupling F by F_π , the physical pion decay constant at NLO. The isospin-conserving relation between these two parameters has already been introduced in Chapter 3 through Eq. (3.7.59).

n	(27)	(8)	(ϵ)	(Z)	(g)
1/2	$\frac{\sqrt{2}}{9}$	$\sqrt{2}$	$-\frac{2}{3}\frac{\sqrt{2}}{\sqrt{3}}$	$\frac{4\sqrt{2}}{3}$	$\frac{2\sqrt{2}}{3}$
3/2	$\frac{10}{9}$	0	$\frac{4}{3\sqrt{3}}$	$\frac{4}{3}$	$\frac{2}{3}$

Table 4.1: $a_n^{(X)}$ values for $n = 1/2, 3/2$. $a_{5/2}^{(X)} = 0$ for all X and $a_n^{(\gamma)} = 0$ for all n .

Including isospin-breaking effects, they are related through [172, 208]

$$\begin{aligned}
F = F_\pi \left\{ 1 - \frac{4}{F^2} \left[L_4^r(\nu_\chi) (M_\pi^2 + 2M_K^2) + L_5^r(\nu_\chi) M_\pi^2 \right] \right. \\
+ \frac{1}{2(4\pi)^2 F^2} \left[2M_\pi^2 \log\left(\frac{M_\pi^2}{\nu_\chi^2}\right) + M_K^2 \log\left(\frac{M_K^2}{\nu_\chi^2}\right) \right] \\
\left. + \frac{2\epsilon^{(2)}}{\sqrt{3}} (M_K^2 - M_\pi^2) \left[\frac{8L_4^r(\nu_\chi)}{F^2} - \frac{1}{2(4\pi)^2 F^2} \left(1 + \log\left(\frac{M_K^2}{\nu_\chi^2}\right) \right) \right] \right\}, \quad (4.2.8)
\end{aligned}$$

so that those corrections get reabsorbed into the different NLO terms.

Each amplitude $\mathcal{A}_n^{(X)}$ in Eq. (4.2.7) can be decomposed as

$$\mathcal{A}_n^{(X)} = \begin{cases} a_n^{(X)} \left[1 + \Delta_L \mathcal{A}_n^{(X)} + \Delta_C \mathcal{A}_n^{(X)} \right], & \text{if } a_n^{(X)} \neq 0, \\ \Delta_L \mathcal{A}_n^{(X)} + \Delta_C \mathcal{A}_n^{(X)}, & \text{if } a_n^{(X)} = 0, \end{cases} \quad (4.2.9)$$

with $a_n^{(X)}$, $\Delta_L \mathcal{A}_n^{(X)}$ and $\Delta_C \mathcal{A}_n^{(X)}$ being the LO, NLO loop and NLO local contributions, respectively as we have already seen in Chapter 3. The amplitudes $\mathcal{A}_n^{(X)}$ and their components $a_n^{(X)}$, $\Delta_L \mathcal{A}_n^{(X)}$ and $\Delta_C \mathcal{A}_n^{(X)}$ are dimensionless by construction. In Table 4.1, we give the values of the LO factors $a_n^{(X)}$. The loop corrections $\Delta_L \mathcal{A}_n^{(X)}$ account for the requirements of unitarity and analyticity; these non-local contributions are fully predicted in terms of the pseudoscalar masses and the pion decay constant. The local components $\Delta_C \mathcal{A}_n^{(X)}$ contain the explicit dependence on the NLO LECs that renormalize the ultraviolet loop divergences. Therefore, both $\Delta_L \mathcal{A}_n^{(X)}$ and $\Delta_C \mathcal{A}_n^{(X)}$ depend on the χ PT renormalization scale, but this dependence exactly cancels in their sum. The full expressions for $\Delta_L \mathcal{A}_n^{(X)}$ and $\Delta_C \mathcal{A}_n^{(X)}$ can be found in Appendix B and in Section 4.4 of Ref. [150] respectively.

4.3 Determination of chiral LECs

In the last section, we have introduced the general structure of the $K \rightarrow \pi\pi$ amplitudes at NLO, accounting for isospin-breaking effects too. The only remaining ingredients are the χ PT LECs, which are not fixed by symmetry considerations. However, these couplings can be determined performing a matching in the large- N_C limit between the short-distance Lagrangian and its chiral realization as we have seen in Section 3.6. As a result, we obtain the electroweak chiral couplings ($g_8, g_{27}, g_8 g_{\text{ewk}}, g_8 N_i, g_{27} D_i, g_8 Z_i$) in terms of the strong and electromagnetic LECs of $\mathcal{O}(p^n)$ with $n = 2, 4, 6$ and $\mathcal{O}(e^2 p^2)$, respectively.

4.3.1 Weak couplings at $\mathcal{O}(G_F p^2)$ and $\mathcal{O}(e^2 G_8 p^0)$

At leading order in $1/N_C$, the chiral couplings of the nonleptonic electroweak Lagrangian of $\mathcal{O}(G_F p^2, e^2 G_8 p^0)$ given by Eq. (3.5.40), take the values of Eqs. (3.6.48) [88,150]. These large- N_C expressions imply²

$$g_8^\infty = \left(1.15_{-0.17}^{+0.14}(\mu) \pm 0.04_{(L_i)} \pm 0.01_{(m_s)} \right) + \tau \left(0.76_{-0.25}^{+0.12}(\mu) \pm 0.20_{(L_i)} \pm 0.03_{(m_s)} \right), \quad (4.3.10)$$

$$g_{27}^\infty = 0.46 \pm 0.02(\mu), \quad (4.3.11)$$

$$(g_8 g_{\text{ewk}})^\infty = \left(-1.54_{-0.87}^{+1.41}(\mu) \pm 0.14_{(L_i)} \pm 0.17_{(K_i)} \pm 0.05_{(m_s)} \right) + \tau \left(-19.9_{-2.2}^{+5.7}(\mu) \pm 1.8_{(L_i)} \pm 0.83_{(K_i)} \pm 0.7_{(m_s)} \right), \quad (4.3.12)$$

where the first uncertainty has been estimated through the variation of the scale μ between 0.77 GeV and 1.3 GeV, while the second and third ones reflect the current errors on the strong LECs of $\mathcal{O}(p^4)$ and the electromagnetic couplings of $\mathcal{O}(e^2 p^2)$. The last error

²The numerical inputs for K_9 and K_{10} are presented below. Although this results have been already presented in Tables 3.2 and 3.3, we decide to put them since the numerical inputs used for this chapter differ slightly from the previous one.

indicates the parametric uncertainty induced by the quark mass factor, which has been taken within the range $(m_s + m_d)(\mu = 1 \text{ GeV}) = 131.8 \pm 2.2 \text{ MeV}$ [259].

The numerical results in Eqs. (4.3.10) and (4.3.11) are quite far from their phenomenologically extracted values, including chiral loop corrections, $g_8 \approx 3.6$ and $g_{27} \approx 0.29$ [53]. This fact just reflects the importance of $\mathcal{O}(1/N_C)$ corrections in the CP-conserving amplitudes. In Section 4.5.2, we will perform a fit to $K \rightarrow \pi\pi$ data in order to obtain reliable predictions for the CP-conserving parts of g_8 and g_{27} .

4.3.2 Weak couplings at $\mathcal{O}(G_F p^4)$ and $\mathcal{O}(e^2 G_8 p^2)$

At NLO, the large- N_C matching fixes the couplings $G_8 N_i$, $G_{27} D_i$ and $G_8 Z_i$ of the non-leptonic weak and electroweak Lagrangians given by Eq. (3.5.42). In this section, we compile the results obtained in Ref. [150]. Taking the definitions,

$$\tilde{C}_1(\mu) \equiv -\frac{2}{5}C_1(\mu) + \frac{3}{5}C_2(\mu) + C_4(\mu), \quad (4.3.13)$$

$$\tilde{C}_2(\mu) \equiv +\frac{3}{5}C_1(\mu) - \frac{2}{5}C_2(\mu) + C_3(\mu) - C_5(\mu), \quad (4.3.14)$$

the non-vanishing LECs contributing to the $K \rightarrow \pi\pi$ amplitudes can be parametrized as follows:

$$(g_{27} D_4)^\infty = 4 L_5 g_{27}^\infty, \quad (4.3.15)$$

$$\begin{aligned} (g_8 N_i)^\infty &= n_i L_5 \tilde{C}_1(\mu) + \mathcal{X}_i B(\mu) C_6(\mu) \\ &= n_i L_5 \left(g_8^\infty + B(\mu) C_6(\mu) \left[16 L_5 + \frac{\mathcal{X}_i}{n_i L_5} \right] \right), \end{aligned} \quad (4.3.16)$$

with n_i and \mathcal{X}_i defined in Table E.1 of Appendix E as functions of the LECs of Eqs. (3.5.34) and (3.5.35), and

$$\begin{aligned} (g_8 Z_i)^\infty &= \mathcal{K}_i^{(1)} \tilde{C}_1(\mu) + \mathcal{K}_i^{(2)} \tilde{C}_2(\mu) + \mathcal{K}_i^{(3)} B(\mu) C_6(\mu) \\ &+ \frac{1}{e^2} \left\{ \mathcal{K}_i^{(4)} C_7(\mu) + \mathcal{K}_i^{(5)} B(\mu) C_8(\mu) + \mathcal{K}_i^{(6)} C_9(\mu) + \mathcal{K}_i^{(7)} C_{10}(\mu) \right\}, \end{aligned} \quad (4.3.17)$$

where the constants $\mathcal{K}_i^{(k)}$ are defined in Table E.2 of Appendix E.

The dependence on the χ PT renormalization scale ν_χ is of $\mathcal{O}(1/N_C)$ and, therefore, is absent from these large- N_C expressions. To account for this systematic uncertainty, we will vary ν_χ between 0.6 GeV and 1 GeV in the loop contributions and the resulting numerical fluctuations will be added as an additional error in the predicted amplitudes.

4.3.3 Strong couplings of $\mathcal{O}(p^4)$ and $\mathcal{O}(p^6)$

The $K \rightarrow \pi\pi$ amplitudes have an explicit dependence on some LECs of the $\mathcal{O}(p^4)$ strong Lagrangian as we have seen in Chapter 3. The values for L_5 and L_8 have been introduced in Section 3.6. For L_7 , we use

$$L_7 = (-0.34 \pm 0.09) \cdot 10^{-3}, \quad (4.3.18)$$

which has been extracted from an $\mathcal{O}(p^6)$ phenomenological fit to kaon and pion data [167]. Note that L_7 does not depend on the χ PT renormalization scale. This input value is in perfect agreement with the large- N_C estimate [153, 155],

$$L_7^\infty = -\frac{F_\pi^2}{48M_{\eta_1}^2} = -2.7 \cdot 10^{-4}, \quad (4.3.19)$$

with $M_{\eta_1} = 804$ MeV [153].

The strong LECs of the $\mathcal{O}(p^6)$ Lagrangian enter into the amplitudes through the coefficients \mathcal{X}_i of Eq. (4.3.16), which only depend on X_{12} , X_{14-20} , X_{31} , X_{33} , X_{34} , X_{37} , X_{38} , X_{91} and X_{94} . The dependence on X_{37} and X_{94} exactly cancels, however, in all $\Delta_C \mathcal{A}_n^{(X)}$ amplitudes; thus these couplings are not needed. Using Resonance Chiral Theory (R χ T) [153, 154], these LECs can be estimated in terms of meson resonance parameters, through the tree-level exchange of the lightest resonance states. This amounts to perform the matching between the χ PT and R χ T Lagrangians at leading order in $1/N_C$, in the single-resonance approximation. An analysis of all resonance contributions to the X_i couplings can be found in Ref. [156]. Furthermore, a complete analysis of the η_1 contributions to the chiral low-energy constants of $\mathcal{O}(p^6)$ was presented in Ref. [157], the only $\tilde{X}_i^{\eta_1}$ that contribute to $K \rightarrow \pi\pi$ are

$$\tilde{X}_{18}^{\eta_1} = 3 \tilde{X}_{19}^{\eta_1} = -2 \tilde{X}_{20}^{\eta_1} = \tilde{X}_{31}^{\eta_1} = \frac{L_7^\infty}{M_{\eta_1}^2}, \quad \tilde{X}_{33}^{\eta_1} = 0. \quad (4.3.20)$$

Combining both results, we obtain the values given in Table 4.2. As expected for the $K \rightarrow \pi\pi$ amplitudes, the relevant couplings do not receive contributions from vector and axial-vector exchanges. Moreover, all η_1 contributions coming from the $\tilde{X}_i^{\eta_1}$ factors in Table 4.2 cancel also in the combinations \mathcal{X}_i that govern the $(g_8 N_i)^\infty$ LECs, as it should. The exchange of η_1 mesons can only contribute indirectly to $K \rightarrow \pi\pi$, through the dependence on L_7 of the $\pi^0 - \eta$ mixing correction $\epsilon_S^{(4)}$ in Eq. (4.2.4), which gives rise to the term proportional to $L_7 L_8$ in \mathcal{X}_{13} . This unique η_1 contribution appears in the NLO local corrections $\Delta_C \mathcal{A}_{1/2,3/2}^{(\epsilon)}$ and represents one of the largest sources of uncertainty in our numerical results.

X_i/F^2	Large- N_C prediction
12	$-\frac{c_d c_m}{2 M_S^4}$
14	$-\frac{d_m^2}{4 M_P^4} + (\bar{\lambda}_1^{SS})' + 2 \frac{c_d}{c_m} (\bar{\lambda}_3^{SS})'$
15	0
16	0
17	$-\frac{d_m^2}{4 M_P^4} + \bar{\lambda}_2^{SS}$
18	$\tilde{X}_{18}^{\eta_1}$
19	$\frac{c_d c_m}{27 M_S^4} + \frac{\bar{\lambda}_4^S}{9} + (\bar{\lambda}_3^{SS})' + \tilde{X}_{19}^{\eta_1}$
20	$-\frac{c_d c_m}{18 M_S^4} - \frac{\bar{\lambda}_4^S}{6} + \tilde{X}_{20}^{\eta_1}$
31	$-\frac{d_m^2}{2 M_P^4} - \frac{7}{18} \frac{c_d c_m}{M_S^4} + \frac{\bar{\lambda}_4^S}{3} - 2 (\bar{\lambda}_2^{SP})' + \tilde{X}_{31}^{\eta_1}$
33	$\frac{d_m^2}{6 M_P^4} + \frac{2}{9} \frac{c_d c_m}{M_S^4} + \frac{\bar{\lambda}_4^S}{6} + \bar{\lambda}_5^S - \bar{\lambda}_3^P + \tilde{X}_{33}^{\eta_1}$
34	$\frac{d_m^2}{2 M_P^4} + \frac{c_d c_m}{2 M_S^4} + \frac{c_m^2}{2 M_S^4} - \frac{d_m^2}{M_P^2 M_S^2}$
38	$-\frac{d_m^2}{2 M_P^4} + \frac{c_m^2}{2 M_S^4}$
91	$2 \frac{d_m^2}{M_P^4}$

Table 4.2: Large- N_C predictions for the relevant strong LECs of $\mathcal{O}(p^6)$ [156].

Thus, only contributions from scalar and pseudoscalar resonance-exchange enter into the relevant X_i LECs in Table 4.2. The LO R χ T couplings have been determined within

the single-resonance approximation, which gives the relations [155]:

$$c_m = c_d = \sqrt{2} d_m = F_\pi/2, \quad M_P = \sqrt{2} M_S. \quad (4.3.21)$$

These couplings correspond to $\mathcal{O}(p^2)$ chiral structures with Goldstone fields coupled to a single resonance multiplet, either scalar ($c_{d,m}$) or pseudoscalar (d_m). The table contains, in addition, contributions from $\mathcal{O}(p^4)$ chiral structures with one resonance ($\bar{\lambda}_i^R$) and $\mathcal{O}(p^2)$ terms with two resonances ($\bar{\lambda}_i^{RR'}$) that are currently unknown. We are only aware of one estimate of $\lambda_3^{SS} \equiv \bar{\lambda}_3^{SS} M_S^4/c_m^2$, determined from the scalar resonance spectrum [211], which we update in Appendix F. We obtain:

$$M_S = 1478 \text{ MeV}, \quad \lambda_3^{SS} = 0.1548. \quad (4.3.22)$$

In the absence of better information, we will take null values for the unknown $\bar{\lambda}_i^R$ and $\bar{\lambda}_i^{RR'}$ couplings. In order to estimate the size of uncertainties in any observable F associated to the LECs X_i , we will take:

$$\text{error of } F = \frac{|F(X_i) - F(0)|}{N_C}. \quad (4.3.23)$$

4.3.4 Electromagnetic couplings of $\mathcal{O}(e^2 p^2)$

The electromagnetic LECs K_i can be expressed as convolutions of QCD correlators with a photon propagator [213], and their evaluation involves an integration over the virtual photon momenta. Therefore, they have an explicit dependence on the χ PT renormalization scale ν_χ , already at leading order in $1/N_C$. In Ref. [266], the couplings K_{1-6}^r have been estimated by computing 4-point Green functions (two currents and two electromagnetic spurion fields) in χ PT and matching them with their $R\chi$ T estimate (neglecting pseudoscalar contributions). The $R\chi$ T couplings are obtained by imposing short-distance constraints. They find

$$\begin{aligned} K_1^r(M_\rho) &= -K_3^r(M_\rho) = -2.71 \cdot 10^{-3}, & K_5^r(M_\rho) &= 11.59 \cdot 10^{-3}, \\ K_2^r(M_\rho) &= \frac{1}{2} K_4^r(M_\rho) = 0.69 \cdot 10^{-3}, & K_6^r(M_\rho) &= 2.77 \cdot 10^{-3}. \end{aligned} \quad (4.3.24)$$

The remaining couplings can be accessed through the study of two- and three-point functions. $K_{7,8}^r$ turn out to be $1/N_C$ suppressed, *i.e.*, $K_7^r(M_\rho) \approx K_8^r(M_\rho) \approx 0$ [213]. K_{9-13}^r are gauge dependent, while K_{9-12}^r depend also on the short-distance renormalization scale μ . Those dependences cancel with the photon loop contributions in the physical decay amplitudes. The explicit values we quote below refer to the Feynman gauge ($\xi = 1$) and $\mu = 1$ GeV [150, 213, 214, 266, 267]:

$$\begin{aligned} K_9^r(M_\rho) &= 2.2 \cdot 10^{-3}, & K_{10}^r(M_\rho) &= 6.5 \cdot 10^{-3}, & (4.3.25) \\ K_{11}^r(M_\rho) &= 1.26 \cdot 10^{-3}, & K_{12}^r(M_\rho) &= -4.2 \cdot 10^{-3}, & K_{13}^r(M_\rho) &= 4.7 \cdot 10^{-3}. \end{aligned}$$

The uncertainties associated with these LECs will be also estimated following the method indicated in Eq. (4.3.23).

4.4 Anatomy of isospin-breaking parameters

To first order in isospin breaking ε' can be written as indicated in (3.2.10). In order to determine the different sources of isospin-breaking effects, it is useful to write the CP-violating amplitudes as

$$\begin{aligned} A_0 e^{i\chi_0} &= \mathcal{A}_{1/2}^{(0)} + \delta\mathcal{A}_{1/2}, \\ A_2 e^{i\chi_2} &= \mathcal{A}_{3/2}^{(0)} + \delta\mathcal{A}_{3/2} + \mathcal{A}_{5/2}, \end{aligned} \quad (4.4.26)$$

where $\delta\mathcal{A}_{1/2,3/2}$ and $\mathcal{A}_{5/2}$ are first order in isospin violation. The amplitudes $\mathcal{A}_{\Delta I}$ have both absorptive, Abs $\mathcal{A}_{\Delta I}$, and dispersive, Disp $\mathcal{A}_{\Delta I}$, parts. Therefore, the loop-induced phases χ_I have to be carefully separated from the CP-violating ones. Expanding to first

order in CP and isospin violation, one finds [150]:

$$\begin{aligned}
\text{Im}A_0^{(0)} &= \left| \mathcal{A}_{1/2}^{(0)} \right|^{-1} \left\{ \text{Im}[\text{Disp } \mathcal{A}_{1/2}^{(0)}] \text{Re}[\text{Disp } \mathcal{A}_{1/2}^{(0)}] \right. \\
&\quad \left. + \text{Im}[\text{Abs } \mathcal{A}_{1/2}^{(0)}] \text{Re}[\text{Abs } \mathcal{A}_{1/2}^{(0)}] \right\} , \\
\text{Im}A_2 &= \left| \mathcal{A}_{3/2}^{(0)} \right|^{-1} \left\{ \text{Im}[\text{Disp } (\delta \mathcal{A}_{3/2} + \mathcal{A}_{5/2})] \text{Re}[\text{Disp } \mathcal{A}_{3/2}^{(0)}] \right. \\
&\quad \left. + \text{Im}[\text{Abs } (\delta \mathcal{A}_{3/2} + \mathcal{A}_{5/2})] \text{Re}[\text{Abs } \mathcal{A}_{3/2}^{(0)}] \right\} , \\
\Delta_0 &= -2 \left| \mathcal{A}_{1/2}^{(0)} \right|^{-2} \left(\text{Re}[\text{Disp } \mathcal{A}_{1/2}^{(0)}] \text{Re}[\text{Disp } \delta \mathcal{A}_{1/2}] + \text{Re}[\text{Abs } \mathcal{A}_{1/2}^{(0)}] \text{Re}[\text{Abs } \delta \mathcal{A}_{1/2}] \right) \\
&\quad + \left[\text{Im}[\text{Disp } \mathcal{A}_{1/2}^{(0)}] \text{Re}[\text{Disp } \mathcal{A}_{1/2}^{(0)}] + \text{Im}[\text{Abs } \mathcal{A}_{1/2}^{(0)}] \text{Re}[\text{Abs } \mathcal{A}_{1/2}^{(0)}] \right]^{-1} \\
&\quad \times \left\{ \text{Im}[\text{Disp } \delta \mathcal{A}_{1/2}] \text{Re}[\text{Disp } \mathcal{A}_{1/2}^{(0)}] + \text{Im}[\text{Disp } \mathcal{A}_{1/2}^{(0)}] \text{Re}[\text{Disp } \delta \mathcal{A}_{1/2}] \right. \\
&\quad \left. + \text{Im}[\text{Abs } \delta \mathcal{A}_{1/2}] \text{Re}[\text{Abs } \mathcal{A}_{1/2}^{(0)}] + \text{Im}[\text{Abs } \mathcal{A}_{1/2}^{(0)}] \text{Re}[\text{Abs } \delta \mathcal{A}_{1/2}] \right\} , \\
f_{5/2} &= \frac{5}{3} \left| \mathcal{A}_{3/2}^{(0)} \right|^{-2} \left\{ \text{Re}[\text{Disp } \mathcal{A}_{3/2}^{(0)}] \text{Re}[\text{Disp } \mathcal{A}_{5/2}] + \text{Re}[\text{Abs } \mathcal{A}_{3/2}^{(0)}] \text{Re}[\text{Abs } \mathcal{A}_{5/2}] \right\} ,
\end{aligned} \tag{4.4.27}$$

which are all the quantities that we need to determine the different sources of isospin violation in Eq. (3.2.15).

4.5 Numerical results

At this point, we have all the theoretical ingredients to provide a numerical prediction for the isospin-breaking effects in $K \rightarrow \pi\pi$. In the following subsections, we present each of the numerical results that enter in the estimation of these corrections.

4.5.1 Amplitudes at NLO

In this subsection, we present the numerical results of the different isospin amplitudes, \mathcal{A}_n with $n = 1/2, 3/2$ and $5/2$. Tables 4.3, 4.4 and 4.5, which supersede Tables 1, 2 and 3 of Ref. [150] display the following information:

- The type of contribution (X) in the first column.
- The LO contributions $a_n^{(X)}$ in the second column.

(X)	$a_{1/2}^{(X)}$	$\Delta_L \mathcal{A}_{1/2}^{(X)}$	$[\Delta_C \mathcal{A}_{1/2}^{(X)}]^+$	$[\Delta_C \mathcal{A}_{1/2}^{(X)}]^-$
27	$\frac{\sqrt{2}}{9}$	$1.03 + 0.47 i$	$0.01 \begin{smallmatrix} +0.00 & +0.65 \\ -0.00 & -0.62 \end{smallmatrix}$	$0.01 \begin{smallmatrix} +0.00 & +0.65 \\ -0.00 & -0.62 \end{smallmatrix}$
8	$\sqrt{2}$	$0.27 + 0.47 i$	$0.02 \begin{smallmatrix} +0.00 & +0.05 \\ -0.01 & -0.05 \end{smallmatrix}$	$0.11 \begin{smallmatrix} +0.01 & +0.05 \\ -0.00 & -0.05 \end{smallmatrix}$
ε	$-\frac{2\sqrt{2}}{3\sqrt{3}}$	$0.26 + 0.47 i$	$-0.32 \begin{smallmatrix} +0.04 & +0.05 \\ -0.16 & -0.06 \end{smallmatrix}$	$1.54 \begin{smallmatrix} +0.08 & +0.05 \\ -0.02 & -0.06 \end{smallmatrix}$
γ	-	-1.39	$-0.48 \begin{smallmatrix} +0.28 & +0.26 \\ -0.12 & -0.27 \end{smallmatrix}$	$-11.16 \begin{smallmatrix} +1.22 & +0.26 \\ -3.45 & -0.27 \end{smallmatrix}$
Z	$\frac{4\sqrt{2}}{3}$	$-1.07 + 0.80 i$	$-0.11 \begin{smallmatrix} +0.01 & +0.17 \\ -0.02 & -0.18 \end{smallmatrix}$	$0.14 \begin{smallmatrix} +0.01 & +0.17 \\ -0.00 & -0.18 \end{smallmatrix}$
g	$\frac{2\sqrt{2}}{3}$	$0.28 + 0.47 i$	$-0.19 \begin{smallmatrix} +0.00 & +0.01 \\ -0.00 & -0.01 \end{smallmatrix}$	$-0.19 \begin{smallmatrix} +0.00 & +0.01 \\ -0.00 & -0.01 \end{smallmatrix}$

Table 4.3: NLO loop and local counterterm amplitudes $\mathcal{A}_{1/2}$. The two uncertainties in the local amplitudes are associated with the variations of the short-distance scale μ and the chiral scale ν_χ , respectively.

(X)	$a_{3/2}^{(X)}$	$\Delta_L \mathcal{A}_{3/2}^{(X)}$	$[\Delta_C \mathcal{A}_{3/2}^{(X)}]^+$	$[\Delta_C \mathcal{A}_{3/2}^{(X)}]^-$
27	$\frac{10}{9}$	$-0.04 - 0.21 i$	$0.01 \begin{smallmatrix} +0.00 & +0.05 \\ -0.00 & -0.05 \end{smallmatrix}$	$0.01 \begin{smallmatrix} +0.00 & +0.05 \\ -0.00 & -0.05 \end{smallmatrix}$
ε	$\frac{4}{3\sqrt{3}}$	$-0.70 - 0.21 i$	$-0.30 \begin{smallmatrix} +0.04 & +0.48 \\ -0.17 & -0.50 \end{smallmatrix}$	$1.65 \begin{smallmatrix} +0.08 & +0.48 \\ -0.02 & -0.50 \end{smallmatrix}$
γ	-	-0.47	$0.40 \begin{smallmatrix} +0.15 & +0.08 \\ -0.04 & -0.09 \end{smallmatrix}$	$-0.22 \begin{smallmatrix} +0.78 & +0.08 \\ -0.11 & -0.09 \end{smallmatrix}$
Z	$\frac{4}{3}$	$-0.87 - 0.79 i$	$0.01 \begin{smallmatrix} +0.00 & +0.32 \\ -0.01 & -0.33 \end{smallmatrix}$	$0.07 \begin{smallmatrix} +0.00 & +0.32 \\ -0.00 & -0.33 \end{smallmatrix}$
g	$\frac{2}{3}$	$-0.50 - 0.21 i$	$-0.19 \begin{smallmatrix} +0.00 & +0.19 \\ -0.00 & -0.20 \end{smallmatrix}$	$-0.19 \begin{smallmatrix} +0.00 & +0.19 \\ -0.00 & -0.20 \end{smallmatrix}$

Table 4.4: NLO loop and local counterterm amplitudes $\mathcal{A}_{3/2}$. The two uncertainties in the local amplitudes are associated with the variations of the short-distance scale μ and the chiral scale ν_χ , respectively.

(X)	$a_{5/2}^{(X)}$	$\Delta_L \mathcal{A}_{5/2}^{(X)}$	$[\Delta_C \mathcal{A}_{5/2}^{(X)}]^+$	$[\Delta_C \mathcal{A}_{5/2}^{(X)}]^-$
γ	-	-0.51	$-0.15 \begin{smallmatrix} +0.04 & +0.10 \\ -0.01 & -0.11 \end{smallmatrix}$	$-0.57 \begin{smallmatrix} +0.00 & +0.10 \\ -0.02 & -0.11 \end{smallmatrix}$
Z	-	$-0.93 - 1.16 i$	$-0.16 \begin{smallmatrix} +0.01 & +0.41 \\ -0.02 & -0.43 \end{smallmatrix}$	$0.09 \begin{smallmatrix} +0.01 & +0.41 \\ -0.00 & -0.43 \end{smallmatrix}$

Table 4.5: NLO loop and local counterterm amplitudes $\mathcal{A}_{5/2}$. The two uncertainties in the local amplitudes are associated with the variations of the short-distance scale μ and the chiral scale ν_χ , respectively.

- The NLO loop contributions $\Delta_L \mathcal{A}_n^{(X)}$ with the absorptive and dispersive components in the third column. Absorptive contributions are independent on the chiral renormalization scale ν_χ . For the dispersive contributions, ν_χ is fixed to 0.77 GeV.
- The NLO local corrections to the CP-even and CP-odd amplitudes, $[\Delta_C \mathcal{A}_n^{(X)}]^+$ and $[\Delta_C \mathcal{A}_n^{(X)}]^-$ respectively in the last columns, where

$$[\Delta_C \mathcal{A}_n^{(X)}]^\pm = \begin{cases} \frac{\text{Re} \left(G_{27} \Delta_C \mathcal{A}_n^{(27)} \right)}{\text{Im} \left(G_{27} \right)}, & X = 27, \\ \frac{\text{Re} \left(G_8 g_{\text{ewk}} \Delta_C \mathcal{A}_n^{(g)} \right)}{\text{Im} \left(G_8 g_{\text{ewk}} \right)}, & X = g, \\ \frac{\text{Re} \left(G_8 \Delta_C \mathcal{A}_n^{(X)} \right)}{\text{Im} \left(G_8 \right)}, & X = 8, Z, \epsilon, \gamma. \end{cases} \quad (4.5.28)$$

The estimation of NLO local contributions represents the main uncertainty in our results. In Tables 4.3, 4.4 and 4.5, we quote the two different sources of uncertainties. The first error is related with the lack of cancellation of the short-distance scale μ . We estimate it by varying this scale from 0.77 GeV to 1.3 GeV. The second error is associated to the missed logarithmic dependence on the χ PT scale ν_χ due to applying the large- N_C limit. In order to estimate it, we vary the chiral renormalization scale between 0.6 and 1 GeV. In most of the cases, this non-perturbative error dominates over the first one.

The results are in good agreement with the ones of the previous analysis. While the underlying physics behind the large values of $\Delta_L \mathcal{A}_{1/2,3/2}^{(Z)}$ and $[\Delta_C \mathcal{A}_{1/2}^{(\gamma)}]^-$ is well understood [150], the larger than expected values of $[\Delta_C \mathcal{A}_{1/2,3/2}^{(\epsilon)}]^-$ are not. It might be consequence of a numerical accident. While the size of the $g_8 N_i^r$ is not larger than expected, their role appears enhanced in the amplitudes with huge numerical prefactors.

4.5.2 χ PT fit to $K \rightarrow \pi\pi$ data

In Section 4.3.1, we have seen the price of taking the large- N_C limit in the CP-even sector, reflected in an unphysical short-distance scale dependence for the observables. The

large- N_C estimate is unable to correctly predict the CP-conserving parts of g_8 and g_{27} . However, one can fit them to data. The observables [150],

$$C_n = \left(\frac{2 \sqrt{s_n} \Gamma_n}{\tilde{G}_n \Phi_n} \right)^{1/2}, \quad (4.5.29)$$

where Γ_n with $n = +-, 00, +0$ are the decay rates, $\tilde{G}_n \equiv \text{Br}_n/\tau_n$, Br_n and τ_n are respectively the branching ratios and the kaon lifetimes, $\sqrt{s_n}$ is the total center of mass energy and Φ_n is the two-body phase space; are directly related to the amplitudes of Eq. (3.2.4):

$$\begin{aligned} A_2^+ &= \frac{2}{3} C_{+0}, & (A_0)^2 + (A_2)^2 &= \frac{2}{3} C_{+-}^2 + \frac{1}{3} C_{00}^2, \\ \frac{A_2}{A_0} \cos(\chi_0 - \chi_2) &= \frac{r - 1 + (\frac{A_2}{A_0})^2 (2r - \frac{1}{2})}{\sqrt{2}(1 + 2r)}, \end{aligned} \quad (4.5.30)$$

where $r \equiv (C_{+-}/C_{00})^2$. Then, using the partial widths $\Gamma_{+-,00,+0}$ from Ref. [31] as experimental inputs to obtain the C_n and using χ PT for A_I , we can perform a fit to g_8 , g_{27} and the phase difference $\chi_0 - \chi_2$. We obtain the results of Tables 4.8, 4.9, 4.6 and 4.7, which supersede Eqs. (7.11), (7.12) and (7.13) and the discussion therein of Ref. [150]. We obtain numerical values in good agreement with that work. In the next section, we use the results presented in Table 4.9 as inputs to compute the isospin-breaking parameters presented in Section 4.4.

4.5.3 Isospin-breaking parameters in the CP-odd sector

Once the NLO amplitudes have been updated (Section 4.5.1) and the CP-conserving components of g_8 and g_{27} have been fitted to experimental data (Section 4.5.2), we have all needed ingredients to compute the different IB parameters in the CP-odd sector given in Section 4.4. Since this work is an update of Ref. [150], it is worth it to compare the impact of the different updated inputs in the different (central) final NLO $\alpha \neq 0$ values. This is shown in Table 4.10, where Δ_i corresponds to the difference between the updated set-up and the same one but with the old input for the variable i ($i = \text{WC}$ stands for Wilson Coefficients). The impact of the different changed inputs is comparable in size,

	Value
Re g_8	4.985 ± 0.002 (exp)
Re g_{27}	0.286 ± 0.001 (exp)
Re A_0 /Re A_2	22.36 ± 0.05 (exp)
Re A_0 /Re A_2^+	22.36 ± 0.05 (exp)
$f_{5/2}$	0
$\chi_0 - \chi_2$ ($^\circ$)	44.78 ± 0.98 (exp)
Re A_0 ($\cdot 10^{-7}$ GeV)	2.711 ± 0.001 (exp)
Re A_2 ($\cdot 10^{-8}$ GeV)	1.212 ± 0.003 (exp)

Table 4.6: Tree-level (LO) isospin-conserving amplitudes.

	Value
Re g_8	3.599 ± 0.001 (exp) $^{+0.139}_{-0.135}$ (ν_χ) $^{+0.018}_{-0.004}$ (μ)
Re g_{27}	0.288 ± 0.001 (exp) ± 0.014 (ν_χ)
Re A_0 /Re A_2	22.36 ± 0.05 (exp)
Re A_0 /Re A_2^+	22.36 ± 0.05 (exp)
$f_{5/2}$	0
$\chi_0 - \chi_2$ ($^\circ$)	44.78 ± 0.98 (exp)
Re A_0 ($\cdot 10^{-7}$ GeV)	2.711 ± 0.001 (exp)
Re A_2 ($\cdot 10^{-8}$ GeV)	1.212 ± 0.003 (exp)

Table 4.7: NLO isospin-conserving amplitudes.

and typically slightly smaller than the central values. In particular, the sensitivity to L_7 is remarkable.

	Value
Re g_8	5.002 ± 0.002 (exp) $^{+0.013}_{-0.006}$ (μ)
Re g_{27}	0.251 ± 0.001 (exp) $^{+0.011}_{-0.004}$ (μ)
Re A_0 /Re A_2	22.13 ± 0.05 (exp) $^{+0.10}_{-0.06}$ (μ)
Re A_0 /Re A_2^+	22.13 ± 0.05 (exp) $^{+0.10}_{-0.06}$ (μ)
$f_{5/2}$	0
$\chi_0 - \chi_2$ ($^\circ$)	47.97 ± 0.92 (exp) $^{+0.12}_{-0.22}$ (μ)
Re A_0 ($\cdot 10^{-7}$ GeV)	2.704 ± 0.001 (exp)
Re A_2 ($\cdot 10^{-8}$ GeV)	1.222 ± 0.003 (exp) $^{+0.003}_{-0.006}$ (μ)

Table 4.8: Tree-level (LO) isospin-breaking amplitudes.

	Value
Re g_8	3.581 ± 0.001 (exp) $^{+0.144}_{-0.141}$ (ν_χ) $^{+0.024}_{-0.008}$ (μ)
Re g_{27}	0.296 ± 0.001 (exp) $^{+0.000}_{-0.001}$ (ν_χ) $^{+0.010}_{-0.003}$ (μ)
Re A_0 /Re A_2	20.54 ± 0.04 (exp) $^{+0.49}_{-0.50}$ (ν_χ) $^{+0.00}_{-0.02}$ (μ)
Re A_0 /Re A_2^+	22.29 ± 0.05 (exp) $^{+0.01}_{-0.06}$ (ν_χ) $^{+0.00}_{-0.03}$ (μ)
$f_{5/2}$	0.0853 ± 0.0002 (exp) $^{+0.0239}_{-0.0250}$ (ν_χ) $^{+0.0000}_{-0.0007}$ (μ)
$\chi_0 - \chi_2$ ($^\circ$)	51.395 ± 0.806 (exp) $^{+1.033}_{-1.041}$ (ν_χ) $^{+0.033}_{-0.007}$ (μ)
Re A_0 ($\cdot 10^{-7}$ GeV)	2.704 ± 0.001 (exp)
Re A_2 ($\cdot 10^{-8}$ GeV)	1.317 ± 0.003 (exp) $^{+0.033}_{-0.031}$ (ν_χ) $^{+0.001}_{-0.000}$ (μ)

Table 4.9: NLO isospin-breaking amplitudes.

In Tables 4.11, 4.12, 4.13 and 4.14, we update Table 4 of Ref. [150] separating the estimate for the different sources of uncertainties, being σ_i the error associated to the variable i .³

³The label $B(\mu)$ refers to the running of the quark masses.

Set-up	Δ_0	$f_{5/2}$	Ω_{IB}	Ω_{eff}
Central Ref. [150]	0.08346	0.08360	0.2267	0.05967
New value	0.05650	0.08202	0.2597	0.1212
Δ_{WC}	-0.011	-0.0009	0.0018	0.013
Δ_{L_5}	-0.016	0.0009	-0.032	-0.017
Δ_{L_8}	0.0032	0.0013	-0.0049	-0.0094
Δ_{L_7}	-0.0007	0.0000	0.043	0.044
Δ_{K_i}	0.0013	-0.0036	0.022	0.024
Δ_{X_i}	-0.0018	0.0001	-0.0008	-0.0026
$\Delta_{\epsilon^{(2)}}$	-0.0003	0.0000	0.012	0.012
$\Delta_{B(\mu)}$	-0.0051	0.0005	-0.0067	-0.0024

Table 4.10: NLO central values for $\alpha \neq 0$ and impact of the different modified inputs.

Set-up	Δ_0	$f_{5/2}$	Ω_{IB}	Ω_{eff}
Central	-0.00002	0	0.1370	0.1370

Table 4.11: LO central values for $\alpha = 0$.

Set-up	Δ_0	$f_{5/2}$	Ω_{IB}	Ω_{eff}
Central	-0.0051	0.0	0.171	0.176
σ_μ	+0.0000 -0.0004	0.0	+0.006 -0.002	+0.007 -0.001
σ_{ν_χ}	0.0001	0.0	+0.048 -0.047	+0.048 -0.047
σ_{γ_5}	0.0004	0.0	0.001	0.002
$\sigma_{L_{5,8}}$	0.0001	0.0	0.033	0.033
σ_{L_7}	0.0011	0.0	0.060	0.061
σ_{X_i}	0.0000	0.0	0.006	0.006

Table 4.12: NLO central values for $\alpha = 0$ and their parametric errors.

Set-up	Δ_0	$f_{5/2}$	Ω_{IB}	Ω_{eff}
Central	0.0563	0.0	0.196	0.140
σ_μ	+0.0021 -0.0000	0.0	+0.004 -0.001	+0.002 -0.002
σ_{ν_χ}	0.0000	0.0	0.000	0.000
σ_{γ_5}	0.0067	0.0	0.001	0.006
$\sigma_{L_{5,8}}$	0.0143	0.0	0.028	0.014
σ_{K_i}	0.0021	0.0	0.039	0.037

Table 4.13: LO central values for $\alpha \neq 0$ and their parametric errors.

Set-up	Δ_0	$f_{5/2}$	Ω_{IB}	Ω_{eff}
Central	0.0565	0.0820	0.260	0.121
σ_μ	+0.0066 -0.0015	+0.0003 -0.0011	+0.008 -0.002	+0.001 -0.000
σ_{ν_χ}	0.0017	+0.0232 -0.0244	0.034	+0.057 -0.055
σ_{γ_5}	0.0067	0.0009	0.001	0.004
$\sigma_{L_{5,8}}$	0.0136	0.0017	0.040	0.029
σ_{L_7}	0.0011	0.0000	0.060	0.061
σ_{K_i}	0.0019	0.0031	0.018	0.013
σ_{X_i}	0.0021	0.0003	0.003	0.005

Table 4.14: NLO central values for $\alpha \neq 0$ and their parametric errors.

Since its sensitivity to L_7 is particularly strong, we show in Figure 4.1 the dependence of the central value of Ω_{eff} with L_7 . The dashed line is the L_7 value from Ref. [167] with its error (dotted line). The red line is the large- N_C prediction for L_7 .

4.6 Impact on the ε'/ε prediction

In this chapter, we have presented a re-analysis of the isospin-breaking corrections in $K \rightarrow \pi\pi$ [150]. Due to the $\Delta I = 1/2$ rule, these corrections get strongly enhanced in the

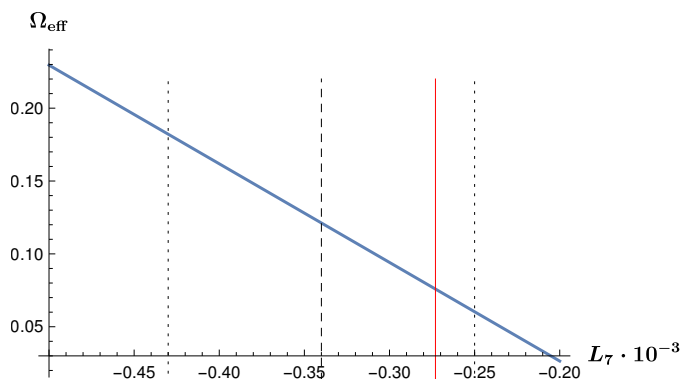
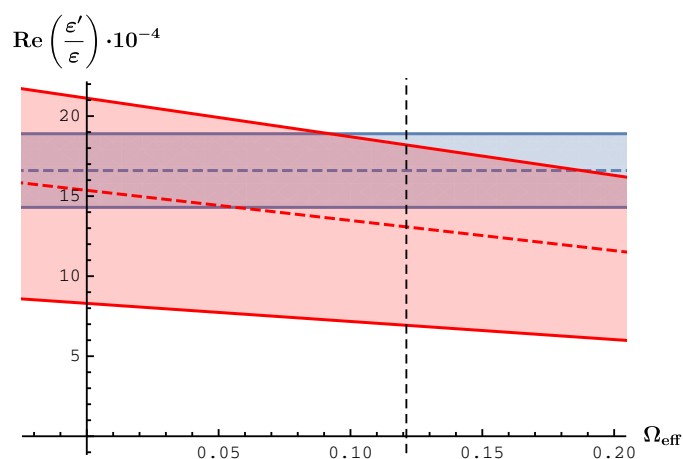
Figure 4.1: Central value of Ω_{eff} as a function of L_7 .

Figure 4.2: SM prediction for $\text{Re}(\varepsilon'/\varepsilon)$ (red dashed line) as a function of Ω_{eff} . The red band has been obtained adding all sources of uncertainty in quadrature for a fixed value of Ω_{eff} . The vertical dashed line indicates the central value of Ω_{eff} in (4.6.31) and the blue horizontal band the measured value of $\text{Re}(\varepsilon'/\varepsilon)$.

direct CP-violating ratio ε'/ε , then it is necessary to re-analyze them in order to make a reliable prediction for this observable. After reviewing the different improvements on many of the inputs, we have obtained updated amplitudes, which lead to a new value for the different relevant isospin-breaking parameters. Among them, it is worth it to remark

the value of Ω_{eff} that encodes the isospin-breaking corrections in ε'/ε . Our prediction is

$$\Omega_{\text{eff}} = (12.1_{-8.8}^{+9.0}) \cdot 10^{-2}, \quad (4.6.31)$$

where the final uncertainty has been obtained by conservatively adding all the errors in quadrature. Figure 4.2 shows the dependence of $\text{Re}(\varepsilon'/\varepsilon)$ on Ω_{eff} . Taking into account the updated value, our prediction for $\text{Re}(\varepsilon'/\varepsilon)$ is

$$\begin{aligned} \text{Re}(\varepsilon'/\varepsilon) &= \left(13.1 \pm 0.4_{m_s} \pm 2.2_{\mu} \pm 3.0_{\nu_\chi} \pm 1.2_{\gamma_5} \pm 4.3_{L_{5,8}} \pm 1.1_{L_7} \pm 0.2_{K_i} \pm 0.3_{X_i} \right) \cdot 10^{-4} \\ &= \left(13_{-7}^{+6} \right) \cdot 10^{-4}, \end{aligned} \quad (4.6.32)$$

which is in perfect agreement with the experimental one [64–72]. We find that the impact of this updated value on ε'/ε is small, finding a central value a slightly smaller than the one obtained in Chapter 3. In spite of the large uncertainty, mostly coming from our ignorance of non-perturbative effects in the matching region.

Chapter 5

Neutral meson mixing in Multi-Higgs-Doublet Models

In this chapter, we present a complete one-loop computation of the Wilson coefficients for the neutral meson mixing in the Aligned-Multi-Higgs-Doublet Model (AMHDM). We contemplate the possibility of extending the $N - 1$ Higgs doublets to colour-octet scalars. After giving a detailed technical summary of the computation, we particularize our analytical results to the wide casuistry of NP models, and finally we obtain combined constraints on the parameters of these models from the current flavour data.

5.1 Introduction

Since the discovery of the Higgs boson, the search for physics beyond the SM has become a priority task for the high-energy-physics community. One of the simplest extensions is to include in the SM one additional Higgs doublet that transforms under the $SU(2)_L$ gauge group, this model is known as Two-Higgs-Doublet Model (2HDM) [268, 269]. It has a rich scalar spectrum (two charged and three neutral scalar fields, in addition to the three Goldstones needed to generate the gauge boson masses) which incorporates interesting phenomenological features, such as potential new sources of CP violation, axion

phenomenology or dark matter candidates, just to mention a few of them. In the most general version of the 2HDM [270–272], the fermionic couplings of the neutral scalars are non-diagonal in flavour, then this gives rise to Flavour Changing Neutral Current (FCNC) interactions which represent the main deficiency of this model because these phenomena are experimentally very constrained [2]. One of the possible ways to avoid the FCNC interactions consists in using flavour alignment [273–275]. Assuming that the couplings of all scalar doublets to a given right-handed fermion have the same flavour structure, then all the Yukawas can be diagonalized simultaneously and these unwanted FCNC interactions disappear at tree level.

Due to the GIM mechanism, the scalar mediators of this type of models play an important role in some low-energy processes. An example can be found in the neutral meson mixing, where the charged particles contribute at the same order as does the W^\pm bosons in the SM, therefore one could expect significant NP contributions. Although some recent works have studied these type of contributions [276–279], we can go a step further and generalize the results present in the literature in four different ways:

- Including “Generalized Alignment” [275] in the Yukawa matrices, where (in the fermion mass-eigenstate basis) $Y_d^{(2)} = \zeta_d^{(2)} M_d$ and $Y_u^{(2)} = [\zeta_u^{(2)}]^\dagger M_u$ with 3×3 diagonal complex matrices in flavour space $\zeta_{d,u}$ which in general are not proportional to the identity matrix.
- Extending to N Higgs doublets instead of two. This type of models are called Multi-Higgs-Doublet Models (MHDMs).
- Giving a wide meson-mixing phenomenology (B^0 , B_s^0 , K^0 and D^0) through a single master formula.
- For the computation, keeping all external quark momenta and all external masses up to second order.

In Sections 5.2.1 and 5.2.2, we present the theoretical framework used in this chapter. In Sections 5.2.3 and 5.2.4, we present the complete one-loop computation of the Wilson

coefficients for the meson mixing, providing a detailed guide for the computation of the box diagrams. In Section 5.2.5, we compare our results with those present in the literature [276–278]. Finally, in Section 5.3, we particularize our analytical results to some specific models and we obtain combined constraints from the currently measured mixing observables.

5.2 Theoretical framework

5.2.1 Multi-Higgs-Doublet Model

The 2HDM is based on a $SU(3)_C \otimes SU(2)_L \otimes U(1)_Y$ symmetry with two scalar doublets $\phi_i(x)$ ($i = 1, 2$) with hypercharge $Y = \frac{1}{2}$ and the same SM fermion content. Using a global $SU(2)$ transformation in the scalar space (ϕ_1, ϕ_2) takes us to the so-called Higgs basis (Φ_1, Φ_2) where only one doublet acquires Vacuum Expectation Value (VEV), $\langle \Phi_1 \rangle \equiv \frac{v}{\sqrt{2}} \neq 0$. In this basis, the doublets can be parametrized as

$$\Phi_1 = \begin{bmatrix} G^+ \\ \frac{1}{\sqrt{2}}(v + S_1 + iG^0) \end{bmatrix}, \quad \Phi_2 = \begin{bmatrix} H^+ \\ \frac{1}{\sqrt{2}}(S_2 + iS_3) \end{bmatrix}, \quad (5.2.1)$$

where G^\pm and G^0 are the Goldstone boson fields and $\langle H^\pm \rangle = \langle G^{\pm,0} \rangle = \langle S_i \rangle = 0$.

Let us generalize the previous result assuming that the second Higgs doublet can be either a singlet or an octet of $SU(3)_C$. Then, we can rewrite Φ_2 as

$$\Phi_2 = T^a \begin{bmatrix} (H^+)_a \\ \frac{1}{\sqrt{2}}[(S_2)_a + i(S_3)_a] \end{bmatrix} \equiv T^a \Phi_2^{(a)}. \quad (5.2.2)$$

where T^a are 3×3 matrices that encode the colour nature of the second Higgs doublet. For instance, the usual 2HDM is obtained by setting these matrices to the identity matrix in colour space, while in the colour-octet 2HDM [280] these matrices are the generators of $SU(3)_C$ being $a = 1, \dots, 8$ the adjoint colour index.

A more general extension of the scalar sector can be constructed considering N doublets instead of two, the so-called Multi-Higgs-Doublet Model (MHDM). In this extension,

Eq. (5.2.2) has to be modified to

$$\Phi_A = T^a \begin{bmatrix} (H_A^+)_a \\ \frac{1}{\sqrt{2}} [(S_2^A)_a + i(S_3^A)_a] \end{bmatrix} \equiv T^a \Phi_A^{(a)}, \quad (5.2.3)$$

where $A = 2, \dots, N$ with N the number of Higgs doublets.

5.2.2 Yukawa interactions and alignment

The most general Yukawa Lagrangian in the MHDM is given by¹

$$\mathcal{L}_Y = -\frac{\sqrt{2}}{v} \bar{Q}'_L \left\{ \left(M'_d \Phi_1 + \sum_{A=2}^N [Y_d^{(A)}]' \Phi_A \right) d'_R + \left(M'_u \tilde{\Phi}_1 + \sum_{A=2}^N [Y_u^{(A)}]' \tilde{\Phi}_A \right) u'_R \right\} + \text{h.c.},$$

where Q'_L is the left-handed quark doublet and $\tilde{\Phi}_A = i \sigma_2 \Phi_A^*$ is the charge-conjugated doublet with hypercharge $Y = -\frac{1}{2}$. All fermionic fields are written as 3 dimensional flavour vectors, *i.e.*, $d'_R = (d'_R, s'_R, b'_R)$ and similarly for u'_R and Q'_L . The matrices M'_f ($f = u, d$) are the non-diagonal fermion mass matrices, while the matrices $[Y_f^{(A)}]'$ contain the Yukawa couplings to the scalar doublets Φ_A . In general, these matrices cannot be diagonalized simultaneously. Therefore, in the fermion mass-eigenstate basis, with diagonal mass matrices M_f , the Yukawa matrices are non-diagonal, which results in flavour-changing interactions of the neutral scalars. One of the possible ways to avoid these non-diagonal neutral couplings consist in requiring the alignment in flavour space of the Yukawa matrices [273–275]. The Yukawa alignment guarantees that these matrices can be simultaneously diagonalized by imposing (in the fermion mass-eigenstate basis)

$$Y_d^{(A)} = \varsigma_d^{(A)} M_d, \quad Y_u^{(A)} = [\varsigma_u^{(A)}]^\dagger M_u, \quad (5.2.4)$$

where $\varsigma_{d,u}^{(A)}$ are 3×3 diagonal complex matrices in flavour space,

$$\varsigma_d^{(A)} = \text{diag}(\varsigma_{d_1}^{(A)}, \varsigma_{d_2}^{(A)}, \varsigma_{d_3}^{(A)}), \quad \varsigma_u^{(A)} = \text{diag}(\varsigma_{u_1}^{(A)}, \varsigma_{u_2}^{(A)}, \varsigma_{u_3}^{(A)}). \quad (5.2.5)$$

¹The lepton part has been skipped.

The matrices $\varsigma_d^{(A)}$ and $\varsigma_u^{(A)}$ introduce family-dependent complex quantities which represent new sources of CP violation. For $N = 2$ with $\varsigma_{d_i} = \varsigma_d$ and $\varsigma_{u_i} = \varsigma_u$, we recover the family-universal Aligned 2HDM (A2HDM) [273] case, in which for particular real values of these parameters², indicated in Table 5.1 one restores all different versions of the 2HDM with Natural Flavour Conservation (NFC).

Model	ς_d	ς_u	ς_l
Type I	$\cot \beta$	$\cot \beta$	$\cot \beta$
Type II	$-\tan \beta$	$\cot \beta$	$-\tan \beta$
Type X	$\cot \beta$	$\cot \beta$	$-\tan \beta$
Type Y	$-\tan \beta$	$\cot \beta$	$\cot \beta$

Table 5.1: Two-Higgs-doublet models with NFC.

In the mass-eigenstate basis, the charged-current Yukawa Lagrangian can be expressed as

$$\mathcal{L}_Y = -\frac{\sqrt{2}}{v} \sum_{A=2}^N \sum_{B=2}^N (\varphi_B^+)_a \mathcal{R}_{BA}^+ \bar{u} T^a \left[\varsigma_d^{(A)} V M_d P_R - \varsigma_u^{(A)} M_u V P_L \right] d + \text{h.c.}, \quad (5.2.6)$$

where V denotes the CKM matrix, $P_{R,L} = \frac{1 \pm \gamma_5}{2}$ are the right-handed and left-handed projectors respectively. For $N > 2$, the charged Higgs particles $(H_A^{(+)})_a$ are not mass eigenstates and we must diagonalize them through a rotation matrix $\mathcal{R}^{(+)}$ to put them in terms of the mass eigenstates $(\varphi_A^{(+)})_a$.³ In order to simplify our analytical results, we use the following definition,

$$\varsigma_{u,d}^A \equiv \sum_{B=2}^N \mathcal{R}_{AB}^+ \varsigma_{u,d}^{(B)}, \quad (5.2.7)$$

in general $\varsigma_{u,d}^A \neq \varsigma_{u,d}^{(A)}$. In addition, for the numerical analysis presented in Section 5.3, we introduce the following definitions: $\varsigma_{u,d} \equiv \varsigma_{u,d}^{(2)}$ in the A2HDM, and $\varsigma_{u,d} \equiv \mathcal{R}_{22}^+ \varsigma_{u,d}^{(2)} + \mathcal{R}_{23}^+ \varsigma_{u,d}^{(3)}$, $\tilde{\varsigma}_{u,d} \equiv \mathcal{R}_{32}^+ \varsigma_{u,d}^{(2)} + \mathcal{R}_{33}^+ \varsigma_{u,d}^{(3)}$ in the Aligned-Three-Higgs Doublet Model (A3HDM).

² $\tan \beta \equiv \frac{v_2}{v_1}$ and $v \equiv \sqrt{v_1^2 + v_2^2}$ where v_1 and v_2 are the VEVs of ϕ_1 and ϕ_2 .

³ Notice that the colour-charged Higgs particles do not mix with those that are colourless.

5.2.3 $M^0 - \bar{M}^0$ mixing within the SM and beyond

In Chapter 1, we have seen that $M^0 - \bar{M}^0$ mixing is governed by box diagrams with $M^0 \equiv q_1 \bar{q}_2$ and $\bar{M}^0 \equiv \bar{q}_1 q_2$, see Figure 5.1. In the SM, the short-distance contributions to B^0 , B_s^0 and K^0 (D^0) mixing are given by box diagrams mediated by up-type (down-type) quarks and W^\pm bosons (Goldstone bosons depending on the gauge choice ξ_W , see Figures 5.1a, 5.1b and 5.1f). In the AMHDM, the Yukawa interactions introduce additional diagrams, mediated by charged Higgs particles $(\varphi_A^\pm)_a$ that can be either colour-singlet or colour-octet scalars, see Figures 5.1c, 5.1d and 5.1e.

To be specific, in the following discussion we consider neutral mesons composed of down-type quarks (B^0 , K^0). The modifications for the D^0 case are going to be obvious. The $M^0 - \bar{M}^0$ mixing is described by the following effective weak Hamiltonian,

$$\begin{aligned} \mathcal{H}_{\text{eff}}^{\Delta F=2} &= \frac{G_F^2 M_W^2}{16\pi^2} \sum_{ijk} \lambda_i \lambda_j (C_k)^{ij}(\mu) \mathcal{O}_k(\mu), \\ (C_k)^{ij}(\mu) &\equiv (C_k^{\text{SM}})^{ij}(\mu) + \sum_{\text{AB}} (\delta C_k^{\text{AB}})^{ij}(\mu), \end{aligned} \quad (5.2.8)$$

where the A and B labels refer to the $N - 1$ Higgs doublets with $\langle \Phi_{\text{A,B}} \rangle = 0$, i and j represent the internal quarks flowing inside the loop, G_F is the Fermi coupling constant, $\lambda_i \equiv V_{iq_2}^* V_{iq_1}$ and $(C_k)^{ij}(\mu)$ are the Wilson coefficients associated to the eight four-quark operators \mathcal{O}_k ,

$$\begin{aligned} \mathcal{O}^{\text{VLL,VRR}} &= [\bar{q}_2^\alpha \gamma^\mu P_{L,R} q_1^\alpha] [\bar{q}_2^\beta \gamma_\mu P_{L,R} q_1^\beta], \\ \mathcal{O}_1^{\text{LR}} &= [\bar{q}_2^\alpha \gamma^\mu P_L q_1^\alpha] [\bar{q}_2^\beta \gamma_\mu P_R q_1^\beta], \\ \mathcal{O}_2^{\text{LR}} &= [\bar{q}_2^\alpha P_L q_1^\alpha] [\bar{q}_2^\beta P_R q_1^\beta], \\ \mathcal{O}_1^{\text{SLL,SRR}} &= [\bar{q}_2^\alpha P_{L,R} q_1^\alpha] [\bar{q}_2^\beta P_{L,R} q_1^\beta], \\ \mathcal{O}_2^{\text{SLL,SRR}} &= [\bar{q}_2^\alpha \sigma_{\mu\nu} P_{L,R} q_1^\alpha] [\bar{q}_2^\beta \sigma^{\mu\nu} P_{L,R} q_1^\beta], \end{aligned} \quad (5.2.9)$$

with α and β being colour indices and $\sigma^{\mu\nu} \equiv \frac{1}{2} [\gamma^\mu, \gamma^\nu]$.⁴

⁴Other works use $i\sigma_{\mu\nu}$ instead of $\sigma_{\mu\nu}$. One can change to this basis through a simple shift $\sigma_{\mu\nu} \rightarrow i\sigma_{\mu\nu}$ which only adds an extra minus sign in the Wilson coefficient $(C_2^{\text{SLL,SRR}})^{ij}$.

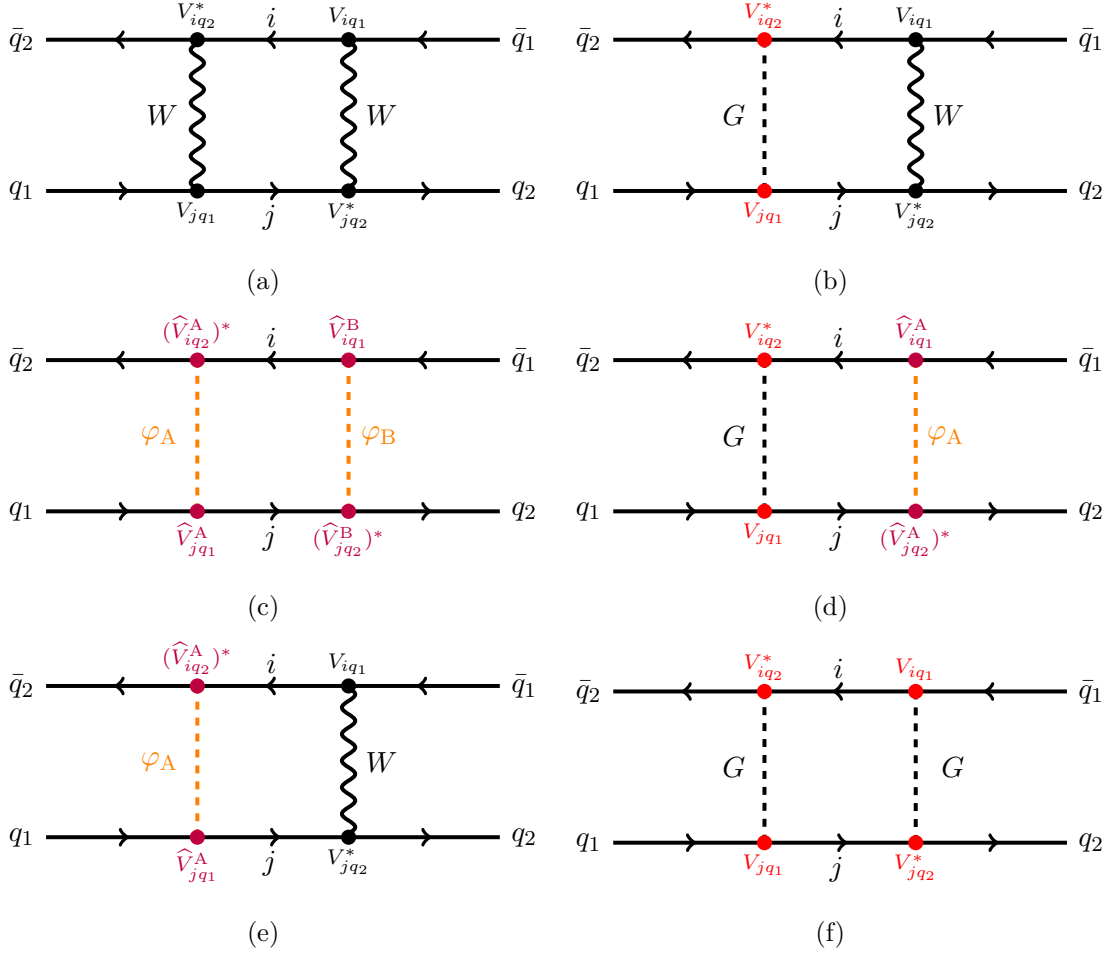


Figure 5.1: Box diagrams contributing to meson mixing in the AMHDM. The omitted crossed diagrams can be obtained exchanging the external lines.

5.2.3.1 Technical details for the computation

For the computation of the box diagrams shown in Figure 5.1, we have taken into account the following prescriptions:

1. The Feynman rules are in Appendix G.
2. The contributions from the box diagrams in Figure 5.1, have been calculated keeping all the external quark masses and momenta up to second order $\mathcal{O}\left(\frac{m_{q_1}^2}{M_W^2}, \frac{m_{q_2}^2}{M_W^2}, \frac{m_{q_1}m_{q_2}}{M_W^2}\right)$.

3. Since the external momenta l are much smaller than the masses of some internal quarks, gauge bosons and charged scalars M , the Feynman integrands are expanded in powers of external momenta before performing the loop integration,

$$\frac{1}{(k+l)^2 - M^2} = \frac{1}{k^2 - M^2} \left[1 - \frac{l^2 + 2(k \cdot l)}{k^2 - M^2} + \frac{4(k \cdot l)^2}{(k^2 - M^2)^2} \right] + \mathcal{O}\left(\frac{l^4}{M^4}\right),$$

where k is the loop momenta.

4. We have applied the partial fraction decomposition

$$\frac{1}{(k^2 - m_1^2)(k^2 - m_2^2)} = \frac{1}{m_1^2 - m_2^2} \left[\frac{1}{k^2 - m_1^2} - \frac{1}{k^2 - m_2^2} \right], \quad (5.2.10)$$

which allows to reduce all Feynman integrals into one-propagator integrals. After the reduction of tensor integrals to scalar ones through Lorentz invariance,

$$\int_k k_\mu k_\nu f(k^2) = \frac{g_{\mu\nu}}{D} \int_k k^2 f(k^2), \quad (5.2.11)$$

$$\int_k k_\mu k_\nu k_\alpha k_\beta f(k^2) = \frac{g_{\mu\nu}g_{\alpha\beta} + g_{\mu\beta}g_{\alpha\nu} + g_{\nu\beta}g_{\mu\alpha}}{D(D-2)} \int_k k^4 f(k^2), \quad (5.2.12)$$

where $\int_k \equiv \int \frac{d^D k}{(2\pi)^D}$, the only non-vanishing one-loop integrals take the form

$$\int_k \frac{(k^2)^\alpha}{(k^2 - m^2)^\beta} = \frac{i(-)^{\alpha-\beta}}{(4\pi)^{D/2}} (m^2)^{D/2+\alpha-\beta} \frac{\Gamma(\beta - \alpha - D/2) \Gamma(\alpha + D/2)}{\Gamma(\beta) \Gamma(D/2)},$$

where α and β are arbitrary integer powers and $m \neq 0$.

In this computation, we have been able to express all loop integrals in terms of the loop functions D_0 and D_2 , defined in Appendix H, and derivatives of these functions using recursively the following formulas:

$$\frac{d}{dm^2} \left(\int_k \frac{(k^2)^\alpha}{(k^2 - m^2)^\beta} \right) = \beta \int_k \frac{(k^2)^\alpha}{(k^2 - m^2)^{\beta+1}}, \quad (5.2.13)$$

$$\int_k \frac{(k^2)^\alpha}{(k^2 - m^2)^\beta} = \int_k \frac{(k^2)^{\alpha-1}}{(k^2 - m^2)^{\beta-1}} + m^2 \int_k \frac{(k^2)^{\alpha-1}}{(k^2 - m^2)^\beta}, \quad (5.2.14)$$

where Eqs. (5.2.13) and (5.2.14) reduce in one unit the powers of the loop momenta in the denominator and numerator respectively.

5. We have applied the Fierz identity (1.4.99), followed by some Dirac reductions, *i.e.*, $\gamma^\mu \gamma^\nu \gamma_\mu = -2\gamma^\nu$, etc. Even so, there have appeared irreducible spinor structures, such as

$$\left[\bar{q}_2^\alpha \not{p}_{\text{ext}} P_{L,R} q_1^\alpha \right] \left[\bar{q}_2^\beta P_{L,R} q_1^\beta \right], \left[\bar{q}_2^\alpha \not{p}_{\text{ext}}^{(1)} P_{L,R} q_1^\alpha \right] \left[\bar{q}_2^\beta \not{p}_{\text{ext}}^{(2)} P_{L,R} q_1^\beta \right], \dots \quad (5.2.15)$$

where q_1 and q_2 in this case represent the Dirac spinors for abbreviation reasons. These structures have been reduced by choosing the kinematical framework in which the initial particles do not have trimomentum.

6. After the computation of all box diagrams, we have summed all the contributions taking into account the relative signs between the Feynman diagrams. Finally with the fundamental amplitude, we have obtained the Wilson coefficients performing a matching between the effective amplitude obtained through Eq. (5.2.8) and the fundamental amplitude.
7. In order to validate our results, we have checked the gauge invariance. For that reason, we have performed the calculation in the Feynman ($\xi_W = 1$) gauge and in the unitary ($\xi_W = \infty$) gauge,⁵ and we have obtained the same results in both gauges. It is important to stress that in the unitary gauge, the result is divergent but when we take into account the GIM mechanism ($\sum_i \lambda_i = 0$), the divergences disappear.

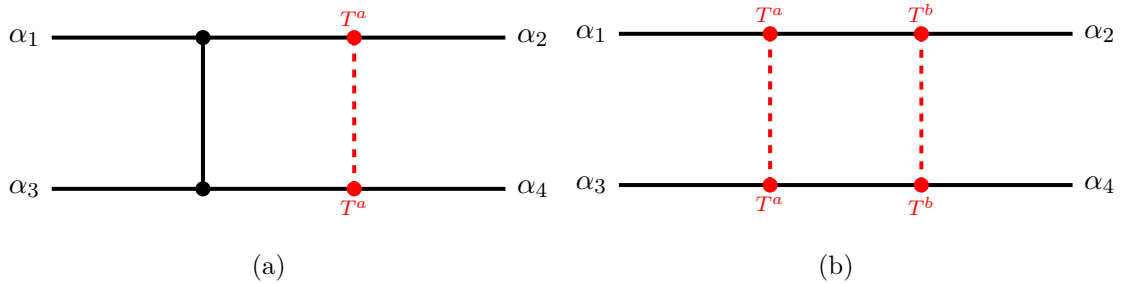


Figure 5.2: Topologies generated by the colour-octet scalar.

⁵In the unitary gauge, the contribution of the Goldstone bosons is zero.

8. Extending the colourless results to the colour-AMHDM can be easily done because the only differences appear in the number of colour structure insertions. In the colour-AMHDM, there are two types of topologies, as shown Figure 5.2, those with one colour-octet scalar particle and those with two. These diagrams generate the following colour structures

$$[T^a]_{\alpha_1 \alpha_2} [T^a]_{\alpha_3 \alpha_4} = -\frac{1}{2 N_C} \delta_{\alpha_1 \alpha_2} \delta_{\alpha_3 \alpha_4} + \frac{1}{2} \delta_{\alpha_1 \alpha_4} \delta_{\alpha_3 \alpha_2} , \quad (5.2.16)$$

$$[T^a T^b]_{\alpha_1 \alpha_2} [T^b T^a]_{\alpha_3 \alpha_4} = \frac{1}{(2 N_C)^2} \delta_{\alpha_1 \alpha_2} \delta_{\alpha_3 \alpha_4} + \frac{N_C^2 - 2}{4 N_C} \delta_{\alpha_1 \alpha_4} \delta_{\alpha_2 \alpha_3} . \quad (5.2.17)$$

The contributions given by Figure 5.2a can be distinguished from the ones given by Figure 5.2b simply by counting the number of couplings. For instance, an operator with two couplings $(\varsigma_{d_j}^A (\varsigma_{u_i}^A)^* , \dots)$ is a clear contribution of one colour-octet scalar particle and, therefore, we have to use Eq. (5.2.16), while an operator with four couplings $((\varsigma_{u_i}^A)^* \varsigma_{u_i}^B (\varsigma_{u_j}^B)^* \varsigma_{u_j}^A , \dots)$ is a two scalar contribution and we have to use Eq. (5.2.17). Let us consider the following example of an operator with four couplings

$$(\varsigma_{u_i}^A)^* \varsigma_{u_i}^B (\varsigma_{u_j}^B)^* \varsigma_{u_j}^A \mathcal{O}_2^{\text{LR}} = (\varsigma_{u_i}^A)^* \varsigma_{u_i}^B (\varsigma_{u_j}^B)^* \varsigma_{u_j}^A [\bar{q}_2^\alpha P_L q_1^{\alpha 1}] [\bar{q}_2^\beta P_R q_1^{\beta 1}] . \quad (5.2.18)$$

Using the previous rules, $\mathcal{O}_2^{\text{LR}}$ corresponds to an operator with two colour scalar particles. Then, in the colour-AMHDM, it has to be replaced by $\tilde{\mathcal{O}}_2^{\text{LR}} \equiv [\bar{q}_2^{\alpha 1} (T^a T^b)_{\alpha_1 \alpha_2} P_L q_1^{\alpha 2}] [\bar{q}_2^{\alpha 3} (T^b T^a)_{\alpha_3 \alpha_4} P_R q_1^{\alpha 4}]$. The operator $\tilde{\mathcal{O}}_2^{\text{LR}}$ can be reduced to the basis of eight four-quark operators given by Eqs. (5.2.9), using Eq. (5.2.17) and the Fierz identities of Appendix J. Finally, we obtain the following result

$$\tilde{\mathcal{O}}_2^{\text{LR}} = \frac{1}{(2 N_C)^2} \mathcal{O}_2^{\text{LR}} - \frac{N_C^2 - 2}{8 N_C} \mathcal{O}_1^{\text{LR}} . \quad (5.2.19)$$

Two important facts can be derived from Eq. (5.2.19), when extending the results to the colour-AMHDM:

- From the first term of Eq. (5.2.19), we can conclude that when a colour operator is reduced to the colourless basis given by Eq. (5.2.9), produces a colour factor

(N_i) in the same colour operator but with $T^a = I$ where I is the identity matrix in the colour space.

- The reduction of a colour operator also produces a colour factor (\tilde{N}_i) in other colourless operators different from the one with $T^a = I$. This operator comes from the second term of Eqs (5.2.16) and (5.2.17) after the Fierz rearrangement is applied.

Taking into account all these facts, we can generalize our results as follows, the colourless-AMHDM will be obtained by making $N_i = 1$ and $\tilde{N}_i = 0$, while the colour-AMHDM fixing N_i and \tilde{N}_i to the values given in Appendix I.

5.2.3.2 Analytical results

The previous technical aspects have allowed us to obtain the following results for the Wilson coefficients in the Feynman gauge, before applying the GIM mechanism.

SM contributions

$$(C_{\text{VLL}}^{\text{SM}})^{ij} = (4 + \beta_i \beta_j) M_W^2 D_2(m_i^2, m_j^2, M_W^2) - 8 \beta_i \beta_j M_W^4 D_0(m_i^2, m_j^2, M_W^2), \quad (5.2.20)$$

$$(C_{\text{ISRR}}^{\text{SM}})^{ij} = x_{q1} \frac{2}{3} \beta_i \beta_j M_W^4 \left[3 D_0(m_i^2, m_j^2, M_W^2) - 2 \left(F_2^{\text{WW}21} + F_2^{\text{WW}31} + F_2^{\text{WW}41} \right) \right], \quad (5.2.21)$$

$$(C_{\text{2SRR}}^{\text{SM}})^{ij} = x_{q1} 4 M_W^4 \left[\frac{1}{3} \left(F_2^{\text{WW}31} + F_2^{\text{WW}41} + F_2^{\text{WW}21} \right) - \frac{1}{2} \left(\frac{1}{2} \frac{d}{dM_W^2} D_2(m_i^2, m_j^2, M_W^2) + \frac{d}{dm_j^2} D_2(m_i^2, m_j^2, M_W^2) \right) \right]. \quad (5.2.22)$$

AMHDM contributions

$$\begin{aligned} (\delta C_{\text{VLL}}^{\text{AB}})^{ij} &= (\varsigma_{u_i}^{\text{A}})^* \varsigma_{u_i}^{\text{B}} (\varsigma_{u_j}^{\text{B}})^* \varsigma_{u_j}^{\text{A}} N_1 (f_1^{\text{AB}})^{ij} \\ &+ \varsigma_{d_j}^{\text{A}} (\varsigma_{u_i}^{\text{A}})^* N_2 (f_2^{\text{AB}})^{ij} + \varsigma_{u_j}^{\text{A}} (\varsigma_{u_i}^{\text{A}})^* N_3 (f_3^{\text{AB}})^{ij}, \end{aligned} \quad (5.2.23)$$

$$(\delta C_{\text{VRR}}^{\text{AB}})^{ij} = (\varsigma_{d_i}^{\text{A}})^* \varsigma_{d_i}^{\text{B}} (\varsigma_{d_j}^{\text{B}})^* \varsigma_{d_j}^{\text{A}} N_4 (f_4^{\text{AB}})^{ij} + \text{Re} [(\varsigma_{d_i}^{\text{A}})^* \varsigma_{d_j}^{\text{A}}] N_5 (f_5^{\text{AB}})^{ij} , \quad (5.2.24)$$

$$\begin{aligned} (\delta C_{\text{1LR}}^{\text{AB}})^{ij} &= (\varsigma_{d_i}^{\text{A}})^* \varsigma_{d_i}^{\text{B}} (\varsigma_{u_j}^{\text{B}})^* \varsigma_{u_j}^{\text{A}} N_6 (f_6^{\text{AB}})^{ij} + \text{Re} [(\varsigma_{d_i}^{\text{A}})^* \varsigma_{u_j}^{\text{A}}] N_7 (f_7^{\text{AB}})^{ij} \\ &+ \varsigma_{d_i}^{\text{A}} (\varsigma_{d_j}^{\text{A}})^* \tilde{N}_8 (f_8^{\text{AB}})^{ij} + \text{Re} [(\varsigma_{d_j}^{\text{A}})^* \varsigma_{u_i}^{\text{A}}] \tilde{N}_9 (f_9^{\text{AB}})^{ij} \\ &+ \text{Re} [(\varsigma_{u_i}^{\text{A}})^* \varsigma_{u_j}^{\text{A}} \varsigma_{d_i}^{\text{B}} (\varsigma_{u_j}^{\text{B}})^*] \tilde{N}_{10} (f_{10}^{\text{AB}})^{ij} + (\varsigma_{u_i}^{\text{A}})^* \varsigma_{u_j}^{\text{A}} \varsigma_{u_i}^{\text{B}} (\varsigma_{u_j}^{\text{B}})^* \tilde{N}_{11} (f_{11}^{\text{AB}})^{ij} \\ &+ (\varsigma_{u_i}^{\text{A}})^* \varsigma_{u_j}^{\text{A}} \varsigma_{d_i}^{\text{B}} (\varsigma_{d_j}^{\text{B}})^* \tilde{N}_{12} (f_{12}^{\text{AB}})^{ij} + \varsigma_{u_j}^{\text{A}} (\varsigma_{u_i}^{\text{A}})^* \tilde{N}_{13} (f_{13}^{\text{AB}})^{ij} , \end{aligned} \quad (5.2.25)$$

$$\begin{aligned} (\delta C_{\text{2LR}}^{\text{AB}})^{ij} &= \varsigma_{d_i}^{\text{A}} (\varsigma_{d_j}^{\text{A}})^* N_8 (f_8^{\text{AB}})^{ij} + \text{Re} [(\varsigma_{d_j}^{\text{A}})^* \varsigma_{u_i}^{\text{A}}] N_9 (f_9^{\text{AB}})^{ij} \\ &+ \text{Re} [(\varsigma_{u_i}^{\text{A}})^* \varsigma_{u_j}^{\text{A}} \varsigma_{d_i}^{\text{B}} (\varsigma_{u_j}^{\text{B}})^*] N_{10} (f_{10}^{\text{AB}})^{ij} + (\varsigma_{u_i}^{\text{A}})^* \varsigma_{u_j}^{\text{A}} \varsigma_{u_i}^{\text{B}} (\varsigma_{u_j}^{\text{B}})^* N_{11} (f_{11}^{\text{AB}})^{ij} \\ &+ (\varsigma_{u_i}^{\text{A}})^* \varsigma_{u_j}^{\text{A}} \varsigma_{d_i}^{\text{B}} (\varsigma_{d_j}^{\text{B}})^* N_{12} (f_{12}^{\text{AB}})^{ij} + \varsigma_{u_j}^{\text{A}} (\varsigma_{u_i}^{\text{A}})^* N_{13} (f_{13}^{\text{AB}})^{ij} \\ &+ (\varsigma_{d_i}^{\text{A}})^* \varsigma_{d_i}^{\text{B}} (\varsigma_{u_j}^{\text{B}})^* \varsigma_{u_j}^{\text{A}} \tilde{N}_6 (f_6^{\text{AB}})^{ij} + \text{Re} [(\varsigma_{d_i}^{\text{A}})^* \varsigma_{u_j}^{\text{A}}] \tilde{N}_7 (f_7^{\text{AB}})^{ij} , \end{aligned} \quad (5.2.26)$$

$$\begin{aligned} (\delta C_{\text{1SLL}}^{\text{AB}})^{ij} &= (\varsigma_{u_i}^{\text{A}})^* \varsigma_{u_i}^{\text{B}} (\varsigma_{u_j}^{\text{B}})^* \varsigma_{u_j}^{\text{A}} N_{14} (f_{14}^{\text{AB}})^{ij} + (\varsigma_{d_i}^{\text{A}})^* (\varsigma_{d_j}^{\text{B}})^* \varsigma_{u_i}^{\text{B}} \varsigma_{u_j}^{\text{A}} N_{15} (f_{15}^{\text{AB}})^{ij} \\ &+ (\varsigma_{u_i}^{\text{A}})^* \varsigma_{u_i}^{\text{B}} (\varsigma_{d_j}^{\text{B}})^* \varsigma_{u_j}^{\text{A}} N_{16} (f_{16}^{\text{AB}})^{ij} + (\varsigma_{u_i}^{\text{A}})^* \varsigma_{u_j}^{\text{A}} N_{17} (f_{17}^{\text{AB}})^{ij} \\ &+ (\varsigma_{d_j}^{\text{A}})^* \varsigma_{u_i}^{\text{A}} N_{18} (f_{18}^{\text{AB}})^{ij} , \end{aligned} \quad (5.2.27)$$

$$\begin{aligned} (\delta C_{\text{1SRR}}^{\text{AB}})^{ij} &= (\varsigma_{u_i}^{\text{A}})^* \varsigma_{u_i}^{\text{B}} (\varsigma_{u_j}^{\text{B}})^* \varsigma_{u_j}^{\text{A}} N_{19} (f_{19}^{\text{AB}})^{ij} + \varsigma_{d_i}^{\text{B}} \varsigma_{d_j}^{\text{A}} (\varsigma_{u_i}^{\text{A}})^* (\varsigma_{u_j}^{\text{B}})^* N_{20} (f_{20}^{\text{AB}})^{ij} \\ &+ (\varsigma_{u_i}^{\text{A}})^* \varsigma_{u_i}^{\text{B}} (\varsigma_{u_j}^{\text{B}})^* \varsigma_{d_j}^{\text{A}} N_{21} (f_{21}^{\text{AB}})^{ij} + (\varsigma_{u_i}^{\text{A}})^* \varsigma_{u_j}^{\text{A}} N_{22} (f_{22}^{\text{AB}})^{ij} \\ &+ \varsigma_{d_j}^{\text{A}} (\varsigma_{u_i}^{\text{A}})^* N_{23} (f_{23}^{\text{AB}})^{ij} , \end{aligned} \quad (5.2.28)$$

$$\begin{aligned} (\delta C_{\text{2SLL}}^{\text{AB}})^{ij} &= (\varsigma_{u_i}^{\text{A}})^* \varsigma_{u_i}^{\text{B}} (\varsigma_{u_j}^{\text{B}})^* \varsigma_{u_j}^{\text{A}} \tilde{N}_{14} (f_{14}^{\text{AB}})^{ij} + (\varsigma_{d_i}^{\text{A}})^* (\varsigma_{d_j}^{\text{B}})^* \varsigma_{u_i}^{\text{B}} \varsigma_{u_j}^{\text{A}} \tilde{N}_{15} (f_{15}^{\text{AB}})^{ij} \\ &+ (\varsigma_{u_i}^{\text{A}})^* \varsigma_{u_i}^{\text{B}} (\varsigma_{d_j}^{\text{B}})^* \varsigma_{u_j}^{\text{A}} \tilde{N}_{16} (f_{16}^{\text{AB}})^{ij} + (\varsigma_{u_i}^{\text{A}})^* \varsigma_{u_j}^{\text{A}} \tilde{N}_{17} (f_{17}^{\text{AB}})^{ij} \\ &+ (\varsigma_{d_j}^{\text{A}})^* \varsigma_{u_i}^{\text{A}} \tilde{N}_{18} (f_{18}^{\text{AB}})^{ij} , \end{aligned} \quad (5.2.29)$$

$$\begin{aligned}
(\delta C_{2\text{SRR}}^{\text{AB}})^{ij} &= (\varsigma_{u_i}^{\text{A}})^* \varsigma_{u_i}^{\text{B}} (\varsigma_{u_j}^{\text{B}})^* \varsigma_{u_j}^{\text{A}} \tilde{N}_{19} (f_{19}^{\text{AB}})^{ij} + \varsigma_{d_i}^{\text{B}} \varsigma_{d_j}^{\text{A}} (\varsigma_{u_i}^{\text{A}})^* (\varsigma_{u_j}^{\text{B}})^* \tilde{N}_{20} (f_{20}^{\text{AB}})^{ij} \\
&+ (\varsigma_{u_i}^{\text{A}})^* \varsigma_{u_i}^{\text{B}} (\varsigma_{u_j}^{\text{B}})^* \varsigma_{d_j}^{\text{A}} \tilde{N}_{21} (f_{21}^{\text{AB}})^{ij} + (\varsigma_{u_i}^{\text{A}})^* \varsigma_{u_j}^{\text{A}} \tilde{N}_{22} (f_{22}^{\text{AB}})^{ij} \\
&+ \varsigma_{d_j}^{\text{A}} (\varsigma_{u_i}^{\text{A}})^* \tilde{N}_{23} (f_{23}^{\text{AB}})^{ij} ,
\end{aligned} \tag{5.2.30}$$

where $\beta_i \equiv \frac{m_i^2}{M_W^2}$, $x_{q_{1,2}} \equiv \frac{m_{q_{1,2}}^2}{M_W^2}$ and the couplings $\varsigma_{u_i, d_i}^{\text{A}}$ are defined in Eq. (5.2.7). The loop functions f_i functions are defined in Appendix H. The N_i and \tilde{N}_i are colour factors which are given in Appendix I.

5.2.4 GIM mechanism

After computing all the Feynman diagrams given in Figure 5.1, the amplitude for neutral meson mixing can be written as

$$\langle \bar{M}^0 | \mathcal{H}_{\Delta F=2}^{\text{eff}} | M^0 \rangle \sim \sum_i \sum_j \lambda_i \lambda_j F(x_i, x_j) , \tag{5.2.31}$$

which sums over all quarks flavours flowing into the loop ($i, j = u(1), c(2), t(3)$), λ_i is the product of the CKM matrix elements and $F(x_i, x_j)$ is the loop function that depends on the internal quark masses ($x_i \equiv m_i^2/M_{W, \varphi_{\text{A,B}}^\pm}^2$) and products of the NP couplings ($((\varsigma_{u_i}^{\text{A}})^* \varsigma_{u_i}^{\text{B}} (\varsigma_{u_j}^{\text{B}})^* \varsigma_{u_j}^{\text{A}} , \dots)$). Considering the unitarity of the CKM matrix, $\lambda_1 + \lambda_2 + \lambda_3 = 0$, the amplitude can be expressed as

$$\sum_i \sum_j \lambda_i \lambda_j F(x_i, x_j) = \lambda_2^2 \mathcal{F}_{22} + 2 \lambda_2 \lambda_3 \mathcal{F}_{23} + \lambda_3^2 \mathcal{F}_{33} , \tag{5.2.32}$$

where

$$\mathcal{F}_{22} \equiv F(x_1, x_1) - F(x_2, x_1) - F(x_1, x_2) + F(x_2, x_2) , \tag{5.2.33}$$

$$\begin{aligned}
\mathcal{F}_{23} &\equiv F(x_1, x_1) - \frac{1}{2} F(x_2, x_1) - \frac{1}{2} F(x_3, x_1) \\
&- \frac{1}{2} F(x_1, x_2) - \frac{1}{2} F(x_1, x_3) + \frac{1}{2} F(x_3, x_2) + \frac{1}{2} F(x_2, x_3) ,
\end{aligned} \tag{5.2.34}$$

$$\mathcal{F}_{33} \equiv F(x_1, x_1) - F(x_3, x_1) - F(x_1, x_3) + F(x_3, x_3) . \tag{5.2.35}$$

Finally, when the GIM mechanism is applied in Eqs. (5.2.20) to (5.2.30) with Eq. (5.2.32), the effective weak Hamiltonian becomes

$$\mathcal{H}_{\text{eff}}^{\Delta F=2} = \frac{G_F^2 M_W^2}{16\pi^2} \left[\lambda_t^2 \mathcal{C}_{tt} + 2 \lambda_c \lambda_t \mathcal{C}_{ct} + \lambda_c^2 \mathcal{C}_{cc} \right], \quad (5.2.36)$$

where

$$\begin{aligned} \mathcal{C}_{ij} = & \mathcal{C}_{\text{VLL}}^{ij} \mathcal{O}^{\text{VLL}} + \mathcal{C}_{\text{VRR}}^{ij} \mathcal{O}^{\text{VRR}} + \mathcal{C}_{\text{1LR}}^{ij} \mathcal{O}_1^{\text{LR}} + \mathcal{C}_{\text{2LR}}^{ij} \mathcal{O}_2^{\text{LR}} \\ & + \mathcal{C}_{\text{1SLL}}^{ij} \mathcal{O}_1^{\text{SLL}} + \mathcal{C}_{\text{1SRR}}^{ij} \mathcal{O}_1^{\text{SRR}} + \mathcal{C}_{\text{2SLL}}^{ij} \mathcal{O}_2^{\text{SLL}} + \mathcal{C}_{\text{2SRR}}^{ij} \mathcal{O}_2^{\text{SRR}}, \end{aligned} \quad (5.2.37)$$

where \mathcal{C}_k^{ij} plays the same role as \mathcal{F}_{ij} with $ij = tt, ct, cc$ in Eq. (5.2.32) being $k = \text{VLL}, \text{VRR}, \text{1LR}, \dots$ and $(\mathcal{C}_k)^{ij}$ are the Wilson coefficients defined by Eq. (5.2.8) which correspond to F_{ij} in Eq. (5.2.32). Eq. (5.2.36) can be applied to all the phenomenology (B^0, B_s^0, K^0) because we have kept all the contributions ($\mathcal{C}_{tt}, \mathcal{C}_{ct}$ and \mathcal{C}_{cc}) which in some cases are important. In the SM, the application of the GIM mechanism results in some contributions proportional to $\ln \beta_u$ that do not vanish in the massless limit. This infrared-sensitive terms only appear for $(\mathcal{C}_{\text{2SRR}}^{\text{SM}})^{ij}$, in Appendix K we show how to deal with these terms. The different Wilson coefficients \mathcal{C}_k^{ij} can be found applying Eq. (5.2.32) to their respective Wilson coefficients $(\mathcal{C}_k)^{ij}$. The explicit expressions will be accessible on a webpage after the publication of this work.

The QCD renormalization group evolution of the Wilson coefficients from the scale μ_t down to the lower scale μ_b for B^0 mixing or μ_c for K^0 mixing, has been calculated in Ref. [283], as well as the corresponding parametrization for the hadronic matrix elements of the four-quark operators. More details can be found in Appendices L and M. In addition, we have taken into account the NLO QCD corrections for the SM which have been calculated in [37, 41] and for the charged scalar the top contribution from [38] in those cases that apply.

5.2.5 Comparison with the literature

In this section, we compare our results with the current ones in the literature [276–278]. To compare with Ref. [276], we particularize our results to $m_{q_2} \rightarrow 0$ and we ignore all

the contributions of $\mathcal{O}(x_{q_1})$ to our C_{VLL}^{ij} coefficient, then we obtain the same results for all Wilson coefficients except for $C_{\text{SM } 2\text{SRR}}$ because they do not follow a correct treatment for the infrared divergences. In order to eliminate these infrared divergences, they put them equal to zero, a correct treatment is presented in the Appendix K. For Ref. [277], we particularize again to $m_{q_2} \rightarrow 0$ and we observe that our result disagrees in the term proportional to $\varsigma_{d_j}^A (\varsigma_{u_i}^A)^* N_2 (f_2^{\text{AB}})^{ij}$ in Eq. (5.2.23). In Figure 5.3, we plot this discrepancy between both Wilson coefficients which is less than 2% for $M_{H^\pm} \geq 25$ GeV. We also compare with Ref. [278]. Our results disagree with their Eqs. (26) and (29) in the terms proportional to $A_u^2 A_u^{*2}$. Basically, they have only considered the corrections of $\mathcal{O}(x_s)$ in \mathcal{O}^{VLL} but there are leading order corrections independent of x_s as shown in our Eq. (H.0.1). Finally, we would like to point out that Ref. [278] quotes results that are inconsistent with those previously given in Ref. [276] by authors of the same group, see for instance \mathcal{O}^{VLL} for the case of $B_s^0 - \bar{B}_s^0$ mixing.

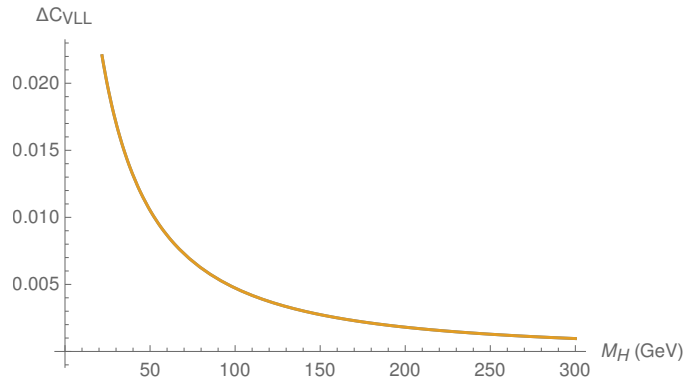


Figure 5.3: Dependence with M_{H^\pm} of the difference between the Wilson coefficient $(\delta C_{\text{VLL}}^{\text{AB}})^{ij}$ of this work and the one extracted from Ref. [277].

5.3 Numerical results

In this section, we present the numerical results extracted from $\bar{B}_{s,d}^0 - B_{s,d}^0$ and $\bar{K}^0 - K^0$ data. In $\bar{B}_q^0 - B_q^0$ mixing, we obtain combined constraints from ΔM_q , $\Delta \Gamma_q$, a_{SL}^q and $\phi_q^{c\bar{c}q}$

where $q = s, d$. The relation of these observables with the off-diagonal transition matrix element has been given in Chapter 1.

In $\bar{K}^0 - K^0$ mixing, ΔM_K is dominated by large long-distance contributions, so it is difficult to put accurate constraints using this observable. However, there exists another observable, the CP-violating parameter ε_K , that is mostly dominated by the short-distance contributions,

$$\varepsilon_K = \frac{\kappa_\varepsilon e^{i\phi_\varepsilon}}{\sqrt{2}} \frac{\text{Im}(M_{12}^{K^0})}{\Delta M_K}, \quad (5.3.38)$$

where $\kappa_\varepsilon = 0.94 \pm 0.02$ [284] takes into account the small long-distance corrections. In order to reduce the theoretical uncertainties, we fix ΔM_K and ϕ_ε to their experimental values, $\Delta M_K^{\text{exp}} = 3.484(6) \cdot 10^{-12}$ MeV [31] and $\phi_\varepsilon = 43.52(5)^\circ$ [31].

5.3.1 Standard Model predictions

Our SM predictions for the $\bar{B}_q^0 - B_q^0$ mixing observables are given in the third row of Tables 5.2 and 5.3 for $q = d, s$ respectively. For the computation of $\Delta\Gamma_q|_{\text{SM}}$ and $a_{st}^q|_{\text{SM}}$, we have used the ratio $\frac{\Gamma_{12}^q}{M_{12}^q}$ from Ref. [285]. The input parameters used in our analysis are provided in Tables N.1, N.2 and N.3. The theoretical uncertainties are obtained by varying each input of these tables within its allowed range and finally adding the individual uncertainties in quadrature. The experimental values averaged by HFLAV [32] are displayed in the second row. At the current level of precision, the SM predictions do not show any strong deviation from their experimental values. Therefore, these observables will set strong constraints on the parameters of NP.

	ΔM_d [ps ⁻¹]	$\phi_d^{c\bar{c}d}$ [rad]	$\Delta\Gamma_d$ [ps ⁻¹]	a_{st}^d [%]
Exp.	0.506 ± 0.002	–	–	-0.21 ± 0.17
SM	0.502 ± 0.071	0.816 ± 0.068	$(2.5 \pm 0.5) \cdot 10^{-3}$	-0.0512 ± 0.0075

Table 5.2: Numerical results for ΔM_d , $\Delta\Gamma_d$, $\phi_d^{c\bar{c}d}$ and a_{st}^d within the SM.

	ΔM_s [ps ⁻¹]	$\phi_s^{c\bar{c}s}$ [rad]	$\Delta\Gamma_s$ [ps ⁻¹]	a_{sl}^s [%]
Exp.	17.757 ± 0.021	-0.030 ± 0.033	0.086 ± 0.006	-0.06 ± 0.28
SM	17.279 ± 1.765	-0.038 ± 0.001	0.085 ± 0.013	0.0023 ± 0.0003

Table 5.3: Numerical results for ΔM_s , $\Delta\Gamma_s$, $\phi_s^{c\bar{c}s}$ and a_{sl}^s within the SM.

In $\bar{K}^0 - K^0$ mixing, we have computed the SM prediction for ε_K , adding all the individual uncertainties in quadrature, we obtain

$$\varepsilon_K|_{\text{SM}} = (2.22 \pm 0.32) \cdot 10^{-3}, \quad (5.3.39)$$

which is in very good agreement with the experimental value [31]

$$\varepsilon_K|_{\text{Exp.}} = (2.228 \pm 0.011) \cdot 10^{-3}. \quad (5.3.40)$$

This gives very strong constraints on the NP models.

In the next section, we present our numerical results. These have been obtained imposing that the NP contributions to the different observables X_j^{NP} have to be lower than the difference between the experimental value and its prediction in the SM,

$$|X_j^{\text{exp}} - X_j^{\text{SM}}| \geq |X_j^{\text{NP}}|, \quad (5.3.41)$$

where $j = 1, \dots, n_O$ and n_O is the number of observables. Finally, we obtain combined constraints plotting those points that fulfill Eq. (5.3.41).

5.3.2 Aligned Two-Higgs-Doublet Model

In this section, we present the numerical results for the colourless- and colour- A2HDM. In the Table 5.4, we display the wide range of models to which our result can be applied.

A₂ and B₂ models

The A₂ (A2HDM) [273] and B₂ (Manohar-Wise) [280] models correspond to the case of real coupling constants with normal flavour alignment. In Figure 5.4, we study how the

Model	Real (\mathbb{R})/Complex (\mathbb{C})	Aligned (A)/Generalized Alignment (GA)	Colour (C)/Colourless (\mathcal{C})
A_n	\mathbb{R}	A	\mathcal{C}
B_n	\mathbb{R}	A	C
C_n	\mathbb{C}	A	\mathcal{C}
D_n	\mathbb{C}	A	C
E_n	\mathbb{R}	GA	\mathcal{C}
F_n	\mathbb{R}	GA	C
G_n	\mathbb{C}	GA	\mathcal{C}
H_n	\mathbb{C}	GA	C

Table 5.4: Casuistry of AMHDM depending on the number of doublets n . First column denotes the name of the model. Second column refers to the couplings, ς_{u_i, d_i} , which can be real (\mathbb{R}) or complex (\mathbb{C}). The third column indicates if the model is aligned ($\varsigma_{u_1} = \varsigma_{u_2} = \varsigma_{u_3} = \varsigma_u$ and $\varsigma_{d_1} = \varsigma_{d_2} = \varsigma_{d_3} = \varsigma_d$) or it has generalized alignment ($\varsigma_{u_1} \neq \varsigma_{u_2} \neq \varsigma_{u_3}$ and $\varsigma_{d_1} \neq \varsigma_{d_2} \neq \varsigma_{d_3}$). The last column makes reference to the nature of $n - 1$ doublets if they are singlets (\mathcal{C}) or octets (C) of $SU(3)_C$.

different mixing observables constraint the $(\varsigma_u, \varsigma_d)$ plane for the A_2 and the B_2 models. In the A_2 model, using $\bar{B}_d^0 - B_d^0$ mixing we observe for $M_{H^\pm} = 100$ GeV that ς_u is bounded between $[-0.3, 0.3]$ and it quickly decreases with the increase of ς_d which is unbounded for this case. For $\bar{B}_s^0 - B_s^0$ mixing, we find that ς_u is bounded between $[-0.3, 0.3]$, until ς_d reaches values of 50 and -50 where ς_u breaks into two vertical legs with 0.4 and -0.4 values. In addition, the lower part of Figure 5.4 displays how the parameter space of ς_u is strongly constrained from $\bar{K}^0 - K^0$ mixing data while ς_d remains unconstrained. Combining all mixings, we obtain the following constraints for the A_2 model,

$$\varsigma_u \in [-0.3, 0.3] \ , \quad M_{H^\pm} = 100 \text{ GeV} \ , \quad (5.3.42)$$

$$\varsigma_u \in [-0.4, 0.4] \ , \quad M_{H^\pm} = 250 \text{ GeV} \ , \quad (5.3.43)$$

$$\varsigma_u \in [-0.6, 0.6] \ , \quad M_{H^\pm} = 500 \text{ GeV} \ , \quad (5.3.44)$$

while the bounds for ς_d lie above its perturbative limit, $|\varsigma_d| < \frac{v}{\sqrt{2}m_b} \approx 40$.

In the B_2 model, we find similar behaviours for both B_q^0 mixings, in contrast to the A_2 model, we observe oblique legs that allow large values of ς_u . However, these fine-tuned regions completely disappear when we consider the $\bar{K}^0 - K^0$ mixing data. Combining all mixings, we find

$$\varsigma_u \in [-0.5, 0.5] \ , \quad M_{H^\pm} = 100 \text{ GeV} \ , \quad (5.3.45)$$

$$\varsigma_u \in [-0.7, 0.7] \ , \quad M_{H^\pm} = 250 \text{ GeV} \ , \quad (5.3.46)$$

$$\varsigma_u \in [-0.9, 0.9] \ , \quad M_{H^\pm} = 500 \text{ GeV} \ , \quad (5.3.47)$$

while ς_d remains unconstrained. Notice in Figure 5.4 for the A_2 model that we obtain a different pattern than the one obtained in Ref. [276] because the authors of Ref. [276] have neglected the mass of the light quarks ($m_q = 0$). These contributions can be proportional to $(\varsigma_d)^2$ and $(\varsigma_d)^4$, then they can have strong repercussions for large values of ς_d . In Figure 5.5, we make a numerical cross-check, in the left side with $(\varsigma_d)^2$ and $(\varsigma_d)^4$ contributions and in the right side without these contributions. The right plot is completely equivalent to the plot of Ref. [276]. Finally, we would like to point out the constraints on ς_d obtained thanks to these contributions (see Figure 5.4), while in Ref. [276] the coupling ς_d remains unconstrained.

C₂ and D₂ models

In the C_2 and D_2 models, there are four parameters that contribute to the mixing, $|\varsigma_u|$, $|\varsigma_d|$, M_{H^\pm} and θ , where the last one is the phase between the two alignment parameters, $\varsigma_u^* \varsigma_d = |\varsigma_u^* \varsigma_d| e^{i\theta}$. In Figures 5.6, we display the different mixing constraints for the C_2 (left) and the D_2 (right) models. In the C_2 model, the $\bar{B}_{s,d}^0 - B_{s,d}^0$ mixings allow large values of $|\varsigma_d|$ and $|\varsigma_u|$ for $\theta \sim \frac{\pi}{2}, \pi, \frac{3\pi}{2}$. Around the vicinity of these angles, there are destructive interferences between the different contributions that result into a linear relation as Figure 5.6 shows. The vertical legs correspond to $\theta \sim \pi$ while the horizontal lines belong to $\theta \sim \frac{\pi}{2}, \frac{3\pi}{2}$. However, when we take into account the $\bar{K}^0 - K^0$ mixing, the

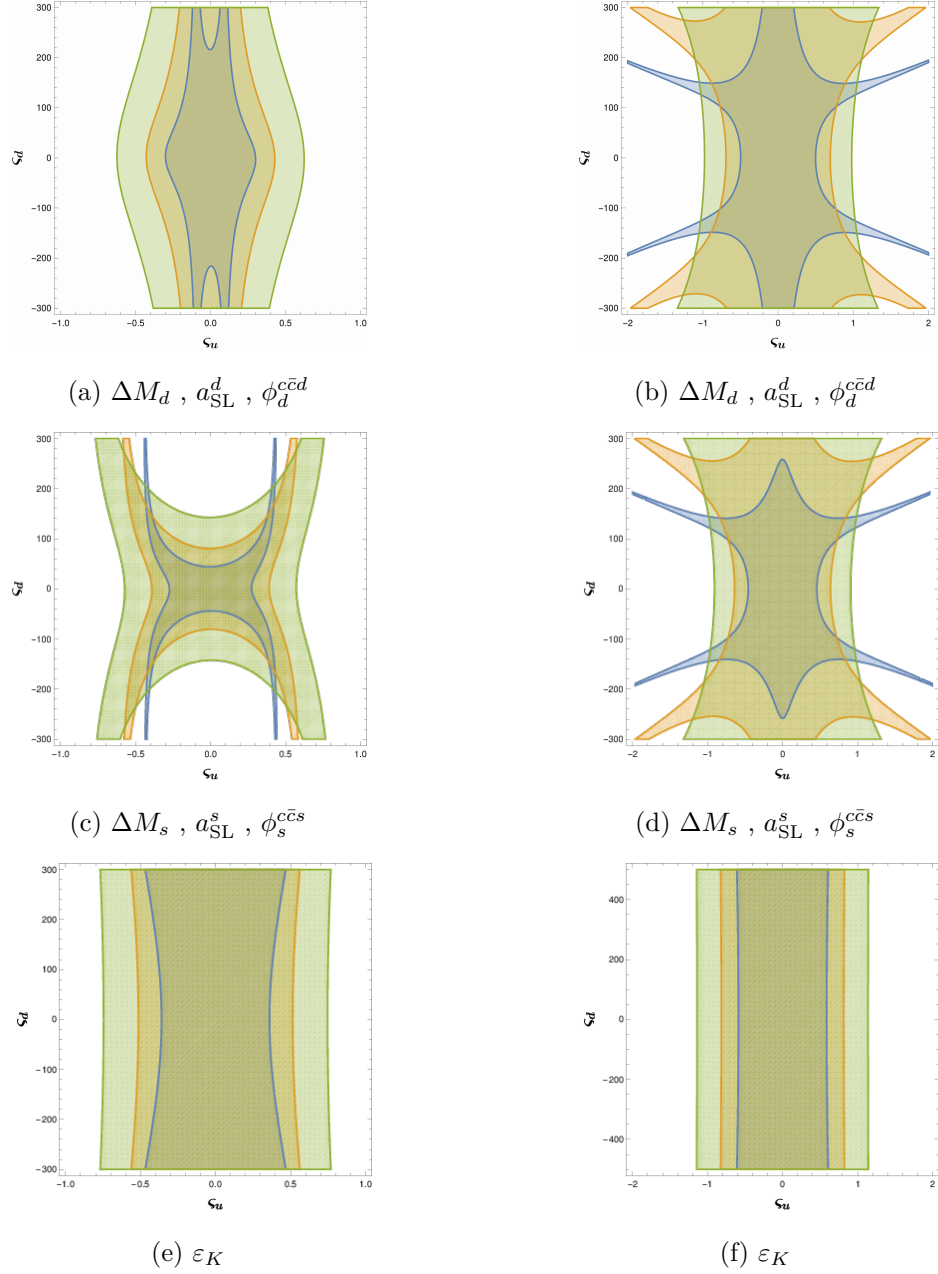


Figure 5.4: Allowed parameter space for ς_u and ς_d in the A_2 (left) and B_2 (right) models under combined constraints from $\Delta M_q, a_{SL}^q, \phi_q^{c\bar{c}q}$ and ε_K . The blue, orange and green regions are obtained with $M_{H^\pm} = 100, 250$ and 500 GeV, respectively.

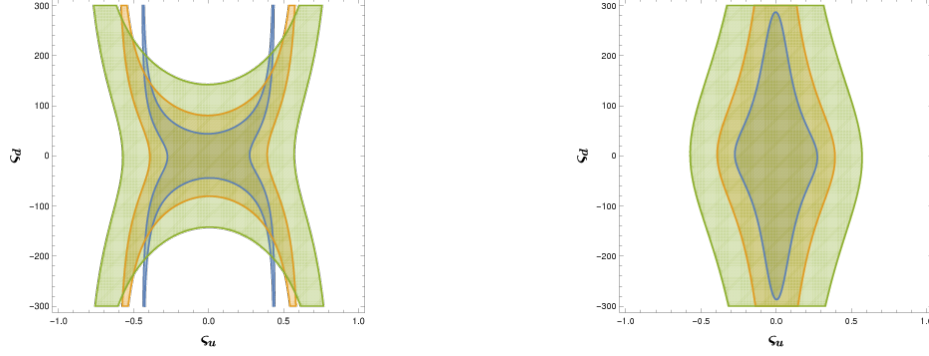


Figure 5.5: Constraints on the A_2 model from ΔM_s . Left side with $(\varsigma_d)^2$ and $(\varsigma_d)^4$ contributions and right side without them. The blue, orange and green regions are obtained with $M_{H^\pm} = 100$, 250 and 500 GeV, respectively.

horizontal lines disappear and give rise to the following bounds for the C_2 model,

$$|\varsigma_u| \in [0, 0.3] , \quad M_{H^\pm} = 100 \text{ GeV} , \quad (5.3.48)$$

$$|\varsigma_u| \in [0, 0.4] , \quad M_{H^\pm} = 250 \text{ GeV} , \quad (5.3.49)$$

$$|\varsigma_u| \in [0, 0.6] , \quad M_{H^\pm} = 500 \text{ GeV} . \quad (5.3.50)$$

while ς_d is again above its perturbative limit, $|\varsigma_d| < 40$.

In the D_2 model, the constraints are less stringent than in the C_2 model. The cancellations appear around $\theta \sim 0, \pi$. Finally, we obtain the following limits for the the D_2 model,

$$|\varsigma_u| \in [0, 0.5] , \quad M_{H^\pm} = 100 \text{ GeV} , \quad (5.3.51)$$

$$|\varsigma_u| \in [0, 0.6] , \quad M_{H^\pm} = 250 \text{ GeV} , \quad (5.3.52)$$

$$|\varsigma_u| \in [0, 0.9] , \quad M_{H^\pm} = 500 \text{ GeV} , \quad (5.3.53)$$

while $|\varsigma_d|$ remains unbounded.

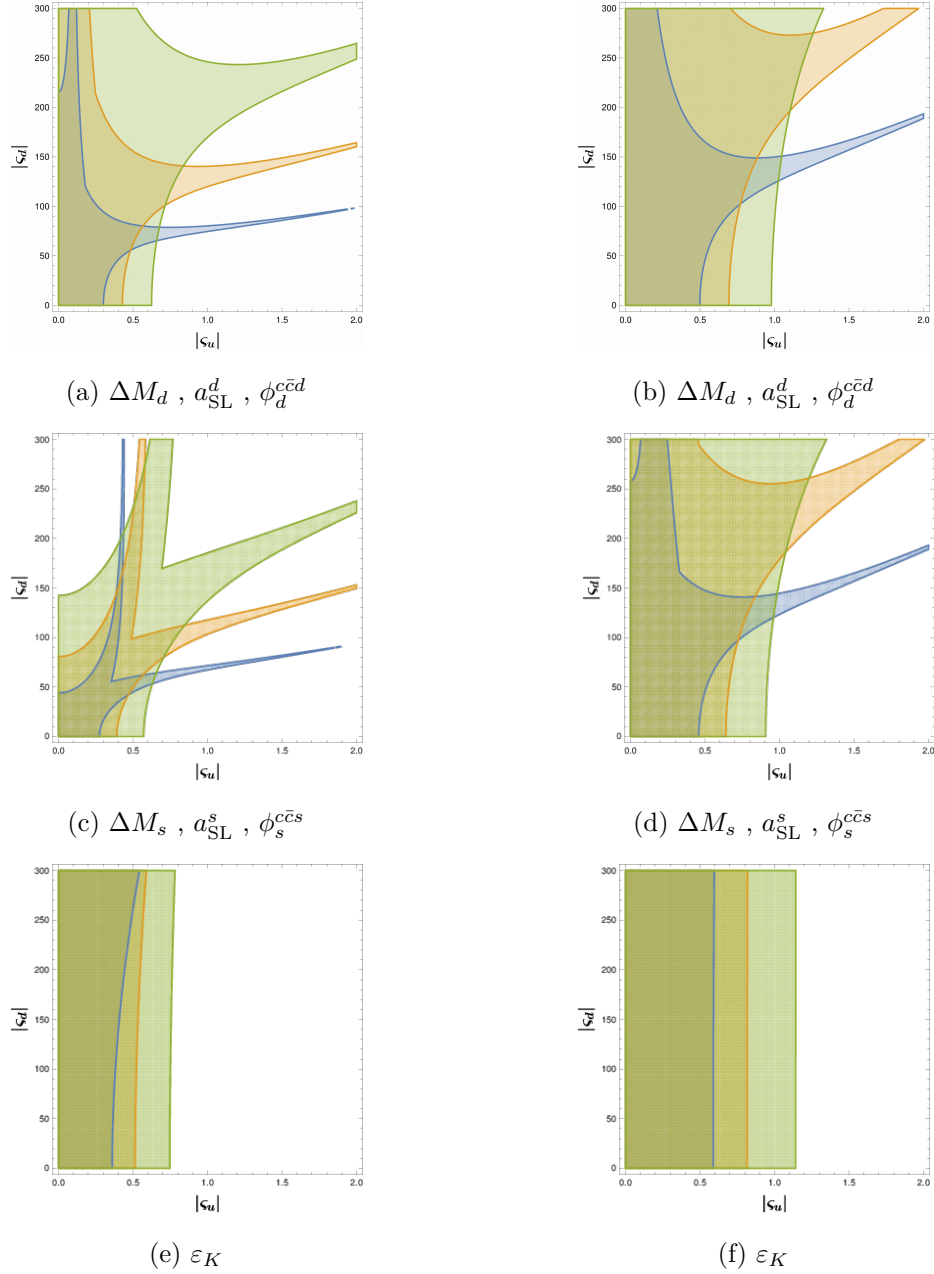


Figure 5.6: Allowed parameter space for $|s_u|$ and $|s_d|$ in the C_2 (left) and the D_2 (right) models under combined constraints from $\Delta M_q, a_{\text{SL}}^q, \phi_q^{c\bar{c}q}$ and ε_K . The blue, orange and green regions are obtained with $M_{H^\pm} = 100, 250$ and 500 GeV, respectively.

Generalized alignment

In the generalized alignment, there are in total 12 parameters, 6 modulus $|\varsigma_{d,s,b,u,c,t}|$, 1 mass M_{H^\pm} and 5 phases, in contrast to the E_2 and F_2 models where the number of parameters is reduced to 6.

Limits on the $|\varsigma_t|$ and $|\varsigma_b|$ parameters can be extracted from the B^0 mixing data. In Figure 5.7, we represent the allowed parameter space for these couplings in the E_2 model. Since the B^0 mixing contribution is dominated by diagrams with internal top quarks, the constraints obtained are completely equivalent to the A_2 model shown in Figure 5.4.

In the F_2 , G_2 and H_2 models, we obtain similar bounds as the B_2 , C_2 and D_2 models, respectively, which again reflects that the NP couplings ς_{u_i} and ς_{d_j} in the $B_{s,d}^0$ mixing are completely dominated by the coupling with the top quark ($i = 3$ and $j = 2$).

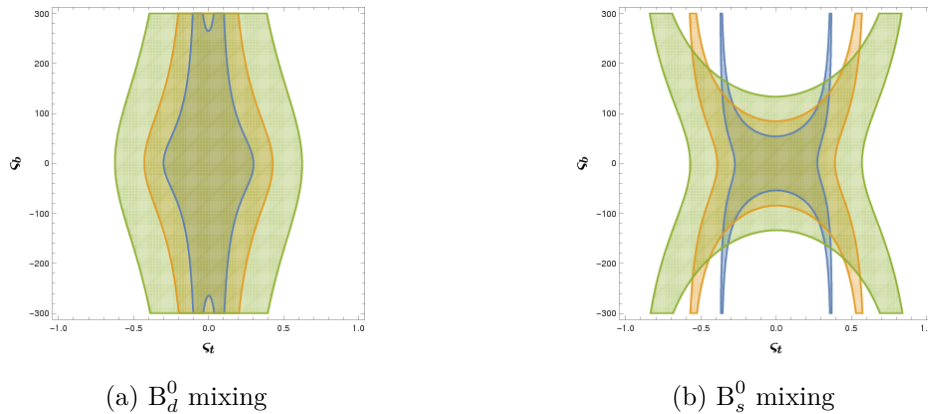


Figure 5.7: Allowed parameter space for ς_b and ς_t in the E_2 model under combined constraints from ΔM_q , a_{SL}^q and $\phi_q^{c\bar{c}q}$. The blue, orange and green regions are obtained with $M_{H^\pm} = 100, 250$ and 500 GeV, respectively.

The $\bar{K}^0 - K^0$ mixing allows us to study the $|\varsigma_c|$ and $|\varsigma_s|$ couplings. In Figure 5.8, we present the parameter space for $|\varsigma_c|$ and $|\varsigma_s|$, observing that while large values for $|\varsigma_c|$ are allowed,

values for $|\zeta_s|$ are not, instead we obtain the following bounds

$$|\zeta_s| \in [0, 15] , [0, 25] , [0, 40] , \quad M_{H^\pm} = 100 , 250 , 500 \text{ GeV} , \quad (\text{E}_2 \text{ and G}_2) \quad (5.3.54)$$

$$|\zeta_s| \in [0, 100] , [0, 160] , [0, 270] , \quad M_{H^\pm} = 100 , 250 , 500 \text{ GeV} , \quad (\text{F}_2 \text{ and H}_2) \quad (5.3.55)$$

which are remarkable stronger than its perturbative bound, $|\zeta_s| < \frac{v}{\sqrt{2}m_s} \approx 1850$.

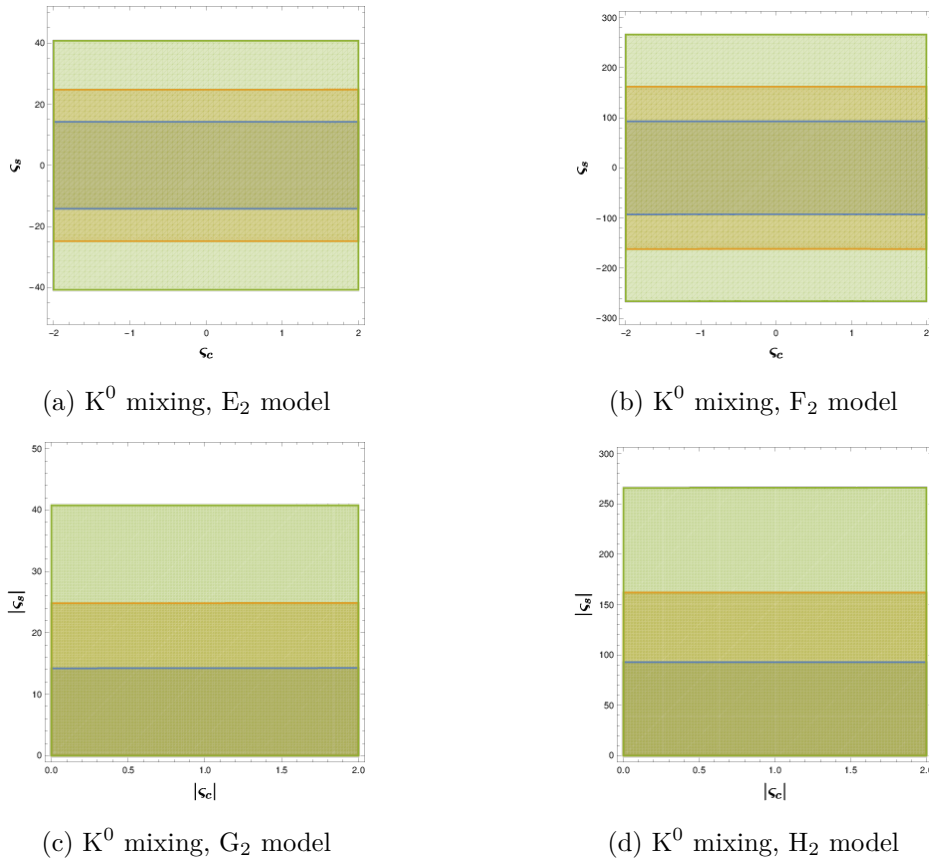


Figure 5.8: Allowed parameter space for ζ_s and ζ_c in the E_2 , F_2 , G_2 and H_2 models under constraints from ε_K . The blue, orange and green regions are obtained with $M_{H^\pm} = 100$, 250 and 500 GeV, respectively.

5.3.3 Aligned Three-Higgs-Doublet Model

In this section, we present our numerical analysis for the colour- and colourless- A3HDM which corresponds to $n = 3$ in Table 5.4. The parameter space is enlarged by the additional charged Higgs particle which in general can have different mass and different couplings constants. In view of this, we simplify our discussion to two quite general scenarios:

- **Scenario I:** The values of the up- and down- type couplings are equal, $\varsigma_{u,d} = \tilde{\varsigma}_{u,d}$. We analyze the allowed region for the ς_u and ς_d parameters for both equal, $M_{\varphi_1^\pm} = M_{\varphi_2^\pm} \equiv M_{H^\pm}$, and different masses, $M_{\varphi_1^\pm} \neq M_{\varphi_2^\pm}$.
- **Scenario II:** The values of the down-type couplings (ς_d and $\tilde{\varsigma}_d$) are fixed to some value ($\varsigma_d = \tilde{\varsigma}_d = 20$ for our study) below its perturbative limit. We set constrains in the ς_u - $\tilde{\varsigma}_u$ plane for equal, $M_{\varphi_1^\pm} = M_{\varphi_2^\pm} \equiv M_{H^\pm}$, and different masses, $M_{\varphi_1^\pm} \neq M_{\varphi_2^\pm}$.

Due to the large number of parameters in the NP models with the generalized alignment, we limit our analysis only to aligned models.

A₃, B₃, C₃, D₃ models in Scenario I

In Scenario I, we obtain the same behaviour as in the A2HDM with a pertinent scale factor. Since, diagrams with two exchanges of charged Higgs particles (Figure 5.1c) are suppressed by a factor $M_W^2/M_{\varphi_{1,2}^\pm}^2$ with respect to those with only one (Figures 5.1d and 5.1e), the main contributions come from the Feynman diagrams with only one exchange of charged particle. In that limit, the total amplitude for the meson mixing can be approximated by two A2HDM. Therefore, we can directly extract the bounds on the A3HDM from the A2HDM with

$$|\varsigma_{u,d}^{X_3}| = \frac{1}{2} |\varsigma_{u,d}^{X_2}|, \quad (5.3.56)$$

where $\varsigma_{u,d}^{X_2}$ are the bounds in $X_2 = A_2, B_2, C_2, D_2$ model for $M_{H^\pm} = M_{\varphi_1^\pm}$. It is interesting to remark that the factor 1/2 allows us to extract better bounds on $|\varsigma_d^{X_3}|$ than the ones obtained by perturbativity.

For different masses $M_{\varphi_1^\pm} \neq M_{\varphi_2^\pm}$, the amplitude is dominated for the lightest charged Higgs contribution, and then the scale factor disappears leading into

$$|\zeta_{u,d}^{X_3}| = |\zeta_{u,d}^{X_2}| . \quad (5.3.57)$$

A₃, B₃, C₃, D₃ models in Scenario II

For Scenario II, the strongest bounds are set by B_s^0 mixing. We have performed an analysis for equal, $M_{\varphi_1^\pm} = M_{\varphi_2^\pm} \equiv M_{H^\pm}$ (Figure 5.9), and different masses, $M_{\varphi_1^\pm} \neq M_{\varphi_2^\pm}$ (Figure 5.10). In the A₃ model, using the $\bar{B}_s^0 - B_s^0$ mixing data we find that for a given charged Higgs mass, the parameters ζ_u and $\tilde{\zeta}_u$ are bounded by a circular region, which leads into the following limits

$$\zeta_u \in [-0.25, 0.25] , \quad \tilde{\zeta}_u \in [-0.25, 0.25] , \quad M_{H^\pm} = 100 \text{ GeV} . \quad (5.3.58)$$

$$\zeta_u \in [-0.30, 0.30] , \quad \tilde{\zeta}_u \in [-0.30, 0.30] , \quad M_{H^\pm} = 250 \text{ GeV} . \quad (5.3.59)$$

$$\zeta_u \in [-0.45, 0.45] , \quad \tilde{\zeta}_u \in [-0.45, 0.45] , \quad M_{H^\pm} = 500 \text{ GeV} . \quad (5.3.60)$$

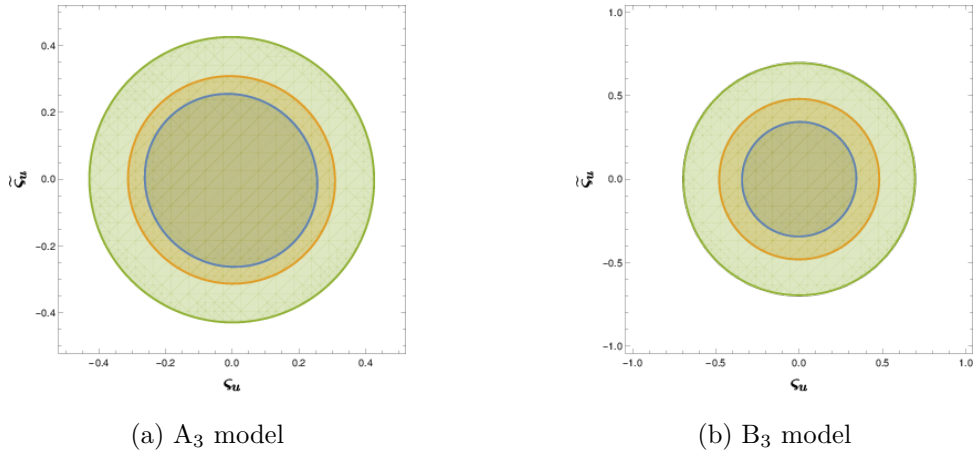


Figure 5.9: Allowed parameter space for ζ_u and $\tilde{\zeta}_u$ in the A₃ (left) and B₃ (right) models in scenario II under combined constraints from ΔM_s , a_{SL}^s and $\phi_s^{c\bar{c}s}$. The blue, orange and green regions are obtained with $M_{H^\pm} = 100, 250$ and 500 GeV, respectively.

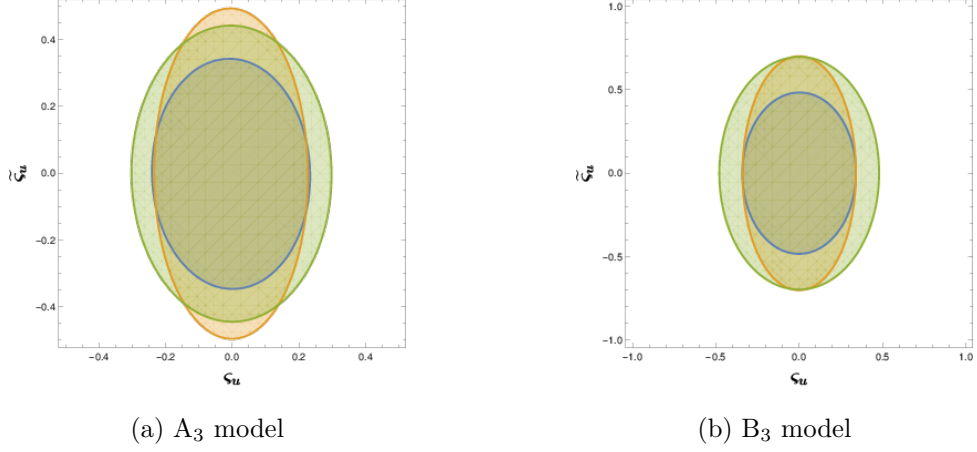


Figure 5.10: Allowed parameter space for ς_u and $\tilde{\varsigma}_u$ in the A₃ (left) and B₃ (right) models in scenario II under combined constraints from ΔM_s , a_{SL}^s and $\phi_s^{c\bar{c}s}$. The blue, orange and green regions are obtained for $(M_{\varphi_1^\pm}, M_{\varphi_2^\pm}) = (100, 250), (100, 500), (250, 500)$ GeV, respectively.

In the B₃ model, we find the same behaviour as in the A₃ model but less stringent,

$$\varsigma_u \in [-0.35, 0.35] \quad , \quad \tilde{\varsigma}_u \in [-0.35, 0.35] \quad , \quad M_{H^\pm} = 100 \text{ GeV} \quad . \quad (5.3.61)$$

$$\varsigma_u \in [-0.5, 0.5] \quad , \quad \tilde{\varsigma}_u \in [-0.5, 0.5] \quad , \quad M_{H^\pm} = 250 \text{ GeV} \quad . \quad (5.3.62)$$

$$\varsigma_u \in [-0.7, 0.7] \quad , \quad \tilde{\varsigma}_u \in [-0.7, 0.7] \quad , \quad M_{H^\pm} = 500 \text{ GeV} \quad . \quad (5.3.63)$$

In contrast to the previous cases, for different masses, we find that the ς_u - $\tilde{\varsigma}_u$ plane is constrained by ellipses, see Figure 5.10, that lead into the following bounds

$$\varsigma_u \in [-0.25, 0.25] \quad , \quad \tilde{\varsigma}_u \in [-0.35, 0.35] \quad , \quad (M_{\varphi_1^\pm}, M_{\varphi_2^\pm}) = (100, 250) \text{ GeV} \quad . \quad (5.3.64)$$

$$\varsigma_u \in [-0.5, 0.5] \quad , \quad \tilde{\varsigma}_u \in [-0.25, 0.25] \quad , \quad (M_{\varphi_1^\pm}, M_{\varphi_2^\pm}) = (100, 500) \text{ GeV} \quad . \quad (5.3.65)$$

$$\varsigma_u \in [-0.45, 0.45] \quad , \quad \tilde{\varsigma}_u \in [-0.3, 0.3] \quad , \quad (M_{\varphi_1^\pm}, M_{\varphi_2^\pm}) = (250, 500) \text{ GeV} \quad . \quad (5.3.66)$$

for the A_3 model, and

$$\varsigma_u \in [-0.25, 0.25] \ , \quad \tilde{\varsigma}_u \in [-0.35, 0.35] \ , \quad (M_{\varphi_1^\pm}, M_{\varphi_2^\pm}) = (100, 250) \text{ GeV} \ . \quad (5.3.67)$$

$$\varsigma_u \in [-0.5, 0.5] \ , \quad \tilde{\varsigma}_u \in [-0.25, 0.25] \ , \quad (M_{\varphi_1^\pm}, M_{\varphi_2^\pm}) = (100, 500) \text{ GeV} \ . \quad (5.3.68)$$

$$\varsigma_u \in [-0.45, 0.45] \ , \quad \tilde{\varsigma}_u \in [-0.3, 0.3] \ , \quad (M_{\varphi_1^\pm}, M_{\varphi_2^\pm}) = (250, 500) \text{ GeV} \ . \quad (5.3.69)$$

for the B_3 model.

For the C_3 and D_3 models, the number of parameters increase with additional phases between the different NP couplings. Studying the C_3 and D_3 models in the $|\varsigma_u|$ - $|\tilde{\varsigma}_u|$ plane, we obtain similar bounds to the A_3 and B_3 models, respectively. The additional phases have been varied from 0 to 2π .

It is interesting to remark the geometrical shape obtained for this scenario, circles and ellipses. The bounds are controlled by ΔM_s via the condition given by Eq. 5.3.41. For large values of $M_{\varphi_2^\pm}$, it is a good approximation if one just considers the contributions with one exchange of a charged Higgs boson (Figures 5.1d and 5.1e) to the Wilson coefficient $\mathcal{C}_{\text{VLL}}^{tt}$. In that limit, the condition given by Eq. (5.3.41) can be simply written as

$$|\varsigma_u|^2 N_3 f(M_{\varphi_1^\pm}^2) + |\tilde{\varsigma}_u|^2 N_3 f(M_{\varphi_2^\pm}^2) \leq \frac{\delta\Delta M_s 24 \pi^2}{G_F^2 M_W^2 \lambda_t^2 f_{B_s^0}^2 M_{B_s^0} \widehat{\mathcal{B}}_{B_s^0} \eta_{B_s^0}} \ , \quad (5.3.70)$$

where N_3 is a colour factor ($N_3 = 1/3$ and $N_3 = 1$ for the colour- and colourless- cases, respectively), $\delta\Delta M_s$ is the uncertainty associated with the difference between the experimental value of ΔM_s and its SM prediction and f is a non-trivial loop function that depends on mass parameters like M_W , m_t , $M_{\varphi_{1,2}^\pm}$, etc. For $M_{\varphi_1^\pm}^2 = M_{\varphi_2^\pm}^2 = M_{H^\pm}^2$, Eq. (5.3.70) simplifies to

$$|\varsigma_u|^2 + |\tilde{\varsigma}_u|^2 \leq \frac{\delta\Delta M_s 24 \pi^2}{G_F^2 M_W^2 \lambda_t^2 f_{B_s^0}^2 M_{B_s^0} \widehat{\mathcal{B}}_{B_s^0} \eta_{B_s^0} N_3 f(M_{H^\pm}^2)} \equiv R(M_{H^\pm}^2)^2 \ , \quad (5.3.71)$$

that corresponds to a circular region of radius $R(M_{H^\pm}^2)$ and explains why we have obtained the circular regions shown in Figure 5.9. Since the loop function f decreases with the increase of M_{H^\pm} , we get stronger bounds for light charged Higgs masses. In addition, it is interesting to point out that the differences between the A_3 and the B_3 models can

be explained with the colour factor ($N_3 = 1/3$) which clearly produces an increase in the radius of the circle.

In the case of different masses, Eq. (5.3.70) turns to be an ellipse which is precisely the same behaviour that shows Figure 5.10. Eq. (5.3.70) shows that large values of $M_{\varphi_1^\pm}$ ($M_{\varphi_2^\pm}$) imply an enlargement for $|\varsigma_u|$ ($|\tilde{\varsigma}_u|$), since the masses are different we get different bounds for each coupling.

5.4 Conclusions

The good agreement between the SM prediction and the measured values in the mixing observables makes the neutral meson mixing a formidable phenomenological application to test the quantum structure of some NP extensions. In this chapter, we have performed a complete one-loop computation of the $M^0 - \bar{M}^0$ mixing within a quite general extension of the SM, the AMHDM where the $N - 1$ additional Higgs doublets can be singlet or octets of $SU(3)_C$ and we have also included the possibility of generalized alignment.

Our analytical results, presented in Section 5.2.3, have been computed as generally as possible. Unlike the results present in the literature [276–278], we have provided our results in a compact manner without specifying any phenomenological application, *i.e.* $B^0 - \bar{B}^0$, $B_s^0 - \bar{B}_s^0$, $K^0 - \bar{K}^0$, etc. They have been computed keeping up to the second order the masses and momenta of all external quarks in the box diagrams, so the number of dimension-six operators increase up to 8 in contrast to the 3 operators of the current literature [276–278]. Although these additional contributions are very small because they are proportional to the external light quark masses, we have observed that they can give non-trivial contributions for large values of ς_d .

Using the current experimental mixing observables in Section 5.3, we have analysed the allowed parameter space in the A2HDM and the A3HDM for singlet or octet colour doublets. In the A2HDM for real couplings (A_2 and B_2 models), we have obtained stronger bounds for $|\varsigma_{u,d}|$ than the ones presented in Refs. [276–278]. In the A_2 (B_2) model, we

have obtained $|\zeta_u| < 0.6$ (0.9) for a $M_{H^\pm} = 500$ GeV . For complex couplings (C_2 and D_2 models), we obtain similar constraints to the A_2 and the B_2 models.

Our analytical results have been particularized to the case of generalized alignment. From the B^0 mixing data, we have been able to extract bounds on the NP couplings $|\zeta_b|$ and $|\zeta_t|$. Since the B^0 mixing is dominated by the internal top quark contributions, the bounds extracted for these models are of the same size as the ones presented in the aligned case. In addition, the K^0 mixing has allowed us to strongly constraint the $|\zeta_s|$ coupling, while for the $|\zeta_c|$ parameter, large values of $|\zeta_c|$ remain allowed.

In the A3HDM, due to the large number of parameters, we have particularized our study to two quite general cases. For scenario I, we have obtained the same limits as in the A2HDM with the pertinent scale factor because in that limit the amplitude is dominated by the diagrams with a single exchange of the lightest charged Higgs particle. For scenario II, we have obtained a simple dependence on our constrains, circles and ellipses. Finally, we have given the arguments that explain the appearance of these geometric forms

In summary, we have presented all the different behaviours followed by the different types of A2HDM and A3HDM. The current experimental data is unable to reveal which one of them fits better, instead we have obtained stringent bounds on their parameter space. However, in the future, our analytical results together with the improvements on the experimental and theoretical uncertainties could disclose which types of MHDM are preferred by experimental data.

Chapter 6

Improved bounds on heavy quark electric dipole moments

In this chapter, we obtain new bounds on the electric dipole moment (EDM) of charm and bottom quarks using the stringent limits on their chromo-EDMs. The new limits, $|d_c| < 1.5 \times 10^{-21} e \text{ cm}$ and $|d_b| < 1.2 \times 10^{-20} e \text{ cm}$, improve the previous ones by about three orders of magnitude. These indirect bounds can have important implications for models of new physics. The content of this chapter is based on Ref. [287].

6.1 Introduction

Searches for EDMs are currently setting stringent constraints on NP models with additional CP violation sources [288–292]. Since the SM predictions are well below the current experimental accuracy, any signal of a non-zero EDM would be a clear sign of NP. Moreover, the persisting B-anomalies suggest a non-trivial flavour structure in NP models, which can enhance the heavy quark EDMs [293, 294].

Due to their very small lifetime, direct EDM searches on heavy-flavoured hadrons represent an experimental challenge and only indirect limits on heavy quark dipole couplings have

been obtained to date. However, this situation may change with the new proposals to search for the EDM of charmed and bottom baryons at the LHC [295–298].

In this chapter, we present a new approach for setting indirect bounds on quark EDM couplings. By exploiting the mixing of operators under the renormalization group and using current constraints on the chromo-EDM of charm and bottom quarks [299, 300], we extract new bounds on their corresponding EDMs that improve the current ones by several orders of magnitude.

6.2 Renormalization group equations

Let us consider the following flavour-conserving CP-violating effective Lagrangian

$$\mathcal{L}_{\text{eff}} = \sum_{i=1}^2 \sum_q C_i^q(\mu) O_i^q(\mu) + C_3(\mu) O_3(\mu) , \quad (6.2.1)$$

where the index q runs over the relevant flavours at the chosen renormalization scale. The effective operators are defined as

$$\begin{aligned} O_1^q &\equiv -\frac{i}{2} e Q_q m_q \bar{q}^\alpha \sigma^{\mu\nu} \gamma_5 q^\alpha F_{\mu\nu} , \\ O_2^q &\equiv -\frac{i}{2} g_s m_q \bar{q}^\alpha \sigma^{\mu\nu} T_a \gamma_5 q^\alpha G_{\mu\nu}^a , \\ O_3 &\equiv -\frac{1}{6} g_s f_{abc} \epsilon^{\mu\nu\lambda\sigma} G_{\mu\rho}^a G_\nu^{b\rho} G_{\lambda\sigma}^c , \end{aligned} \quad (6.2.2)$$

where Q_q and m_q are the quark charge and quark mass, respectively. The quark EDM, chromo-EDM, and the usually defined coefficient $\omega(\mu)$ of the Weinberg operator are related to the Wilson coefficients by

$$\begin{aligned} d_q(\mu) &= e Q_q m_q(\mu) C_1^q(\mu) , \\ \tilde{d}_q(\mu) &= m_q(\mu) C_2^q(\mu) , \\ \omega(\mu) &= -\frac{1}{2} g_s(\mu) C_3(\mu) . \end{aligned} \quad (6.2.3)$$

When a heavy quark is integrated out, its chromo-EDM gives a finite contribution to the Weinberg operator [300–302], which is strongly constrained from the limits on the neutron

EDM. This allows to bound the quark chromo-EDMs to be [299, 300],

$$\begin{aligned} |\tilde{d}_c(m_c)| &< 1.0 \times 10^{-22} \text{ cm} , \\ |\tilde{d}_b(m_b)| &< 1.1 \times 10^{-21} \text{ cm} . \end{aligned} \quad (6.2.4)$$

Attempts to constraint heavy quark EDMs have followed different strategies: flavour-mixing contributions into light-quark EDMs [299,303,304], $b \rightarrow s\gamma$ transitions [299], mixing into the electron EDM via light-by-light scattering diagrams [304] and tree-level contributions to the $e^+e^- \rightarrow q\bar{q}$ total cross section [305,306]. All of these approaches yield results within the same order of magnitude, the most restrictive ones being [299, 306]

$$\begin{aligned} |d_c(m_c)| &< 4.4 \times 10^{-17} e \text{ cm} , \\ |d_b(m_b)| &< 2.0 \times 10^{-17} e \text{ cm} . \end{aligned} \quad (6.2.5)$$

We follow a new strategy that relates the EDM and chromo-EDM operators in order to find new limits on d_q from the already available strong bounds on \tilde{d}_q . This relation is done in a model-independent way using the RGEs, which mix the effective operators when the energy scale is changed as we have seen in Chapter 2. The relevant diagrams include photon loops which have been neglected in previous works due to its small size compared with pure QCD corrections. Nevertheless, they represent the first non-zero contribution to the mixing we are interested in as we will see in the next section.

The evolution of the Wilson coefficients is given by

$$\frac{d}{d \ln \mu} \vec{C}(\mu) = \hat{\gamma}^T \vec{C}(\mu) , \quad (6.2.6)$$

where $\vec{C} \equiv (C_1^q, C_2^q, C_3)$ and $\hat{\gamma}$ is the anomalous dimension matrix. This matrix can be expanded in powers of the QCD and QED coupling constants, α_s and α , respectively,

$$\hat{\gamma} = \frac{\alpha_s}{4\pi} \gamma_s^{(0)} + \left(\frac{\alpha_s}{4\pi}\right)^2 \gamma_s^{(1)} + \frac{\alpha}{4\pi} \gamma_e^{(0)} + \dots , \quad (6.2.7)$$

where $\gamma_s^{(0)}$ and $\gamma_s^{(1)}$ represent the one- and two-loop QCD anomalous corrections, while $\gamma_e^{(0)}$ encodes the one-loop QED correction [301, 307–310]. The one- and two-loop QCD

anomalous dimensions are given by¹

$$\gamma_s^{(0)} = \begin{bmatrix} 8 C_F & 0 & 0 \\ 8 C_F & 16 C_F - 4 N_C & 0 \\ 0 & -2 N_C & N_C + 2f + \beta_0 \end{bmatrix}, \quad (6.2.8)$$

$$\gamma_s^{(1)} = \begin{bmatrix} \left(\frac{548}{9} N_C - 16 C_F - \frac{56}{9} f\right) C_F & 0 & 0 \\ \left(\frac{404}{9} N_C - 32 C_F - \frac{56}{9} f\right) C_F & -\frac{458}{9} - \frac{12}{N_C^2} + \frac{214}{9} N_C^2 + \frac{56}{9} \frac{f}{N_C} - \frac{13}{9} N_C f & 0 \\ \times & \times & \times \end{bmatrix},$$

respectively. At $\mathcal{O}(\alpha_s)$ and $\mathcal{O}(\alpha_s^2)$, the quark EDM does not mix into the chromo-EDM, see the matrix elements $(\gamma_s^{(0)})_{12}$ and $(\gamma_s^{(1)})_{12}$, and the first contribution only appears at $\mathcal{O}(\alpha)$ from photon-loop diagrams as shown in Figure 6.1. Applying the standard techniques for the computation of anomalous dimensions [49, 50] which have been introduced in the Chapter 2, we obtain the following matrix element

$$(\gamma_e)_{12}^{(0)} = 8, \quad (6.2.9)$$

in agreement with a previous calculation [310]. In Appendix O, we provide detailed information on the computation of (6.2.9).

Solving Eq. (6.2.6) by adding this contribution, the evolution of the charm and bottom chromo-EDMs read

$$\begin{bmatrix} d_c(m_c) \\ \tilde{d}_c(m_c) \end{bmatrix} = \begin{bmatrix} 0.64 e & -0.47 e \\ -0.04 & 0.74 \end{bmatrix} \begin{bmatrix} \frac{d_c(M_{\text{NP}})}{e} \\ \tilde{d}_c(M_{\text{NP}}) \end{bmatrix}, \quad (6.2.10)$$

¹The matrix elements with crosses in the $\gamma_s^{(1)}$ are unknown. However, since we have neglected the contributions of the Weinberg operator, these elements do not contribute to the RGEs.

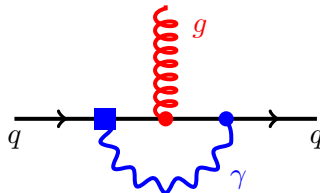


Figure 6.1: The quark EDM coupling (blue square) induces a chromo-EDM through photon-loop diagrams. These represent the leading contributions to the matrix element $(\gamma_e)_{12}^{(0)}$.

$$\begin{bmatrix} d_b(m_b) \\ \tilde{d}_b(m_b) \end{bmatrix} = \begin{bmatrix} 0.80 e & 0.19 e \\ 0.08 & 0.88 \end{bmatrix} \begin{bmatrix} \frac{d_b(M_{\text{NP}})}{e} \\ \tilde{d}_b(M_{\text{NP}}) \end{bmatrix}, \quad (6.2.11)$$

where we have taken $M_{\text{NP}} \sim 1$ TeV as the scale of NP. The mixing of \tilde{d}_q and d_q into themselves, described by the diagonal matrix elements of Eqs. (6.2.10) and (6.2.11), has leading contributions from pure QCD corrections, then corrections of $\mathcal{O}(\alpha)$ can be safely neglected. In the way down to low energies, we do not include the threshold effect of heavy quarks like bottom or top since these corrections represent less than 10% of the contribution to the RGEs.

6.3 Extracting the new bounds

Taking the first rows of Eqs. (6.2.10) and (6.2.11), together with the bounds on the chromo-EDMs at the low scales quoted in Eq. (6.2.4), we obtain the following inequalities

$$\left| 0.04 \frac{d_c(M_{\text{NP}})}{e} - 0.74 \tilde{d}_c(M_{\text{NP}}) \right| < 1.0 \times 10^{-22} \text{ cm}, \quad (6.3.12)$$

$$\left| 0.08 \frac{d_b(M_{\text{NP}})}{e} + 0.88 \tilde{d}_b(M_{\text{NP}}) \right| < 1.1 \times 10^{-21} \text{ cm}, \quad (6.3.13)$$

which can be plotted in the \tilde{d}_q - d_q plane as shown in Figure 6.2. We observe an allowed region extending along a straight line, these strong fine-tuned cancellations come from the destructive interference between the two pieces of Eqs. (6.3.12) and (6.3.13). Since

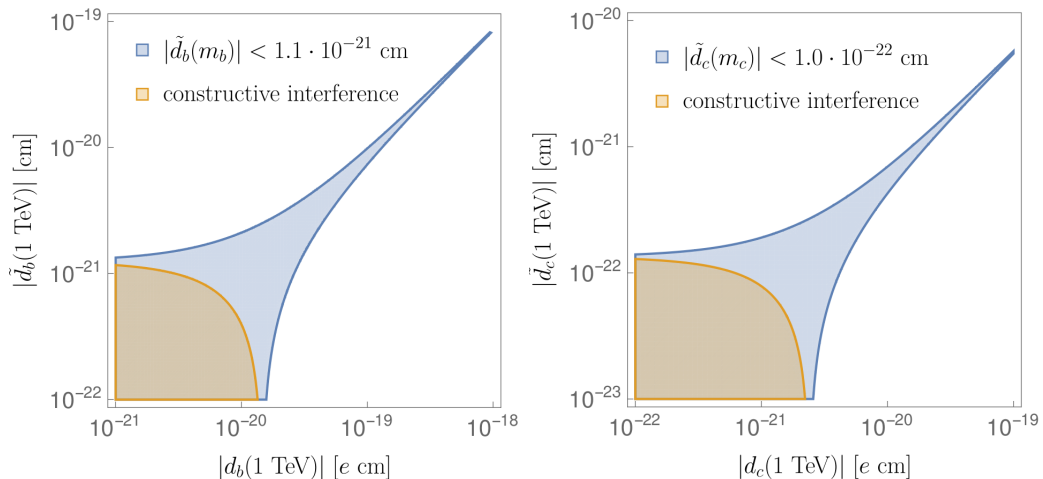


Figure 6.2: Bounds on the charm (bottom) chromo-EDM constrain the \tilde{d}_c - d_c (\tilde{d}_b - d_b) plane to the allowed blue region. Notice that strong fine-tuned cancellations result in a straight line region that is not present in the case with constructive interference, displayed in orange.

this fine-tuned region is unlikely to be realised in NP models, we assume constructive interference between the EDM and chromo-EDM contributions at the NP scale which allow us to extract the following bounds on $d_q(M_{\text{NP}})$,

$$\begin{aligned} |d_c(M_{\text{NP}})| &< 2.5 \times 10^{-21} e \text{ cm} , \\ |d_b(M_{\text{NP}})| &< 1.3 \times 10^{-20} e \text{ cm} . \end{aligned} \quad (6.3.14)$$

Then, using the evolution of the EDM operator, given by the second rows of Eqs. (6.2.10) and (6.2.11), to bring these bounds down to the quark mass scale, the new bounds on the charm and bottom quark EDMs are

$$\begin{aligned} |d_c(m_c)| &< 1.5 \times 10^{-21} e \text{ cm} , \\ |d_b(m_b)| &< 1.2 \times 10^{-20} e \text{ cm} , \end{aligned} \quad (6.3.15)$$

which improve the previous ones quoted in Eq. (6.2.5) by three and four orders of magnitude, respectively. This approach does not improve the current bounds on the top quark EDM [312] given that the limit on its chromo-EDM is of similar size [313]. The theoretical

uncertainty of this result is dominated by the contribution of the Weinberg operator to the neutron EDM, since it determines the size of the chromo-EDM bounds. Note also that higher values of the NP scale yield less conservative results, e.g. a 30% stronger bounds for $M_{\text{NP}} = 10 \text{ TeV}$.

The new constraints for the charm and bottom quark EDMs are in tension with the predictions of different theories beyond the standard model [314–317] and will provide valuable input for future phenomenological analysis of NP models.

Conclusions

This thesis is focused on the study of physical systems with CP violation. Since the SM of particle physics is unable to predict the large size of the observed matter-antimatter asymmetry in the Universe, new sources of CP violation from SM extensions are needed. The SM of particle physics is currently considered as the theoretical framework of reference for any NP theory because along the years it has successfully overcome a large number of experimental tests. In Chapter 1, we have seen how its interactions emerge from gauge symmetry principles and how the SSB is able to generate the masses of the weak bosons through the Higgs mechanism. Finally, we have presented the flavour sector, introducing the CP violation phenomena and the different ways in which this appears in nature.

In Chapter 2, we have introduced the EFT approach which provides a formidable framework to deal with the different physical systems. The techniques used along this thesis have been illustrated there by the Fermi's theory.

The first phenomenological application is the theoretical determination of the CP-violating ratio ε'/ε in the SM which has been presented in Chapter 3. We have reviewed the current status, discussing in detail the different ingredients that enter into the calculation of this observable and the reasons why seemingly contradictory predictions were obtained in the past by several groups. We have included all known short- and long-distance contributions and our SM prediction is in complete agreement with the experimental measurement.

The known isospin-breaking contributions to the $K \rightarrow \pi\pi$ amplitudes have been reanalyzed in Chapter 4. Taking into account these contributions, we have presented a complete numerical re-evaluation of the previous ε'/ε prediction. We have obtained the following

Standard Model prediction

$$\text{Re}(\varepsilon'/\varepsilon) = \left(13 \begin{smallmatrix} +6 \\ -7 \end{smallmatrix}\right) \cdot 10^{-4} ,$$

which is again in good agreement with its measured ratio. The central value of ε'/ε is slightly smaller than the previous one due to the increase in Ω_{eff} ,

$$\Omega_{\text{eff}} = (12.1 \begin{smallmatrix} +9.0 \\ -8.8 \end{smallmatrix}) \cdot 10^{-2} .$$

A complete one-loop computation of the Wilson coefficients for the neutral meson mixing in the AMHDM has been presented in Chapter 5. Since this type of process appears at loop level in the SM, it could be very sensitive to NP contributions. We have given a detailed summary of the computation and finally we have obtained combined constraints on the parameters of these models using the current flavour data.

Finally, we have focused on the study of the heavy quark EDMs. The quark EDM coupling produces a chromo-EDM contribution at loop level through photon-loop diagrams. Including these corrections in the RGEs and using the stringent bounds on their chromo-EDMs, we have obtained the following limits of the charm and bottom quark EDMs

$$\begin{aligned} |d_c(m_c)| &< 1.5 \times 10^{-21} \text{ e cm} , \\ |d_b(m_b)| &< 1.2 \times 10^{-20} \text{ e cm} , \end{aligned}$$

which improve the previous ones by about three orders of magnitude. These new limits could place strong constraints on NP extensions of the SM.

Appendix A

OPE in the charged-current SM Lagrangian

The charged-current SM Lagrangian is given by

$$\begin{aligned}\mathcal{L}_{\text{CC}} &= -\frac{1}{2} \left(\partial_\mu W_\nu^\dagger - \partial_\nu W_\mu^\dagger \right) \left(\partial^\mu W^\nu - \partial^\nu W^\mu \right) + M_W^2 W_\mu^\dagger W^\mu \\ &\quad - \frac{g}{\sqrt{2}} \left(W_\mu^\dagger \mathcal{J}^{\mu\dagger} + W_\mu \mathcal{J}^\mu \right),\end{aligned}\tag{A.0.1}$$

where the first and the second terms correspond to the kinetic and the mass terms of W^\pm bosons respectively. The first two pieces can be written as

$$\begin{aligned}\mathcal{L}_{\text{kin}}^W &= -\partial_\mu W_\nu^\dagger \partial^\mu W^\nu + \partial_\mu W_\nu^\dagger \partial^\nu W^\mu + M_W^2 W_\mu^\dagger W^\mu \\ &= W_\nu^\dagger \square W^\nu + M_W^2 W_\mu^\dagger W^\mu - W_\nu^\dagger \partial_\mu \partial^\nu W^\mu \\ &= W_\mu^\dagger \left[g^{\mu\nu} \left(\square + M_W^2 \right) - \partial^\mu \partial^\nu \right] W_\nu \\ &= \int d^D y W_\mu^\dagger(x) \delta^{(D)}(x-y) \left[g^{\mu\nu} \left(\square_y + M_W^2 \right) - \partial_y^\mu \partial_y^\nu \right] W_\nu(x),\end{aligned}$$

where we have eliminated all the total derivatives, in the second line, and we have used $\int d^D y \delta^{(D)}(x-y) = 1$, in the last line. Then, the normalized generating functional is

given by

$$Z_{\text{CC}}[\mathcal{J}^\dagger, \mathcal{J}] \equiv \frac{\int [\mathcal{D} W_\mu^\dagger] [\mathcal{D} W_\mu] e^{iS_{\text{CC}}[\mathcal{J}^\dagger, \mathcal{J}]} }{\int [\mathcal{D} W_\mu^\dagger] [\mathcal{D} W_\mu] e^{iS_{\text{CC}}[0,0]}}, \quad (\text{A.0.2})$$

where the action of the charged-current SM Lagrangian is given by

$$S_{\text{CC}}[\mathcal{J}^\dagger, \mathcal{J}] \equiv \int d^D x \left[\int d^D y W_\mu^\dagger(x) K^{\mu\nu}(x-y) W_\nu(y) - \frac{g}{\sqrt{2}} \left(W_\mu \mathcal{J}^\mu + W_\mu^\dagger \mathcal{J}^{\mu\dagger} \right) \right],$$

and

$$K_W^{\mu\nu}(x-y) \equiv \delta^{(D)}(x-y) \left[g^{\mu\nu} \left(\square_y + M_W^2 \right) - \partial_y^\mu \partial_y^\nu \right] \quad (\text{A.0.3})$$

is the inverse of the W^\pm boson propagator, defined by

$$\int d^D y K_{\mu\nu}^W(x-y) \Delta_W^{\nu\lambda}(y-z) = g_\mu^\lambda \delta^{(D)}(x-z), \quad (\text{A.0.4})$$

with

$$\Delta_W^{\nu\lambda}(x-y) = - \int \frac{d^D k}{(2\pi)^D} \frac{e^{-ik(x-y)}}{k^2 - M_W^2} \left(g^{\nu\lambda} - \frac{k^\nu k^\lambda}{M_W^2} \right). \quad (\text{A.0.5})$$

At low energy scales ($E \ll M_W$), we can perform an integration over the W_μ fields in Eq. (A.0.2). Let us introduce the following auxiliary fields $\widetilde{W}_\mu^\dagger$ and \widetilde{W}_μ :

$$W_\mu = \widetilde{W}_\mu + \widehat{W}_\mu, \quad W_\mu^\dagger = \widetilde{W}_\mu^\dagger + \widehat{W}_\mu^\dagger, \quad (\text{A.0.6})$$

where \widehat{W}_μ^\dagger and \widehat{W}_μ satisfy the classical equations of motion

$$\left[g^{\mu\nu} \left(\square + M_W^2 \right) - \partial^\mu \partial^\nu \right] \widehat{W}_\mu = \frac{g}{\sqrt{2}} \mathcal{J}^{\nu\dagger}, \quad \left[g^{\mu\nu} \left(\square + M_W^2 \right) - \partial^\mu \partial^\nu \right] \widehat{W}_\mu^\dagger = \frac{g}{\sqrt{2}} \mathcal{J}^\nu,$$

with the following solutions

$$\widehat{W}_\mu(x) = \frac{g}{\sqrt{2}} \int d^D y \Delta_{\mu\nu}^W(x-y) \mathcal{J}^{\nu\dagger}(y), \quad \widehat{W}_\mu^\dagger(x) = \frac{g}{\sqrt{2}} \int d^D y \Delta_{\mu\nu}^W(x-y) \mathcal{J}^\nu(y).$$

Expanding the charged-current Lagrangian around \widehat{W}_μ^\dagger and \widehat{W}_μ , we obtain

$$Z_{\text{CC}}[\mathcal{J}^\dagger, \mathcal{J}] = e^{-i \frac{g^2}{2} \int d^D x d^D y \mathcal{J}_\mu^\dagger(x) \Delta_W^{\mu\nu}(x-y) \mathcal{J}_\nu(y)}, \quad (\text{A.0.7})$$

with

$$\mathcal{L} = -\frac{g^2}{2} \int d^D y \mathcal{J}_\mu^\dagger(x) \Delta_W^{\mu\nu}(x-y) \mathcal{J}_\nu(y) . \quad (\text{A.0.8})$$

Then, performing a Taylor expansion of $\mathcal{J}_\nu(y)$ around $y \approx x$, the Lagrangian becomes

$$\mathcal{L} = -\frac{g^2}{2} \lim_{N \rightarrow \infty} \sum_{n=0}^N \frac{i^n}{n!} \mathcal{J}_\alpha^\dagger(x) \widehat{\mathcal{J}}_\beta^{\mu_1 \dots \mu_n}(x) \mathcal{P}_{\mu_1 \dots \mu_n}^{\alpha\beta}(0) , \quad (\text{A.0.9})$$

where

$$\widehat{\mathcal{J}}_\beta^{\mu_1 \dots \mu_n}(x) \equiv (\partial_z^{\mu_1} \dots \partial_z^{\mu_n} \mathcal{J}_\beta(z))|_{z=x} , \quad (\text{A.0.10})$$

$$\mathcal{P}_{\mu_1 \dots \mu_n}^{\alpha\beta}(0) \equiv \left[\partial_{\mu_1}^k \dots \partial_{\mu_n}^k f^{\alpha\beta}(k) \right] \Big|_{k=0} , \quad (\text{A.0.11})$$

with

$$f^{\alpha\beta}(k) = -\frac{1}{(k^2 - M_W^2)} \left(g^{\alpha\beta} - \frac{k^\alpha k^\beta}{M_W^2} \right) . \quad (\text{A.0.12})$$

Finally, we can truncate the Lagrangian given by Eq. (A.0.9) for $N = 1$,

$$\mathcal{L}_{\text{eff}}^{\text{weak}} \approx -\frac{g^2}{2M_W^2} \mathcal{J}_\alpha^\dagger(x) \mathcal{J}^\alpha(x) , \quad (\text{A.0.13})$$

which is the usual Fermi's Lagrangian.

Appendix B

Feynman rules for $q_1 \bar{q}_3 \rightarrow q_2 \bar{q}_4$

Propagators

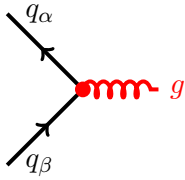
$$\begin{array}{c} W \\ \text{~~~~~} \\ \text{~~~~~} \end{array} \quad -i \frac{1}{k^2 - M_W^2 + i\epsilon} \left[g_{\mu\nu} - (1 - \xi_W) \frac{k_\mu k_\nu}{k^2 - \xi_W M_W^2} \right] \quad (\text{B.0.1})$$

$$\begin{array}{c} g \\ \text{~~~~~} \\ \text{~~~~~} \end{array} \quad -i \delta_{ab} \frac{1}{k^2 + i\epsilon} \left[g_{\mu\nu} - (1 - \xi_G) \frac{k_\mu k_\nu}{k^2} \right] \quad (\text{B.0.2})$$

$$\begin{array}{c} p \\ \text{-----} \\ \text{-----} \end{array} \quad \frac{i (\not{p} + m_f)}{p^2 + m_f^2 + i\epsilon} \quad (\text{B.0.3})$$

Vertices

$$\begin{array}{c} u_\alpha (d_\beta) \\ \text{-----} \\ \text{-----} \\ d_\beta (u_\alpha) \end{array} \quad \begin{array}{c} \text{-----} \\ \text{-----} \\ \text{-----} \end{array} W_\mu^{+(-)} \quad -i \frac{g}{\sqrt{2}} \gamma_\mu P_L V_{\alpha\beta}^{(*)} \quad (\text{B.0.4})$$



$$-i g_s \gamma_\mu T_{\alpha\beta}^a$$

(B.0.5)

Appendix C

Inputs values of Chapter 3

Parameter	Value	Ref.
λ	0.22506 ± 0.00050	[63]
A	0.811 ± 0.026	[63]
ρ	0.124 ± 0.019	[63]
η	0.356 ± 0.011	[63]
$\alpha^{-1}(M_Z^2)$	128.947 ± 0.012	[252]
$\alpha_s^{(n_f=3)}(M_\tau)$	0.325 ± 0.015	[63, 197]
$\sin^2 \theta_W(M_Z)_{\overline{\text{MS}}}$	0.23129 ± 0.00005	[63]
M_W	$(80.385 \pm 0.015) \text{ GeV}$	[63]
M_τ	$(1.77686 \pm 0.00012) \text{ GeV}$	[63]
$\overline{m}_u(2 \text{ GeV})$	$(2.36 \pm 0.24) \text{ MeV}$	[152]
$\overline{m}_d(2 \text{ GeV})$	$(5.03 \pm 0.26) \text{ MeV}$	[152]
$\overline{m}_s(2 \text{ GeV})$	$(93.9 \pm 1.1) \text{ MeV}$	[152]
$\overline{m}_c(\overline{m}_c)$	$(1.286 \pm 0.030) \text{ GeV}$	[152]
$\overline{m}_b(\overline{m}_b)$	$(4.190 \pm 0.021) \text{ GeV}$	[152]
$\overline{m}_t(\overline{m}_t)$	$(165.9 \pm 2.1) \text{ GeV}$	[253, 254]

Table C.1: Input values adopted for the relevant SM parameters.

Appendix D

NLO $\Delta S = 1$ Wilson coefficients

In this appendix, we give all technical details to obtain the Wilson coefficients of Table 3.1. Further details can be found in Refs. [189–192].

D.1 Effective $\Delta S = 1$ short-distance Hamiltonian

We have introduced the effective Lagrangian for $\Delta S = 1$ in Eq. (3.3.19). The operators in Eq. (3.3.19) correspond to an energy scale $\mu < m_c$, where the charm quark c has already been integrated out. Therefore, in that case the sum would be about u , d and s . For an energy scale $m_b > \mu > m_c$, the charm quark c must be included; and in this case it gives rise to the appearance of two new operators,

$$Q_1^c = (\bar{s}_\alpha c_\beta)_{V-A} (\bar{c}_\beta d_\alpha)_{V-A} , \quad Q_2^c = (\bar{s}c)_{V-A} (\bar{c}d)_{V-A} . \quad (\text{D.1.1})$$

D.2 Renormalization group equations

The RGEs for $\vec{C}(\mu)$ are given by

$$\left[\mu \frac{\partial}{\partial \mu} + \beta(g) \frac{\partial}{\partial g} \right] \vec{C}(t, g^2, \alpha) = \hat{\gamma}^T(g^2, \alpha) \vec{C}(t, g^2, \alpha) , \quad t \equiv \frac{M_W^2}{\mu^2} , \quad (\text{D.2.2})$$

where $\beta(g)$ is the beta function of QCD

$$\beta(g) = -\beta_0 \frac{g^3}{16\pi^2} - \beta_1 \frac{g^5}{(16\pi^2)^2} - \beta_{1e} \frac{e^2 g^3}{(16\pi^2)^2} , \quad (\text{D.2.3})$$

with

$$\beta_0 = 11 - \frac{2}{3}f, \quad \beta_1 = 102 - \frac{38}{3}f, \quad \beta_{1e} = -\frac{8}{9}\left(u + \frac{d}{4}\right), \quad (\text{D.2.4})$$

and $f = u + d$ is the number of active flavours being u and d the number of up- and down-type flavours respectively. $\hat{\gamma}(g^2, \alpha)$ is the anomalous dimension, in this case a 10×10 matrix, which can be expanded as

$$\hat{\gamma}(g^2, \alpha) = \hat{\gamma}_s(g^2) + \frac{\alpha}{4\pi}\hat{\Gamma}(g^2) + \dots, \quad (\text{D.2.5})$$

where the QCD and QED parts are given by

$$\hat{\gamma}_s(g^2) = \frac{\alpha_s}{4\pi}\hat{\gamma}_s^{(0)} + \frac{\alpha_s^2}{(4\pi)^2}\hat{\gamma}_s^{(1)} + \dots, \quad (\text{D.2.6})$$

$$\hat{\Gamma}(g^2) = \hat{\gamma}_e^{(0)} + \frac{\alpha_s}{4\pi}\hat{\gamma}_{se}^{(1)} + \dots, \quad (\text{D.2.7})$$

where $\alpha = \frac{e^2}{4\pi}$ and $\alpha_s = \frac{g^2}{4\pi}$. The expressions of $(\hat{\gamma}_s^{(0)}, \hat{\gamma}_s^{(1)})$ and $(\hat{\gamma}_e^{(0)}, \hat{\gamma}_{se}^{(1)})$ can be found in Refs. [190, 191].

The solution of (D.2.2) is given by

$$\vec{C}\left(\frac{M_W^2}{\mu^2}, g^2, \alpha\right) = \left[T_g \exp\left(\int_{g(M_W)}^{g(\mu)} dg' \frac{\hat{\gamma}^T(g'^2, \alpha)}{\beta(g')}\right)\right] \vec{C}(1, g^2(M_W), \alpha), \quad (\text{D.2.8})$$

where T_g is responsible to order the coupling constant of QCD in such a way that increases from right to left.

D.3 General evolution matrix

The general evolution matrix from m_2 to $m_1 < m_2$, is defined by

$$\hat{U}(m_1, m_2, \alpha) \equiv T_g \exp\left(\int_{g(m_2)}^{g(m_1)} dg' \frac{\hat{\gamma}^T(g'^2, \alpha)}{\beta(g')}\right). \quad (\text{D.3.9})$$

Then, Eq. (D.2.8) can be written more compactly as

$$\vec{C}(\mu) = \hat{U}(\mu, M_W, \alpha) \vec{C}(M_W). \quad (\text{D.3.10})$$

In addition, the evolution matrix $\hat{U}(m_1, m_2, \alpha)$ can be decomposed as

$$\hat{U}(m_1, m_2, \alpha) = \hat{U}(m_1, m_2) + \frac{\alpha}{4\pi}\hat{R}(m_1, m_2), \quad (\text{D.3.11})$$

where

$$\hat{U}(m_1, m_2) = T_g \exp \left(\int_{g(m_2)}^{g(m_1)} dg' \frac{\gamma_s^T(g')}{\beta(g')} \right), \quad (\text{D.3.12})$$

$$\hat{R}(m_1, m_2) = \int_{g(m_2)}^{g(m_1)} dg' \frac{\hat{U}(m_1, m') \Gamma^T(g') \hat{U}(m', m_2)}{\beta(g')}, \quad (\text{D.3.13})$$

where $g' \equiv g'(m')$ and $\hat{U}(m_1, m_2)$ represents the QCD evolution matrix, while $\hat{R}(m_1, m_2)$ is the QED evolution matrix.

D.4 QCD evolution matrix

The NLO QCD evolution matrix can be written as

$$\hat{U}(m_1, m_2) = \left(\hat{1} + \frac{\alpha_s(m_1)}{4\pi} \hat{J} \right) \hat{U}^{(0)}(m_1, m_2) \left(\hat{1} - \frac{\alpha_s(m_2)}{4\pi} \hat{J} \right), \quad (\text{D.4.14})$$

where $\hat{U}^{(0)}(m_1, m_2)$ represents the evolution matrix to LO and \hat{J} contains NLO corrections. Notice, in $\hat{U}(m_1, m_2)$, that terms proportional to α_s^2 should not be considered since they correspond to contributions of NNLO. Taking into account the following definitions

$$(\hat{\gamma}_s^{(0)})_D \equiv \hat{V}^{-1} \hat{\gamma}_s^{(0)T} \hat{V}, \quad \hat{G} \equiv \hat{V}^{-1} \hat{\gamma}_s^{(1)T} \hat{V}, \quad (\text{D.4.15})$$

where $(\hat{\gamma}_s^{(0)})_D$ is a diagonal matrix, we obtain

$$\hat{U}^{(0)}(m_1, m_2) = \hat{V} \left[\left(\frac{\alpha_s(m_2)}{\alpha_s(m_1)} \right)^{\vec{a}} \right]_D \hat{V}^{-1} \quad \text{with} \quad \vec{a} = \frac{\vec{\gamma}_s^{(0)}}{2\beta_0}. \quad (\text{D.4.16})$$

The matrix \hat{J} is given by

$$\hat{J} = \hat{V} \hat{S} \hat{V}^{-1}, \quad (\text{D.4.17})$$

while the matrix elements of \hat{S} are given by

$$S_{ij} = \delta_{ij} \gamma_{s,i}^{(0)} \frac{\beta_1}{2\beta_0^2} - \frac{G_{ij}}{2\beta_0 + \gamma_{s,i}^{(0)} - \gamma_{s,j}^{(0)}}, \quad (\text{D.4.18})$$

where $\gamma_{s,i}^{(0)}$ are the components of $\vec{\gamma}_s^{(0)}$ and G_{ij} are the matrix elements of \hat{G} . Eq. (D.4.18) develops singularities for certain combinations of $2\beta_0 + \gamma_{s,i}^{(0)} - \gamma_{s,j}^{(0)}$ (for $f = 3$, $i = 10$ and

$j = 1$).¹ However, Eq. (D.4.14) remains finite after making a proper combination of the relevant terms. After this rearrangement, Eq. (D.4.14) can be written as

$$\hat{U}(m_1, m_2) = \hat{U}_0(m_1, m_2) + \frac{1}{4\pi} \hat{V} A(m_1, m_2) \hat{V}^{-1}, \quad (\text{D.4.19})$$

where

$$\hat{V} A(m_1, m_2) \hat{V}^{-1} = \alpha_s(m_1) \hat{J} \hat{U}_0(m_1, m_2) - \alpha_s(m_2) \hat{U}_0(m_1, m_2) \hat{J}. \quad (\text{D.4.20})$$

Notice that when the matrices \hat{S} and \hat{J} have no singularities, A is given by

$$A_{ij} = S_{ij} \left[\alpha_s(m_1) \left(\frac{\alpha_s(m_2)}{\alpha_s(m_1)} \right)^{a_j} - \alpha_s(m_2) \left(\frac{\alpha_s(m_2)}{\alpha_s(m_1)} \right)^{a_i} \right], \quad (\text{D.4.21})$$

while when S_{ij} is singular ($i = 10$ and $j = 1$), this expression diverges and it can not be used to perform numerical calculations. In this case, A_{ij} is finite

$$A_{ij} = \frac{G_{ij}}{2\beta_0} \alpha_s(m_2) \left(\frac{\alpha_s(m_2)}{\alpha_s(m_1)} \right)^{a_i} \ln \left(\frac{\alpha_s(m_2)}{\alpha_s(m_1)} \right), \quad (\text{D.4.22})$$

for $1 + a_i - a_j = 0$ with $i \neq j$. Since, the matrix \hat{S} can be expressed as

$$S_{ij} = -\frac{G_{ij}}{2\beta_0(1 + a_i - a_j)}, \quad (\text{D.4.23})$$

for $i \neq j$, then

$$A_{ij} = -\frac{G_{ij}}{2\beta_0(1 + a_i - a_j)} \left[\alpha_s(m_1) \left(\frac{\alpha_s(m_2)}{\alpha_s(m_1)} \right)^{a_j} - \alpha_s(m_2) \left(\frac{\alpha_s(m_2)}{\alpha_s(m_1)} \right)^{a_i} \right].$$

and we can regularize the divergence through a change of variable $a_j = 1 + a_i - \epsilon$. Finally, we obtain

$$A_{ij} = \left(\frac{G_{ij}}{2\beta_0} \right) \frac{1}{\epsilon} \alpha_s(m_2) \left(\frac{\alpha_s(m_2)}{\alpha_s(m_1)} \right)^{a_i} \left[\epsilon \ln \left(\frac{\alpha_s(m_2)}{\alpha_s(m_1)} \right) + \mathcal{O}(\epsilon^2) \right], \quad (\text{D.4.24})$$

which in the limit of $\epsilon \rightarrow 0$ becomes Eq. (D.4.22).

¹The components i and j of the divergences depend on the order of the eigenvalues of $(\hat{\gamma}_s^{(0)})_D$.

D.5 QED evolution matrix

The evolution matrix $R(m_1, m_2)$ (D.3.13) can be expanded in powers of g^2 as

$$\hat{R}(m_1, m_2) = \hat{R}^{(0)}(m_1, m_2) + \hat{R}^{(1)}(m_1, m_2) + \dots . \quad (\text{D.5.25})$$

At this point, it is useful to split the different contributions using the following counting rules $\hat{R}^{(0)} \sim \mathcal{O}(1/\alpha_s)$ and $\hat{R}^{(1)} \sim \mathcal{O}(1)$, then

$$\hat{R}(m_1, m_2) = -\frac{2\pi}{\beta_0} \hat{V} \hat{K}(m_1, m_2) \hat{V}^{-1} , \quad (\text{D.5.26})$$

$$\hat{K}(m_1, m_2) = \hat{K}^{(0)}(m_1, m_2) + \frac{1}{4\pi} \sum_{i=1}^3 \hat{K}_i^{(1)}(m_1, m_2) , \quad (\text{D.5.27})$$

$$\hat{R}^{(0)}(m_1, m_2) = -\frac{2\pi}{\beta_0} \hat{V} \hat{K}^{(0)}(m_1, m_2) \hat{V}^{-1} , \quad (\text{D.5.28})$$

$$\hat{R}^{(1)}(m_1, m_2) = -\frac{2\pi}{\beta_0} \frac{1}{4\pi} \sum_{i=1}^3 \hat{V} \hat{K}_i^{(1)}(m_1, m_2) \hat{V}^{-1} . \quad (\text{D.5.29})$$

The first contribution $\hat{K}^{(0)}$ can be obtained using Eq. (D.3.13),

$$(\hat{K}^{(0)}(m_1, m_2))_{ij} = \frac{\hat{M}_{ij}^{(0)}}{a_i - a_j - 1} \left[\left(\frac{\alpha_s(m_2)}{\alpha_s(m_1)} \right)^{a_j} \frac{1}{\alpha_s(m_1)} - \left(\frac{\alpha_s(m_2)}{\alpha_s(m_1)} \right)^{a_i} \frac{1}{\alpha_s(m_2)} \right] ,$$

where $\hat{M}^{(0)}$ is

$$\hat{M}^{(0)} = \hat{V}^{-1} \hat{\gamma}_e^{(0)T} \hat{V} . \quad (\text{D.5.30})$$

Similar to S_{ij} , $\hat{K}^{(0)}(m_1, m_2)$ can also develop singularities for $(i, j) = (10, 1)$ since $a_{10} = a_1 + 1$ when $f = 3$. However, the numerator also cancels and $(\hat{K}^{(0)}(m_1, m_2))_{ij}$ becomes finite

$$(\hat{K}^{(0)}(m_1, m_2))_{ij} = M_{ij}^{(0)} \frac{1}{\alpha_s(m_1)} \left(\frac{\alpha_s(m_2)}{\alpha_s(m_1)} \right)^{a_j} \ln \left(\frac{\alpha_s(m_1)}{\alpha_s(m_2)} \right) . \quad (\text{D.5.31})$$

The NLO QED corrections are given by $\hat{K}_i^{(1)}(m_1, m_2)$. For this type of corrections, it is useful to define

$$\hat{\Gamma}^{(1)} \equiv \hat{\gamma}_{se}^{(1)T} - \frac{\beta_1}{\beta_0} \hat{\gamma}_e^{(0)T} - \frac{\beta_{1e}}{\beta_0} \hat{\gamma}_s^{(0)T} , \quad \hat{M}^{(1)} \equiv \hat{V}^{-1} \left(\hat{\Gamma}^{(1)} + [\hat{\gamma}_e^{(0)T}, \hat{J}] \right) \hat{V} , \quad (\text{D.5.32})$$

then, $\hat{K}_i^{(1)}(m_1, m_2)$ is given by

$$\left(\hat{K}_1^{(1)}(m_1, m_2)\right)_{ij} = \begin{cases} \frac{\hat{M}_{ij}^{(1)}}{a_i - a_j} \left[\left(\frac{\alpha_s(m_2)}{\alpha_s(m_1)}\right)^{a_j} - \left(\frac{\alpha_s(m_2)}{\alpha_s(m_1)}\right)^{a_i} \right] & \text{if } a_i \neq a_j \text{ and } i \neq j , \\ \hat{M}_{ij}^{(1)} \left(\frac{\alpha_s(m_2)}{\alpha_s(m_1)}\right)^{a_i} \ln \left(\frac{\alpha_s(m_1)}{\alpha_s(m_2)}\right) & \text{if } a_i = a_j \text{ and } i \neq j , \\ \hat{M}_{ii}^{(1)} \left(\frac{\alpha_s(m_2)}{\alpha_s(m_1)}\right)^{a_i} \ln \left(\frac{\alpha_s(m_1)}{\alpha_s(m_2)}\right) & \text{if } a_i = a_j \text{ and } i = j , \end{cases}$$

$$\hat{K}_2^{(1)}(m_1, m_2) = -\alpha_s(m_2) \hat{K}^{(0)}(m_1, m_2) \hat{S} ,$$

$$\hat{K}_3^{(1)}(m_1, m_2) = \alpha_s(m_1) \hat{S} \hat{K}^{(0)}(m_1, m_2) .$$

Since the previous equations depend on the matrices \hat{S} or \hat{J} , they develop singularities for $f = 3$ that cancel in the evolution matrix $\hat{R}(m_1, m_2)$. The procedure used is described in Ref. [255]. Let us to introduce a new non-singular matrix \hat{H}_{ij} which is finite by definition,

$$\hat{H}_{ij} = S_{ij}(1 - \delta_{a_j, a_i+1}) . \quad (\text{D.5.33})$$

Expressing $\hat{R}(m_1, m_2)$ as:

$$\hat{R}(m_1, m_2) = -\frac{2\pi}{\beta_0} \hat{V} \hat{K}(m_1, m_2) \hat{V}^{-1} , \quad (\text{D.5.34})$$

$$\hat{K}(m_1, m_2) = \hat{K}^{(0)}(m_1, m_2) + \frac{1}{4\pi} \sum_{i=1}^4 \tilde{K}_i^{(1)}(m_1, m_2) , \quad (\text{D.5.35})$$

we can write the matrices $\tilde{K}_i^{(1)}$ as

$$[\tilde{K}_1^{(1)}]_{ij} = [\hat{V}^{-1} \hat{\Gamma}^{(1)} \hat{V} + [\hat{M}^{(0)}, \hat{H}]]_{ij} Q_{ij} , \quad (\text{D.5.36})$$

$$[\tilde{K}_2^{(1)}]_{ij} = -\alpha_s(m_2) [\hat{K}^{(0)} \hat{H}]_{ij} , \quad (\text{D.5.37})$$

$$[\tilde{K}_3^{(1)}]_{ij} = \alpha_s(m_1) [\hat{H} \hat{K}^{(0)}]_{ij} , \quad (\text{D.5.38})$$

$$[\tilde{K}_4^{(1)}]_{ij} = \delta_{a_\alpha, a_i+1} \left[\frac{\hat{G}_{i\alpha} \hat{M}_{\alpha j}^{(0)}}{2\beta_0} \right] [I_1]_{ij} + \delta_{a_j, a_\alpha+1} \left[\frac{\hat{M}_{i\alpha}^{(0)} \hat{G}_{\alpha j}}{2\beta_0} \right] [I_2]_{ij} , \quad (\text{D.5.39})$$

where

$$Q_{ij} = \begin{cases} \frac{1}{a_i - a_j} \left[\left(\frac{\alpha_s(m_2)}{\alpha_s(m_1)}\right)^{a_j} - \left(\frac{\alpha_s(m_2)}{\alpha_s(m_1)}\right)^{a_i} \right] & \text{if } a_i \neq a_j , \\ \left(\frac{\alpha_s(m_2)}{\alpha_s(m_1)}\right)^{a_i} \ln \left(\frac{\alpha_s(m_1)}{\alpha_s(m_2)}\right) & \text{if } a_i = a_j , \end{cases} \quad (\text{D.5.40})$$

and

$$[I_1]_{ij} = \begin{cases} \frac{1}{a_i - a_j} \left(\frac{\alpha_s(m_2)}{\alpha_s(m_1)} \right)^{a_i} \ln \left(\frac{\alpha_s(m_1)}{\alpha_s(m_2)} \right) \\ - \frac{1}{(a_i - a_j)^2} \left[\left(\frac{\alpha_s(m_2)}{\alpha_s(m_1)} \right)^{a_j} - \left(\frac{\alpha_s(m_2)}{\alpha_s(m_1)} \right)^{a_i} \right] & \text{if } a_i \neq a_j, \\ -\frac{1}{2} \left(\frac{\alpha_s(m_2)}{\alpha_s(m_1)} \right)^{a_j} \left[\ln \left(\frac{\alpha_s(m_2)}{\alpha_s(m_1)} \right) \right]^2 & \text{if } a_i = a_j, \end{cases} \quad (\text{D.5.41})$$

$$[I_2]_{ij} = \begin{cases} \frac{1}{a_i - a_j} \left(\frac{\alpha_s(m_2)}{\alpha_s(m_1)} \right)^{a_j} \ln \left(\frac{\alpha_s(m_2)}{\alpha_s(m_1)} \right) \\ + \frac{1}{(a_i - a_j)^2} \left[\left(\frac{\alpha_s(m_2)}{\alpha_s(m_1)} \right)^{a_j} - \left(\frac{\alpha_s(m_2)}{\alpha_s(m_1)} \right)^{a_i} \right] & \text{if } a_i \neq a_j, \\ -\frac{1}{2} \left(\frac{\alpha_s(m_2)}{\alpha_s(m_1)} \right)^{a_j} \left[\ln \left(\frac{\alpha_s(m_2)}{\alpha_s(m_1)} \right) \right]^2 & \text{if } a_i = a_j. \end{cases} \quad (\text{D.5.42})$$

Notice that $\tilde{K}_i^{(1)}$ ($i = 1, 2, 3$) matrices are equal to the $\hat{K}_i^{(1)}$ matrices when \hat{S} is replaced by \hat{H} . $\tilde{K}_4^{(1)}$ corresponds to the contribution of the singular element of the matrix \hat{S} .

D.6 Wilson coefficients at $\mu < m_c$

The Wilson coefficients are defined by

$$C_i(\mu) \equiv z_i(\mu) + \tau y_i(\mu), \quad y_i(\mu) \equiv v_i(\mu) - z_i(\mu),$$

where $z_i(\mu)$ and $v_i(\mu)$ are the components of \vec{z} and \vec{v} , given by

$$\vec{z}(\mu) = \hat{U}_3(\mu, m_c, \alpha) \vec{z}(m_c), \quad (\text{D.6.43})$$

and

$$\vec{v}(\mu) = \hat{U}_3(\mu, m_c, \alpha) \hat{M}(m_c) \hat{U}_4(m_c, m_b, \alpha) \hat{M}(m_b) \hat{U}_5(m_b, M_W, \alpha) \vec{C}(M_W). \quad (\text{D.6.44})$$

where $\hat{M}(m_i)$ encodes the threshold effects,

$$\hat{M}(m) = \hat{1} + \frac{\alpha_s(m)}{4\pi} \delta \hat{r}_s^T + \frac{\alpha}{4\pi} \delta \hat{r}_e^T. \quad (\text{D.6.45})$$

The only elements of $\delta\hat{r}_s$ that contribute are:

$$\delta\hat{r}_s(Q_4) = \delta\hat{r}_s(Q_6) = -2 \delta\hat{r}_s(Q_8) = -2 \delta\hat{r}_s(Q_{10}) = -\frac{5}{9} P, \quad \mu = m_b, \quad (\text{D.6.46})$$

$$\delta\hat{r}_s(Q_4) = \delta\hat{r}_s(Q_6) = \delta\hat{r}_s(Q_8) = \delta\hat{r}_s(Q_{10}) = -\frac{5}{9} P, \quad \mu = m_c, \quad (\text{D.6.47})$$

where

$$P = \left(0, 0, -\frac{1}{3}, 1, -\frac{1}{3}, 1, 0, 0, 0, 0\right). \quad (\text{D.6.48})$$

In the case of $\delta\hat{r}_e$,

$$\delta\hat{r}_e(Q_3) = 3 \delta\hat{r}_e(Q_4) = \delta\hat{r}_e(Q_5) = 3 \delta\hat{r}_e(Q_6) = \frac{20}{27} \bar{P}, \quad \mu = m_b, \quad (\text{D.6.49})$$

$$\delta\hat{r}_e(Q_7) = 3 \delta\hat{r}_e(Q_8) = \delta\hat{r}_e(Q_9) = 3 \delta\hat{r}_e(Q_{10}) = -\frac{10}{27} \bar{P}, \quad \mu = m_b, \quad (\text{D.6.50})$$

and

$$\delta\hat{r}_e(Q_3) = \delta\hat{r}_e(Q_5) = \delta\hat{r}_e(Q_7) = \delta\hat{r}_e(Q_9) = -\frac{40}{27} \bar{P}, \quad \mu = m_c, \quad (\text{D.6.51})$$

$$\delta\hat{r}_e(Q_4) = \delta\hat{r}_e(Q_6) = \delta\hat{r}_e(Q_8) = \delta\hat{r}_e(Q_{10}) = -\frac{40}{81} \bar{P}, \quad \mu = m_c, \quad (\text{D.6.52})$$

where

$$\bar{P} = (0, 0, 0, 0, 0, 0, 1, 0, 1, 0). \quad (\text{D.6.53})$$

When we use Eqs. (D.6.43) and (D.6.44), we must eliminate higher-order contributions because the matrix $\hat{U}_f(m_1, m_2, \alpha)$ has only been calculated at the order $\mathcal{O}(1, \alpha_s, \frac{\alpha}{\alpha_s}, \alpha)$. For instance, products that involve $\hat{J}\hat{R}^{(1)}$ terms must be eliminated because they belong to higher-order contributions of $\mathcal{O}(\alpha \alpha_s)$.

The $\vec{C}(M_W)$ values in the NDR scheme are given by

$$C_1(M_W) = \frac{\alpha_s(M_W)}{4\pi} B_{s,1}^{\text{NDR}} + \frac{\alpha}{4\pi} B_{e,1}^{\text{NDR}} , \quad (\text{D.6.54})$$

$$C_2(M_W) = 1 + \frac{\alpha_s(M_W)}{4\pi} B_{s,2}^{\text{NDR}} + \frac{\alpha}{4\pi} B_{e,2}^{\text{NDR}} , \quad (\text{D.6.55})$$

$$C_3(M_W) = -\frac{\alpha_s(M_W)}{24\pi} \tilde{E}(x_t) + \frac{\alpha}{6\pi} \frac{1}{\sin^2 \theta_W} [2B(x_t) + C(x_t)] , \quad (\text{D.6.56})$$

$$C_4(M_W) = \frac{\alpha_s(M_W)}{8\pi} \tilde{E}(x_t) , \quad (\text{D.6.57})$$

$$C_5(M_W) = -\frac{\alpha_s(M_W)}{24\pi} \tilde{E}(x_t) , \quad (\text{D.6.58})$$

$$C_6(M_W) = \frac{\alpha_s(M_W)}{8\pi} \tilde{E}(x_t) , \quad (\text{D.6.59})$$

$$C_7(M_W) = \frac{\alpha}{6\pi} [4C(x_t) + \tilde{D}(x_t)] , \quad (\text{D.6.60})$$

$$C_8(M_W) = 0 , \quad (\text{D.6.61})$$

$$C_9(M_W) = \frac{\alpha}{6\pi} \left[4C(x_t) + \tilde{D}(x_t) + \frac{1}{\sin^2 \theta_W} (10B(x_t) - 4C(x_t)) \right] , \quad (\text{D.6.62})$$

$$C_{10}(M_W) = 0 , \quad (\text{D.6.63})$$

where

$$B_{s,1}^{\text{NDR}} = 11/2 , \quad B_{s,2}^{\text{NDR}} = -11/6 , \quad (\text{D.6.64})$$

$$B_{e,1}^{\text{NDR}} = 0 , \quad B_{e,2}^{\text{NDR}} = -35/18 ,$$

and

$$\tilde{E}(x_t) = E(x_t) - \frac{2}{3} , \quad \tilde{D}(x_t) = D(x_t) - \frac{4}{9} , \quad x_t = \frac{m_t^2}{M_W^2} , \quad (\text{D.6.65})$$

and

$$B(x) = \frac{1}{4} \left[\frac{x}{1-x} + \frac{x \ln x}{(x-1)^2} \right], \quad (\text{D.6.66})$$

$$C(x) = \frac{x}{8} \left[\frac{x-6}{x-1} + \frac{3x+2}{(x-1)^2} \ln x \right], \quad (\text{D.6.67})$$

$$D(x) = -\frac{4}{9} \ln x + \frac{-19x^3 + 25x^2}{36(x-1)^3} + \frac{x^2(5x^2 - 2x - 6)}{18(x-1)^4} \ln x, \quad (\text{D.6.68})$$

$$E(x) = -\frac{2}{3} \ln x + \frac{x(18 - 11x - x^2)}{12(1-x)^3} + \frac{x^2(15 - 16x + 4x^2)}{6(1-x)^4} \ln x. \quad (\text{D.6.69})$$

Due to the GIM mechanism, the $z_i(\mu)$ $i \neq 1, 2$ coefficients are zero for f equal to 4 and 5. Then, for $\mu > m_c$, the evolution only involves the operators $Q_{1,2}$ with the following initial conditions

$$z_1(M_W) = \frac{\alpha_s(M_W)}{4\pi} B_{s,1}^{\text{NDR}} + \frac{\alpha(M_W)}{4\pi} B_{e,1}^{\text{NDR}}, \quad (\text{D.6.70})$$

$$z_2(M_W) = 1 + \frac{\alpha_s(M_W)}{4\pi} B_{s,2}^{\text{NDR}} + \frac{\alpha(M_W)}{4\pi} B_{e,2}^{\text{NDR}}. \quad (\text{D.6.71})$$

Therefore,

$$\begin{pmatrix} z_1(m_c) \\ z_2(m_c) \end{pmatrix} = \hat{U}_4(m_c, m_b, \alpha) \hat{M}(m_b) \hat{U}_5(m_b, M_W, \alpha) \begin{pmatrix} z_1(M_W) \\ z_2(M_W) \end{pmatrix}, \quad (\text{D.6.72})$$

where the evolution matrices $\hat{U}_{4,5}$ only contain the 2×2 anomalous dimension. When the charm quark is integrated out, the operators $Q_{1,2}^c$ disappear and the coefficients $z_i(\mu)$ for $i \neq 1, 2$ cease to be zero. To calculate $z_i(m_c)$, we have to perform a matching between the $f = 4$ and $f = 3$ theories that leads in the NDR scheme

$$\begin{aligned} \vec{z}^{\text{NDR}}(m_c) = & \left(z_1^{\text{NDR}}(m_c), z_2^{\text{NDR}}(m_c), -\frac{\alpha_s}{(24\pi)} F_s^{\text{NDR}}(m_c), \right. \\ & \frac{\alpha_s}{(8\pi)} F_s^{\text{NDR}}(m_c), -\frac{\alpha_s}{(24\pi)} F_s^{\text{NDR}}(m_c), \frac{\alpha_s}{(8\pi)} F_s^{\text{NDR}}(m_c), \\ & \left. \frac{\alpha}{(6\pi)} F_e^{\text{NDR}}(m_c), 0, \frac{\alpha}{(6\pi)} F_e^{\text{NDR}}(m_c), 0 \right), \quad (\text{D.6.73}) \end{aligned}$$

where

$$F_s^{\text{NDR}}(\mu) = -\frac{2}{3} \left(\ln \left(\frac{m_c^2}{\mu^2} \right) + 1 \right) z_2(\mu) , \quad (\text{D.6.74})$$

$$F_e^{\text{NDR}}(\mu) = -\frac{4}{9} \left(\ln \left(\frac{m_c^2}{\mu^2} \right) + 1 \right) [3z_1(\mu) + z_2(\mu)] , \quad (\text{D.6.75})$$

for $\mu \approx \mathcal{O}(m_c)$.

D.7 Wilson coefficient in the HV scheme

The changes for the HV renormalization scheme are the following:

1. Anomalous dimensions of HV scheme:

- $\hat{\gamma}_s^{(0)}$ and $\hat{\gamma}_e^{(0)}$ do not depend on the renormalization scheme.
- $\hat{\gamma}_{se, \text{HV}}^{(1)} = \hat{\gamma}_{se, \text{NDR}}^{(1)} + [\Delta \hat{r}_s, \hat{\gamma}_e^{(0)}] + [\Delta \hat{r}_e, \hat{\gamma}_s^{(0)}]$.
- $\hat{\gamma}_{s, \text{HV}}^{(1)} = \hat{\gamma}_{s, \text{NDR}}^{(1)} + [\Delta \hat{r}_s, \hat{\gamma}_s^{(0)}] + 2\beta_0 \Delta \hat{r}_s$.
- We must perform the following changes:

$$\begin{aligned} [\hat{\gamma}_{HV}^{(1)}] &\longrightarrow [\hat{\gamma}_{HV}^{(1)}]_{\text{eff}} \equiv \hat{\gamma}_{\text{HV}}^{(1)} - 2[\gamma_C^{(1)}]_{\text{HV}} \hat{1} . \\ \Delta \hat{r}_s &\longrightarrow \Delta \hat{r}_s - 4C_F \hat{1} . \end{aligned}$$

where $[\gamma_c^{(1)}]_{\text{HV}} \equiv 4C_F \beta_0$ and $C_F = \frac{N_C^2 - 1}{2N_C}$.

2. The Wilson coefficients can be extracted from the relationship between two renormalization schemes a and b :

$$\vec{C}_b(\mu) = \left[\hat{1} - \frac{\alpha_s(\mu)}{4\pi} \Delta \hat{r}_s^{\text{T}} - \frac{\alpha}{4\pi} \Delta \hat{r}_e^{\text{T}} \right] \vec{C}_a(\mu) ,$$

where $\Delta \hat{r}_i = (\hat{r}_i)_b - (\hat{r}_i)_a$.

Finally, we get

$$C_1^{\text{HV}}(M_W) = \frac{\alpha_s(M_W)}{4\pi} \left(B_{s,1}^{\text{NDR}} - 2 \right) + \frac{\alpha}{4\pi} B_{e,1}^{\text{NDR}} , \quad (\text{D.7.76})$$

$$C_2^{\text{HV}}(M_W) = 1 + \frac{\alpha_s(M_W)}{4\pi} \left(B_{s,2}^{\text{NDR}} - \frac{14}{3} \right) + \frac{\alpha}{4\pi} \left(B_{e,2}^{\text{NDR}} - \frac{2}{9} \right) , \quad (\text{D.7.77})$$

$$\begin{aligned} C_3^{\text{HV}}(M_W) &= -\frac{\alpha_s(M_W)}{24\pi} \left(\tilde{E}(x_t) + \frac{2}{3} \right) \\ &+ \frac{\alpha}{6\pi \sin^2 \theta_W} [2B(x_t) + C(x_t)] , \end{aligned} \quad (\text{D.7.78})$$

$$C_4^{\text{HV}}(M_W) = \frac{\alpha_s(M_W)}{8\pi} \left(\tilde{E}(x_t) + \frac{2}{3} \right) , \quad (\text{D.7.79})$$

$$C_5^{\text{HV}}(M_W) = -\frac{\alpha_s(M_W)}{24\pi} \left(\tilde{E}(x_t) + \frac{2}{3} \right) , \quad (\text{D.7.80})$$

$$C_6^{\text{HV}}(M_W) = \frac{\alpha_s(M_W)}{8\pi} \left(\tilde{E}(x_t) + \frac{2}{3} \right) , \quad (\text{D.7.81})$$

$$C_7^{\text{HV}}(M_W) = \frac{\alpha}{6\pi} \left[4C(x_t) + \tilde{D}(x_t) + \frac{4}{9} \right] , \quad (\text{D.7.82})$$

$$C_8^{\text{HV}}(M_W) = 0 , \quad (\text{D.7.83})$$

$$\begin{aligned} C_9^{\text{HV}}(M_W) &= \frac{\alpha}{6\pi} \left[4C(x_t) + \tilde{D}(x_t) + \frac{4}{9} \right. \\ &\left. + \frac{1}{\sin^2 \theta_W} (10B(x_t) - 4C(x_t)) \right] , \end{aligned} \quad (\text{D.7.84})$$

$$C_{10}^{\text{HV}}(M_W) = 0 . \quad (\text{D.7.85})$$

D.8 Errors on the Wilson coefficients

In Table D.1, we show the numerical errors of the Wilson coefficients for different inputs. We have obtained them generating $N = 1000$ inputs considering that they follow a Gaus-

sian distribution. Then, we have evaluated the Wilson coefficients with these values and plot them in a histogram from which we have extracted the error. During the analysis of each input, we have kept the other inputs fixed to their central value. Table D.1 shows that the error of the Wilson coefficients is dominated by $\alpha_s^{(3)}(M_\tau)$.

	$\alpha_s^{(3)}(M_\tau)$	$\sin^2 \hat{\theta}(M_Z)_{\overline{\text{MS}}}$	m_c	m_b	m_t	M_W	M_τ
z_1	± 0.0373	$\pm \mathcal{O}(10^{-8})$	± 0.0008	± 0.0004	$\pm \mathcal{O}(10^{-8})$	$\pm \mathcal{O}(10^{-5})$	$\pm \mathcal{O}(10^{-5})$
z_2	± 0.0258	$\pm \mathcal{O}(10^{-7})$	± 0.0005	± 0.0003	$\pm \mathcal{O}(10^{-7})$	$\pm \mathcal{O}(10^{-5})$	$\pm \mathcal{O}(10^{-5})$
z_3	± 0.0024	$\pm \mathcal{O}(10^{-9})$	± 0.0007	$\pm \mathcal{O}(10^{-6})$	$\pm \mathcal{O}(10^{-9})$	$\pm \mathcal{O}(10^{-7})$	$\pm \mathcal{O}(10^{-6})$
z_4	± 0.0060	$\pm \mathcal{O}(10^{-9})$	± 0.0016	$\pm \mathcal{O}(10^{-6})$	$\pm \mathcal{O}(10^{-9})$	$\pm \mathcal{O}(10^{-7})$	$\pm \mathcal{O}(10^{-6})$
z_5	± 0.0007	$\pm \mathcal{O}(10^{-9})$	± 0.0001	$\pm \mathcal{O}(10^{-7})$	$\pm \mathcal{O}(10^{-9})$	$\pm \mathcal{O}(10^{-8})$	$\pm \mathcal{O}(10^{-6})$
z_6	± 0.0060	$\pm \mathcal{O}(10^{-9})$	± 0.0017	$\pm \mathcal{O}(10^{-6})$	$\pm \mathcal{O}(10^{-9})$	$\pm \mathcal{O}(10^{-7})$	$\pm \mathcal{O}(10^{-6})$
z_7/α	± 0.0030	$\pm \mathcal{O}(10^{-9})$	± 0.0005	$\pm \mathcal{O}(10^{-5})$	$\pm \mathcal{O}(10^{-9})$	$\pm \mathcal{O}(10^{-6})$	$\pm \mathcal{O}(10^{-6})$
z_8/α	± 0.0028	$\pm \mathcal{O}(10^{-9})$	± 0.0016	$\pm \mathcal{O}(10^{-6})$	$\pm \mathcal{O}(10^{-9})$	$\pm \mathcal{O}(10^{-7})$	$\pm \mathcal{O}(10^{-6})$
z_9/α	± 0.0044	$\pm \mathcal{O}(10^{-9})$	± 0.0002	$\pm \mathcal{O}(10^{-5})$	$\pm \mathcal{O}(10^{-9})$	$\pm \mathcal{O}(10^{-6})$	$\pm \mathcal{O}(10^{-6})$
z_{10}/α	± 0.0013	$\pm \mathcal{O}(10^{-9})$	± 0.0009	$\pm \mathcal{O}(10^{-6})$	$\pm \mathcal{O}(10^{-9})$	$\pm \mathcal{O}(10^{-7})$	$\pm \mathcal{O}(10^{-6})$
y_3	± 0.0030	$\pm \mathcal{O}(10^{-6})$	± 0.0006	$\pm \mathcal{O}(10^{-5})$	± 0.0002	$\pm \mathcal{O}(10^{-7})$	$\pm \mathcal{O}(10^{-6})$
y_4	± 0.0038	$\pm \mathcal{O}(10^{-7})$	± 0.0014	$\pm \mathcal{O}(10^{-5})$	± 0.0001	$\pm \mathcal{O}(10^{-6})$	$\pm \mathcal{O}(10^{-6})$
y_5	± 0.0032	$\pm \mathcal{O}(10^{-7})$	$\pm \mathcal{O}(10^{-5})$	$\pm \mathcal{O}(10^{-5})$	$\pm \mathcal{O}(10^{-5})$	$\pm \mathcal{O}(10^{-6})$	$\pm \mathcal{O}(10^{-6})$
y_6	± 0.0160	$\pm \mathcal{O}(10^{-7})$	± 0.0016	$\pm \mathcal{O}(10^{-5})$	± 0.0002	$\pm \mathcal{O}(10^{-5})$	$\pm \mathcal{O}(10^{-5})$
y_7/α	± 0.0004	$\pm \mathcal{O}(10^{-9})$	± 0.0004	$\pm \mathcal{O}(10^{-5})$	± 0.0075	± 0.0001	$\pm \mathcal{O}(10^{-7})$
y_8/α	± 0.0244	$\pm \mathcal{O}(10^{-8})$	± 0.0018	± 0.0002	± 0.0103	± 0.0001	$\pm \mathcal{O}(10^{-5})$
y_9/α	± 0.0420	± 0.0011	± 0.0002	± 0.0001	± 0.0538	± 0.0008	$\pm \mathcal{O}(10^{-5})$
y_{10}/α	± 0.0617	± 0.0005	± 0.0005	± 0.0003	± 0.0264	± 0.0003	$\pm \mathcal{O}(10^{-5})$

Table D.1: Errors of the Wilson coefficients $\mu = 1 \text{ GeV}$. $y_1 = y_2 \equiv 0$.

Appendix E

Parameters of large- N_C matching at NLO

E.1 $(g_8 N_i)$ couplings

i	n_i	\mathcal{X}_i
5	-2	$-16 X_{14} + 32 X_{17} - 24 X_{38} - 4 X_{91}$
6	4	$-32 X_{17} - 32 X_{18} + 32 X_{37} + 16 X_{38}$
7	2	$-32 X_{16} - 16 X_{17} + 8 X_{38}$
8	4	$-16 X_{15} - 32 X_{17} + 16 X_{38}$
9	0	$-64 L_5 L_8 - 8 X_{34} + 8 X_{38} + 4 X_{91}$
10	0	$-48 X_{19} - 8 X_{38} - 2 X_{91} - 4 X_{94}$
11	0	$-32 X_{20} + 4 X_{94}$
12	0	$128 L_8 L_8 + 16 X_{12} - 16 X_{31} + 8 X_{38} - 2 X_{91} - 4 X_{94}$
13	0	$256 L_7 L_8 - \frac{32}{3} X_{12} - 16 X_{33} + 16 X_{37} + \frac{4}{3} X_{91} + 4 X_{94}$

Table E.1: Large- N_C parameters determining the $(g_8 N_i)$ couplings in (4.3.16).

The strong LEC X_{94} only appears in \mathcal{X}_i for $i = 10, 11, 12, 13$. The corresponding couplings N_i contribute to $\Delta_C \mathcal{A}_{1/2}^{(8)}$ and $\Delta_C \mathcal{A}_{1/2,3/2}^{(\epsilon)}$, but X_{94} always appear in combinations of the form $\sum_{i=10}^{13} a_i N_i$ with $a_{10} + a_{12} = a_{11} + a_{13}$. Thus, X_{94} drops completely from the $K \rightarrow \pi\pi$ amplitudes. The same happens with X_{37} , because \mathcal{X}_6 and \mathcal{X}_{13} only enter through the combination $N_6^r - 2N_{13}^r$.

E.2 ($g_8 Z_i$) couplings

i	$\mathcal{K}_i^{(1)}$	$\mathcal{K}_i^{(2)}$	$\mathcal{K}_i^{(3)}$	$\mathcal{K}_i^{(4)}$	$\mathcal{K}_i^{(5)}$	$\mathcal{K}_i^{(6)}$	$\mathcal{K}_i^{(7)}$
1	$\frac{1}{3} K_{12} - K_{13}$	0	$64 L_8 (-\frac{1}{3} K_9 + \frac{5}{3} K_{10} + K_{11})$	0	$-24 L_8$	0	0
2	$\frac{4}{3} K_{13}$	0	$-\frac{256}{3} L_8 (K_{10} + K_{11})$	0	0	0	0
3	K_{13}	0	$-64 L_8 (K_{10} + K_{11})$	0	0	0	0
4	$-K_{13}$	0	$64 L_8 (K_{10} + K_{11})$	0	0	0	0
5	$\frac{4}{3} (4 K_1 + 3 K_5 + 3 K_{12})$	0	$-\frac{64}{3} L_5 (2K_7 + K_9)$	0	0	0	1
6	$-\frac{2}{3} (K_5 + K_6) + 2 (K_{12} + K_{13})$	0	$-\frac{32}{3} L_5 (K_9 + K_{10} + 3K_{11})$	0	$-12 L_5$	0	0
7	$8 K_2 + 6 K_6 - 4 K_{13}$	0	$-32 L_5 (2K_8 + K_{10} + K_{11})$	0	0	0	0
8	$\frac{8}{3} K_3 + 4 K_{12}$	$\frac{4}{3} K_5$	0	0	0	$\frac{3}{2}$	$\frac{3}{2}$
9	$-\frac{4}{3} (K_4 + K_{12} + K_{13})$	$\frac{4}{3} K_5$	0	$-\frac{3}{2}$	0	0	0
10	$-2 K_{13}$	$4 K_6$	0	0	0	0	0
11	$2 (K_4 + K_{13})$	0	0	0	0	0	0
12	$-4 K_3$	0	0	0	0	0	0

Table E.2: Large- N_C parameters determining the ($g_8 Z_i$) couplings in (4.3.17).

Appendix F

Updated estimate of λ_3^{SS}

The $R\chi T$ coupling λ_3^{SS} splits the masses of the different isospin components of the scalar-resonance nonet multiplet through the term

$$\mathcal{L}_S^{\text{mass}} = -\frac{M_S^2}{2} \langle S^2 \rangle + \lambda_3^{SS} 4B_0 \langle S^2 \mathcal{M} \rangle . \quad (\text{F.0.1})$$

The common multiplet mass and λ_3^{SS} can then be determined through the relations [211]:

$$\lambda_3^{SS} = \frac{M_{I=1}^2 - M_{I=1/2}^2}{4(M_K^2 - M_\pi^2)} , \quad M_S^2 = M_{I=1}^2 + \frac{M_\pi^2 (M_{I=1}^2 - M_{I=1/2}^2)}{M_K^2 - M_\pi^2} , \quad (\text{F.0.2})$$

with M_I the mass of the scalar meson with isospin I .

In order to identify the members of the scalar resonance nonet, we must exclude the lightest observed scalars that are well understood as dynamically-generated poles arising from 2-Goldstone scattering: $f_0(500)$ (σ), $K_0^*(700)$ (κ), $a_0(980)$ and $f_0(980)$ [261–265]. The $I = 1/2$ and $I = 1$ members of the resonance nonet are identified without controversy with $K_0^*(1430)$ and $a_0(1450)$ respectively. For the $I = 0$ states, we have three possible candidates: $f_0(1370)$, $f_0(1500)$ and $f_0(1710)$. Thus, there are two possible scenarios:

$$\mathbf{A:} \quad f_0(1370) , K_0^*(1430) , a_0(1450) , f_0(1500) .$$

$$\mathbf{B:} \quad f_0(1370) , K_0^*(1430) , a_0(1450) , f_0(1710) .$$

One can figure out the favoured dynamical option, comparing these candidates with the predicted isosinglet masses. Using the relation [211],

$$M_{L,H}^2 = M_{I=1/2}^2 \mp |M_{I=1/2}^2 - M_{I=1}^2|, \quad (\text{F.0.3})$$

we find $M_L = 1374$ MeV and $M_H = 1474$ MeV for the lighter and heavier isosinglet scalar states, respectively. Therefore, we can conclude that the lightest scalar-resonance nonet is given by the scenario **A**. Moreover, since the values of $M_{L,H}$ are very close to the measured masses, additional nonet-symmetry-breaking corrections to the scalar masses can be neglected (*i.e.*, $k_m^R = \gamma_R = 0$, in Ref. [211]). Inserting the scalar resonance masses in the relations (F.0.2), one finally finds the values of M_S and λ_3^{SS} given in Eq. (4.3.22).

Appendix G

Feynman rules for meson mixing

Propagators

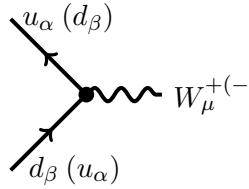
$$\begin{array}{c} W \\ \text{~~~~~} \end{array} \quad -i \frac{1}{k^2 - M_W^2 + i\epsilon} \left[g_{\mu\nu} - (1 - \xi_W) \frac{k_\mu k_\nu}{k^2 - \xi_W M_W^2} \right] \quad (\text{G.0.1})$$

$$\begin{array}{c} p \\ \text{—————} \end{array} \quad \frac{i(\not{p} + m_f)}{p^2 + m_f^2 + i\epsilon} \quad (\text{G.0.2})$$

$$\begin{array}{c} G^\pm \\ \text{-----} \end{array} \quad \frac{i}{p^2 - \xi_W M_W^2 + i\epsilon} \quad (\text{G.0.3})$$

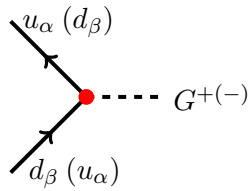
$$\begin{array}{c} \varphi_A^\pm \\ \text{-----} \end{array} \quad \frac{i}{p^2 - M_{\varphi_A^\pm}^2 + i\epsilon} \quad (\text{G.0.4})$$

Vertices



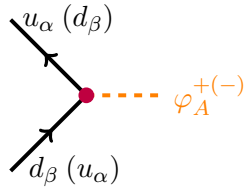
A Feynman diagram showing a vertex where two quark lines meet. The top-left line is labeled $u_\alpha (d_\beta)$ and the bottom-left line is labeled $d_\beta (u_\alpha)$. A wavy line representing a $W_\mu^{+(-)}$ boson extends to the right from a black dot at the vertex.

$$-i \frac{g}{\sqrt{2}} \gamma_\mu P_L V_{\alpha\beta}^{(*)} \quad (\text{G.0.5})$$



A Feynman diagram showing a vertex where two quark lines meet. The top-left line is labeled $u_\alpha (d_\beta)$ and the bottom-left line is labeled $d_\beta (u_\alpha)$. A dashed line representing a $G^{+(-)}$ boson extends to the right from a red dot at the vertex.

$$i \frac{g}{\sqrt{2}} \left(\frac{m_{u_\alpha}}{M_W} P_{L(R)} - \frac{m_{d_\beta}}{M_W} P_{R(L)} \right) V_{\alpha\beta}^{(*)} \quad (\text{G.0.6})$$



A Feynman diagram showing a vertex where two quark lines meet. The top-left line is labeled $u_\alpha (d_\beta)$ and the bottom-left line is labeled $d_\beta (u_\alpha)$. A dashed orange line representing a $\varphi_A^{+(-)}$ boson extends to the right from a red dot at the vertex.

$$-i \frac{g T^a}{\sqrt{2}} \left[(a_{\alpha\beta}^A)^{(*)} P_{L(R)} + (b_{\alpha\beta}^A)^{(*)} P_{R(L)} \right] \equiv -i \frac{g T^a}{\sqrt{2}} (\widehat{V}_{\alpha\beta}^A)^{(*)} \quad (\text{G.0.7})$$

where g is the SU(2) coupling constant which is related with the VEV through $g = \frac{2M_W}{v}$, $(a_{\alpha\beta}^A)^{(*)} \equiv -\frac{1}{M_W} (\zeta_{u_\alpha}^A)^{(*)} m_{u_\alpha} V_{\alpha\beta}^{(*)}$ and $(b_{\alpha\beta}^A)^{(*)} \equiv \frac{1}{M_W} (\zeta_{d_\alpha}^A)^{(*)} m_{d_\beta} V_{\alpha\beta}^{(*)}$ where $(\zeta_{u,d}^A)^{(*)}$ are defined in Eq. (5.2.7).

Appendix H

Loop functions for meson mixing

In this appendix, we present the loop functions that appear in the Wilson coefficients before applying the GIM mechanism.

$$(f_1^{\text{AB}})^{ij} = \beta_i \beta_j M_W^2 A_1^{\text{AB}} \quad (\text{H.0.1})$$

$$- x_{q_1} \frac{1}{6} \beta_i \beta_j M_W^4 \left[6 A_3^{\text{ABj}} + 3 A_2^{\text{AB}} - 4 \left(F_2^{\text{AB111}} + F_2^{\text{AB121}} + F_2^{\text{AB131}} \right) \right] ,$$

$$(f_2^{\text{AB}})^{ij} = x_{q_1} 4 \beta_i M_W^4 \left(C_3^{\text{Ai}} + E_2^{\text{A}} \right) , \quad (\text{H.0.2})$$

$$(f_3^{\text{AB}})^{ij} = -2 \beta_i \beta_j M_W^2 \left(4 M_W^2 D_1^{\text{A}} - C_1^{\text{A}} \right) \quad (\text{H.0.3})$$

$$+ x_{q_1} \frac{2}{3} \beta_i \beta_j M_W^4 \left\{ 12 M_W^2 \left(D_3^{\text{Aj}} + D_2^{\text{A}} - F_1^{\text{AW111}} - F_1^{\text{AW121}} - F_1^{\text{AW131}} \right) \right. \\ \left. - 3 D_1^{\text{A}} + F_2^{\text{AW111}} + F_2^{\text{AW113}} + F_2^{\text{AW121}} + F_2^{\text{AW131}} + F_2^{\text{WA122}} + F_2^{\text{WA131}} \right\} ,$$

$$(f_4^{\text{AB}})^{ij} = x_{q_1} x_{q_2} M_W^2 A_1^{\text{AB}} , \quad (\text{H.0.4})$$

$$(f_5^{\text{AB}})^{ij} = x_{q_1} x_{q_2} 2 M_W^2 C_1^{\text{A}} , \quad (\text{H.0.5})$$

$$(f_6^{\text{AB}})^{ij} = \sqrt{x_{q_1} x_{q_2}} 2 M_W^2 \beta_j A_1^{\text{AB}}, \quad (\text{H.0.6})$$

$$(f_7^{\text{AB}})^{ij} = \sqrt{x_{q_1} x_{q_2}} 4 M_W^2 \beta_j \left\{ C_1^{\text{A}} - 2 M_W^2 (C_3^{\text{Aj}} + C_2^{\text{A}}) \right\}, \quad (\text{H.0.7})$$

$$(f_8^{\text{AB}})^{ij} = -\sqrt{x_{q_1} x_{q_2}} 8 M_W^2 (C_1^{\text{A}} - \beta_i \beta_j M_W^2 D_1^{\text{A}}), \quad (\text{H.0.8})$$

$$(f_9^{\text{AB}})^{ij} = -\sqrt{x_{q_1} x_{q_2}} 8 \beta_i M_W^4 \left\{ 2 (C_2^{\text{A}} + C_3^{\text{Ai}}) + \beta_j (C_3^{\text{Aj}} + E_2^{\text{A}}) \right\}, \quad (\text{H.0.9})$$

$$(f_{10}^{\text{AB}})^{ij} = -\sqrt{x_{q_1} x_{q_2}} 4 \beta_i \beta_j M_W^4 (A_2^{\text{AB}} + 2 A_3^{\text{ABi}}), \quad (\text{H.0.10})$$

$$(f_{11}^{\text{AB}})^{ij} = \sqrt{x_{q_1} x_{q_2}} \frac{4}{3} \beta_i \beta_j M_W^4 \left\{ F_2^{\text{AB112}} + F_2^{\text{AB121}} + F_2^{\text{AB122}} + 2 F_2^{\text{AB131}} \right\}, \quad (\text{H.0.11})$$

$$(f_{12}^{\text{AB}})^{ij} = \sqrt{x_{q_1} x_{q_2}} 8 \beta_i \beta_j M_W^4 B_1^{\text{AB}}, \quad (\text{H.0.12})$$

$$(f_{13}^{\text{AB}})^{ij} = \sqrt{x_{q_1} x_{q_2}} \frac{4}{3} \beta_i \beta_j M_W^4 \left\{ 3 (E_2^{\text{A}} - 2 C_2^{\text{A}}) + F_2^{\text{AW112}} + F_2^{\text{AW121}} + F_2^{\text{AW122}} \right. \\ \left. + 2 F_2^{\text{AW131}} + F_2^{\text{WA112}} + F_2^{\text{WA121}} + F_2^{\text{WA122}} + 2 F_2^{\text{WA131}} \right\}, \quad (\text{H.0.13})$$

$$(f_{14}^{\text{AB}})^{ij} = x_{q_2} \frac{1}{3} \beta_i \beta_j M_W^4 \left\{ 3 (A_2^{\text{AB}} + 2 A_3^{\text{ABi}}) \right. \\ \left. - 4 (F_2^{\text{AB113}} + F_2^{\text{AB122}} + F_2^{\text{AB131}}) \right\}, \quad (\text{H.0.14})$$

$$(f_{15}^{\text{AB}})^{ij} = x_{q_2} 4 \beta_i \beta_j M_W^4 B_1^{\text{AB}}, \quad (\text{H.0.15})$$

$$(f_{16}^{\text{AB}})^{ij} = x_{q_2} \beta_i \beta_j M_W^4 \left\{ 2 (A_3^{\text{ABi}} - A_3^{\text{ABj}}) + (A_2^{\text{AB}} - A_2^{\text{BA}}) - 4 B_1^{\text{AB}} \right\}, \quad (\text{H.0.16})$$

$$(f_{17}^{\text{AB}})^{ij} = -x_{q_2} \frac{4}{3} \beta_i \beta_j M_W^4 \left\{ 3 (D_1^{\text{A}} - C_2^{\text{A}} - C_3^{\text{Ai}}) + F_2^{\text{AW111}} + F_2^{\text{AW113}} \right. \\ \left. + F_2^{\text{AW122}} + F_2^{\text{AW131}} + F_2^{\text{WA121}} + F_2^{\text{WA131}} \right\}, \quad (\text{H.0.17})$$

$$(f_{18}^{\text{AB}})^{ij} = x_{q_2} 2 \beta_i \beta_j M_W^4 \left(C_3^{\text{Ai}} - C_3^{\text{Aj}} - C_2^{\text{A}} + 2 D_1^{\text{A}} + E_2^{\text{A}} \right), \quad (\text{H.0.18})$$

$$(f_{19}^{\text{AB}})^{ij} = x_{q_1} \frac{1}{3} \beta_i \beta_j M_W^4 \left\{ 3 (A_2^{\text{AB}} + 2A_3^{\text{ABj}}) - 4 (F_2^{\text{AB111}} + F_2^{\text{AB121}} + F_2^{\text{AB131}}) \right\}, \quad (\text{H.0.19})$$

$$(f_{20}^{\text{AB}})^{ij} = x_{q_1} 4 \beta_i \beta_j M_W^4 B_1^{\text{AB}}, \quad (\text{H.0.20})$$

$$(f_{21}^{\text{AB}})^{ij} = x_{q_1} \beta_i \beta_j M_W^4 \left\{ 2 (A_3^{\text{ABi}} - A_3^{\text{ABj}}) + (A_2^{\text{BA}} - A_2^{\text{AB}}) - 4 B_1^{\text{AB}} \right\}, \quad (\text{H.0.21})$$

$$(f_{22}^{\text{AB}})^{ij} = -x_{q_1} \frac{4}{3} \beta_i \beta_j M_W^4 \left\{ 3 (D_1^{\text{A}} - C_2^{\text{A}} - C_3^{\text{Aj}}) + F_2^{\text{AW111}} + F_2^{\text{AW113}} + F_2^{\text{AW121}} + F_2^{\text{AW131}} + F_2^{\text{WA122}} + F_2^{\text{WA131}} \right\}, \quad (\text{H.0.22})$$

$$(f_{23}^{\text{AB}})^{ij} = x_{q_2} 2 \beta_i \beta_j M_W^4 \left(C_3^{\text{Ai}} - C_3^{\text{Aj}} - C_2^{\text{A}} + 2 D_1^{\text{A}} + E_2^{\text{A}} \right), \quad (\text{H.0.23})$$

where the capital-letter functions are defined by

$$A_1^{\text{AB}} \equiv D_2(m_i^2, m_j^2, M_{\varphi_{\text{A}}}^2, M_{\varphi_{\text{B}}}^2), \quad (\text{H.0.24})$$

$$A_2^{\text{AB}} \equiv 2 \frac{\text{d}}{\text{d}M_{\varphi_{\text{B}}}^2} D_2(m_i^2, m_j^2, M_{\varphi_{\text{A}}}^2, M_{\varphi_{\text{B}}}^2), \quad (\text{H.0.25})$$

$$A_3^{\text{ABi}} \equiv \frac{\text{d}}{\text{d}m_i^2} D_2(m_i^2, m_j^2, M_{\varphi_{\text{A}}}^2, M_{\varphi_{\text{B}}}^2), \quad (\text{H.0.26})$$

$$B_1^{\text{AB}} \equiv D_0(m_i^2, m_j^2, M_{\varphi_{\text{A}}}^2, M_{\varphi_{\text{B}}}^2), \quad (\text{H.0.27})$$

$$C_1^{\text{A}} \equiv D_2(m_i^2, m_j^2, M_W^2, M_{\varphi_{\text{A}}}^2), \quad (\text{H.0.28})$$

$$C_2^{\text{A}} \equiv \frac{\text{d}}{\text{d}M_W^2} D_2(m_i^2, m_j^2, M_W^2, M_{\varphi_{\text{A}}}^2), \quad (\text{H.0.29})$$

$$C_3^{\text{Ai}} \equiv \frac{d}{dm_i^2} D_2(m_i^2, m_j^2, M_W^2, M_{\varphi_A^\pm}^2), \quad (\text{H.0.30})$$

$$D_1^{\text{A}} \equiv D_0(m_i^2, m_j^2, M_W^2, M_{\varphi_A^\pm}^2), \quad (\text{H.0.31})$$

$$D_2^{\text{A}} \equiv \frac{d}{dM_W^2} D_0(m_i^2, m_j^2, M_W^2, M_{\varphi_A^\pm}^2), \quad (\text{H.0.32})$$

$$D_3^{\text{Ai}} \equiv \frac{d}{dm_i^2} D_0(m_i^2, m_j^2, M_W^2, M_{\varphi_A^\pm}^2), \quad (\text{H.0.33})$$

$$E_2^{\text{A}} \equiv \frac{d}{dM_{\varphi_A^\pm}^2} D_2(m_i^2, m_j^2, M_W^2, M_{\varphi_A^\pm}^2), \quad (\text{H.0.34})$$

and¹

$$F_1^{\text{AB } abc} \equiv \int_0^\infty dx \frac{2x^5}{(x^2 + M_A^2)^a (x^2 + M_B^2)^b (x^2 + m_i^2)^c (x^2 + m_j^2)^{6-a-b-c}},$$

$$F_2^{\text{AB } abc} \equiv - \int_0^\infty dx \frac{2x^7}{(x^2 + M_A^2)^a (x^2 + M_B^2)^b (x^2 + m_i^2)^c (x^2 + m_j^2)^{6-a-b-c}},$$

$$F_2^{\text{AA } a+b c} \equiv F_2^{\text{AA } abc},$$

where

$$D_0(a, b, c, d) = \frac{b \ln\left(\frac{b}{a}\right)}{(b-a)(b-c)(b-d)} + \frac{c \ln\left(\frac{c}{a}\right)}{(c-a)(c-b)(c-d)} + \frac{d \ln\left(\frac{d}{a}\right)}{(d-a)(d-b)(d-c)},$$

$$D_2(a, b, c, d) = \frac{b^2 \ln\left(\frac{b}{a}\right)}{(b-a)(b-c)(b-d)} + \frac{c^2 \ln\left(\frac{c}{a}\right)}{(c-a)(c-b)(c-d)} + \frac{d^2 \ln\left(\frac{d}{a}\right)}{(d-a)(d-b)(d-c)},$$

being

$$D_i(m_1, m_2, M) \equiv \lim_{M_2 \rightarrow M} D_i(m_1, m_2, M, M_2),$$

with $i = 0, 2$.

¹The loop functions $F_1^{\text{AB } abc}$ and $F_2^{\text{AB } abc}$ are $\int \frac{d^4 k}{\pi^2} \frac{i k^2}{(k^2 - M_A^2)^a (k^2 - M_B^2)^b (k^2 - m_i^2)^c (k^2 - m_j^2)^{6-a-b-c}}$ and $\int \frac{d^4 k}{\pi^2} \frac{i k^4}{(k^2 - M_A^2)^a (k^2 - M_B^2)^b (k^2 - m_i^2)^c (k^2 - m_j^2)^{6-a-b-c}}$ respectively, but we have converted them into simple Riemann integrals performing a Wick rotation.

Appendix I

Colour factors

In Tables I.1 and I.2 , we present the colour factors N_i and \tilde{N}_i respectively which have been computed following the arguments given in Section 5.2.3.

i	N_i
1, 4	$\frac{N_C^3 - 2 N_C + 1}{4 N_C^2}$
2, 3, 5	$\frac{N_C - 1}{2 N_C}$
6, 10, 11, 12	$\frac{1}{(2 N_C)^2}$
7, 8, 9, 13	$-\frac{1}{2 N_C}$
14, 15, 16, 19, 20, 21	$\frac{-N_C^3 + 2 N_C + 2}{8 N_C^2}$
17, 18, 22, 23	$-\left(\frac{N_C + 2}{4 N_C}\right)$

Table I.1: N_i colour factors.

i	\tilde{N}_i
6	$-2 \left(\frac{N_C^2 - 2}{4 N_C}\right)$
7	-1
8, 9, 13	$-\frac{1}{4}$
10, 11, 12	$-\left(\frac{N_C^2 - 2}{8 N_C}\right)$
14, 15, 16, 19, 20, 21	$\frac{1}{8} \left(\frac{N_C^2 - 2}{4 N_C}\right)$
17, 18, 22, 23	$\frac{1}{16}$

Table I.2: \tilde{N}_i colour factors.

Appendix J

Fierz transformations

The Fierz rearrangements used in Chapter 5 are

$$\left[\gamma^\mu P_{L(R)} \right]_{ij} \left[\gamma_\mu P_{L(R)} \right]_{kl} = \left[\gamma^\mu P_{L(R)} \right]_{il} \left[\gamma_\mu P_{L(R)} \right]_{kj} ,$$

$$\left[\gamma^\mu P_{L(R)} \right]_{ij} \left[\gamma_\mu P_{R(L)} \right]_{kl} = -2 \left[P_{R(L)} \right]_{il} \left[P_{L(R)} \right]_{kj} ,$$

$$\left[\sigma^{\mu\nu} P_{L(R)} \right]_{ij} \left[\sigma_{\mu\nu} P_{R(L)} \right]_{kl} = 0 ,$$

$$\left[P_{L(R)} \right]_{ij} \left[P_{L(R)} \right]_{kl} = -\frac{1}{2} \left[P_{L(R)} \right]_{il} \left[P_{L(R)} \right]_{kj} + \frac{1}{8} \left[\sigma^{\mu\nu} P_{L(R)} \right]_{il} \left[\sigma_{\mu\nu} P_{L(R)} \right]_{kj} ,$$

$$\left[\sigma^{\mu\nu} P_{L(R)} \right]_{ij} \left[\sigma_{\mu\nu} P_{L(R)} \right]_{kl} = 6 \left[P_{L(R)} \right]_{il} \left[P_{L(R)} \right]_{kj} + \frac{1}{2} \left[\sigma^{\mu\nu} P_{L(R)} \right]_{il} \left[\sigma_{\mu\nu} P_{L(R)} \right]_{kj} ,$$

where $\sigma_{\mu\nu} \equiv \frac{1}{2} [\gamma_\mu, \gamma_\nu]$. These Fierz transformations are valid at the operator level, *i.e.*, they include the Fermi-statistics minus sign from the permutation of the two fermion fields. The minus sign is absent in the analogous relations between spinor bilineals.

Appendix K

GIM mechanism in $C_{\text{SM } 2\text{SRR}}^{ij}$

When the GIM mechanism is applied to the Wilson coefficients, $C_{\text{SM } 2\text{SRR}}^{ij}$ has $\ln \beta_u$ contributions that do not vanish in the massless limit. These infrared terms coming from Figure 5.1a correspond to virtual contributions from the up and the charm quarks, see Figure K.1. When these new contributions are realized in the low-energy effective theory, all the infrared divergencies cancel in the matching process because both theories have the same infrared behaviour. The low-energy effective Lagrangian is

$$\mathcal{L}_{\text{EFT}} = -\frac{4 G_F}{\sqrt{2}} \sum_{ij=u,c} V_{iq_1} V_{jq_2}^* [\bar{i} \gamma_\mu P_L q_1] [\bar{q}_2 \gamma^\mu P_L j] . \quad (\text{K.0.1})$$

There are eight diagrams with the topologies depicted in Figure K.1: four **a**)-topology diagrams with $(i, j) = (c, c), (c, u), (u, c), (u, u)$ and another four which are related to the previous ones by interchanging the external legs, **b**)-topology.

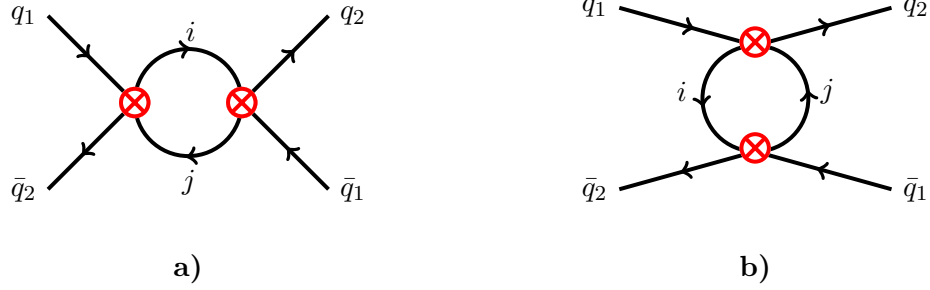
Computing the amplitude of diagram **b**), we obtain

$$\mathcal{M}_{\mathbf{b}}^{ij} = 8 G_F^2 \lambda_i \lambda_j \Lambda^{\alpha\beta} [\bar{u}_{q_2}(k_2) \gamma_\mu \gamma_\alpha \gamma_\nu P_L v_{q_1}(k_1)] [\bar{v}_{q_2}(p_1) \gamma^\nu \gamma_\beta \gamma^\mu P_L u_{q_1}(p_2)] , \quad (\text{K.0.2})$$

where

$$\Lambda^{\alpha\beta} \equiv \int_k \frac{\mathcal{K}_1^\alpha \mathcal{K}_2^\beta}{(\mathcal{K}_1^2 - m_j^2)(\mathcal{K}_2^2 - m_i^2)} ,$$

with $\mathcal{K}_1 \equiv k$ and $\mathcal{K}_2 \equiv k + p_2 - k_2$.

Figure K.1: Diagrams from the low-energy effective theory with $i, j = u, c$.

Expanding $\Lambda^{\alpha\beta}$ in powers of external momenta and taking the external momenta of the light quarks equal to zero (k_2 and p_1), we obtain

$$\Lambda^{\alpha\beta} = \frac{g^{\alpha\beta}}{4} f_1(m_i^2, m_j^2, m_{q_1}^2) - \frac{p_2^\alpha p_2^\beta}{2} f_2(m_i^2, m_j^2), \quad (\text{K.0.3})$$

where

$$\begin{aligned} f_1(m_i^2, m_j^2, m_{q_1}^2) &\equiv \int_k \frac{k^2}{(k^2 - m_j^2)(k^2 - m_i^2)} - \int_k \frac{k^4}{(k^2 - m_j^2)(k^2 - m_i^2)^2} \\ &\quad + \frac{1}{6} m_{q_1}^2 \int_k \frac{k^4}{(k^2 - m_j^2)(k^2 - m_i^2)^3}, \\ f_2(m_i^2, m_j^2) &\equiv \int_k \frac{k^2}{(k^2 - m_j^2)(k^2 - m_i^2)^2} - \frac{2}{3} \int_k \frac{k^4}{(k^2 - m_j^2)(k^2 - m_i^2)^3}. \end{aligned}$$

Then, Eq. (K.0.2) can be simplified by using the Fierz identities defined in Appendix J and the Dirac spinor equation,

$$\mathcal{M}_{\mathbf{b}}^{ij} = 8 G_F^2 \lambda_i \lambda_j \left(f_1(m_i^2, m_j^2, 0) \mathcal{O}_1^X - \frac{1}{2} m_{q_1}^2 f_2(m_i^2, m_j^2) \mathcal{O}_{19}^X \right), \quad (\text{K.0.4})$$

where

$$\mathcal{O}_1^X \equiv [\bar{u}_{q_2}(k_2) \gamma_\mu P_L v_{q_1}(k_1)][\bar{v}_{q_2}(p_1) \gamma^\mu P_L u_{q_1}(p_2)] \sim \mathcal{O}^{\text{VLL}}, \quad (\text{K.0.5})$$

$$\mathcal{O}_{19}^X \equiv [\bar{u}_{q_2}(k_2) \sigma_{\mu\nu} P_R v_{q_1}(k_1)][\bar{v}_{q_2}(p_1) \sigma^{\mu\nu} P_R u_{q_1}(p_2)] \sim \mathcal{O}_2^{\text{SRR}}. \quad (\text{K.0.6})$$

In the computation of Eq. (K.0.4), we must neglect contributions of $\mathcal{O}\left(\frac{m_{q_1}^2}{M_W^2}\right)$ in \mathcal{O}^{VLL} because we have not computed up to this order. Similarly for the Feynman diagram **a**), we find

$$\mathcal{M}_{\mathbf{a}}^{ij} = 8 G_F^2 \lambda_i \lambda_j \left(f_1(m_i^2, m_j^2, 0) \mathcal{O}_2^X - \frac{1}{2} m_{q_1}^2 f_2(m_i^2, m_j^2) \mathcal{O}_{20}^X \right), \quad (\text{K.0.7})$$

where

$$\begin{aligned} \mathcal{O}_2^X &\equiv [\bar{u}_{q_2}(k_2) \gamma_\mu P_L u_{q_1}(p_2)][\bar{v}_{q_2}(p_1) \gamma^\mu P_L v_{q_1}(k_1)] \sim \mathcal{O}^{VLL}, \\ \mathcal{O}_{20}^X &\equiv [\bar{u}_{q_2}(k_2) \sigma_{\mu\nu} P_R u_{q_1}(p_2)][\bar{v}_{q_2}(p_1) \sigma^{\mu\nu} P_R v_{q_1}(k_1)] \sim \mathcal{O}_2^{\text{SRR}}. \end{aligned}$$

Then, the total amplitude taking the relative signs given by the Wick's theorem is given by

$$\begin{aligned} \mathcal{M}_{\text{eff}} &= \sum_{ij} \mathcal{M}_{\mathbf{a}}^{ij} - \sum_{ij} \mathcal{M}_{\mathbf{b}}^{ij} \\ &= i \frac{G_F^2}{2 \pi^2} \left[\tilde{F}^{\text{VLL}} (\mathcal{O}_2^X - \mathcal{O}_1^X) - \frac{m_{q_1}^2}{6} \tilde{F}_2^{\text{SRR}} (\mathcal{O}_{20}^X - \mathcal{O}_{19}^X) \right], \quad (\text{K.0.8}) \end{aligned}$$

where

$$\begin{aligned} \tilde{F}^{\text{VLL}} &\equiv \lambda_u^2 \tilde{f}_1(m_u^2, m_u^2) + \lambda_u \lambda_c \left[\tilde{f}_1(m_u^2, m_c^2) + \tilde{f}_1(m_c^2, m_u^2) \right] + \lambda_c^2 \tilde{f}_1(m_c^2, m_c^2), \\ \tilde{F}_2^{\text{SRR}} &\equiv \lambda_u^2 \tilde{f}_2(m_u^2, m_u^2) + \lambda_u \lambda_c \left[\tilde{f}_2(m_u^2, m_c^2) + \tilde{f}_2(m_c^2, m_u^2) \right] + \lambda_c^2 \tilde{f}_2(m_c^2, m_c^2), \end{aligned}$$

and

$$\begin{aligned} \tilde{f}_1(m_i^2, m_j^2) &= \frac{m_i^2 m_j^2}{(m_i^2 - m_j^2)^2} \left[A_0(m_i^2) - A_0(m_j^2) \right] - \frac{m_i^4}{m_i^2 - m_j^2} \frac{d}{dm_i^2} A_0(m_i^2), \\ \tilde{f}_2(m_i^2, m_j^2) &= \frac{m_j^2(m_j^2 - 3m_i^2)}{(m_i^2 - m_j^2)^3} \left[A_0(m_i^2) - A_0(m_j^2) \right] + \frac{m_i^2(m_i^2 + m_j^2)}{(m_i^2 - m_j^2)^2} \frac{d}{dm_i^2} A_0(m_i^2) \\ &\quad - \frac{m_i^4}{m_i^2 - m_j^2} \frac{d}{dm_i^2} \frac{d}{dm_i^2} A_0(m_i^2), \end{aligned}$$

where

$$\tilde{f}_1(m_i^2, m_j^2) \equiv -i 16 \pi^2 f_1(m_i^2, m_j^2, 0),$$

$$\tilde{f}_2(m_i^2, m_j^2) \equiv -i 48 \pi^2 f_2(m_i^2, m_j^2),$$

$$A_0(a) \equiv -\mu^{D-4} a \left\{ \frac{1}{\hat{\epsilon}} + \ln \left(\frac{a}{\mu^2} \right) \right\}.$$

At this point, it is convenient to express \tilde{F}^{VLL} and \tilde{F}_2^{SRR} in terms of $\lambda_{t,c}$. For that purpose, we use the unitarity of the CKM matrix, so Eq. (K.0.8) becomes

$$\begin{aligned} \mathcal{M}_{\text{eff}} = & i \frac{G_F^2 \lambda_t^2}{2 \pi^2} \left[\tilde{F}_{tt}^{\text{VLL}} (\mathcal{O}_2^X - \mathcal{O}_1^X) - \frac{m_{q1}^2}{6} \tilde{F}_{2tt}^{\text{SRR}} (\mathcal{O}_{20}^X - \mathcal{O}_{19}^X) \right] \\ & + i \frac{G_F^2 \lambda_t \lambda_c}{2 \pi^2} \left[\tilde{F}_{tc}^{\text{VLL}} (\mathcal{O}_2^X - \mathcal{O}_1^X) - \frac{m_{q1}^2}{6} \tilde{F}_{2tc}^{\text{SRR}} (\mathcal{O}_{20}^X - \mathcal{O}_{19}^X) \right] \\ & + i \frac{G_F^2 \lambda_c^2}{2 \pi^2} \left[\tilde{F}_{cc}^{\text{VLL}} (\mathcal{O}_2^X - \mathcal{O}_1^X) - \frac{m_{q1}^2}{6} \tilde{F}_{2cc}^{\text{SRR}} (\mathcal{O}_{20}^X - \mathcal{O}_{19}^X) \right], \end{aligned} \quad (\text{K.0.9})$$

where

$$\tilde{F}^{\text{VLL}} \equiv \lambda_t^2 \tilde{F}_{tt}^{\text{VLL}} + \lambda_t \lambda_c \tilde{F}_{tc}^{\text{VLL}} + \lambda_c^2 \tilde{F}_{cc}^{\text{VLL}},$$

$$\tilde{F}_2^{\text{SRR}} \equiv \lambda_t^2 \tilde{F}_{2tt}^{\text{SRR}} + \lambda_t \lambda_c \tilde{F}_{2tc}^{\text{SRR}} + \lambda_c^2 \tilde{F}_{2cc}^{\text{SRR}},$$

and

$$\tilde{F}_{tt}^{\text{VLL}} = \tilde{f}_1(m_u^2, m_u^2),$$

$$\tilde{F}_{tc}^{\text{VLL}} = 2 \tilde{f}_1(m_u^2, m_u^2) - \tilde{f}_1(m_u^2, m_c^2) - \tilde{f}_1(m_c^2, m_u^2),$$

$$\tilde{F}_{cc}^{\text{VLL}} = \tilde{f}_1(m_u^2, m_u^2) - \tilde{f}_1(m_u^2, m_c^2) - \tilde{f}_1(m_c^2, m_u^2) + \tilde{f}_1(m_c^2, m_c^2),$$

$$\tilde{F}_{2tt}^{\text{SRR}} = \tilde{f}_2(m_u^2, m_u^2),$$

$$\tilde{F}_{2tc}^{\text{SRR}} = 2 \tilde{f}_2(m_u^2, m_u^2) - \tilde{f}_2(m_u^2, m_c^2) - \tilde{f}_2(m_c^2, m_u^2),$$

$$\tilde{F}_{2cc}^{\text{SRR}} = \tilde{f}_2(m_u^2, m_u^2) - \tilde{f}_2(m_u^2, m_c^2) - \tilde{f}_2(m_c^2, m_u^2) + \tilde{f}_2(m_c^2, m_c^2).$$

K.1 B mixing

In B mixing, in the limit of $m_{u,c} \rightarrow 0$, we obtain

$$\begin{aligned}\tilde{F}_{tt}^{\text{VLL}} &= 0, & \tilde{F}_{2tt}^{\text{SRR}} &= \tilde{f}_2(0, 0), \\ \tilde{F}_{tc}^{\text{VLL}} &= 0, & \tilde{F}_{2tc}^{\text{SRR}} &= 0, \\ \tilde{F}_{cc}^{\text{VLL}} &= 0, & \tilde{F}_{2cc}^{\text{SRR}} &= 0,\end{aligned}\tag{K.1.10}$$

where

$$\tilde{f}_2(0, 0) = -\frac{1}{\hat{\epsilon}} + \ln\left(\frac{\mu^2}{M_W^2}\right) - \ln\left(\frac{m_u^2}{M_W^2}\right) - \frac{5}{6}, \quad \text{with } m_u \rightarrow 0.\tag{K.1.11}$$

This limit depends on the way we do it. This means that $\lim_{m_c \rightarrow 0} \lim_{m_u \rightarrow \alpha m_c} f(m_u, m_c) = \hat{f}(\alpha)$. The result depends on α , however when we take the limit in the fundamental theory, we get the same α -dependence as in the low-energy theory which exactly cancels out in the matching procedure. Therefore, it does not matter the α chosen, in particular our results are for $\alpha = 1$ in both effective and fundamental theories.

Finally, the effective amplitude is given by

$$\mathcal{M}_{\text{eff}}^{\text{B}} = -i \frac{G_F^2 M_W^2 \lambda_t^2}{12 \pi^2} x_{q_1} \tilde{F}_{2tt}^{\text{SRR}} (\mathcal{O}_{20}^{\text{X}} - \mathcal{O}_{19}^{\text{X}}),\tag{K.1.12}$$

with

$$\tilde{F}_{2tt}^{\text{SRR}} = -\frac{1}{\hat{\epsilon}} + \ln\left(\frac{\mu^2}{M_W^2}\right) - \ln\left(\frac{m_u^2}{M_W^2}\right) - \frac{5}{6}, \quad \text{with } m_u \rightarrow 0.\tag{K.1.13}$$

In Eq. (K.1.13), we can see the ultraviolet divergence given by the first two pieces, which has to be renormalized with a dimension-8 four-quark operator, and the infrared divergence given by the third piece that will cancel out with the coming ones from the fundamental theory.

K.2 K mixing

In K mixing, in the limit of $m_u \rightarrow 0$, we obtain

$$\begin{aligned}
\tilde{F}_{tt}^{\text{VLL}} &= 0, \quad \tilde{F}_{tc}^{\text{VLL}} = -m_c^2 \left[\frac{1}{\hat{\epsilon}} - \ln \left(\frac{\mu^2}{M_W^2} \right) + \ln \left(\frac{m_c^2}{M_W^2} \right) + 1 \right], \quad \tilde{F}_{cc}^{\text{VLL}} = \frac{m_c^2}{2}, \\
\tilde{F}_{2tt}^{\text{SRR}} &= -\frac{1}{\hat{\epsilon}} + \ln \left(\frac{\mu^2}{M_W^2} \right) - \ln \left(\frac{m_u^2}{M_W^2} \right) - \frac{5}{6}, \\
\tilde{F}_{2tc}^{\text{SRR}} &= -2 \ln \left(\frac{m_u^2}{M_W^2} \right) + 2 \ln \left(\frac{m_c^2}{M_W^2} \right) - \frac{5}{3}, \\
\tilde{F}_{2cc}^{\text{SRR}} &= -\ln \left(\frac{m_u^2}{M_W^2} \right) + \ln \left(\frac{m_c^2}{M_W^2} \right) - \frac{5}{3},
\end{aligned} \tag{K.2.14}$$

Therefore, the effective amplitude is

$$\begin{aligned}
\mathcal{M}_{\text{eff}}^{\text{K}} &= i \frac{G_F^2 \lambda_t^2}{2 \pi^2} \left[-\frac{m_{q_1}^2}{6} \tilde{F}_{2tt}^{\text{SRR}} (\mathcal{O}_{20}^X - \mathcal{O}_{19}^X) \right] \\
&\quad + i \frac{G_F^2 \lambda_t \lambda_c}{2 \pi^2} \left[\tilde{F}_{tc}^{\text{VLL}} (\mathcal{O}_2^X - \mathcal{O}_1^X) - \frac{m_{q_1}^2}{6} \tilde{F}_{2tc}^{\text{SRR}} (\mathcal{O}_{20}^X - \mathcal{O}_{19}^X) \right] \\
&\quad + i \frac{G_F^2 \lambda_c^2}{2 \pi^2} \left[\tilde{F}_{cc}^{\text{VLL}} (\mathcal{O}_2^X - \mathcal{O}_1^X) - \frac{m_{q_1}^2}{6} \tilde{F}_{2cc}^{\text{SRR}} (\mathcal{O}_{20}^X - \mathcal{O}_{19}^X) \right].
\end{aligned} \tag{K.2.15}$$

K.3 Matching procedure

We have proved that the effective amplitude is given by

$$\begin{aligned}
\mathcal{M}_{\text{eff}} &= X_{\text{eff}}^{\text{VLL}} (\mathcal{O}_2^X - \mathcal{O}_1^X) + X_{\text{eff}}^{2\text{SRR}} (\mathcal{O}_{20}^X - \mathcal{O}_{19}^X) \\
&\quad + i \frac{G_F^2 \lambda_t^2}{2 \pi^2} \left[\tilde{F}_{tt}^{\text{VLL}} (\mathcal{O}_2^X - \mathcal{O}_1^X) - \frac{m_{q_1}^2}{6} \tilde{F}_{2tt}^{\text{SRR}} (\mathcal{O}_{20}^X - \mathcal{O}_{19}^X) \right] \\
&\quad + i \frac{G_F^2 \lambda_t \lambda_c}{2 \pi^2} \left[\tilde{F}_{ct}^{\text{VLL}} (\mathcal{O}_2^X - \mathcal{O}_1^X) - \frac{m_{q_1}^2}{6} \tilde{F}_{2ct}^{\text{SRR}} (\mathcal{O}_{20}^X - \mathcal{O}_{19}^X) \right] \\
&\quad + i \frac{G_F^2 \lambda_c^2}{2 \pi^2} \left[\tilde{F}_{cc}^{\text{VLL}} (\mathcal{O}_2^X - \mathcal{O}_1^X) - \frac{m_{q_1}^2}{6} \tilde{F}_{2cc}^{\text{SRR}} (\mathcal{O}_{20}^X - \mathcal{O}_{19}^X) \right],
\end{aligned} \tag{K.3.16}$$

where $X_{\text{eff}}^{\text{VLL}}$ and $X_{\text{eff}}^{2\text{SRR}}$ are tree-level amplitudes from the low-energy effective theory defined as

$$\begin{aligned} X_{\text{eff}}^{\text{VLL}} &\equiv \lambda_t^2 X_{\text{eff VLL}}^{tt} + 2 \lambda_t \lambda_c X_{\text{eff VLL}}^{ct} + \lambda_c^2 X_{\text{eff VLL}}^{cc} , \\ X_{\text{eff}}^{2\text{SRR}} &\equiv \lambda_t^2 X_{\text{eff 2SRR}}^{tt} + 2 \lambda_t \lambda_c X_{\text{eff 2SRR}}^{ct} + \lambda_c^2 X_{\text{eff 2SRR}}^{cc} . \end{aligned}$$

On the other hand, the fundamental amplitude is give by

$$\mathcal{M}_{\text{fun}} = X_{\text{fun}}^{\text{VLL}} (\mathcal{O}_2^X - \mathcal{O}_1^X) + X_{\text{fun}}^{2\text{SRR}} (\mathcal{O}_{20}^X - \mathcal{O}_{19}^X) , \quad (\text{K.3.17})$$

where

$$\begin{aligned} X_{\text{fun}}^{\text{VLL}} &\equiv \lambda_t^2 X_{\text{fun VLL}}^{tt} + 2 \lambda_t \lambda_c X_{\text{fun VLL}}^{ct} + \lambda_c^2 X_{\text{fun VLL}}^{cc} , \\ X_{\text{fun}}^{2\text{SRR}} &\equiv \lambda_t^2 X_{\text{fun 2SRR}}^{tt} + 2 \lambda_t \lambda_c X_{\text{fun 2SRR}}^{ct} + \lambda_c^2 X_{\text{fun 2SRR}}^{cc} . \end{aligned}$$

Therefore, performing a matching between both theories, $\mathcal{M}_{\text{eff}} = \mathcal{M}_{\text{fun}}$, we obtain the following relations

$$\begin{aligned} X_{\text{eff VLL}}^{tt} &= X_{\text{fun VLL}}^{tt} - i \frac{G_F^2}{2 \pi^2} \tilde{F}_{tt}^{\text{VLL}} , \\ X_{\text{eff VLL}}^{ct} &= X_{\text{fun VLL}}^{ct} - i \frac{G_F^2}{4 \pi^2} \tilde{F}_{ct}^{\text{VLL}} , \\ X_{\text{eff VLL}}^{cc} &= X_{\text{fun VLL}}^{cc} - i \frac{G_F^2}{2 \pi^2} \tilde{F}_{cc}^{\text{VLL}} , \\ X_{\text{eff 2SRR}}^{tt} &= X_{\text{fun 2SRR}}^{tt} + i \frac{G_F^2 M_W^2}{12 \pi^2} x_{q1} \tilde{F}_{2 tt}^{\text{SRR}} , \\ X_{\text{eff 2SRR}}^{ct} &= X_{\text{fun 2SRR}}^{ct} + i \frac{G_F^2 M_W^2}{24 \pi^2} x_{q1} \tilde{F}_{2 ct}^{\text{SRR}} , \\ X_{\text{eff 2SRR}}^{cc} &= X_{\text{fun 2SRR}}^{cc} + i \frac{G_F^2 M_W^2}{12 \pi^2} x_{q1} \tilde{F}_{2 cc}^{\text{SRR}} . \end{aligned} \quad (\text{K.3.18})$$

Translating Eqs. (K.3.18) in terms of Wilson coefficients, we find¹

$$\begin{aligned}
C_{SM\ VLL}^{tt} &= C_{SM\ VLL}^{tt\ \text{fun}} + \frac{4}{M_W^2} \tilde{F}_{tt}^{\text{VLL}}, \\
C_{SM\ VLL}^{ct} &= C_{SM\ VLL}^{ct\ \text{fun}} + \frac{2}{M_W^2} \tilde{F}_{ct}^{\text{VLL}}, \\
C_{SM\ VLL}^{cc} &= C_{SM\ VLL}^{cc\ \text{fun}} + \frac{4}{M_W^2} \tilde{F}_{cc}^{\text{VLL}}, \\
C_{SM\ 2SRR}^{tt} &= -x_{q1} \left[\frac{2}{3} \tilde{F}_{2\ tt}^{\text{SRR}} - 4 M_W^4 \tilde{\mathcal{S}}_0(m_u, m_t) \right], \\
C_{SM\ 2SRR}^{ct} &= -x_{q1} \left[\frac{1}{3} \tilde{F}_{2\ ct}^{\text{SRR}} - 4 M_W^4 \tilde{\mathcal{S}}_0(m_u, m_c, m_t) \right], \\
C_{SM\ 2SRR}^{cc} &= -x_{q1} \left[\frac{2}{3} \tilde{F}_{2\ cc}^{\text{SRR}} - 4 M_W^4 \tilde{\mathcal{S}}_0(m_u, m_c) \right],
\end{aligned} \tag{K.3.19}$$

where

$$\tilde{\mathcal{S}}_0(m_u, m_t) = \mathcal{F}_{\text{fun}}(m_u, m_u) - [\mathcal{F}_{\text{fun}}(m_u, m_t) + \mathcal{F}_{\text{fun}}(m_t, m_u)] + \mathcal{F}_{\text{fun}}(m_t, m_t),$$

$$\tilde{\mathcal{S}}_0(m_u, m_c) = \mathcal{F}_{\text{fun}}(m_u, m_u) - [\mathcal{F}_{\text{fun}}(m_u, m_c) + \mathcal{F}_{\text{fun}}(m_c, m_u)] + \mathcal{F}_{\text{fun}}(m_c, m_c),$$

$$\begin{aligned}
\tilde{\mathcal{S}}_0(m_u, m_c, m_t) &= \mathcal{F}_{\text{fun}}(m_u, m_u) - \frac{1}{2} [\mathcal{F}_{\text{fun}}(m_u, m_c) + \mathcal{F}_{\text{fun}}(m_c, m_u)] \\
&\quad - \frac{1}{2} [\mathcal{F}_{\text{fun}}(m_u, m_t) + \mathcal{F}_{\text{fun}}(m_t, m_u)] \\
&\quad + [\mathcal{F}_{\text{fun}}(m_c, m_t) + \mathcal{F}_{\text{fun}}(m_t, m_c)],
\end{aligned}$$

with

$$\begin{aligned}
\mathcal{F}_{\text{fun}} &= \frac{1}{3} \left[F_2^{\text{WW}31} + F_2^{\text{WW}41} + F_2^{\text{WW}21} \right] \\
&\quad - \frac{1}{2} \left[\frac{1}{2} \frac{d}{d M_W^2} D_2(m_i^2, m_j^2, M_W^2) + \frac{d}{d m_j^2} D_2(m_i^2, m_j^2, M_W^2) \right].
\end{aligned} \tag{K.3.20}$$

¹Without the renormalization of the ultraviolet divergences.

K.4 Renormalization procedure

The contributions from the Feynman diagrams given by Figure K.1 generate ultraviolet divergences in $\tilde{F}_{2tt}^{\text{SRR}}$ and $\tilde{F}_{tc}^{\text{VLL}}$. These divergences have to be renormalized with dimension-eight four-quark operators ($\mathcal{O}_{2\text{SRR}}^{D=8}$ and $\mathcal{O}_{\text{VLL}}^{D=8}$). Then, the $\Delta B = 2$ and $\Delta S = 2$ counter-terms Lagrangians are

$$\mathcal{L}_R^{\Delta B=2} = \mathcal{L}_R^{2\text{SRR}}, \quad (\text{K.4.21})$$

$$\mathcal{L}_R^{\Delta S=2} = \mathcal{L}_R^{\text{VLL}} + \mathcal{L}_R^{2\text{SRR}}, \quad (\text{K.4.22})$$

where

$$\begin{aligned} \mathcal{L}_R^{2\text{SRR}} &= + \frac{G_F^2 \lambda_t^2}{24 \pi^2} C_0(\mu) \mathcal{O}_{2\text{SRR}}^{D=8}, \\ \mathcal{L}_R^{\text{VLL}} &= - \frac{G_F^2 \lambda_t \lambda_c}{4 \pi^2} C_0(\mu) \mathcal{O}_{\text{VLL}}^{D=8}, \end{aligned}$$

with

$$\begin{aligned} \mathcal{O}_{2\text{SRR}}^{D=8} &\equiv [\bar{q}_2 \sigma_{\mu\nu} \vec{\partial}_\alpha P_R q_1] [\bar{q}_2 \sigma^{\mu\nu} \vec{\partial}^\alpha P_R q_1], \\ \mathcal{O}_{\text{VLL}}^{D=8} &\equiv m_c^2 [\bar{q}_2 \gamma_\mu P_L q_1] [\bar{q}_2 \gamma^\mu P_L q_1], \end{aligned}$$

and

$$C_0(\mu) \equiv \ln \left(\frac{\mu^2}{M_W^2} \right).$$

After the renormalization of the Wilson coefficients given by Eq (K.3.19), we obtain

$$\begin{aligned} \mathcal{C}_{\text{SM VLL}}^{tt} &= \mathcal{C}_{\text{SM VLL}}^{tt \text{ fun}} + \frac{4}{M_W^2} \tilde{F}_{tt}^{\text{VLL}}, \\ \mathcal{C}_{\text{SM VLL}}^{ct} &= \mathcal{C}_{\text{SM VLL}}^{ct \text{ fun}} + \frac{2}{M_W^2} \tilde{F}_{ct}^{\text{VLL}}, \\ \mathcal{C}_{\text{SM VLL}}^{cc} &= \mathcal{C}_{\text{SM VLL}}^{cc \text{ fun}} + \frac{4}{M_W^2} \tilde{F}_{cc}^{\text{VLL}}, \\ \mathcal{C}_{\text{SM 2SRR}}^{tt} &= -x_{q1} \left[\frac{2}{3} \tilde{f}_{2tt}^{\text{SRR}} - 4 M_W^4 \tilde{\mathcal{S}}_0(m_u, m_t) \right], \end{aligned}$$

$$C_{SM\ 2SRR}^{ct} = -x_{q1} \left[\frac{1}{3} \tilde{f}_{2\ ct}^{SRR} - 4 M_W^4 \tilde{\mathcal{S}}_0(m_u, m_c, m_t) \right],$$

$$C_{SM\ 2SRR}^{cc} = -x_{q1} \left[\frac{2}{3} \tilde{f}_{2\ cc}^{SRR} - 4 M_W^4 \tilde{\mathcal{S}}_0(m_u, m_c) \right],$$

with

$$\tilde{F}_{tt}^{VLL} = 0, \quad \tilde{F}_{tc}^{VLL} = -m_c^2 \left[\ln \left(\frac{m_c^2}{M_W^2} \right) + 1 \right], \quad \tilde{F}_{cc}^{VLL} = \frac{m_c^2}{2},$$

$$\tilde{f}_{2\ tt}^{SRR} = -\ln \left(\frac{m_u^2}{M_W^2} \right) - \frac{5}{6},$$

$$\tilde{f}_{2\ tc}^{SRR} = -2 \ln \left(\frac{m_u^2}{M_W^2} \right) + 2 \ln \left(\frac{m_c^2}{M_W^2} \right) - \frac{5}{3},$$

$$\tilde{f}_{2\ cc}^{SRR} = -\ln \left(\frac{m_u^2}{M_W^2} \right) + \ln \left(\frac{m_c^2}{M_W^2} \right) - \frac{5}{3}. \quad (\text{K.4.23})$$

Appendix L

Hadronic matrix elements for meson mixing

The matrix elements $\langle \mathcal{O}_i(\mu) \rangle \equiv \langle \bar{M}^0 | \mathcal{O}_i(\mu) | M^0 \rangle$ can be written as

$$\langle \mathcal{O}^{\text{VLL}}(\mu) \rangle = \frac{1}{3} M_{M^0} f_{M^0}^2 B_1^{\text{VLL}}(\mu) , \quad (\text{L.0.1})$$

$$\langle \mathcal{O}^{\text{VRR}}(\mu) \rangle = \frac{1}{3} M_{M^0} f_{M^0}^2 B_1^{\text{VRR}}(\mu) , \quad (\text{L.0.2})$$

$$\langle \mathcal{O}_1^{\text{LR}}(\mu) \rangle = -\frac{1}{6} R(\mu) M_{M^0} f_{M^0}^2 B_1^{\text{LR}}(\mu) , \quad (\text{L.0.3})$$

$$\langle \mathcal{O}_2^{\text{LR}}(\mu) \rangle = \frac{1}{4} R(\mu) M_{M^0} f_{M^0}^2 B_2^{\text{LR}}(\mu) , \quad (\text{L.0.4})$$

$$\langle \mathcal{O}_1^{\text{SLL}}(\mu) \rangle = -\frac{5}{24} R(\mu) M_{M^0} f_{M^0}^2 B_1^{\text{SLL}}(\mu) , \quad (\text{L.0.5})$$

$$\langle \mathcal{O}_2^{\text{SLL}}(\mu) \rangle = -\frac{1}{2} R(\mu) M_{M^0} f_{M^0}^2 B_2^{\text{SLL}}(\mu) , \quad (\text{L.0.6})$$

$$\langle \mathcal{O}_1^{\text{SRR}}(\mu) \rangle = -\frac{5}{24} R(\mu) M_{M^0} f_{M^0}^2 B_1^{\text{SRR}}(\mu) , \quad (\text{L.0.7})$$

$$\langle \mathcal{O}_2^{\text{SRR}}(\mu) \rangle = -\frac{1}{2} R(\mu) M_{M^0} f_{M^0}^2 B_2^{\text{SRR}}(\mu) , \quad (\text{L.0.8})$$

where

$$R(\mu) = \left(\frac{M_{M^0}}{m_{q_1}(\mu) + m_{q_2}(\mu)} \right)^2 \quad (\text{L.0.9})$$

and f_{M^0} is the M-meson decay constant, $f_{B^0} = (192.0 \pm 4.3) \text{ MeV}$ [152],

$f_{B^0_s} = (228.4 \pm 3.7) \text{ MeV}$ [152] and $f_{K^0} = (155.6 \pm 0.4) \text{ MeV}$ [32]. The $B_i^a(\mu)$ parametrize

$i =$	1	2	3	4	5
$f_{B^0} \sqrt{B_i^{B^0}}$	$174 \pm 8 \text{ MeV}$	$160 \pm 8 \text{ MeV}$	$177 \pm 17 \text{ MeV}$	$185 \pm 9 \text{ MeV}$	$229 \pm 14 \text{ MeV}$
$f_{B_s^0} \sqrt{B_i^{B_s^0}}$	$211 \pm 8 \text{ MeV}$	$195 \pm 7 \text{ MeV}$	$215 \pm 17 \text{ MeV}$	$220 \pm 9 \text{ MeV}$	$285 \pm 14 \text{ MeV}$
B_i^K	$0.506 \pm 0.017 \pm 0.003$	$0.46 \pm 0.01 \pm 0.03$	$0.79 \pm 0.02 \pm 0.05$	$0.78 \pm 0.02 \pm 0.04$	$0.49 \pm 0.03 \pm 0.03$

Table L.1: Determinations of $f_{M^0} \sqrt{B_i^{M^0}}$ ($M^0 = B^0, B_s^0$) [281] and $B_i^{K^0}$ ($M^0 = K^0$) [282], in the $\overline{\text{MS}}$ scheme. The B_q^0 parameters are given at $\mu = m_b$, while the K^0 values refer to $\mu = 3 \text{ GeV}$.

the deviation from the naive factorization limit. These $B_i^a(\mu)$ factors are given by

$$B_1^{\text{VLL}}(\mu) = B_1^{\text{VRR}}(\mu) = B_1^{\text{M}^0}(\mu), \quad (\text{L.0.10})$$

$$B_1^{\text{LR}}(\mu) = B_5^{\text{M}^0}(\mu), \quad (\text{L.0.11})$$

$$B_2^{\text{LR}}(\mu) = B_4^{\text{M}^0}(\mu), \quad (\text{L.0.12})$$

$$B_1^{\text{SLL}}(\mu) = B_1^{\text{SRR}}(\mu) = B_2^{\text{M}^0}(\mu), \quad (\text{L.0.13})$$

$$B_2^{\text{SLL}}(\mu) = B_2^{\text{SRR}}(\mu) = \frac{5}{3} B_2^{\text{M}^0}(\mu) - \frac{2}{3} B_3^{\text{M}^0}(\mu), \quad (\text{L.0.14})$$

where $B_i^{\text{M}^0}(\mu)$, $i = 1, \dots, 5$ are non-perturbative factors that can be found in the Table L.1.

Appendix M

Renormalization group short-distance QCD effects

The renormalization group short-distance QCD effects can be calculated by solving the renormalization group equations that govern the scale dependence of Wilson coefficients $C_i(\mu)$. In this appendix we present the analytic formulae of the $\Delta F = 2$ dimension six four-quark operators \mathcal{O}_i extracted from Ref. [283]. The general expression for $C_i(\mu)$ is given by

$$\vec{\mathcal{C}}(\mu) = \hat{U}(\mu, \mu_0) \vec{\mathcal{C}}(\mu_0), \quad \mu < \mu_0, \quad (\text{M.0.1})$$

where $\vec{\mathcal{C}}$ is a column vector built out of the C_i components and $\hat{U}(\mu, \mu_0)$ is the evolution matrix. $\vec{\mathcal{C}}(\mu_0)$ are the initial Wilson conditions which encode all short-distance physics.

For instance, $(\mu, \mu_0) = (\mu_b, \mu_{tW})$ for B_q^0 and $(\mu, \mu_0) = (\mu_c, \mu_{tW})$ for K^0 :¹

$$\mathcal{C}_1^{\text{VLL}}(\mu) = [\eta(\mu)]_{\text{VLL}} \mathcal{C}_1^{\text{VLL}}(\mu_{tW}) , \quad (\text{M.0.2})$$

$$\begin{pmatrix} \mathcal{C}_1^{\text{LR}}(\mu) \\ \mathcal{C}_2^{\text{LR}}(\mu) \end{pmatrix} = \begin{pmatrix} [\eta_{11}(\mu)]_{\text{LR}} & [\eta_{12}(\mu)]_{\text{LR}} \\ [\eta_{21}(\mu)]_{\text{LR}} & [\eta_{22}(\mu)]_{\text{LR}} \end{pmatrix} \begin{pmatrix} \mathcal{C}_1^{\text{LR}}(\mu_{tW}) \\ \mathcal{C}_2^{\text{LR}}(\mu_{tW}) \end{pmatrix} , \quad (\text{M.0.3})$$

$$\begin{pmatrix} \mathcal{C}_1^{\text{SLL}}(\mu) \\ \mathcal{C}_2^{\text{SLL}}(\mu) \end{pmatrix} = \begin{pmatrix} [\eta_{11}(\mu)]_{\text{SLL}} & [\eta_{12}(\mu)]_{\text{SLL}} \\ [\eta_{21}(\mu)]_{\text{SLL}} & [\eta_{22}(\mu)]_{\text{SLL}} \end{pmatrix} \begin{pmatrix} \mathcal{C}_1^{\text{SLL}}(\mu_{tW}) \\ \mathcal{C}_2^{\text{SLL}}(\mu_{tW}) \end{pmatrix} , \quad (\text{M.0.4})$$

where

$$[\eta(\mu)]_a = [\eta^{(0)}(\mu)]_a + \frac{\alpha_s^{(f)}(\mu)}{4\pi} [\eta^{(1)}(\mu)]_a . \quad (\text{M.0.5})$$

M.1 η -Factors for $B_{s,d}^0 - \bar{B}_{s,d}^0$ mixing

VLL-Sector

$$[\eta^{(0)}(\mu_b)]_{\text{VLL}} = \eta_5^{6/23} , \quad [\eta^{(1)}(\mu_b)]_{\text{VLL}} = 1.6273 (1 - \eta_5) \eta_5^{6/23} .$$

LR-Sector

$$\begin{aligned} [\eta_{11}^{(0)}(\mu_b)]_{\text{LR}} &= \eta_5^{3/23} , & [\eta_{12}^{(0)}(\mu_b)]_{\text{LR}} &= 0 , \\ [\eta_{21}^{(0)}(\mu_b)]_{\text{LR}} &= \frac{2}{3} \left(\eta_5^{3/23} - \eta_5^{-24/23} \right) , & [\eta_{22}^{(0)}(\mu_b)]_{\text{LR}} &= \eta_5^{-24/23} , \\ [\eta_{11}^{(1)}(\mu_b)]_{\text{LR}} &= 0.9250 \eta_5^{-24/23} + \eta_5^{3/23} (-2.0994 + 1.1744 \eta_5) , \\ [\eta_{12}^{(1)}(\mu_b)]_{\text{LR}} &= 1.3875 \left(\eta_5^{26/23} - \eta_5^{-24/23} \right) , \\ [\eta_{21}^{(1)}(\mu_b)]_{\text{LR}} &= (-11.7329 + 0.7829 \eta_5) \eta_5^{3/23} + \eta_5^{-24/23} (-5.3048 + 16.2548 \eta_5) , \\ [\eta_{22}^{(1)}(\mu_b)]_{\text{LR}} &= (7.9572 - 8.8822 \eta_5) \eta_5^{-24/23} + 0.9250 \eta_5^{26/23} . \end{aligned}$$

¹The VRR and SRR sectors are the same as in the VLL and SLL sectors.

SLL-Sector

$$\begin{aligned}
\left[\eta_{11}^{(0)}(\mu_b)\right]_{\text{SLL}} &= 1.0153 \eta_5^{-0.6315} - 0.0153 \eta_5^{0.7184} , \\
\left[\eta_{12}^{(0)}(\mu_b)\right]_{\text{SLL}} &= 1.9325 \left(\eta_5^{-0.6315} - \eta_5^{0.7184}\right) , \\
\left[\eta_{21}^{(0)}(\mu_b)\right]_{\text{SLL}} &= 0.0081 \left(\eta_5^{0.7184} - \eta_5^{-0.6315}\right) , \\
\left[\eta_{22}^{(0)}(\mu_b)\right]_{\text{SLL}} &= 1.0153 \eta_5^{0.7184} - 0.0153 \eta_5^{-0.6315} , \\
\left[\eta_{11}^{(1)}(\mu_b)\right]_{\text{SLL}} &= (4.8177 - 5.2272 \eta_5) \eta_5^{-0.6315} + (0.3371 + 0.0724 \eta_5) \eta_5^{0.7184} , \\
\left[\eta_{12}^{(1)}(\mu_b)\right]_{\text{SLL}} &= (9.1696 - 38.8778 \eta_5) \eta_5^{-0.6315} + (42.5021 - 12.7939 \eta_5) \eta_5^{0.7184} , \\
\left[\eta_{21}^{(1)}(\mu_b)\right]_{\text{SLL}} &= (0.0531 + 0.0415 \eta_5) \eta_5^{-0.6315} - (0.0566 + 0.0380 \eta_5) \eta_5^{0.7184} , \\
\left[\eta_{22}^{(1)}(\mu_b)\right]_{\text{SLL}} &= (0.1011 + 0.3083 \eta_5) \eta_5^{-0.6315} + (-7.1314 + 6.7219 \eta_5) \eta_5^{0.7184} ,
\end{aligned}$$

where $\eta_5 \equiv \frac{\alpha_s^{(5)}(\mu_{tW})}{\alpha_s^{(5)}(\mu_b)}$.

M.2 η -Factors for $K^0 - \bar{K}^0$ mixingVLL-Sector

$$\begin{aligned}
\left[\eta^{(0)}(\mu_c)\right]_{\text{VLL}} &= \eta_4^{6/25} \eta_5^{6/23} , \\
\left[\eta^{(1)}(\mu_c)\right]_{\text{VLL}} &= \eta_4^{6/25} \eta_5^{6/23} (1.7917 - 0.1644 \eta_4 - 1.6273 \eta_4 \eta_5) .
\end{aligned}$$

LR-Sector

$$\begin{aligned}
\left[\eta_{11}^{(0)}(\mu_c)\right]_{\text{LR}} &= \eta_4^{3/25} \eta_5^{3/23} , \\
\left[\eta_{12}^{(0)}(\mu_c)\right]_{\text{LR}} &= 0 , \\
\left[\eta_{21}^{(0)}(\mu_c)\right]_{\text{LR}} &= \frac{2}{3} \left(\eta_4^{3/25} \eta_5^{3/23} - \eta_4^{-24/25} \eta_5^{-24/23}\right) , \\
\left[\eta_{22}^{(0)}(\mu_c)\right]_{\text{LR}} &= \eta_4^{-24/25} \eta_5^{-24/23} , \\
\left[\eta_{11}^{(1)}(\mu_c)\right]_{\text{LR}} &= 0.9279 \eta_4^{-24/25} \eta_5^{-24/23} - 0.0029 \eta_4^{28/25} \eta_5^{-24/23} \\
&\quad + \eta_4^{3/25} \eta_5^{3/23} (-2.0241 - 0.0753 \eta_4 + 1.1744 \eta_4 \eta_5) ,
\end{aligned}$$

$$\begin{aligned}
\left[\eta_{12}^{(1)}(\mu_c)\right]_{\text{LR}} &= -1.3918 \eta_4^{-24/25} \eta_5^{-24/23} + 0.0043 \eta_4^{28/25} \eta_5^{-24/23} \\
&\quad + 1.3875 \eta_4^{28/25} \eta_5^{26/23} , \\
\left[\eta_{21}^{(1)}(\mu_c)\right]_{\text{LR}} &= -0.0019 \eta_4^{28/25} \eta_5^{-24/23} + 5.0000 \eta_4^{1/25} \eta_5^{3/23} \\
&\quad + \eta_4^{3/25} \eta_5^{3/23} (-16.6828 - 0.0502 \eta_4 + 0.7829 \eta_4 \eta_5) \\
&\quad + \eta_4^{-24/25} \eta_5^{-24/23} (-4.4701 - 0.8327 \eta_4 + 16.2548 \eta_4 \eta_5) , \\
\left[\eta_{22}^{(1)}(\mu_c)\right]_{\text{LR}} &= 0.0029 \eta_4^{28/25} \eta_5^{-24/23} + 0.9250 \eta_4^{28/25} \eta_5^{26/23} \\
&\quad + \eta_4^{-24/25} \eta_5^{-24/23} (6.7052 + 1.2491 \eta_4 - 8.8822 \eta_4 \eta_5) .
\end{aligned}$$

SLL-Sector

$$\begin{aligned}
\left[\eta_{11}^{(0)}(\mu_c)\right]_{\text{SLL}} &= 1.0153 \eta_4^{-0.5810} \eta_5^{-0.6315} - 0.0153 \eta_4^{0.6610} \eta_5^{0.7184} , \\
\left[\eta_{12}^{(0)}(\mu_c)\right]_{\text{SLL}} &= 1.9325 \left(\eta_4^{-0.5810} \eta_5^{-0.6315} - \eta_4^{0.6610} \eta_5^{0.7184} \right) , \\
\left[\eta_{21}^{(0)}(\mu_c)\right]_{\text{SLL}} &= 0.0081 \left(\eta_4^{0.6610} \eta_5^{0.7184} - \eta_4^{-0.5810} \eta_5^{-0.6315} \right) , \\
\left[\eta_{22}^{(0)}(\mu_c)\right]_{\text{SLL}} &= 1.0153 \eta_4^{0.6610} \eta_5^{0.7184} - 0.0153 \eta_4^{-0.5810} \eta_5^{-0.6315} , \\
\left[\eta_{11}^{(1)}(\mu_c)\right]_{\text{SLL}} &= 0.0020 \eta_4^{1.6610} \eta_5^{-0.6315} - 0.0334 \eta_4^{0.4190} \eta_5^{0.7184} \\
&\quad + \eta_4^{-0.5810} \eta_5^{-0.6315} (4.2458 + 0.5700 \eta_4 - 5.2272 \eta_4 \eta_5) \\
&\quad + \eta_4^{0.6610} \eta_5^{0.7184} (0.3640 + 0.0064 \eta_4 + 0.0724 \eta_4 \eta_5) , \\
\left[\eta_{12}^{(1)}(\mu_c)\right]_{\text{SLL}} &= 0.0038 \eta_4^{1.6610} \eta_5^{-0.6315} - 4.2075 \eta_4^{0.4190} \eta_5^{0.7184} \\
&\quad + \eta_4^{-0.5810} \eta_5^{-0.6315} (8.0810 + 1.0848 \eta_4 - 38.8778 \eta_4 \eta_5) \\
&\quad + \eta_4^{0.6610} \eta_5^{0.7184} (45.9008 + 0.8087 \eta_4 - 12.7939 \eta_4 \eta_5) , \\
\left[\eta_{21}^{(1)}(\mu_c)\right]_{\text{SLL}} &= -0.0011 \eta_4^{1.6610} \eta_5^{-0.6315} + 0.0003 \eta_4^{0.4190} \eta_5^{0.7184} \\
&\quad + \eta_4^{0.6610} \eta_5^{0.7184} (-0.0534 - 0.0034 \eta_4 - 0.0380 \eta_4 \eta_5) \\
&\quad + \eta_4^{-0.5810} \eta_5^{-0.6315} (0.0587 - 0.0045 \eta_4 + 0.0415 \eta_4 \eta_5) ,
\end{aligned}$$

$$\begin{aligned}
\left[\eta_{22}^{(1)}(\mu_c) \right]_{\text{SLL}} &= -0.0020 \eta_4^{1.6610} \eta_5^{-0.6315} + 0.0334 \eta_4^{0.4190} \eta_5^{0.7184} \\
&+ \eta_4^{-0.5810} \eta_5^{-0.6315} (0.1117 - 0.0086 \eta_4 + 0.3083 \eta_4 \eta_5) \\
&+ \eta_4^{0.6610} \eta_5^{0.7184} (-6.7398 - 0.4249 \eta_4 + 6.7219 \eta_4 \eta_5) ,
\end{aligned}$$

where $\eta_4 \equiv \frac{\alpha_s^{(4)}(\mu_b)}{\alpha_s^{(4)}(\mu_c)}$.

Appendix N

Inputs for meson mixing

Tables N.1, N.2 and N.3 show the inputs values adopted for the different inputs entering in the numerical analysis. ¹

Parameter	Value	Ref.
G_F	$1.1663787(6) \cdot 10^{-5}$ GeV	[63]
M_Z	91.1876(21) GeV	[63]
M_W	80.385(15) GeV	[63]
μ_t	163.427 GeV	Our analysis
μ_W	80.385 GeV	[63]
μ_b	4.18 GeV	[63]

Table N.1: Electroweak parameters.

¹In Tables N.1, N.2 and N.3, “Our analysis” means that we have used the Mathematica package `RunDec` [286] to extract the value.

Parameter	Value	Ref.
$\alpha_s(\mu_t)$	0.1086(10)	Our analysis
$\alpha_s(M_Z)$	0.1182(12)	[63]
$\alpha_s(\mu_W)$	0.1205(12)	Our analysis
$\alpha_s(\mu_b)$	0.2243(45)	Our analysis
$\alpha_s(3 \text{ GeV})$	0.2521(58)	Our analysis

Table N.2: QCD coupling constant.

Parameter	Value	Ref.
m_t^{pole}	173.21(87) GeV	[63]
$\bar{m}_t(\bar{m}_t)$	$163.427^{+0.828}_{-0.829}$ GeV	Our analysis
$m_t(\mu_W)$	$173.235^{+0.946}_{-0.947}$ GeV	Our analysis
$m_b(\mu_t)$	2.75(2) GeV	Our analysis
$m_b(\mu_W)$	2.91(2) GeV	Our analysis
$\bar{m}_b(\bar{m}_b)$	$4.18^{+0.04}_{-0.03}$ GeV	[63]
$m_c(\mu_t)$	0.623(15) GeV	Our analysis
$m_c(\mu_W)$	0.660(16) GeV	Our analysis
$\bar{m}_c(\bar{m}_c)$	1.27(3) GeV	[63]
$m_s(\mu_t)$	$0.054^{+0.005}_{-0.002}$ GeV	Our analysis
$m_s(\mu_W)$	$0.057^{+0.005}_{-0.002}$ GeV	Our analysis
$m_s(\mu_b)$	$0.082^{+0.007}_{-0.003}$ GeV	Our analysis
$m_s(3 \text{ GeV})$	$0.087^{+0.007}_{-0.004}$ GeV	Our analysis
$m_s(2 \text{ GeV})$	$0.096^{+0.008}_{-0.004}$ GeV	[63]
$m_d(\mu_t)$	$0.0026^{+0.0003}_{-0.0002}$ GeV	Our analysis
$m_d(\mu_W)$	$0.0028^{+0.0003}_{-0.0002}$ GeV	Our analysis
$m_d(\mu_b)$	$0.0040^{+0.0004}_{-0.0003}$ GeV	Our analysis
$m_d(3 \text{ GeV})$	$0.0043^{+0.0005}_{-0.0004}$ GeV	Our analysis
$m_d(2 \text{ GeV})$	$0.0047^{+0.0005}_{-0.0004}$ GeV	[63]

Table N.3: Quark masses.

Appendix O

Computation of $(\gamma_e)_{12}^{(0)}$

O.1 Feynman diagrams

In Figure O.1, we show all the Feynman diagrams that contribute to $(\gamma_e)_{12}^{(0)}$. In total, there are six diagrams with d_q couplings inside contributing to \tilde{d}_q .

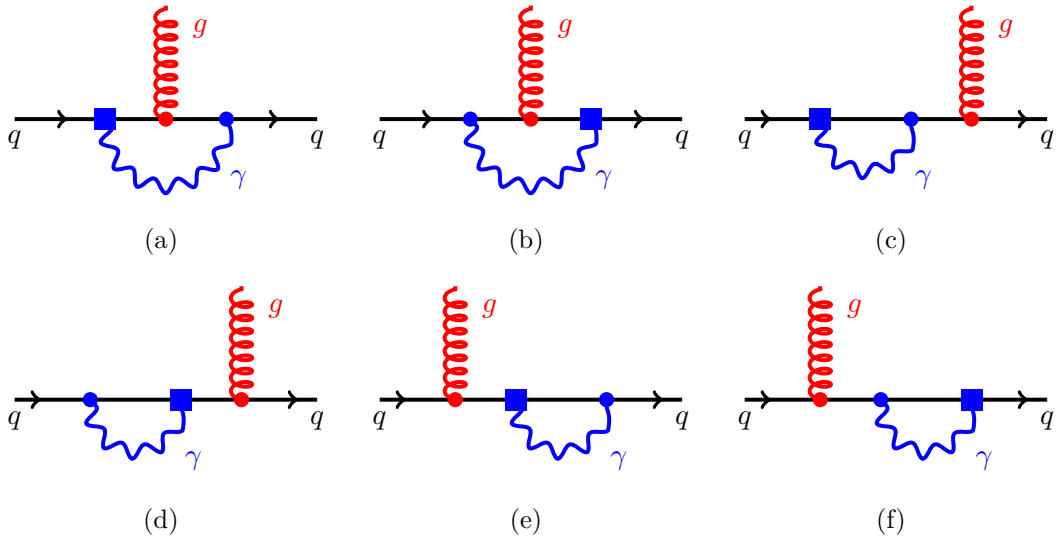
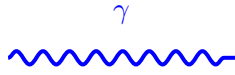
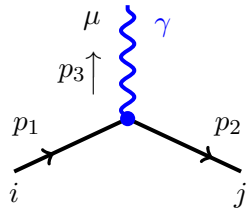


Figure O.1: Feynman diagrams contributing to $(\gamma_e)_{12}^{(0)}$.

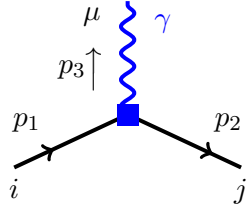
O.2 Feynman Rules



$$-i \frac{1}{k^2 - i\epsilon} \left[g^{\mu\nu} - (1 - \xi_\gamma) \frac{k_\mu k_\nu}{k^2} \right]$$



$$-ie(\gamma^\mu)_{ji}$$



$$D_q e (\sigma^{\mu\nu} \gamma_5)_{ji} p_{3\nu} \quad \text{where} \quad D_q \equiv -C_1^q(\mu) Q_q m_q$$

O.3 Computation

In this section, we compute the Feynman diagrams of Figure O.1. The technical prescriptions adopted for the computation of these diagrams:

1. All the Feynman rules are provided in Appendices B and O.2 .
2. We take the limit of external quark masses equal to zero.

Let us start with the computation of the Feynman diagrams shown in Figure O.1:

Feynman diagram (1 a)

Assuming the momentum directions presented in Figure O.2, the amplitude of the Feynman diagram (1 a) can be written as:

$$\mathcal{M}_{(1a)}^{\bar{x}} = \int \frac{d^D k}{(2\pi)^D} \left(\frac{i g_{\mu\mu_1}}{k^2} \right) \cdot \left[\bar{u}_q(p_2) i e \gamma^\mu \frac{i (\not{p}_2 + \not{k} + m_q)}{(p_2 + k)^2 - m_q^2} i g_s \gamma^{\bar{x}} T^a \frac{i (\not{p}_1 + \not{k} + m_q)}{(p_1 + k)^2 - m_q^2} (e D_q \sigma^{\mu_1\nu} \gamma_5 k_\nu) u_q(p_1) \right],$$

which after some Dirac algebra and putting all external quark masses equal to zero, it becomes

$$\mathcal{M}_{(1\ a)}^{\tilde{x}} = i e^2 g_s D_q \left[\bar{u}_q(p_2) \gamma_\mu \gamma_{\alpha_1} \gamma^{\tilde{x}} \gamma_{\alpha_2} \sigma^{\mu\nu} \gamma_5 T^a u_q(p_1) \right] A_\nu^{\alpha_1 \alpha_2}(p_1, p_2), \quad (\text{O.3.1})$$

where

$$A^{\alpha_1 \alpha_2 \nu}(p_1, p_2) \equiv \int \frac{d^D k}{(2\pi)^D} \frac{(p_2 + k)^{\alpha_1} (p_1 + k)^{\alpha_2} k^\nu}{(p_2 + k)^2 (p_1 + k)^2 k^2}. \quad (\text{O.3.2})$$

We have omitted the gluon polarization, since it is not necessary for our purposes.

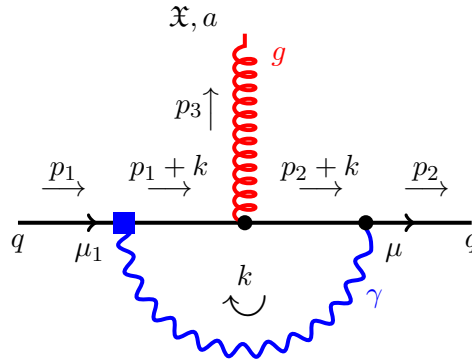


Figure O.2: Feynman diagram (1 a) showing momentum directions.

Feynman diagram (1 b), (1 c), (1 d), (1 e) and (1 f)

Following a similar proceeding as in the diagram (1 a), we obtain the following amplitudes for the rest of diagrams depicted in Figure O.1:

$$\mathcal{M}_{(1\ b)}^{\tilde{x}} = -i e^2 g_s D_q \left[\bar{u}_q(p_2) \sigma^{\mu\nu} \gamma_5 \gamma_{\alpha_1} \gamma^{\tilde{x}} \gamma_{\alpha_2} \gamma_\mu T^a u_q(p_1) \right] A_\nu^{\alpha_1 \alpha_2}(p_1, p_2), \quad (\text{O.3.3})$$

$$\mathcal{M}_{(1\ c)}^{\tilde{x}} = i e^2 g_s D_q \frac{p_1^{\alpha_1}}{p_1^2} \left[\bar{u}_q(p_2) \gamma^{\tilde{x}} T^a \gamma_{\alpha_1} \gamma_\mu \gamma_{\alpha_2} \sigma^{\mu\nu} \gamma_5 u_q(p_1) \right] B_\nu^{\alpha_2}(p_1), \quad (\text{O.3.4})$$

$$\mathcal{M}_{(1\ d)}^{\tilde{x}} = -i e^2 g_s D_q \frac{p_1^{\alpha_1}}{p_1^2} \left[\bar{u}_q(p_2) \gamma^{\tilde{x}} T^a \gamma_{\alpha_1} \sigma^{\mu\nu} \gamma_5 \gamma_{\alpha_2} \gamma_\mu u_q(p_1) \right] B_\nu^{\alpha_2}(p_1), \quad (\text{O.3.5})$$

$$\mathcal{M}_{(1\ e)}^{\tilde{x}} = -i e^2 g_s D_q \frac{p_2^{\alpha_2}}{p_2^2} \left[\bar{u}_q(p_2) \gamma_\mu \gamma_{\alpha_1} \sigma^{\mu\nu} \gamma_5 \gamma_{\alpha_2} \gamma^{\tilde{x}} T^a u_q(p_1) \right] B_\nu^{\alpha_1}(p_2), \quad (\text{O.3.6})$$

$$\mathcal{M}_{(1f)}^{\mathfrak{X}} = i e^2 g_s D_q \frac{p_2^{\alpha_2}}{p_2^2} \left[\bar{u}_q(p_2) \sigma^{\mu\nu} \gamma_5 \gamma_{\alpha_1} \gamma_\mu \gamma_{\alpha_2} \gamma^{\mathfrak{X}} T^a u_q(p_1) \right] B_{\nu}^{\alpha_1}(p_2), \quad (\text{O.3.7})$$

where

$$B^{\alpha\nu}(p) \equiv \int \frac{d^D k}{(2\pi)^D} \frac{(p+k)^\alpha k^\nu}{(p+k)^2 k^2}. \quad (\text{O.3.8})$$

Since we are going to compute the anomalous dimensions, we are only interested in ultra-violet (UV) divergences. The UV parts of $A^{\alpha\beta\nu}(p_1, p_2)$ and $B^{\alpha\nu}(p)$ are given by

$$\begin{aligned} A^{\alpha\beta\nu}(p_1, p_2) &= \frac{i \mu^{2\epsilon}}{(4\pi)^2 12 \hat{\epsilon}} \left[g^{\alpha\beta} (p_1 + p_2)^\nu + g^{\nu\beta} (p_1 - 2p_2)^\alpha \right. \\ &\quad \left. - g^{\nu\alpha} (p_2 - 2p_1)^\beta \right], \end{aligned} \quad (\text{O.3.9})$$

$$B^{\alpha\nu}(p) = \frac{i \mu^{2\epsilon}}{(4\pi)^2 12 \hat{\epsilon}} \left[g^{\alpha\nu} p^2 + 2 p^\nu p^\alpha \right]. \quad (\text{O.3.10})$$

Adding up all the contributions, we obtain the following total amplitude

$$\mathcal{M}_{(1)}^{\mathfrak{X}} = -i e^2 g_s D_q \left(\frac{\mu^{2\epsilon} 4}{(4\pi)^2 \hat{\epsilon}} \right) (p_1 + p_2)^{\mathfrak{X}} [\bar{u}_q(p_2) \gamma_5 T^a u_q(p_1)]. \quad (\text{O.3.11})$$

O.4 Extracting the anomalous dimension matrix

Using Eqs. (O.3.11) and the unrenormalized amplitude which is given by

$$\mathcal{M}_{(1)}^{\mathfrak{X}}|^{(0)} = -i \tilde{D}_q g_s (p_1 + p_2)^{\mathfrak{X}} [\bar{u}_q(p_2) \gamma_5 T^a u(p_1)], \quad (\text{O.4.12})$$

we obtain

$$\langle O_1^g \rangle^{(0)} = Z_{12} \langle O_2^g \rangle, \quad (\text{O.4.13})$$

where

$$Z_{12} = \frac{\alpha(\mu)}{4\pi} \frac{1}{\hat{\epsilon}} 4 \equiv \left[-\frac{1}{\hat{\epsilon}} \right] (\hat{Z}_1)_{12}(e), \quad (\text{O.4.14})$$

and $\alpha(\mu) \equiv \mu^{2\epsilon} \frac{e^2}{4\pi}$. Therefore, the anomalous dimension is given by

$$\hat{\gamma}(g) = -2 g^2 \frac{\partial \hat{Z}_1(g)}{\partial g^2}, \quad (\text{O.4.15})$$

where g in this case is the electric charge e . Finally, we get

$$\frac{\alpha(\mu)}{4\pi} (\gamma^{(2)})_{12} = -2 e^2 \frac{\partial (\hat{Z}_1)_{12}(e)}{\partial e^2} = \frac{\alpha(\mu)}{4\pi} 8, \quad (\text{O.4.16})$$

and then

$$(\gamma^{(2)})_{12} = 8, \quad (\text{O.4.17})$$

which is in perfect agreement with the results present in the literature [310].

Appendix P

Resum de la tesi

El coneixement actual sobre l'estructura de la matèria és el resultat d'un enorme esforç experimental i teòric. El nostre Univers es compon de partícules elementals governades per les quatre forces fonamentals: gravitatòries, febles, electromagnètiques i fortes.

El model estàndard (SM) de la física de partícules és la descripció teòrica més senzilla de com es relacionen aquestes partícules i forces, excepte la força gravitatòria. Al llarg dels anys, el SM ha estat capaç d'explicar totes les dades experimentals amb gran precisió, culminant en 2012 amb el descobriment del bosó de Higgs amb una massa de 125 GeV . La seua elegància, simplicitat i alta predictibilitat han convertit el SM en el millor marc de referència teòric fins ara.

Tot i ser una descripció satisfactòria de la realitat, hi ha alguns fenòmens que el SM no explica, com ara la gran asimetria de matèria-antimatèria. A l'univers prematur, el Big Bang hauria de tenir com a resultat les mateixes proporcions de matèria i antimatèria, però les observacions indiquen que tot el que ens envolta està fet de matèria excepte per una petita quantitat d'antimatèria. Un dels grans reptes de la física és entendre per què observem aquesta asimetria.

La violació de CP és un dels ingredients necessaris per a generar aquesta gran asimetria. La quantitat de violació de CP present al SM no és suficient per a obtenir completament

l'asimetria observada. Per tant, les extensions del SM amb noves fonts de violació de CP podrien explicar la proporció d'aquesta asimetria.

P.1 Objectius assolits

L'objectiu principal d'aquest treball és precisament l'estudi dels sistemes fenomenològics amb violació de CP.

Al Capítol 1, presentem una visió general del SM que mostra com sorgeixen les seues interaccions dels principis de simetria. L'última part està dedicada al sector de sabor al SM, on s'introdueixen els fenòmens de violació de CP a través de la matriu Cabibbo-Kobawashi-Maskawa (CKM). Finalment, es presenten les diferents formes en què aquest fenomen pot aparèixer a la natura.

El concepte de teoria efectiva de camps (EFT) s'introdueix al Capítol 2, proporcionant un potent marc teòric per als sistemes físics estudiats al llarg d'aquesta tesi.

La determinació teòrica de la relació directa de violació de CP ε'/ε en $K \rightarrow \pi\pi$ al SM és la primera aplicació fenomenològica presentada en aquest treball al Capítol 3. Utilitzant la teoria de pertorbacions quirals (χ PT), obtenim una predicció del SM que està d'acord amb el resultat experimental. Al Capítol 4, realitzem una actualització de la predicció anterior incloent les correccions conegudes d'isospín.

Considerant una extensió prou general del SM, el model *Aligned-Multi-Higgs-Doublet* (AMHDM), al Capítol 5, realitzem un càlcul a un *loop* de les contribucions de curta distància per a la mescla de mesons neutres. Aquesta extensió permet acomodar noves fonts de violació de CP que podrien reproduir l'asimetria observada. Finalment, restringim fortament aquestes fonts a partir de les dades de sabor actuals.

Al Capítol 6, obtenim nous límits per als moments dipolars elèctrics (EDM) dels quarks pesats *charm* i *bottom* utilitzant les equacions del grup de renormalització (RGE) junt amb els forts límits dels seus chromo-EDM.

P.2 Metodologia

La metodologia utilitzada al llarg d'aquest treball és pot trobar als Capítols 1 i 2. A continuació fem un resum dels punts més rellevants.

P.2.1 El model estàndard de la física de partícules

El model estàndard electrofeble (EWSM) és una teoria quàntica de camps basada en el grup de simetria gauge $SU(2)_L \otimes U(1)_Y$. El EWSM és capaç de descriure i unificar les interaccions electromagnètiques i dèbils a través de bosons de gauge, un fotó γ sense massa per a la interacció electromagnètica i 3 bosons massius febles, dos carregats i un neutre, W^\pm i Z^0 .

Pel que fa al sector fermiònic, aquest s'organitza en tres generacions amb propietats idèntiques. Les úniques diferències són les seues masses i els seus nombres quàntics. El contingut de partícules en cada generació s'organitza de la següent manera

- **Primera generació:** $\begin{bmatrix} \nu_e \\ e^- \end{bmatrix}_L$, $\begin{bmatrix} u \\ d' \end{bmatrix}_L$, e_R^- , u_R , d'_R
- **Segona generació:** $\begin{bmatrix} \nu_\mu \\ \mu^- \end{bmatrix}_L$, $\begin{bmatrix} c \\ s' \end{bmatrix}_L$, μ_R^- , c_R , s'_R
- **Tercera generació:** $\begin{bmatrix} \nu_\tau \\ \tau^- \end{bmatrix}_L$, $\begin{bmatrix} t \\ b' \end{bmatrix}_L$, τ_R^- , t_R , b'_R

amb les seues antipartícules corresponents. Podem observar com cada generació consta d'1 camp (1 camp de leptons) més 3 camps (1 camp de quark amb 3 colors) que transformen com a doblets de $SU(2)_L$, i a més d'1 camp (1 camp de leptons) més 6 camps (2 camps de quark amb 3 colors) que es transformen com a singlets de $SU(2)_L$.

P.2.1.1 Interaccions al model estàndard

El Lagrangianà cinètic del sector fermiònic és invariant sota transformacions globals del grup de simetria $SU(2)_L \otimes U(1)_Y$. Si volem que aquest Lagrangianà es mantinga invariant local

sota aquest grup de simetria, hem d'imposar el que es coneix com a *principi d'invariància gauge*. Aquest principi consisteix a substituir les derivades de Dirac per derivades covariants. Substituint totes les derivades fermiòniques per les seues derivades covariants corresponents, les quals venen donades per l'equació (1.1.20), s'obtenen les interaccions que constitueixen el SM, que es poden classificar com:

- **Corrents carregades:** interaccions entre fermions i els bosons W^\pm .



Figure P.1: Vèrtexs de Feynman per a les interaccions de corrents carregades.

- **Corrents neutres:** interaccions entre fermions i els bosons γ i Z^0 .



Figure P.2: Vèrtexs de Feynman per a la interacció de corrent neutra.

- **Auto-interaccions dels bosons febles:** interaccions entre els bosons γ , Z^0 i W^\pm .

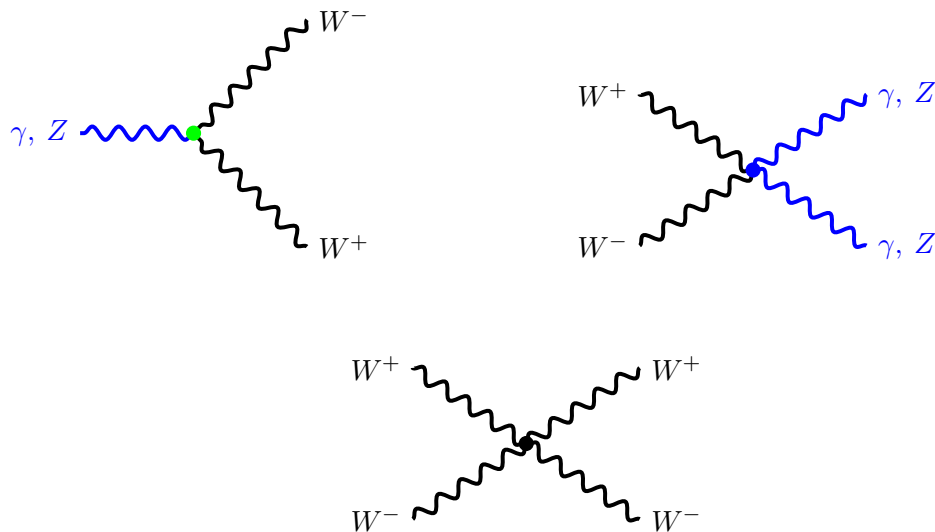


Figure P.3: Vèrtexs de Feynman per a les auto-interaccions dels bosons febles.

P.2.1.2 El mecanisme de Higgs

En l'apartat anterior, hem vist com el principi d'invariància gauge ha sigut capaç de generar totes les interaccions del SM. No obstant això, experimentalment s'observa que els bosons febles són massius. Com que la simetria de gauge no permet termes de masses per a aquests bosons, un nou ingredient és requerit per a resoldre aquest problema, el *mecanisme de Higgs*. El mecanisme de Higgs es basa en el trencament de simetria espontània (SSB) que apareix quan un sistema definit per un Lagrangiana que és simètric sota una determinada transformació, té un estat de buit que no és simètric. D'aquesta manera el bosó d'Higgs adquireix un valor esperat en el buit que indueix una ruptura espontània de la simetria electrofeble, donant lloc a les masses dels bosons W^\pm i Z^0 del SM.

P.2.1.3 Conseqüències del mecanisme de Higgs: el Lagrangia de Yukawa

El mecanisme de Higgs requereix la introducció d'un doblet escalar de $SU(2)_L$ que permet afegir nous termes invariants sota la simetria $SU(2)_L \otimes U(1)_Y$. Aquestes noves interaccions són les responsables de generar les masses de tots els fermions del SM. La diagonalització d'aquestes masses té fortes implicacions físiques que constitueixen els pilars de la física del sabor al SM,

- *Les corrents neutres no canvien sabor al SM*, conegut com el *mecanisme Glashow-Iliopoulos-Maiani* (GIM). El Lagrangia de les corrents neutres no canvia quan s'expressa en termes dels estats propis de massa.
- *Els corrents carregades són les úniques interaccions que canvien sabor al SM*. Quan expressem els estats febles del Lagrangia de corrents carregades en termes dels estats de massa, apareix una matriu unitària coneguda com la matriu CKM. Aquesta matriu és la responsable de la violació de CP al SM com veurem a continuació.

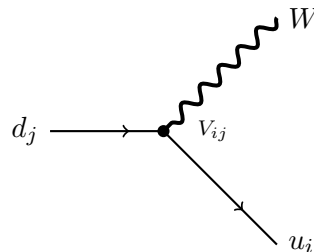


Figure P.4: Vèrtex Feynman per a les interaccions amb canvi de sabor.

P.2.1.4 La matriu CKM

A la literatura, la matriu CKM es pot trobar en diferents parametritzacions equivalents. Una d'aquestes parametritzacions és la de Wolfenstein, que inclou tres paràmetres de mescla (λ, A, ρ) i a més una fase η ; aquesta última és la responsable de descriure el fenomen de violació de CP al SM, tal com s'observa a l'equació 1.3.68. A la matriu

s'observa que les transicions diagonals (V_{ud}, V_{cs}, V_{tb}) són $\mathcal{O}(1)$, les transicions entre la primera i la segona generació (V_{us}, V_{cd}) són $\mathcal{O}(\lambda)$, les transicions entre la segona i la tercera generació (V_{cb}, V_{ts}) són $\mathcal{O}(\lambda^2)$ i les transicions entre la primera i la tercera generació (V_{ub}, V_{td}) són $\mathcal{O}(\lambda^3)$.

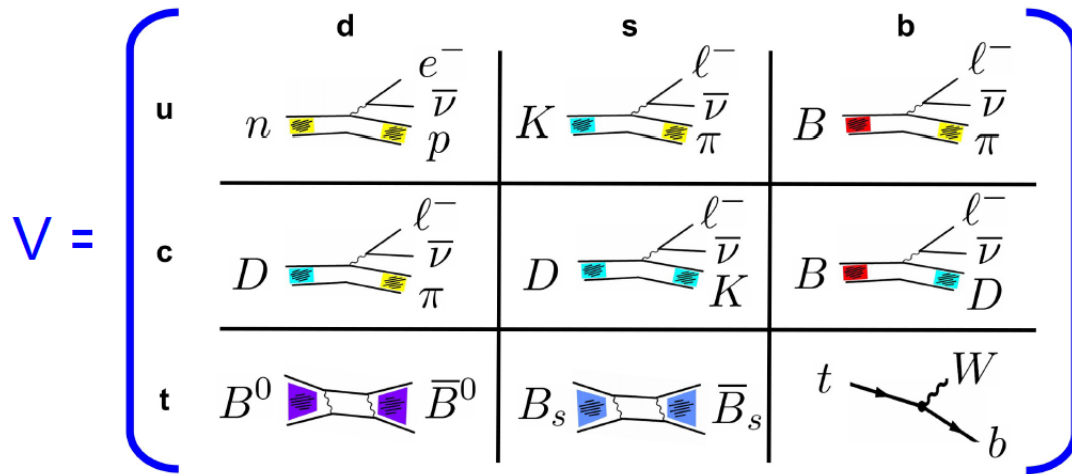


Figure P.5: Processos utilitzats per determinar els elements de la matriu CKM [29].

P.2.1.5 Unitaritat de la matriu CKM

Una de les propietats més interessants de la matriu CKM és la unitarietat. Com que aquesta ens permet provar la consistència del SM, és important determinar els elements de la matriu amb gran precisió. La determinació d'aquests elements suposa un repte perquè consisteix en l'estudi de les desintegracions hadròniques que introdueixen grans incerteses teòriques. La Figura P.5 mostra quins processos s'utilitzen per determinar els elements de la matriu CKM. Una violació de l'unitaritat podria indicar signes de nova física més enllà del SM. Per exemple, amb una quarta generació o uns quarks pesats exòtics, la submatriu 3×3 deixaria de ser unitària conduint a una determinació incorrecta d'alguns elements de la matriu CKM.

Les restriccions experimentals actuals es mostren a la Figura P.6. Un dels costats del triangle s'ha calculat utilitzant l'equació (1.3.70) a través de $|V_{ub}/V_{cb}|$ (regió verda fosca). L'altre costat es pot obtenir utilitzant la mescla $B_d^0 - B_d^0$ (regió groga), $\Delta M_d = 0.5064 \pm 0.0019 \text{ ps}^{-1}$ [31, 32]. També s'obté informació addicional de la mescla de $\Delta M_s = 17.757 \pm 0.021 \text{ ps}^{-1}$ [31, 32] i de la fracció experimental $\Delta M_d/\Delta M_s$ (regió taronja). A més, les restriccions sobre el paràmetre η es determinen a través de $K^0 \rightarrow \pi\pi$ amb el valor mesurat de $|\varepsilon_K| = (2.228 \pm 0.011) \cdot 10^{-3}$ [31] que determina la regió parabòlica de color verd clar. El mesó B^0 es desintegra als estats finals autoconjugats de CP que proporcionen maneres independents de determinar els angles del triangle d'unitaritat. Una de les desintegracions més importants és $B_d^0 \rightarrow J/\psi K_S$, que ens dóna una molt bona mesura de l'angle β , $\sin(2\beta) = 0.691 \pm 0.017$ [32]. Les determinacions dels altres dos angles α i γ , també s'inclouen en l'ajust global. Els diferents conjunts de dades encaixen molt bé i proporcionen una determinació molt precisa dels vèrtexs del triangle d'unitaritat.

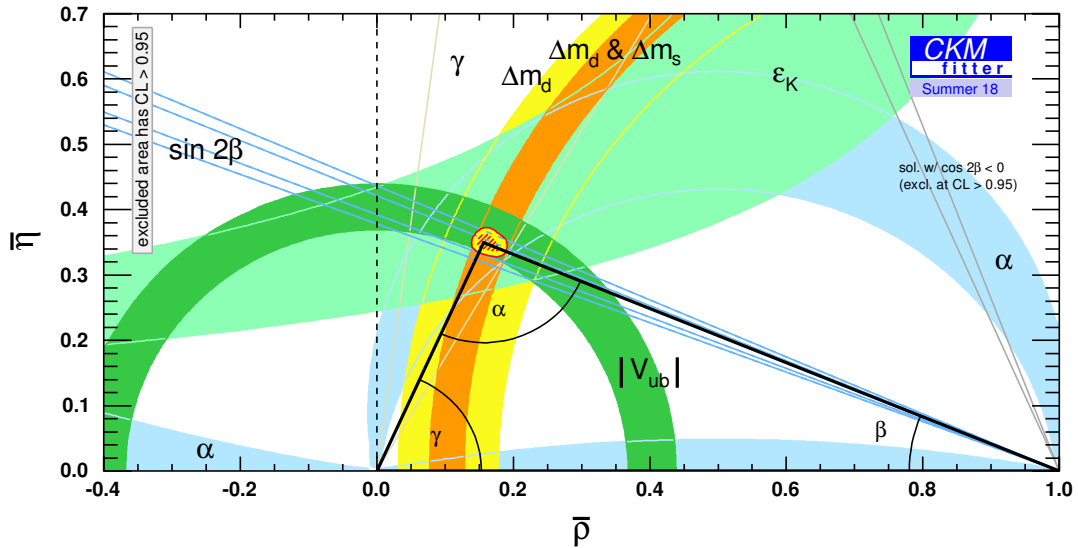


Figure P.6: Restriccions experimentals al triangle d'unitaritat del SM [28].

P.2.1.6 Tipus de violació de CP en sistemes de mesons neutres

La violació de CP apareix en sistemes de mesons neutres a través de dos tipus de fenòmens, mescla i desintegracions. A continuació fem una classificació de les tres formes de violació de CP que poden aparèixer a la natura [43].

1. **Violació de CP a la desintegració**, també coneguda com a *violació directa de CP*.
2. **Violació de CP a la mescla**, també coneguda com a *violació indirecta de CP*.
3. **Violació de CP en la interferència entre desintegració sense mescla i desintegració amb mescla**.

Les aplicacions dels Capítols 3 i 4 corresponen al primer cas, mentre que l'aplicació del Capítol 5 al segon cas.

P.2.2 Teoria de camps efectius

Una teoria de camps efectius (EFT) és una descripció simplificada d'una teoria física subjacent. La EFT proporciona un excel·lent formalisme per a descriure problemes físics que impliquen diverses escales energètiques. Aquesta es basa en utilitzar els graus de llibertat adequats per a descriure un sistema físic a una determinada escala d'energia. Per exemple, no es pot crear una partícula pesada (un grau de llibertat) a escales energètiques més petites que la seua massa, per tant no pot ser un grau de llibertat dinàmic de la teoria efectiva de baixa energia. Les EFTs funcionen millor quan hi ha una gran diferència d'energia entre l'escala que es vol estudiar i l'escala d'energia de la teoria subjacent. La dinàmica a baixes energies no depèn dels detalls de la dinàmica a altes energies, això es garanteix pel *teorema del desacoblament* [51] que indica que els graus de llibertat de les partícules pesades es desvinculen a escales energètiques molt inferiors a la seua massa. Llavors, la física d'alta energia o la física més enllà del SM se suprimeix a baixes energies. Tot sembla indicar que l'extracció d'informació sobre la teoria fonamental a les mesures de baixa energia no es possible. No obstant això, les indicacions de nova física es poden trobar

a través de petites desviacions dels paràmetres de baixa energia del Lagrangiana efectiu, ja que codifiquen la informació en termes de masses que han deixat de ser dinàmiques a eixa escala. Per tant, els experiments d'alta precisió a baixa energia es poden utilitzar per estudiar dinàmiques d'alta energia i proporcionar una alternativa als experiments d'alta energia.

P.2.2.1 Lagrangiana efectiu i comportament dels seus operadors

Un Lagrangiana efectiu es pot expressar com una suma finita d'operadors locals \mathcal{O}_i multiplicats per certs coeficients C_i :

$$\mathcal{L}_{\text{eff}} = \sum_i C_i \mathcal{O}_i . \quad (\text{P.2.1})$$

Aquests coeficients codifiquen tota la informació d'alta energia en termes de les masses pesades, mentre que els operadors \mathcal{O}_i descriuen la dinàmica a baixes energies. Els diferents operadors \mathcal{O}_i es poden classificar utilitzant anàlisi dimensional ($\hbar = c = 1$). Definint la dimensió de l'operador \mathcal{O}_i com a E^{d_i} , la dimensió dels coeficients C_i ha de ser Λ^{D-d_i} , on Λ és una escala d'alta energia. Llavors, l'acció efectiva es pot escriure com:

$$S_{\text{eff}} \equiv \int d^D x \mathcal{L}_{\text{eff}} = \sum_i c_i \left(\frac{E}{\Lambda} \right)^{d_i - D} , \quad (\text{P.2.2})$$

on c_i són constants adimensionals de $\mathcal{O}(1)$. La dependència energètica donada per l'equació (P.2.2) condueix als següents tipus d'operadors:

- $d_i > D$: aquests operadors s'anomenen irrelevants, ja que la seua contribució es feble a baixes energies. Tanmateix, això no vol dir que la seua contribució no siga important, de fet són fonamentals en alguns casos en què són l'únic tipus d'operadors que contribueixen. Aquests operadors es coneixen com a no renormalitzables.
- $d_i = D$: aquests tipus d'operadors s'anomenen marginals. Les seues contribucions no depenen de E/Λ , amb l'excepció de correccions logarítmiques. Aquests operadors corresponen a operadors renormalitzables.

- $d_i < D$: en aquest cas s'anomenen rellevants i són importants a baixes energies. En general, solen estar prohibits per simetries, ja que causen problemes degut als seus efectes a altes escales energètiques. Aquests operadors reben el nom de super-renormalitzables.

Es interessant destacar la relació entre la dimensió dels operadors i la precisió amb què volem realitzar les nostres prediccions. Per exemple, imaginem que volem calcular algun procés fenomenològic fins a un cert nivell de precisió ϵ , per tant hem de truncar el Lagrangiana per a aquells operadors amb dimensió d_i que satisfan

$$d_i \lesssim D + \frac{\ln \epsilon}{\ln \left(\frac{E}{\Lambda} \right)}, \quad (\text{P.2.3})$$

que s'obte de l'equació (P.2.2).

P.2.2.2 Un exemple de EFT: la teoria de Fermi de les interaccions febles

Per tal d'il·lustrar els aspectes generals de les EFTs, a continuació considerem un exemple de teoria efectiva al Lagrangiana de corrents carregades donat per l'equació (1.2.65). Aquest Lagrangiana juga un paper molt important en algunes de les aplicacions fenomenològiques presentades al llarg d'aquesta tesi, en particular als Capítols 3, 4 i 5. A baixes energies els bosons W^\pm deixen de ser graus de llibertat dinàmics del sistema i com a resultat obtenim una suma infinita d'operadors locals que es pot truncar a un determinat ordre, com hem vist a l'equació (P.2.1). Després de tot aquest procés, obtenim el que es coneix com la teoria de Fermi de les interaccions febles:

$$\mathcal{L}_{\text{eff}}^{\text{weak}} = -4 \frac{G_F}{\sqrt{2}} \mathcal{J}_\mu^\dagger \mathcal{J}^\mu + \mathcal{O} \left(\frac{p^2}{M_W^2} \right), \quad (\text{P.2.4})$$

on $\frac{G_F}{\sqrt{2}} \equiv \frac{g^2}{8M_W^2}$ es la constant de Fermi i

$$\mathcal{J}_\mu^\dagger = \sum_{ij} V_{ij} \bar{u}_i \gamma_\mu P_L d_j + \sum_l \bar{\nu}_l \gamma_\mu P_L l. \quad (\text{P.2.5})$$

La constant d'acoblament associada a aquest operador està suprimida per dues potències de M_W , que és el comportament típic que es troba a l'integrar els camps pesats de la teoria

fonamental. La teoria de Fermi es va proposar per a descriure les interaccions febles abans de la formulació del SM amb els seus bosons de gauge. Durant aquest temps, hi havia una forta creença que l'escala de la interacció feble hauria d'estar al voltant de $\left(\frac{\sqrt{2}}{G_F}\right)^{\frac{1}{2}} \approx 10^2$ GeV . Llavors, el descobriment dels bosons febles al voltant d'aquesta escala va ser un èxit molt important per a la comunitat de física de partícules, no sols per l'unificació d'electromagnetisme amb l'interacció feble, sinó també per la poderosa predicció a través del raonament de les EFTs.

El Lagrangià donat per l'equació (P.2.4) esta molt lluny de ser una descripció realista, ja que no té en compte les interaccions de la cromodinàmica quàntica (QCD) que són rellevants a baixes energies. Aquestes correccions s'han de tindre en compte a la nostra EFT. Les contribucions pertorbatives de QCD estan codificades pels coneguts *coeficients de Wilson* \mathcal{C}_i mentre que els efectes no pertorbatius apareixen als operadors \mathcal{O}_i , com s'observa en

$$\mathcal{L}_{\text{eff}}^{\text{weak}} = -4 \frac{G_F}{\sqrt{2}} \sum_i \lambda_i \mathcal{C}_i(\mu) \mathcal{O}_i , \quad (\text{P.2.6})$$

on λ_i conté productes d'elements de la matriu CKM. Els operadors \mathcal{O}_i es construeixen amb els graus de llibertat lleugers (camps de quarks i leptons) utilitzant els principis de simetria. En canvi, els coeficients de Wilson \mathcal{C}_i són les constants d'acoblament dels operadors \mathcal{O}_i , que ens diuen com de grans són les contribucions d'aquests operadors per a un determinat procés fenomenològic. Els coeficients de Wilson només depenen de les masses de les partícules pesades que s'han integrat. Els valors dels coeficients de Wilson es poden calcular tenint en compte que:

1. Els coeficients de Wilson \mathcal{C}_i s'han de determinar de forma pertorbativa a escales d'alta energia en alguna teoria fonamental. Això es pot fer perquè el QCD té llibertat asimptòtica.
2. Per construcció, la EFT a baixes energies té el mateix comportament infraroig que la teoria fonamental, per tant les diferències només apareixen a altes energies on la

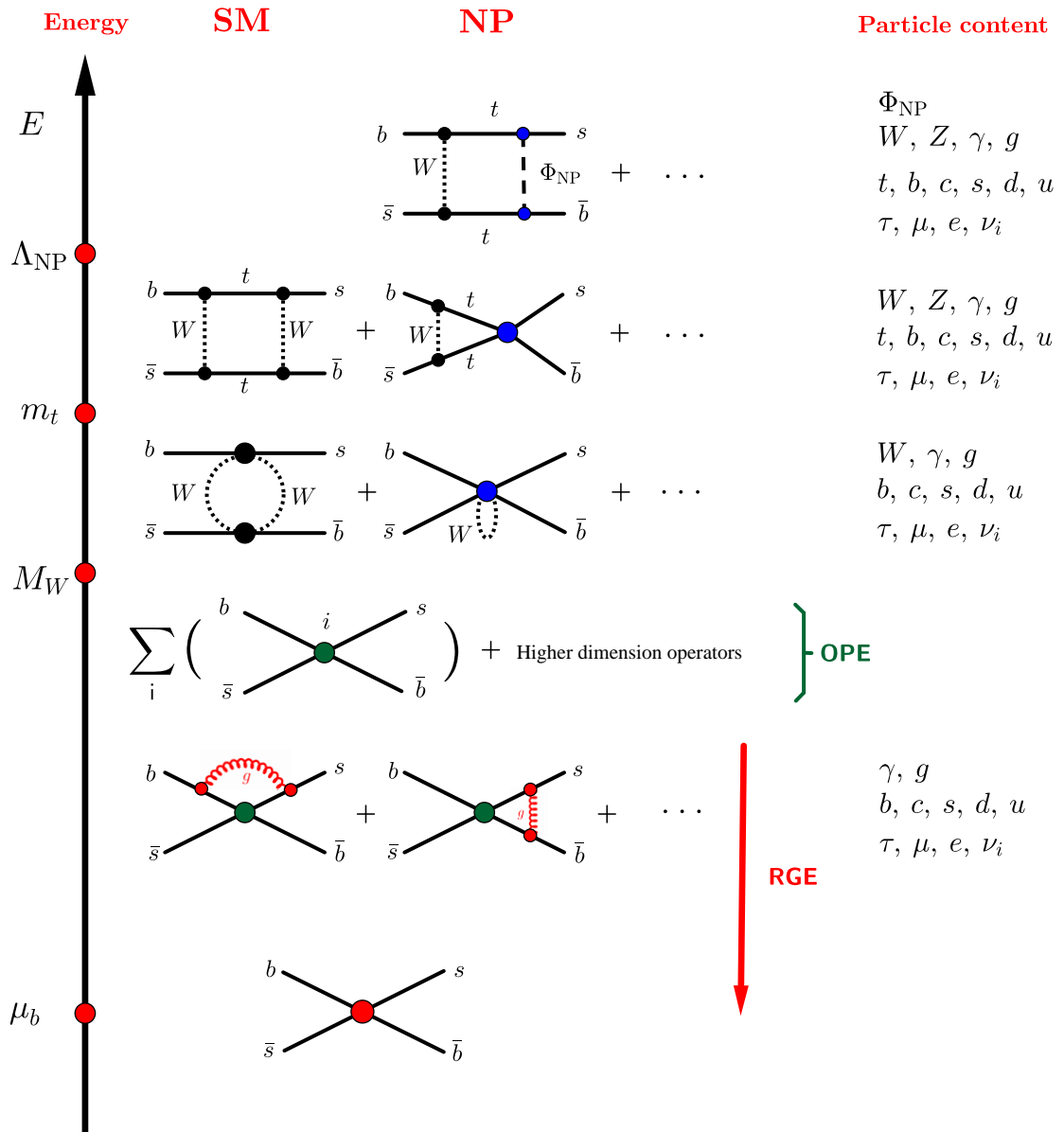


Figure P.7: Imatge de la EFT a la mescla de B_s^0 .

teoria fonamental té graus de llibertat addicionals, com per exemple camps de nova física Φ_{NP} .

3. La determinació de l'amplitud d'alguns processos fenomenològics (a través del càlcul de diagrames de Feynman) tant a la teoria efectiva com a la teoria fonamental permet determinar els coeficients de Wilson $\mathcal{C}_i(\mu_H)$ per a escales energètiques $\mu_H > M_W$ a través de la condició de *matching*:

$$\mathcal{A}_{\text{eff}} = \mathcal{A}_{\text{fun}} \longrightarrow \sum_i \lambda_i \mathcal{C}_i(\mu_H) \langle f | \mathcal{O}_i(\mu_H) | i \rangle = \sum_i \mathcal{X}_i(\mu_H) \langle f | \mathcal{O}_i(\mu_H) | i \rangle ,$$

on $|i\rangle$ and $|f\rangle$ són els estats de les partícules inicials i finals, mentre que \mathcal{X}_i són funcions que depenen de paràmetres de la teoria fonamental.

4. Finalment, utilitzant les RGEs podem transformar els coeficients de Wilson $\mathcal{C}_i(\mu_H)$ d'una escala d'alta energia $\mu_H > M_W$ en uns altres coeficients de Wilson a una escala més baixa $\mu_L \ll M_W$.

A la figura P.7, s'il·lustren els punts anteriors amb un exemple del que ocorre a la mescla de mesons B_s^0 en alguna extensió del SM amb noves partícules Φ_{NP} . S'observa com els graus de llibertat dinàmics són integrats per a energies menors que la seua massa.

P.3 Resultats i conclusions

El SM de la física de partícules es considera actualment com el marc teòric de referència de qualsevol teoria de NP perquè al llarg dels anys ha superat amb èxit un gran nombre de proves experimentals. Hem vist com les seues interaccions surten de principis de simetria de gauge i com el SSB és capaç de generar les masses dels bosons febles a través del mecanisme de Higgs. També, hem presentat el sector del sabor, introduint els fenòmens de violació de CP i les diferents formes en què apareix a la natura. Finalment, hem introduït l'enfocament EFT que proporciona un marc excel·lent per fer front als diferents sistemes físics. Les tècniques utilitzades al llarg d'aquest treball s'han il·lustrat a partir de la teoria de Fermi.

Aquesta tesi se centra en l'estudi de sistemes físics amb violació de CP. Atés que el SM de la física de partícules no és capaç de predir l'asimètrica proporció de matèria-antimatèria

observada a l'Univers, es necessiten noves fonts de violació de CP que podrien vindre d'extensions de SM.

En les següents seccions s'exposaran els resultats i les conclusions assolides en aquesta tesi doctoral. Informació detallada es pot trobar als Capítols 3, 4, 5 i 6.

P.3.1 Violació directa de CP en la desintegració de $K \rightarrow \pi\pi$

En 1988 l'experiment NA31 va presentar la primera evidència d'una violació directa de CP a les amplituds de $K^0 \rightarrow \pi\pi$. Més tard, un senyal clara amb una significança estadística de 7.2σ es va establir amb les mostres de dades completes dels experiments de NA31, E731, NA48 i KTeV, confirmant d'aquesta manera l'existència de la violació de CP associada a la transició amb canvi de sabor $\Delta S = 1$ tal com va predir el SM. No obstant això, la predicció teòrica de la relació mesurada de ε'/ε ha sigut objecte d'una forta controvèrsia al llarg dels anys. Tot i que la física subjacent ja es va aclarir en 2001, la recent actualització de les dades de lattice ha revifat de nou el debat teòric. En aquest capítol, revisem l'estat actual, es discuteix detalladament els diferents ingredients que entren en el càlcul d'aquest observable i els motius pels quals, en el passat, es van obtenir prediccions contradictòries per diversos grups. Finalment, es presenta una actualització de la predicció del SM, que està totalment d'acord amb la mesura experimental, i s'analitzen les perspectives de millora futures. El contingut d'aquest capítol es basa en Ref. [52].

P.3.2 Violació d'isospín en la desintegració de $K \rightarrow \pi\pi$

Mentre que la simetria d'isospín és una excel·lent aproximació per a la majoria d'aplicacions fenomenològiques, les violacions d'isospín induïdes per la diferència de massa de quarks $m_u - m_d$ i la interacció electromagnètica poden generar contribucions grans a alguns observables. Aquest és el cas de la relació directa de violació de CP ε'/ε , on es produeix una subtil cancel·lació numèrica entre les dues contribucions de l'isospín tal com es discuteix a la Secció 3.4. L'esforç teòric actual per predir aquest observable amb una precisió similar a l'experimental requereix una millor comprensió dels efectes de trencament

de l'isospín. El que permetria testejar diferents escenaris de nova física (NP). L'avaluació del paper de les diferents correccions d'isospín és una de les principals motivacions del Capítol 4, on duem a terme una reanàlisi de les contribucions de violació d'isospín a les amplituds de $K \rightarrow \pi\pi$. Per altra banda, presentem una revisió numèrica completa de la relació directa de violació de CP ε'/ε , on aquestes correccions tenen un paper molt important. Després d'incloure els efectes actualitzats de violació d'isospín, obtenim que la predicció de SM

$$\text{Re}(\varepsilon'/\varepsilon) = \left(13 \begin{smallmatrix} +6 \\ -7 \end{smallmatrix}\right) \cdot 10^{-4},$$

torna a estar d'acord amb la seua relació mesurada experimentalment. Com al Capítol 3, la incertesa està dominada per la nostra ignorància actual sobre contribucions suprimides d'ordre $1/N_C$ a alguns acoblaments chirals de baixa energia. El valor central de ε'/ε és lleugerament més petit que l'anterior a causa de l'augment de Ω_{eff} ,

$$\Omega_{\text{eff}} = (12.1 \begin{smallmatrix} +9.0 \\ -8.8 \end{smallmatrix}) \cdot 10^{-2}.$$

P.3.3 Mescla de mesons neutres en extensions del Model Estàndard

Al Capítol 5, presentem un càlcul complet, a un *loop*, dels coeficients de Wilson per a la mescla de mesons neutres al AMHDM on contemplem la possibilitat d'ampliar els $N - 1$ doblets de Higgs a octets escalars de color. Aquest tipus de procés apareix a nivell de *loop* al SM, per tant la mescla de mesons neutres és molt sensible a les contribucions de NP. Finalment, particularitzant els nostres resultats analítics a l'ampla casuística de models de NP i utilitzant les dades experimentals de les factories de sabor actuals, hem obtingut restriccions combinades per als paràmetres que caracteritzen aquests models.

P.3.4 Millora als moments dipolars electrics dels quarks pesats

A l'última aplicació que es pot trobar al Capítol 6, ens centrem a l'estudi dels EDMs dels quarks pesats. L'acoblament del EDM d'un quark produeix una contribució al chromo-EDM mitjançant diagrames a un *loop* de fotons. Incloent aquestes correccions en les RGE

i utilitzant els estrictes límits dels seus chromo-EDMs, hem obtingut els següents límits als EDMs dels quarks *charm* i *bottom*.

$$|d_c(m_c)| < 1.5 \times 10^{-21} e \text{ cm} ,$$

$$|d_b(m_b)| < 1.2 \times 10^{-20} e \text{ cm} ,$$

que milloren els anteriors en tres ordres de magnitud. Aquests nous límits podrien restringir fortament algunes de les extensions proposades per al SM.

Acknowledgements

Hi ha moltes persones que han fet possible que haja pogut aplegar fins ací. Una d'elles ha sigut el meu director de tesi, Toni. La teua tasca com a docent durant el grau i més tard al màster van fer possible que aflorara el meu interés per la física de partícules. Des del primer moment, sempre has estat disposat a ajudar-me en tot el que em fera falta. Moltes gràcies també per donar-me l'oportunitat de realitzar aquesta tesi amb finançament econòmic.

En segon lloc, volia donar-li les gràcies als meus pares, Ramon i Leo. M'havau ensenyat que lluitant amb constància es pot aconseguir tot el que un es proposa. Gràcies als vostres esforços i els vostres sacrificis sóc la persona que sóc.

Moltes gràcies també al meu germà. Ramon, recordes aquella nit a la terrassa de casa quan et vaig confessar que el que realment m'agradava era la física? Si no li ho hagueres dit aquella mateixa nit a la mare, segurament ara mateixa seria un químic frustrat.

Als meus avis que des de menut m'han estimat, i a tota la meua família que amb l'estima demostrada m'han ajudat en tots els moments a seguir endavant.

Durant el grau de física, vaig tindre l'oportunitat de conèixer a molta gent. M'agradaria donar-li les gràcies a Antonio Sánchez, Berna, Faisel, Juanjo, Masià, Òscar, Pacocha, Ponce, Rosello i Yanis. Més tard al màster, Òscar i jo vàrem conèixer a Carlos Sánchez i Clara Remón. El bon record que guarde d'aquells temps va ser en gran part gràcies a ells. Antonio Sánchez, Carlos Sánchez, Clara Remón i Òscar no hi ha suficients pàgines per a agrair-vos tot el que heu fet per mi. Tots els moments que hem viscut al pis, les tonteries, les cerveses, etc. Moltes gràcies!

De forma especial, me gustaría darle las gracias a Antonio Sánchez. Durante todos estos años hemos alcanzado una amistad que el tiempo no podrá erosionar. Muchas gracias por estar ahí siempre que te he necesitado, y también por todas aquellas noches que como unos yonkis estudiábamos física hasta las tantas de la madrugada, alternadas con paseos y videojuegos. Parte de lo que he conseguido es gracias a ti. O.W.

Ja fa més de dos anys que vaig conèixer a una persona molt especial, la meua companya de viatge, que per ironies de la vida havia de ser química. Laura, moltes gràcies per creuar-te al meu camí. Durant aquests anys m'has completat com a persona en molts aspectes i m'has ensenyat a ser una persona millor. Gràcies també per acceptar-me tal com sóc i per compartir-me amb la física. T'estime!

Als amics de Castalla, moltes gràcies per tots eixos bons moments de rialles i cerveses (i algun que altre cubata) quan he baixat, després de molts mesos, al poble. A pesar del temps que he estat fora, sempre m'heu tractat com un mes i eixa bona sensació quan “torne a casa” en part és gràcies a vosaltres.

También me gustaría darle las gracias a Antonio Rodríguez, por su ayuda incondicional desde el primer día que llegue al grupo. Durante estos años, he disfrutado muchísimo trabajando contigo.

Gràcies a Ana, Fernando, Ivan, Joan, Mario i Victor, per tots eixos moments que hem compartit a l'IFIC prenent café mentre parlàvem de física. D'una forma especial a Joan, gràcies també per compartir amb mi el teu interès pels moments dipolars elèctrics. Durant aquest últim any he gaudit moltíssim col·laborant amb tu.

També, volia agrair a tots els membres que formen el “Escuadron IFIC”. Gràcies per totes eixes estones de rialles i “cachondeo” a l'hora de dinar.

Many thanks to Vincenzo Cirigliano for all his help and advices throughout our project. Finally, I would like to thank Ulrich Nierste for his hospitality during my research stay at Karlsruhe Institute of Technology (KIT).

I com estic segur que he oblidat a més d'un, moltes gràcies a tots aquells que de forma voluntària o involuntària han fet possible aquesta tesi.

Bibliography

- [1] A. Pich, “The Standard Model of Electroweak Interactions,” arXiv:1201.0537 [hep-ph].
- [2] A. Pich, “Flavour Dynamics and Violations of the CP Symmetry,” arXiv:1805.08597 [hep-ph].
- [3] A. Pich, “Quantum chromodynamics,” [hep-ph/9505231].
- [4] G. C. Branco, L. Lavoura and J. P. Silva, “CP Violation,” Int. Ser. Monogr. Phys. **103** (1999) 1.
- [5] M. Herrero, “The Standard model,” NATO Sci. Ser. C **534** (1999) 1 [hep-ph/9812242].
- [6] D. J. Gross and F. Wilczek, Phys. Rev. Lett. **30** (1973) 1343.
- [7] S. Weinberg, Phys. Rev. Lett. **31** (1973) 494.
- [8] H. Fritzsch, M. Gell-Mann and H. Leutwyler, Phys. Lett. **47B** (1973) 365.
- [9] H. D. Politzer, Phys. Rev. Lett. **30** (1973) 1346. doi:10.1103/PhysRevLett.30.1346
- [10] P. Pascual and R. Tarrach, Lect. Notes Phys. **194** (1984) 1.
- [11] A. Pich, “Aspects of quantum chromodynamics,” hep-ph/0001118.
- [12] S. Scherer and M. R. Schindler, hep-ph/0505265.

-
- [13] S. Weinberg, "A Model of Leptons," *Phys. Rev. Lett.* **19** (1967) 1264.
- [14] S. L. Glashow, "Partial Symmetries of Weak Interactions," *Nucl. Phys.* **22** (1961) 579.
- [15] A. Salam, "Weak and Electromagnetic Interactions," *Conf. Proc. C* **680519** (1968) 367.
- [16] J. Goldstone, "Field Theories with Superconductor Solutions," *Nuovo Cim.* **19** (1961) 154.
- [17] J. Goldstone, A. Salam and S. Weinberg, "Broken Symmetries," *Phys. Rev.* **127** (1962) 965.
- [18] P. W. Higgs, "Broken Symmetries and the Masses of Gauge Bosons," *Phys. Rev. Lett.* **13** (1964) 508.
- [19] F. Englert and R. Brout, "Broken Symmetry and the Mass of Gauge Vector Mesons," *Phys. Rev. Lett.* **13** (1964) 321.
- [20] G. S. Guralnik, C. R. Hagen and T. W. B. Kibble, "Global Conservation Laws and Massless Particles," *Phys. Rev. Lett.* **13** (1964) 585.
- [21] S. L. Glashow, J. Iliopoulos and L. Maiani, "Weak Interactions with Lepton-Hadron Symmetry," *Phys. Rev. D* **2** (1970) 1285.
- [22] E. Majorana, "Teoria simmetrica dell'elettrone e del positrone," *Nuovo Cim.* **14** (1937) 171.
- [23] N. Cabibbo, "Unitary Symmetry and Leptonic Decays," *Phys. Rev. Lett.* **10** (1963) 531.
- [24] M. Kobayashi and T. Maskawa, "CP Violation in the Renormalizable Theory of Weak Interaction," *Prog. Theor. Phys.* **49** (1973) 652.

- [25] L. L. Chau and W. Y. Keung, “Comments on the Parametrization of the Kobayashi-Maskawa Matrix,” *Phys. Rev. Lett.* **53** (1984) 1802.
- [26] L. Wolfenstein, “Parametrization of the Kobayashi-Maskawa Matrix,” *Phys. Rev. Lett.* **51** (1983) 1945.
- [27] A. J. Buras, M. E. Lautenbacher and G. Ostermaier, *Phys. Rev. D* **50** (1994) 3433 [hep-ph/9403384].
- [28] J. Charles *et al.* [CKMfitter Group], *Eur. Phys. J. C* **41** (2005) no.1, 1 [hep-ph/0406184].
- [29] S. Gori, CERN-2018-008-SP, pp. 65-90 [arXiv:1610.02629 [hep-ph]].
- [30] C. Jarlskog, *Phys. Rev. Lett.* **55** (1985) 1039.
- [31] M. Tanabashi *et al.* [Particle Data Group], *Phys. Rev. D* **98** (2018) no.3, 030001.
- [32] Y. Amhis *et al.* [HFLAV Collaboration], *Eur. Phys. J. C* **77** (2017) no.12, 895 [arXiv:1612.07233 [hep-ex]].
- [33] T. Inami and C. S. Lim, *Prog. Theor. Phys.* **65** (1981) 297 Erratum: [*Prog. Theor. Phys.* **65** (1981) 1772].
- [34] P. Breitenlohner and D. Maison, “Dimensional Renormalization and the Action Principle”, *Commun. Math. Phys.* **52** (1977) 11.
- [35] P. Breitenlohner and D. Maison, “Dimensionally Renormalized Green’s Functions for Theories with Massless Particles. 1.”, *Commun. Math. Phys.* **52** (1977) 39.
- [36] P. Breitenlohner and D. Maison, “Dimensionally Renormalized Green’s Functions for Theories with Massless Particles. 2.”, *Commun. Math. Phys.* **52** (1977) 55.
- [37] A. J. Buras, M. Jamin and P. H. Weisz, *Nucl. Phys. B* **347** (1990) 491.
- [38] J. Urban, F. Krauss, U. Jentschura and G. Soff, *Nucl. Phys. B* **523** (1998) 40 [hep-ph/9710245].

-
- [39] S. Herrlich and U. Nierste, Nucl. Phys. B **419** (1994) 292 [hep-ph/9310311].
- [40] S. Herrlich and U. Nierste, Phys. Rev. D **52** (1995) 6505 [hep-ph/9507262].
- [41] S. Herrlich and U. Nierste, Nucl. Phys. B **476** (1996) 27 [hep-ph/9604330].
- [42] A. J. Buras, W. Slominski and H. Steger, Nucl. Phys. B **245** (1984) 369.
doi:10.1016/0550-3213(84)90437-1
- [43] Y. Nir, hep-ph/0510413.
- [44] E. Fermi, Z. Phys. **88** (1934) 161.
- [45] A. V. Manohar, Lect. Notes Phys. **479** (1997) 311 [hep-ph/9606222].
- [46] M. Neubert, arXiv:1901.06573 [hep-ph].
- [47] M. Neubert, hep-ph/0512222.
- [48] A. Pich, hep-ph/9806303.
- [49] G. Buchalla, A. J. Buras and M. E. Lautenbacher, Rev. Mod. Phys. **68** (1996) 1125
[hep-ph/9512380].
- [50] A. J. Buras, “Weak Hamiltonian, CP violation and rare decays,” hep-ph/9806471.
- [51] T. Appelquist and J. Carazzone, Phys. Rev. D **11** (1975) 2856.
- [52] H. Gisbert and A. Pich, Rept. Prog. Phys. **81** (2018) no.7, 076201 doi:10.1088/1361-6633/aac18e [arXiv:1712.06147 [hep-ph]].
- [53] V. Cirigliano, G. Ecker, H. Neufeld, A. Pich and J. Portolés, “Kaon Decays in the Standard Model”, *Rev. Mod. Phys.* **84** (2012) 399.
- [54] M. Gell-Mann, “Isotopic Spin and New Unstable Particles”, Phys. Rev. **92** (1953) 833.
- [55] A. Pais, “Some Remarks on the V-Particles”, Phys. Rev. **86** (1952) 663.

- [56] R. H. Dalitz, “Decay of tau mesons of known charge”, *Phys. Rev.* **94** (1954) 1046.
- [57] T. D. Lee and C. N. Yang, “Question of Parity Conservation in Weak Interactions”, *Phys. Rev.* **104** (1956) 254.
- [58] M. Gell-Mann and A. Pais, “Behavior of neutral particles under charge conjugation”, *Phys. Rev.* **97** (1955) 1387.
- [59] J. H. Christenson, J. W. Cronin, V. L. Fitch and R. Turlay, “Evidence for the 2π Decay of the K_2^0 Meson”, *Phys. Rev. Lett.* **13** (1964) 138.
- [60] G. D. Rochester and C. C. Butler, “Evidence for the Existence of New Unstable Elementary Particles”, *Nature* **160** (1947) 855.
- [61] M. K. Gaillard and B. W. Lee, “Rare Decay Modes of the K-Mesons in Gauge Theories”, *Phys. Rev. D* **10** (1974) 897.
- [62] A. J. Buras and M. K. Harlander, “A Top quark story: Quark mixing, CP violation and rare decays in the standard model”, *Adv. Ser. Direct. High Energy Phys.* **10** (1992) 58.
- [63] C. Patrignani *et al.* [Particle Data Group], “Review of Particle Physics”, *Chin. Phys. C* **40** (2016) no.10, 100001.
- [64] H. Burkhardt *et al.* [NA31 Collaboration], “First Evidence for Direct CP Violation”, *Phys. Lett. B* **206** (1988) 169.
- [65] G. D. Barr *et al.* [NA31 Collaboration], “A New measurement of direct CP violation in the neutral kaon system”, *Phys. Lett. B* **317** (1993) 233.
- [66] V. Fanti *et al.* [NA48 Collaboration], “A New measurement of direct CP violation in two pion decays of the neutral kaon”, *Phys. Lett. B* **465** (1999) 335 [hep-ex/9909022].
- [67] A. Lai *et al.* [NA48 Collaboration], “A Precise measurement of the direct CP violation parameter $\text{Re}(\varepsilon'/\varepsilon)$ ”, *Eur. Phys. J. C* **22** (2001) 231 [hep-ex/0110019].

- [68] J. R. Batley *et al.* [NA48 Collaboration], “A Precision measurement of direct CP violation in the decay of neutral kaons into two pions”, *Phys. Lett. B* **544** (2002) 97 [hep-ex/0208009].
- [69] L. K. Gibbons *et al.* [E731 Collaboration], “Measurement of the CP violation parameter $\text{Re}(\varepsilon'/\varepsilon)$ ”, *Phys. Rev. Lett.* **70** (1993) 1203.
- [70] A. Alavi-Harati *et al.* [KTeV Collaboration], “Observation of direct CP violation in $K_{S,L} \rightarrow \pi\pi$ decays”, *Phys. Rev. Lett.* **83** (1999) 22 [hep-ex/9905060].
- [71] A. Alavi-Harati *et al.* [KTeV Collaboration], “Measurements of direct CP violation, CPT symmetry, and other parameters in the neutral kaon system”, *Phys. Rev. D* **67** (2003) 012005 [*Erratum-ibid.* *D* **70** (2004) 079904] [hep-ex/0208007].
- [72] E. Abouzaid *et al.* [KTeV Collaboration], “Precise Measurements of Direct CP Violation, CPT Symmetry, and Other Parameters in the Neutral Kaon System”, *Phys. Rev. D* **83** (2011) 092001 [arXiv:1011.0127 [hep-ex]].
- [73] F. J. Gilman and M. B. Wise, “The $\Delta I = 1/2$ Rule and Violation of CP in the Six Quark Model”, *Phys. Lett.* **83B** (1979) 83.
- [74] G. Buchalla, A. J. Buras and M. K. Harlander, “The Anatomy of ε'/ε in the Standard Model”, *Nucl. Phys. B* **337** (1990) 313.
- [75] A. J. Buras, M. Jamin and M. E. Lautenbacher, “The Anatomy of ε'/ε beyond leading logarithms with improved hadronic matrix elements”, *Nucl. Phys. B* **408** (1993) 209 [hep-ph/9303284].
- [76] A. J. Buras, M. Jamin and M. E. Lautenbacher, “A 1996 analysis of the CP violating ratio ε'/ε ”, *Phys. Lett. B* **389** (1996) 749 [hep-ph/9608365].
- [77] S. Bosch, A. J. Buras, M. Gorbahn, S. Jager, M. Jamin, M. E. Lautenbacher and L. Silvestrini, “Standard model confronting new results for ε'/ε ”, *Nucl. Phys. B* **565** (2000) 3 [hep-ph/9904408].

- [78] A. J. Buras, P. Gambino, M. Gorbahn, S. Jager and L. Silvestrini, “ ε'/ε and rare K and B decays in the MSSM”, *Nucl. Phys. B* **592** (2001) 55 [hep-ph/0007313].
- [79] M. Ciuchini, E. Franco, G. Martinelli, L. Reina and L. Silvestrini, “An Upgraded analysis of ε'/ε at the next-to-leading order”, *Z. Phys. C* **68** (1995) 239 [hep-ph/9501265].
- [80] M. Ciuchini, E. Franco, G. Martinelli and L. Reina, “ ε'/ε at the Next-to-leading order in QCD and QED”, *Phys. Lett. B* **301** (1993) 263 [hep-ph/9212203].
- [81] S. Bertolini, J. O. Eeg and M. Fabbrichesi, “A New estimate of ε'/ε ”, *Nucl. Phys. B* **476** (1996) 225 [hep-ph/9512356].
- [82] S. Bertolini, J. O. Eeg, M. Fabbrichesi and E. I. Lashin, “ ε'/ε at $O(p^4)$ in the chiral expansion”, *Nucl. Phys. B* **514** (1998) 93 [hep-ph/9706260].
- [83] S. Bertolini, M. Fabbrichesi and J. O. Eeg, “Theory of the CP violating parameter ε'/ε ”, *Rev. Mod. Phys.* **72** (2000) 65 [hep-ph/9802405].
- [84] S. Bertolini, J. O. Eeg and M. Fabbrichesi, “An Updated analysis of ε'/ε in the standard model with hadronic matrix elements from the chiral quark model”, *Phys. Rev. D* **63** (2001) 056009 [hep-ph/0002234].
- [85] T. Hambye, G. O. Kohler, E. A. Paschos and P. H. Soldan, “Analysis of ε'/ε in the $1/N_c$ expansion”, *Nucl. Phys. B* **564** (2000) 391 [hep-ph/9906434].
- [86] E. Pallante and A. Pich, “Strong enhancement of ε'/ε through final state interactions”, *Phys. Rev. Lett.* **84** (2000) 2568 [hep-ph/9911233].
- [87] E. Pallante and A. Pich, “Final state interactions in kaon decays”, *Nucl. Phys. B* **592** (2001) 294 [hep-ph/0007208].
- [88] E. Pallante, A. Pich and I. Scimemi, “The Standard model prediction for ε'/ε ”, *Nucl. Phys. B* **617** (2001) 441 [hep-ph/0105011].

- [89] J. Bijnens and J. Prades, “ ϵ'_K/ϵ_K in the chiral limit”, JHEP **0006** (2000) 035 [hep-ph/0005189].
- [90] T. Hambye, S. Peris and E. de Rafael, “ $\Delta I = 1/2$ and ϵ'/ϵ in large N_C QCD”, JHEP **0305** (2003) 027 [hep-ph/0305104].
- [91] A. J. Buras and M. Jamin, “ ϵ'/ϵ at the NLO: 10 years later”, JHEP **0401** (2004) 048 [hep-ph/0306217].
- [92] A. Pich, “ ϵ'/ϵ in the standard model: Theoretical update”, hep-ph/0410215.
- [93] L. Maiani and M. Testa, “Final state interactions from Euclidean correlation functions”, Phys. Lett. B **245** (1990) 585.
- [94] D. Pekurovsky and G. Kilcup, “Matrix elements relevant for $\Delta I = 1/2$ rule and ϵ'/ϵ from lattice QCD with staggered fermions”, Phys. Rev. D **64** (2001) 074502 [hep-lat/9812019].
- [95] J. I. Noaki *et al.* [CP-PACS Collaboration], “Calculation of nonleptonic kaon decay amplitudes from $K \rightarrow \pi$ matrix elements in quenched domain wall QCD”, Phys. Rev. D **68** (2003) 014501 [hep-lat/0108013].
- [96] T. Blum *et al.* [RBC Collaboration], “Kaon matrix elements and CP violation from quenched lattice QCD: 1. The three flavor case”, Phys. Rev. D **68** (2003) 114506 [hep-lat/0110075].
- [97] T. Bhattacharya, G. T. Fleming, R. Gupta, G. Kilcup, W. Lee and S. R. Sharpe, “Calculating ϵ'/ϵ using HYP staggered fermions”, Nucl. Phys. Proc. Suppl. **140** (2005) 369 [hep-lat/0409046].
- [98] T. Blum *et al.*, T. Blum *et al.* [RBC and UKQCD Collaborations], “The $K \rightarrow (\pi\pi)_{I=2}$ Decay Amplitude from Lattice QCD”, Phys. Rev. Lett. **108** (2012) 141601; [arXiv:1111.1699 [hep-lat]];

- [99] T. Blum *et al.* [RBC and UKQCD Collaborations], “Lattice determination of the $K \rightarrow (\pi\pi)_{I=2}$ Decay Amplitude A_2 ”, *Phys. Rev. D* **86** (2012) 074513 [arXiv:1206.5142 [hep-lat]].
- [100] T. Blum *et al.*, “ $K \rightarrow \pi\pi$ $\Delta I = 3/2$ decay amplitude in the continuum limit”, *Phys. Rev. D* **91** (2015) no.7, 074502 [arXiv:1502.00263 [hep-lat]].
- [101] P. A. Boyle *et al.* [RBC and UKQCD Collaborations], “Emerging understanding of the $\Delta I = 1/2$ Rule from Lattice QCD”, *Phys. Rev. Lett.* **110** (2013) 152001 [arXiv:1212.1474 [hep-lat]].
- [102] A. Pich and E. de Rafael, “Weak K amplitudes in the chiral and $1/N_c$ expansions”, *Phys. Lett. B* **374** (1996) 186 [hep-ph/9511465].
- [103] A. Pich and E. de Rafael, “Four quark operators and nonleptonic weak transitions”, *Nucl. Phys. B* **358** (1991) 311.
- [104] M. Jamin and A. Pich, “QCD corrections to inclusive $\Delta S = 1, 2$ transitions at the next-to-leading order”, *Nucl. Phys. B* **425** (1994) 15 [hep-ph/9402363].
- [105] S. Bertolini, J. O. Eeg, M. Fabbrichesi and E. I. Lashin, “The $\Delta I = 1/2$ rule and B_K at $O(p^4)$ in the chiral expansion”, *Nucl. Phys. B* **514** (1998) 63 [hep-ph/9705244].
- [106] V. Antonelli, S. Bertolini, J. O. Eeg, M. Fabbrichesi and E. I. Lashin, “The $\Delta S = 1$ weak chiral lagrangian as the effective theory of the chiral quark model”, *Nucl. Phys. B* **469** (1996) 143 [hep-ph/9511255];
- [107] V. Antonelli, S. Bertolini, M. Fabbrichesi and E. I. Lashin, “The $\Delta I = 1/2$ selection rule”, *Nucl. Phys. B* **469** (1996) 181 [hep-ph/9511341].
- [108] T. Hambye, G. O. Kohler, E. A. Paschos, P. H. Soldan and W. A. Bardeen, “ $1/N_c$ corrections to the hadronic matrix elements of Q_6 and Q_8 in $K \rightarrow \pi\pi$ decays”, *Phys. Rev. D* **58** (1998) 014017 [hep-ph/9802300].

- [109] W. A. Bardeen, A. J. Buras and J. M. Gerard, “A Consistent Analysis of the $\Delta I = 1/2$ Rule for K Decays”, *Phys. Lett. B* **192** (1987) 138.
- [110] A. J. Buras, J. M. Gerard and W. A. Bardeen, “Large N Approach to Kaon Decays and Mixing 28 Years Later: $\Delta I = 1/2$ Rule, \hat{B}_K and ΔM_K ”, *Eur. Phys. J. C* **74** (2014) 2871 [arXiv:1401.1385 [hep-ph]].
- [111] J. Bijnens and J. Prades, “The Delta I = 1/2 rule in the chiral limit”, *JHEP* **9901** (1999) 023 [hep-ph/9811472].
- [112] N. Ishizuka, K.-I. Ishikawa, A. Ukawa and T. Yoshié, “Calculation of $K \rightarrow \pi\pi$ decay amplitudes with improved Wilson fermion action in lattice QCD”, *Phys. Rev. D* **92** (2015) no.7, 074503 [arXiv:1505.05289 [hep-lat]].
- [113] Z. Bai *et al.* [RBC and UKQCD Collaborations], “Standard Model Prediction for Direct CP Violation in $K \rightarrow \pi\pi$ Decay”, *Phys. Rev. Lett.* **115** (2015) no.21, 212001 [arXiv:1505.07863 [hep-lat]].
- [114] A. J. Buras and J. M. Gérard, “Upper bounds on ε'/ε parameters $B_6^{(1/2)}$ and $B_8^{(3/2)}$ from large N QCD and other news”, *JHEP* **1512** (2015) 008 [arXiv:1507.06326 [hep-ph]].
- [115] A. J. Buras and J. M. Gerard, “Final state interactions in $K \rightarrow \pi\pi$ decays: $\Delta I = 1/2$ rule vs. ε'/ε ”, *Eur. Phys. J. C* **77** (2017) no.1, 10 [arXiv:1603.05686 [hep-ph]].
- [116] A. J. Buras, M. Gorbahn, S. Jäger and M. Jamin, “Improved anatomy of ε'/ε in the Standard Model”, *JHEP* **1511** (2015) 202 [arXiv:1507.06345 [hep-ph]].
- [117] A. J. Buras, F. De Fazio and J. Girschbach, “ $\Delta I = 1/2$ rule, ε'/ε and $K \rightarrow \pi\nu\bar{\nu}$ in $Z'(Z)$ and G' models with FCNC quark couplings”, *Eur. Phys. J. C* **74** (2014) no.7, 2950 [arXiv:1404.3824 [hep-ph]].
- [118] A. J. Buras, D. Buttazzo and R. Knegjens, “ $K \rightarrow \pi\nu\bar{\nu}$ and ε'/ε in simplified new physics models”, *JHEP* **1511** (2015) 166 [arXiv:1507.08672 [hep-ph]].

- [119] M. Blanke, A. J. Buras and S. Recksiegel, “Quark flavour observables in the Littlest Higgs model with T-parity after LHC Run 1”, *Eur. Phys. J. C* **76** (2016) no.4, 182 [arXiv:1507.06316 [hep-ph]].
- [120] A. J. Buras and F. De Fazio, “ ϵ'/ϵ in 331 Models”, *JHEP* **1603** (2016) 010 [arXiv:1512.02869 [hep-ph]].
- [121] A. J. Buras and F. De Fazio, “331 Models Facing the Tensions in $\Delta F = 2$ Processes with the Impact on ϵ'/ϵ , $B_s \rightarrow \mu^+ \mu^-$ and $B \rightarrow K^* \mu^+ \mu^-$ ”, *JHEP* **1608** (2016) 115 [arXiv:1604.02344 [hep-ph]].
- [122] A. J. Buras, “New physics patterns in ϵ'/ϵ and ϵ_K with implications for rare kaon decays and ΔM_K ”, *JHEP* **1604** (2016) 071 [arXiv:1601.00005 [hep-ph]].
- [123] T. Kitahara, U. Nierste and P. Tremper, “Supersymmetric Explanation of CP Violation in $K \rightarrow \pi\pi$ Decays”, *Phys. Rev. Lett.* **117** (2016) no.9, 091802 [arXiv:1604.07400 [hep-ph]].
- [124] T. Kitahara, U. Nierste and P. Tremper, “Singularity-free next-to-leading order $\Delta S = 1$ renormalization group evolution and ϵ'_K/ϵ_K in the Standard Model and beyond”, *JHEP* **1612** (2016) 078 [arXiv:1607.06727 [hep-ph]].
- [125] M. Endo, S. Mishima, D. Ueda and K. Yamamoto, “Chargino contributions in light of recent ϵ'/ϵ ”, *Phys. Lett. B* **762** (2016) 493 [arXiv:1608.01444 [hep-ph]].
- [126] M. Endo, T. Kitahara, S. Mishima and K. Yamamoto, “Revisiting Kaon Physics in General Z Scenario”, *Phys. Lett. B* **771** (2017) 37 [arXiv:1612.08839 [hep-ph]].
- [127] V. Cirigliano, W. Dekens, J. de Vries and E. Mereghetti, “An ϵ' improvement from right-handed currents”, *Phys. Lett. B* **767** (2017) 1 [arXiv:1612.03914 [hep-ph]].
- [128] S. Alioli, V. Cirigliano, W. Dekens, J. de Vries and E. Mereghetti, “Right-handed charged currents in the era of the Large Hadron Collider”, *JHEP* **1705** (2017) 086 [arXiv:1703.04751 [hep-ph]].

- [129] C. Bobeth, A. J. Buras, A. Celis and M. Jung, “Patterns of Flavour Violation in Models with Vector-Like Quarks”, JHEP **1704** (2017) 079 [arXiv:1609.04783 [hep-ph]].
- [130] C. Bobeth, A. J. Buras, A. Celis and M. Jung, “Yukawa enhancement of Z -mediated new physics in $\Delta S = 2$ and $\Delta B = 2$ processes”, JHEP **1707** (2017) 124 [arXiv:1703.04753 [hep-ph]].
- [131] A. Crivellin, G. D’Ambrosio, T. Kitahara and U. Nierste, “ $K \rightarrow \pi\nu\bar{\nu}$ in the MSSM in light of the ϵ'_K/ϵ_K anomaly”, Phys. Rev. D **96** (2017) no.1, 015023 [arXiv:1703.05786 [hep-ph]].
- [132] V. Chobanova, G. D’Ambrosio, T. Kitahara, M. Lucio Martinez, D. Martinez Santos, I. S. Fernandez and K. Yamamoto, “Probing SUSY effects in $K_S^0 \rightarrow \mu^+\mu^-$ ”, arXiv:1711.11030 [hep-ph].
- [133] C. Bobeth and A. J. Buras, “Leptoquarks meet ϵ'/ϵ and rare Kaon processes”, arXiv:1712.01295 [hep-ph].
- [134] M. Endo, T. Goto, T. Kitahara, S. Mishima, D. Ueda and K. Yamamoto, “Gluino-mediated electroweak penguin with flavor-violating trilinear couplings”, arXiv:1712.04959 [hep-ph].
- [135] C. H. Chen and T. Nomura, “ ϵ_K and ϵ'/ϵ in a diquark model”, arXiv:1808.04097 [hep-ph].
- [136] J. Aebischer *et al.*, “Master formula for ϵ'/ϵ beyond the Standard Model”, arXiv:1807.02520 [hep-ph].
- [137] J. Aebischer, A. J. Buras and J. M. Gérard, “BSM Hadronic Matrix Elements for ϵ'/ϵ and $K \rightarrow \pi\pi$ Decays in the Dual QCD Approach”, arXiv:1807.01709 [hep-ph].

- [138] N. Haba, H. Umeeda and T. Yamada, “Direct CP Violation in Cabibbo-Favored Charmed Meson Decays and ϵ'/ϵ in $SU(2)_L \times SU(2)_R \times U(1)_{B-L}$ Model”, arXiv:1806.03424 [hep-ph].
- [139] S. Matsuzaki, K. Nishiwaki and K. Yamamoto, “Simultaneous interpretation of K and B anomalies in terms of chiral-flavorful vectors”, arXiv:1806.02312 [hep-ph].
- [140] C. H. Chen and T. Nomura, “ ϵ'/ϵ from charged-Higgs-induced gluonic dipole operators”, arXiv:1805.07522 [hep-ph].
- [141] C. H. Chen and T. Nomura, “ $\text{Re}(\epsilon'_K/\epsilon_K)$ and $K \rightarrow \pi\nu\bar{\nu}$ in a two-Higgs doublet model”, JHEP **1808** (2018) 145 [arXiv:1804.06017 [hep-ph]].
- [142] N. Haba, H. Umeeda and T. Yamada, “ ϵ'/ϵ Anomaly and Neutron EDM in $SU(2)_L \times SU(2)_R \times U(1)_{B-L}$ model with Charge Symmetry”, JHEP **1805** (2018) 052 [arXiv:1802.09903 [hep-ph]].
- [143] C. Marzo, L. Marzola and M. Raidal, arXiv:1901.08290 [hep-ph].
- [144] L. Lellouch and M. Luscher, “Weak transition matrix elements from finite volume correlation functions”, Commun. Math. Phys. **219** (2001) 31 [hep-lat/0003023].
- [145] M. Luscher, “Volume Dependence of the Energy Spectrum in Massive Quantum Field Theories. 2. Scattering States”, Commun. Math. Phys. **105** (1986) 153.
- [146] M. Luscher, “Two particle states on a torus and their relation to the scattering matrix”, Nucl. Phys. B **354** (1991) 531.
- [147] X. Feng, “Recent progress in applying lattice QCD to kaon physics”, arXiv:1711.05648 [hep-lat].
- [148] C. Kelly, “Progress in lattice in the kaon system”, talk at CKM 2018 (Heidelberg, September 17th); A. Soni “Current hints of BSM physics and opportunities in the Intensity Frontier”, talk at EW session of the 54th Rencontres de Moriond (La Thuile, March 21st).

- [149] V. Cirigliano, A. Pich, G. Ecker and H. Neufeld, “Isospin violation in ε' ”, *Phys. Rev. Lett.* **91** (2003) 162001 [hep-ph/0307030].
- [150] V. Cirigliano, G. Ecker, H. Neufeld and A. Pich, “Isospin breaking in $K \rightarrow \pi\pi$ decays”, *Eur. Phys. J. C* **33** (2004) 369 [hep-ph/0310351];
- [151] V. Cirigliano, G. Ecker and A. Pich, “Reanalysis of pion pion phase shifts from $K \rightarrow \pi\pi$ decays”, *Phys. Lett. B* **679** (2009) 445 [arXiv:0907.1451 [hep-ph]].
- [152] S. Aoki *et al.*, “Review of lattice results concerning low-energy particle physics”, *Eur. Phys. J. C* **77** (2017) no.2, 112 [arXiv:1607.00299 [hep-lat]].
- [153] G. Ecker, J. Gasser, A. Pich and E. de Rafael, “The Role of Resonances in Chiral Perturbation Theory”, *Nucl. Phys. B* **321** (1989) 311.
- [154] G. Ecker, J. Gasser, H. Leutwyler, A. Pich and E. de Rafael, “Chiral Lagrangians for Massive Spin 1 Fields”, *Phys. Lett. B* **223** (1989) 425.
- [155] A. Pich, “Colorless mesons in a polychromatic world”, Proc. Int. Workshop on *Phenomenology of Large N_C QCD* (Tempe, Arizona, 2002), ed. R. F. Lebed, Proc. Institute for Nuclear Theory – Vol. 12 (World Scientific, Singapore, 2002), p. 239 [hep-ph/0205030].
- [156] V. Cirigliano, G. Ecker, M. Eidemuller, R. Kaiser, A. Pich and J. Portolés, “Towards a consistent estimate of the chiral low-energy constants”, *Nucl. Phys. B* **753** (2006) 139 [hep-ph/0603205].
- [157] R. Kaiser, “ η' contributions to the chiral low-energy constants”, *Nucl. Phys. Proc. Suppl.* **174** (2007) 97.
- [158] V. Cirigliano, G. Ecker, M. Eidemuller, A. Pich and J. Portolés, “ $\langle VAP \rangle$ Green function in the resonance region”, *Phys. Lett. B* **596** (2004) 96 [hep-ph/0404004].

- [159] V. Cirigliano, G. Ecker, M. Eidemuller, R. Kaiser, A. Pich and J. Portolés, “The Green function and SU(3) breaking in K_{l3} decays”, JHEP **0504** (2005) 006 [hep-ph/0503108].
- [160] P. D. Ruiz-Femenia, A. Pich and J. Portolés, “Odd intrinsic parity processes within the resonance effective theory of QCD”, JHEP **0307** (2003) 003 [hep-ph/0306157].
- [161] M. Jamin, J. A. Oller and A. Pich, “Order p^6 chiral couplings from the scalar $K\pi$ form-factor”, JHEP **0402** (2004) 047 [hep-ph/0401080].
- [162] I. Rosell, J. J. Sanz-Cillero and A. Pich, “Quantum loops in the resonance chiral theory: The Vector form-factor”, JHEP **0408** (2004) 042 [hep-ph/0407240].
- [163] I. Rosell, J. J. Sanz-Cillero and A. Pich, “Towards a determination of the chiral couplings at NLO in $1/N_C$: $L_8^r(\mu)$ ”, JHEP **0701** (2007) 039 [hep-ph/0610290].
- [164] A. Pich, I. Rosell and J. J. Sanz-Cillero, “Form-factors and current correlators: Chiral couplings $L_{10}^r(\mu)$ and $C_{87}^r(\mu)$ at NLO in $1/N_C$ ”, JHEP **0807** (2008) 014 [arXiv:0803.1567 [hep-ph]].
- [165] M. Gonzalez-Alonso, A. Pich and J. Prades, “Determination of the Chiral Couplings L_{10} and C_{87} from Semileptonic Tau Decays”, Phys. Rev. D **78** (2008) 116012 [arXiv:0810.0760 [hep-ph]].
- [166] A. Pich, I. Rosell and J. J. Sanz-Cillero, “The vector form factor at the next-to-leading order in $1/N_C$: chiral couplings $L_9(\mu)$ and $C_{88}(\mu) - C_{90}(\mu)$ ”, JHEP **1102** (2011) 109 [arXiv:1011.5771 [hep-ph]].
- [167] J. Bijnens and G. Ecker, “Mesonic low-energy constants”, Ann. Rev. Nucl. Part. Sci. **64** (2014) 149 [arXiv:1405.6488 [hep-ph]].
- [168] M. González-Alonso, A. Pich and A. Rodríguez-Sánchez, “Updated determination of chiral couplings and vacuum condensates from hadronic τ decay data”, Phys. Rev. D **94** (2016) no.1, 014017 [arXiv:1602.06112 [hep-ph]].

- [169] B. Ananthanarayan, J. Bijnens, S. Friot and S. Ghosh, “An analytic representation of F_K/F_π ”, arXiv:1711.11328 [hep-ph].
- [170] S. Weinberg, “Phenomenological Lagrangians”, *Physica A* **96** (1979) 327.
- [171] J. Gasser and H. Leutwyler, “Chiral Perturbation Theory to One Loop”, *Annals Phys.* **158** (1984) 142.
- [172] J. Gasser and H. Leutwyler, “Chiral Perturbation Theory: Expansions in the Mass of the Strange Quark”, *Nucl. Phys. B* **250** (1985) 465.
- [173] G. Ecker, “Chiral perturbation theory”, *Prog. Part. Nucl. Phys.* **35** (1995) 1 [hep-ph/9501357].
- [174] A. Pich, “Chiral perturbation theory”, *Rept. Prog. Phys.* **58** (1995) 563 [hep-ph/9502366].
- [175] J. Bijnens, G. Colangelo and G. Ecker, “The Mesonic chiral Lagrangian of order p^6 ”, *JHEP* **9902** (1999) 020 [hep-ph/9902437].
- [176] J. Bijnens, G. Colangelo and G. Ecker, “Renormalization of chiral perturbation theory to order p^6 ”, *Annals Phys.* **280** (2000) 100 [hep-ph/9907333].
- [177] M. Antonelli *et al.*, “An Evaluation of $|V_{us}|$ and precise tests of the Standard Model from world data on leptonic and semileptonic kaon decays”, *Eur. Phys. J. C* **69** (2010) 399. [arXiv:1005.2323 [hep-ph]].
- [178] G. Ecker, G. Muller, H. Neufeld and A. Pich, “ π^0 - η mixing and CP violation”, *Phys. Lett. B* **477** (2000) 88 [hep-ph/9912264].
- [179] G. Altarelli and L. Maiani, “Octet Enhancement of Nonleptonic Weak Interactions in Asymptotically Free Gauge Theories”, *Phys. Lett.* **52B** (1974) 351.
- [180] M. K. Gaillard and B. W. Lee, “ $\Delta I = 1/2$ Rule for Nonleptonic Decays in Asymptotically Free Field Theories”, *Phys. Rev. Lett.* **33** (1974) 108.

- [181] A. I. Vainshtein, V. I. Zakharov and M. A. Shifman, “A Possible mechanism for the Delta $T = 1/2$ rule in nonleptonic decays of strange particles”, JETP Lett. **22** (1975) 55 [Pisma Zh. Eksp. Teor. Fiz. **22** (1975) 123].
- [182] M. A. Shifman, A. I. Vainshtein and V. I. Zakharov, “Light Quarks and the Origin of the $\Delta I = 1/2$ Rule in the Nonleptonic Decays of Strange Particles”, Nucl. Phys. B **120** (1977) 316.
- [183] F. J. Gilman and M. B. Wise, “Effective Hamiltonian for $\Delta S = 1$ Weak Nonleptonic Decays in the Six Quark Model”, Phys. Rev. D **20** (1979) 2392.
- [184] J. Bijnens and M. B. Wise, “Electromagnetic Contribution to ϵ'/ϵ ”, Phys. Lett. **137B** (1984) 245.
- [185] A. J. Buras and J. M. Gerard, “Isospin Breaking Contributions to ϵ'/ϵ ”, Phys. Lett. B **192** (1987) 156.
- [186] S. R. Sharpe, “On the Contribution of Electromagnetic Penguins to ϵ' ”, Phys. Lett. B **194** (1987) 551.
- [187] M. Lusignoli, “Electromagnetic Corrections to the Effective Hamiltonian for Strangeness Changing Decays and ϵ'/ϵ ”, Nucl. Phys. B **325** (1989) 33.
- [188] J. M. Flynn and L. Randall, “The Electromagnetic Penguin Contribution to ϵ'/ϵ for Large Top Quark Mass”, Phys. Lett. B **224** (1989) 221 [Erratum: Phys. Lett. B **235** (1990) 412].
- [189] A. J. Buras, M. Jamin, M. E. Lautenbacher and P. H. Weisz, “Effective Hamiltonians for $\Delta S = 1$ and $\Delta B = 1$ nonleptonic decays beyond the leading logarithmic approximation”, Nucl. Phys. B **370** (1992) 69 [Addendum: Nucl. Phys. B **375** (1992) 501].

- [190] A. J. Buras, M. Jamin, M. E. Lautenbacher and P. H. Weisz, “Two loop anomalous dimension matrix for $\Delta S = 1$ weak nonleptonic decays. 1. $O(\alpha_s^2)$ ”, *Nucl. Phys. B* **400** (1993) 37 [hep-ph/9211304].
- [191] A. J. Buras, M. Jamin and M. E. Lautenbacher, “Two loop anomalous dimension matrix for $\Delta S = 1$ weak nonleptonic decays. 2. $O(\alpha\alpha_s)$ ”, *Nucl. Phys. B* **400** (1993) 75 [hep-ph/9211321].
- [192] M. Ciuchini, E. Franco, G. Martinelli and L. Reina, “The $\Delta S = 1$ effective Hamiltonian including next-to-leading order QCD and QED corrections”, *Nucl. Phys. B* **415** (1994) 403 [hep-ph/9304257].
- [193] A. J. Buras, P. Gambino and U. A. Haisch, “Electroweak penguin contributions to nonleptonic $\Delta F = 1$ decays at NNLO”, *Nucl. Phys. B* **570** (2000) 117 [hep-ph/9911250].
- [194] M. Gorbahn and U. Haisch, “Effective Hamiltonian for non-leptonic $|\Delta F| = 1$ decays at NNLO in QCD”, *Nucl. Phys. B* **713** (2005) 291 [hep-ph/0411071].
- [195] M. Cerdà-Sevilla, M. Gorbahn, S. Jäger and A. Kokulu, “Towards NNLO accuracy for ϵ'/ϵ ”, *J. Phys. Conf. Ser.* **800** (2017) no.1, 012008 [arXiv:1611.08276 [hep-ph]].
- [196] G. 't Hooft and M. J. G. Veltman, “Regularization and Renormalization of Gauge Fields”, *Nucl. Phys. B* **44** (1972) 189.
- [197] A. Pich, “Precision physics with QCD”, *EPJ Web Conf.* **137** (2017) 01016 [arXiv:1612.05010 [hep-ph]].
- [198] G. 't Hooft, “A Planar Diagram Theory for Strong Interactions”, *Nucl. Phys. B* **72**, 461 (1974).
- [199] E. Witten, “Baryons in the $1/n$ Expansion”, *Nucl. Phys. B* **160** (1979) 57.
- [200] A. J. Buras and J. M. Gerard, “ $1/N$ Expansion for Kaons”, *Nucl. Phys. B* **264** (1986) 371.

- [201] W. A. Bardeen, A. J. Buras and J. M. Gerard, “The $K \rightarrow \pi\pi$ Decays in the Large n Limit: Quark Evolution”, Nucl. Phys. B **293** (1987) 787.
- [202] J. Wess and B. Zumino, “Consequences of anomalous Ward identities”, Phys. Lett. **37B** (1971) 95.
- [203] E. Witten, “Global Aspects of Current Algebra”, Nucl. Phys. B **223** (1983) 422.
- [204] R. Urech, “Virtual photons in chiral perturbation theory”, Nucl. Phys. B **433** (1995) 234 [hep-ph/9405341].
- [205] J. Kambor, J. H. Missimer and D. Wyler, “The Chiral Loop Expansion of the Non-leptonic Weak Interactions of Mesons”, Nucl. Phys. B **346** (1990) 17.
- [206] G. Ecker, J. Kambor and D. Wyler, “Resonances in the weak chiral Lagrangian”, Nucl. Phys. B **394** (1993) 101.
- [207] G. Ecker, G. Isidori, G. Muller, H. Neufeld and A. Pich, “Electromagnetism in nonleptonic weak interactions”, Nucl. Phys. B **591** (2000) 419 [hep-ph/0006172].
- [208] M. Knecht, H. Neufeld, H. Rupertsberger and P. Talavera, “Chiral perturbation theory with virtual photons and leptons”, Eur. Phys. J. C **12** (2000) 469 [hep-ph/9909284].
- [209] J. A. Cronin, “Phenomenological model of strong and weak interactions in chiral $U(3) \times U(3)$ ”, Phys. Rev. **161** (1967) 1483.
- [210] B. Grinstein, S. J. Rey and M. B. Wise, “CP Violation in Charged Kaon Decay”, Phys. Rev. D **33** (1986) 1495.
- [211] V. Cirigliano, G. Ecker, H. Neufeld and A. Pich, “Meson resonances, large N_c and chiral symmetry”, JHEP **0306** (2003) 012 [hep-ph/0305311].
- [212] R. J. Dowdall, C. T. H. Davies, G. P. Lepage and C. McNeile, “ V_{us} from π and K decay constants in full lattice QCD with physical u, d, s and c quarks”, Phys. Rev. D **88** (2013) 074504 [arXiv:1303.1670 [hep-lat]].

- [213] B. Moussallam, “A Sum rule approach to the violation of Dashen’s theorem”, Nucl. Phys. B **504** (1997) 381 [hep-ph/9701400].
- [214] J. Bijnens and J. Prades, “Electromagnetic corrections for pions and kaons: Masses and polarizabilities”, Nucl. Phys. B **490** (1997) 239 [hep-ph/9610360].
- [215] J. Kambor, J. H. Missimer and D. Wyler, “ $K \rightarrow 2\pi$ and $K \rightarrow 3\pi$ decays in next-to-leading order chiral perturbation theory”, Phys. Lett. B **261** (1991) 496.
- [216] J. Bijnens, E. Pallante and J. Prades, “Obtaining $K \rightarrow \pi\pi$ from off-shell $K \rightarrow \pi$ amplitudes”, Nucl. Phys. B **521** (1998) 305 [hep-ph/9801326].
- [217] E. Pallante, “The Generating functional for hadronic weak interactions and its quenched approximation”, JHEP **9901** (1999) 012 [hep-lat/9808018].
- [218] S. Weinberg, “Pion scattering lengths”, Phys. Rev. Lett. **17** (1966) 616.
- [219] V. Cirigliano and E. Golowich, “Analysis of $O(p^2)$ corrections to $\langle \pi\pi | Q_{7,8} | K \rangle$ ”, Phys. Lett. B **475** (2000) 351 [hep-ph/9912513].
- [220] V. Cirigliano and E. Golowich, “Comment on ‘Analysis of $O(p^2)$ corrections to $\langle \pi\pi | Q_{7,8} | K \rangle$ ’”, Phys. Rev. D **65** (2002) 054014 [hep-ph/0109265].
- [221] J. Bijnens, “ K_{l4} Decays and the Low-energy Expansion”, Nucl. Phys. B **337** (1990) 635.
- [222] C. Riggenbach, J. Gasser, J. F. Donoghue and B. R. Holstein, “Chiral symmetry and the large N_c limit in K_{l4} decays”, Phys. Rev. D **43** (1991) 127.
- [223] J. Bijnens, G. Colangelo and J. Gasser, “ K_{l4} decays beyond one loop”, Nucl. Phys. B **427** (1994) 427 [hep-ph/9403390].
- [224] G. Amoros, J. Bijnens and P. Talavera, “Low-energy constants from K_{l4} form-factors”, Phys. Lett. B **480** (2000) 71 [hep-ph/9912398].

- [225] G. Amoros, J. Bijnens and P. Talavera, “ $K_{\ell 4}$ form-factors and $\pi-\pi$ scattering”, Nucl. Phys. B **585** (2000) 293 Erratum: [Nucl. Phys. B **598** (2001) 665] [hep-ph/0003258].
- [226] J. Bijnens, G. Colangelo, G. Ecker, J. Gasser and M. E. Sainio, “Elastic $\pi\pi$ scattering to two loops”, Phys. Lett. B **374** (1996) 210 [hep-ph/9511397].
- [227] J. Bijnens, G. Colangelo, G. Ecker, J. Gasser and M. E. Sainio, “Pion-pion scattering at low energy”, Nucl. Phys. B **508** (1997) 263 Erratum: [Nucl. Phys. B **517** (1998) 639] [hep-ph/9707291].
- [228] B. Ananthanarayan, G. Colangelo, J. Gasser and H. Leutwyler, “Roy equation analysis of $\pi\pi$ scattering”, Phys. Rept. **353** (2001) 207 [hep-ph/0005297].
- [229] G. Colangelo, J. Gasser and H. Leutwyler, “The $\pi\pi$ S wave scattering lengths”, Phys. Lett. B **488** (2000) 261 [hep-ph/0007112].
- [230] G. Colangelo, J. Gasser and H. Leutwyler, “ $\pi\pi$ scattering”, Nucl. Phys. B **603** (2001) 125 [hep-ph/0103088].
- [231] I. Caprini, G. Colangelo, J. Gasser and H. Leutwyler, “On the precision of the theoretical predictions for $\pi\pi$ scattering”, Phys. Rev. D **68** (2003) 074006 [hep-ph/0306122].
- [232] I. Caprini, G. Colangelo and H. Leutwyler, “Regge analysis of the $\pi\pi$ scattering amplitude”, Eur. Phys. J. C **72** (2012) 1860 [arXiv:1111.7160 [hep-ph]].
- [233] S. Descotes-Genon, N. H. Fuchs, L. Girlanda and J. Stern, “Analysis and interpretation of new low-energy $\pi\pi$ scattering data”, Eur. Phys. J. C **24** (2002) 469 [hep-ph/0112088].
- [234] R. Garcia-Martin, R. Kaminski, J. R. Pelaez, J. Ruiz de Elvira and F. J. Yndurain, “The Pion-pion scattering amplitude. IV: Improved analysis with once subtracted Roy-like equations up to 1100 MeV”, Phys. Rev. D **83** (2011) 074004 [arXiv:1102.2183 [hep-ph]].

- [235] G. Colangelo, E. Passemar and P. Stoffer, “A dispersive treatment of $K_{\ell 4}$ decays”, *Eur. Phys. J. C* **75** (2015) 172 [arXiv:1501.05627 [hep-ph]].
- [236] N. Christ and X. Feng, “Including electromagnetism in $K \rightarrow \pi\pi$ decay calculations”, arXiv:1711.09339 [hep-lat].
- [237] C. Lehner, E. Lunghi and A. Soni, “Emerging lattice approach to the K-Unitarity Triangle”, *Phys. Lett. B* **759** (2016) 82 [arXiv:1508.01801 [hep-ph]].
- [238] P. A. Baikov, K. G. Chetyrkin and J. H. Kühn, “Quark Mass and Field Anomalous Dimensions to $\mathcal{O}(\alpha_s^5)$ ”, *JHEP* **1410** (2014) 076 [arXiv:1402.6611 [hep-ph]].
- [239] V. Cirigliano, H. Gisbert, A. Pich and A. Rodríguez-Sánchez, “Isospin-Violating Contributions to ϵ'/ϵ ”, work in progress.
- [240] J. F. Donoghue and E. Golowich, “Anatomy of a weak matrix element”, *Phys. Lett. B* **315** (1993) 406 [hep-ph/9307263].
- [241] M. Knecht, S. Peris and E. de Rafael, “Matrix elements of electroweak penguin operators in the $1/N_c$ expansion”, *Phys. Lett. B* **457** (1999) 227 [hep-ph/9812471].
- [242] J. F. Donoghue and E. Golowich, “Dispersive calculation of $B_7^{(3/2)}$ and $B_8^{(3/2)}$ in the chiral limit”, *Phys. Lett. B* **478** (2000) 172 [hep-ph/9911309].
- [243] M. Knecht, S. Peris and E. de Rafael, “A critical reassessment of Q_7 and Q_8 matrix elements”, *Phys. Lett. B* **508** (2001) 117 [hep-ph/0102017].
- [244] S. Narison, “New QCD estimate of the kaon penguin matrix elements and ϵ'/ϵ ”, *Nucl. Phys. B* **593** (2001) 3 [hep-ph/0004247].
- [245] V. Cirigliano, J. F. Donoghue, E. Golowich and K. Maltman, “Determination of $\langle(\pi\pi)_{I=2}|Q_{7,8}|K^0\rangle$ in the chiral limit”, *Phys. Lett. B* **522** (2001) 245 [hep-ph/0109113].
- [246] J. Bijnens, E. Gamiz and J. Prades, “Matching the electroweak penguins Q_7 , Q_8 and spectral correlators”, *JHEP* **0110** (2001) 009 [hep-ph/0108240].

- [247] V. Cirigliano, J. F. Donoghue, E. Golowich and K. Maltman, “Improved determination of the electroweak penguin contribution to ϵ'/ϵ in the chiral limit”, *Phys. Lett. B* **555** (2003) 71 [hep-ph/0211420].
- [248] A. Rodríguez-Sánchez and A. Pich, *Nucl. Part. Phys. Proc.* **300-302** (2018) 131 [arXiv:1811.06706 [hep-ph]].
- [249] P. Boucaud, V. Gimenez, C. J. D. Lin, V. Lubicz, G. Martinelli, M. Papinutto and C. T. Sachrajda, “An Exploratory lattice study of $\Delta I = 3/2$ $K \rightarrow \pi\pi$ decays at next-to-leading order in the chiral expansion”, *Nucl. Phys. B* **721** (2005) 175 [hep-lat/0412029].
- [250] M. Buchler, G. Colangelo, J. Kambor and F. Orellana, “Dispersion relations and soft pion theorems for $K \rightarrow \pi\pi$ ”, *Phys. Lett. B* **521** (2001) 22 [hep-ph/0102287].
- [251] M. Buchler, “The Chiral logs of the $K \rightarrow \pi\pi$ amplitude”, *Phys. Lett. B* **633** (2006) 497 [hep-ph/0511087].
- [252] M. Davier, A. Hoecker, B. Malaescu and Z. Zhang, “Reevaluation of the hadronic vacuum polarisation contributions to the Standard Model predictions of the muon $g - 2$ and $\alpha(m_Z)$ using newest hadronic cross-section data”, arXiv:1706.09436 [hep-ph].
- [253] J. Fuster, A. Irls, D. Melini, P. Uwer and M. Vos, “Extracting the top-quark running mass using $t\bar{t} + 1$ -jet events produced at the Large Hadron Collider”, arXiv:1704.00540 [hep-ph].
- [254] G. Aad *et al.* [ATLAS Collaboration], “Determination of the top-quark pole mass using $t\bar{t} + 1$ -jet events collected with the ATLAS experiment in 7 TeV pp collisions”, *JHEP* **1510** (2015) 121 [arXiv:1507.01769 [hep-ex]].
- [255] D. H. Adams and W. Lee, *Phys. Rev. D* **75** (2007) 074502 doi:10.1103/PhysRevD.75.074502 [hep-lat/0701014].

- [256] J. Bijnens and F. Borg, Nucl. Phys. B **697** (2004) 319 doi:10.1016/j.nuclphysb.2004.07.011 [hep-ph/0405025].
- [257] J. Bijnens and F. Borg, Eur. Phys. J. C **39** (2005) 347 doi:10.1140/epjc/s2004-02094-9 [hep-ph/0410333].
- [258] J. Bijnens and F. Borg, Eur. Phys. J. C **40** (2005) 383 doi:10.1140/epjc/s2005-02155-7 [hep-ph/0501163].
- [259] S. Aoki *et al.* [Flavour Lattice Averaging Group], arXiv:1902.08191 [hep-lat].
- [260] V. Cirigliano, M. Knecht, H. Neufeld, H. Rupertsberger and P. Talavera, Eur. Phys. J. C **23** (2002) 121 doi:10.1007/s100520100825 [hep-ph/0110153].
- [261] J. A. Oller, Nucl. Phys. A **727** (2003) 353 doi:10.1016/j.nuclphysa.2003.08.002 [hep-ph/0306031].
- [262] M. Jamin, J. A. Oller and A. Pich, Nucl. Phys. B **587** (2000) 331 doi:10.1016/S0550-3213(00)00479-X [hep-ph/0006045].
- [263] T. Ledwig, J. Nieves, A. Pich, E. Ruiz Arriola and J. Ruiz de Elvira, Phys. Rev. D **90** (2014) no.11, 114020 doi:10.1103/PhysRevD.90.114020 [arXiv:1407.3750 [hep-ph]].
- [264] I. Caprini, G. Colangelo and H. Leutwyler, Phys. Rev. Lett. **96** (2006) 132001 doi:10.1103/PhysRevLett.96.132001 [hep-ph/0512364].
- [265] J. R. Pelaez, Phys. Rept. **658** (2016) 1 doi:10.1016/j.physrep.2016.09.001 [arXiv:1510.00653 [hep-ph]].
- [266] B. Ananthanarayan and B. Moussallam, JHEP **0406** (2004) 047 doi:10.1088/1126-6708/2004/06/047 [hep-ph/0405206].
- [267] M. Albaladejo and B. Moussallam, Eur. Phys. J. C **77** (2017) no.8, 508 doi:10.1140/epjc/s10052-017-5052-x [arXiv:1702.04931 [hep-ph]].
- [268] T. D. Lee, Phys. Rev. D **8** (1973) 1226. doi:10.1103/PhysRevD.8.1226

- [269] T. D. Lee, Phys. Rept. **9** (1974) 143. doi:10.1016/0370-1573(74)90020-9
- [270] G. C. Branco, P. M. Ferreira, L. Lavoura, M. N. Rebelo, M. Sher and J. P. Silva, Phys. Rept. **516** (2012) 1 doi:10.1016/j.physrep.2012.02.002 [arXiv:1106.0034 [hep-ph]].
- [271] J. F. Gunion, H. E. Haber, G. L. Kane and S. Dawson, Front. Phys. **80** (2000) 1.
- [272] I. P. Ivanov, Prog. Part. Nucl. Phys. **95** (2017) 160 doi:10.1016/j.ppnp.2017.03.001 [arXiv:1702.03776 [hep-ph]].
- [273] A. Pich and P. Tuzon, Phys. Rev. D **80** (2009) 091702 doi:10.1103/PhysRevD.80.091702 [arXiv:0908.1554 [hep-ph]].
- [274] A. Pich, Nucl. Phys. Proc. Suppl. **209** (2010) 182 doi:10.1016/j.nuclphysbps.2010.12.030 [arXiv:1010.5217 [hep-ph]].
- [275] A. Peñuelas and A. Pich, JHEP **1712** (2017) 084 doi:10.1007/JHEP12(2017)084 [arXiv:1710.02040 [hep-ph]].
- [276] Q. Chang, P. F. Li and X. Q. Li, Eur. Phys. J. **C75** (2015) 594.
- [277] Enomoto, Tetsuya, Watanabe and Ryoutaro, *Flavor constraints on the Two Higgs Doublet Models of Z_2 symmetric and aligned types*, JHEP **05** (2016) 002.
- [278] N. Cho, X. Q. Li, F. Su and X. Zhang, Adv. High Energy Phys. **2017** (2017) 2863647 doi:10.1155/2017/2863647 [arXiv:1705.07638 [hep-ph]].
- [279] R. M. Wang, P. B. Wang, X. D. Cheng, Y. G. Xu and Q. Chang, J. Phys. G **45** (2018) no.12, 125001. doi:10.1088/1361-6471/aaeba1
- [280] A. V. Manohar and M. B. Wise, Phys. Rev. D **74** (2006) 035009 doi:10.1103/PhysRevD.74.035009 [hep-ph/0606172].
- [281] N. Carrasco *et al.* [ETM Collaboration], JHEP **1403** (2014) 016 doi:10.1007/JHEP03(2014)016 [arXiv:1308.1851 [hep-lat]].

- [282] N. Carrasco *et al.* [ETM Collaboration], Phys. Rev. D **92** (2015) no.3, 034516 doi:10.1103/PhysRevD.92.034516 [arXiv:1505.06639 [hep-lat]].
- [283] A. J. Buras, S. Jager and J. Urban, Nucl. Phys. B **605** (2001) 600 doi:10.1016/S0550-3213(01)00207-3 [hep-ph/0102316].
- [284] A. J. Buras, D. Guadagnoli and G. Isidori, Phys. Lett. B **688** (2010) 309 doi:10.1016/j.physletb.2010.04.017 [arXiv:1002.3612 [hep-ph]].
- [285] T. Jubb, M. Kirk, A. Lenz and G. Tetlalmatzi-Xolocotzi, Nucl. Phys. B **915** (2017) 431 doi:10.1016/j.nuclphysb.2016.12.020 [arXiv:1603.07770 [hep-ph]].
- [286] K. G. Chetyrkin, J. H. Kuhn and M. Steinhauser, Comput. Phys. Commun. **133** (2000) 43 doi:10.1016/S0010-4655(00)00155-7 [hep-ph/0004189].
- [287] H. Gisbert and J. Ruiz Vidal, arXiv:1905.02513 [hep-ph].
- [288] T. Chupp, P. Fierlinger, M. Ramsey-Musolf and J. Singh, Rev. Mod. Phys. **91** (2019) no.1, 015001.
- [289] N. Yamanaka, B. K. Sahoo, N. Yoshinaga, T. Sato, K. Asahi and B. P. Das, Eur. Phys. J. A **53** (2017) no.3, 54.
- [290] M. Pospelov and A. Ritz, Annals Phys. **318** (2005) 119.
- [291] J. Engel, M. J. Ramsey-Musolf and U. van Kolck, Prog. Part. Nucl. Phys. **71** (2013) 21.
- [292] W. Dekens, J. de Vries, J. Bsaisou, W. Bernreuther, C. Hanhart, U. G. Meißner, A. Nogga and A. Wirzba, JHEP **1407** (2014) 069.
- [293] D. Buttazzo, A. Greljo, G. Isidori and D. Marzocca, JHEP **1711** (2017) 044.
- [294] W. Dekens, J. de Vries, M. Jung and K. K. Vos, JHEP **1901** (2019) 069.
- [295] F. J. Botella, L. M. Garcia Martin, D. Marangotto, F. Martínez Vidal, A. Merli, N. Neri, A. Oyanguren and J. Ruiz Vidal, Eur. Phys. J. C **77** (2017) no.3, 181.

-
- [296] E. Bagli *et al.*, Eur. Phys. J. C **77** (2017) no.12, 828.
- [297] A. S. Fomin *et al.*, JHEP **1708** (2017) 120.
- [298] V. G. Baryshevsky, Phys. Lett. B **757** (2016) 426.
- [299] F. Sala, JHEP **1403** (2014) 061.
- [300] D. Chang, W. Y. Keung, C. S. Li and T. C. Yuan, Phys. Lett. B **241** (1990) 589.
- [301] E. Braaten, C. S. Li and T. C. Yuan, Phys. Rev. Lett. **64** (1990) 1709.
- [302] G. Boyd, A. K. Gupta, S. P. Trivedi and M. B. Wise, Phys. Lett. B **241** (1990) 584.
- [303] A. Cordero-Cid, J. M. Hernandez, G. Tavares-Velasco and J. J. Toscano, J. Phys. G **35** (2008) 025004.
- [304] A. G. Grozin, I. B. Khriplovich and A. S. Rudenko, Nucl. Phys. B **821** (2009) 285.
- [305] R. Escribano and E. Masso, Nucl. Phys. B **429** (1994) 19.
- [306] A. E. Blinov and A. S. Rudenko, Nucl. Phys. Proc. Suppl. **189** (2009) 257.
- [307] S. Weinberg, Phys. Rev. Lett. **63** (1989) 2333.
- [308] F. Wilczek and A. Zee, Phys. Rev. D **15** (1977) 2660.
- [309] G. Degrassi, E. Franco, S. Marchetti and L. Silvestrini, JHEP **0511** (2005) 044.
- [310] E. E. Jenkins, A. V. Manohar and P. Stoffer, JHEP **1801** (2018) 084.
- [311] C. A. Baker *et al.*, Phys. Rev. Lett. **97** (2006) 131801.
- [312] V. Cirigliano, W. Dekens, J. de Vries and E. Mereghetti, Phys. Rev. D **94** (2016) no.1, 016002.
- [313] J. F. Kamenik, M. Papucci and A. Weiler, Phys. Rev. D **85** (2012) 071501 Erratum:
[Phys. Rev. D **88** (2013) no.3, 039903].

- [314] S. M. Zhao, T. F. Feng, Z. J. Yang, H. B. Zhang, X. X. Dong and T. Guo, Eur. Phys. J. C **77** (2017) no.2, 102.
- [315] R. Martinez and G. Valencia, Phys. Rev. D **95** (2017) no.3, 035041.
- [316] Z. Z. Aydin and U. Erkarslan, Phys. Rev. D **67** (2003) 036006.
- [317] D. A. Demir and M. B. Voloshin, Phys. Rev. D **63** (2001) 115011.